UNIVERSITÉ DE NEUCHÂTEL
FACULTÉ DES SCIENCES
INSTITUT DE GÉOLOGIE
CENTRE D'HYDROGÉOLOGIE

Shallow depth karst structure imaging with the Very Low Frequency-Electromagnetics GRADIENT method (VLF-EM GRAD):

A new geophysical contribution to aquifer protection strategies compared with other near surface mapping geophysics

by

FRANK P. BOSCH

Centre d'Hydrogéologie

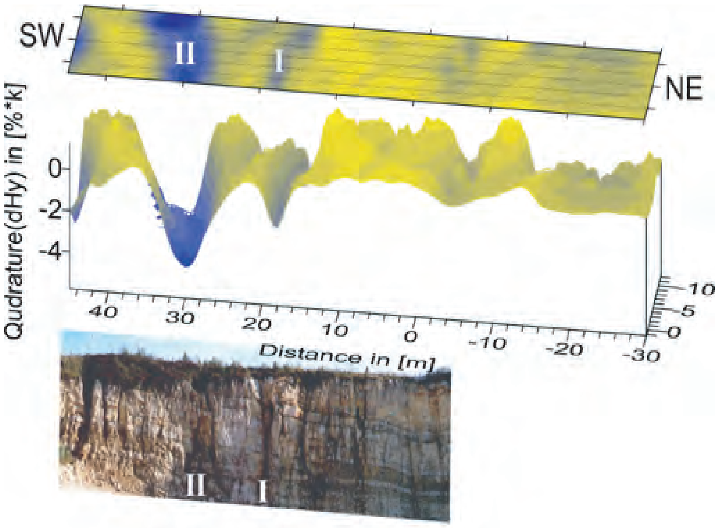

Abstract

In order to provide useful information relating to karst aquifer protection strategies, geophysical methods have to be capable of mapping heterogeneously distributed high permeability zones in carbonate rocks. High horizontal and vertical resolution of a method is as necessary as the ability to cover large areas.

Within this objective in mind, a Very Low Frequency-Electromagnetic GRADIENT device has been developed for high-resolution mapping at shallow depth. Joint surveys using different geophysical methods at different sites allowing in-situ validation demonstrate its efficiency and reliability. Apart from the particular focus on the gradient method, this work shows that the combination of electromagnetic methods provides an appropriate tool-set for obtaining integrated subsurface information necessary to characterise the high permeability zone distribution at local scale over large areas.

Moreover, this work indicates that the self-potential method is a promising tool for mapping hydrogeologically important aspects of karst structures.

The development and application of a null-array electrode configuration has demonstrated that the technique provides a significant sensitivity increase for geoelectrical methods to detect narrow, vertical structures at shallow depths.

THÈSE

présentée à
la Faculté des Sciences
de l'Université de Neuchâtel
pour obtenir le titre de
Docteur ès Sciences

Soutenue le 30. Août 2002 devant le jury composé de:

Prof. François Zwahlen (Directeur)
Université de Neuchâtel (Suisse)

Prof. Imre Müller (Codirecteur)
Université de Neuchâtel (Suisse)

Prof. Alain Dassargues (Expert)
Université de Liège (Belgique)

Prof. Stanislav Mares (Expert)
Univerzita Karlova v Praze (Tchéquie)

Prof. Jacques Mudry (Expert)
Université de Franche-Comté, Besançon (France)

Dr. Pierre-André Schnegg (Expert)
Université de Neuchâtel (Suisse)

NEUCHÂTEL, 2002

IMPRIMATUR POUR LA THESE

Shallow depth karst structure imaging with the Very Low Frequency-Electromagnetics Gradient (VLF-EM GRAD) method: A new geophysical contribution to aquifer protection strategies compared with other near surface mapping geophysics

de M. Frank P. Bosch

UNIVERSITE DE NEUCHATEL

FACULTE DES SCIENCES

La Faculté des sciences de l'Université de Neuchâtel sur le rapport des membres du jury,

MM. F. Zwahlen (directeur de thèse),
I. Müller (co-directeur de thèse),
P.-A. Schnegg, A. Dassargues (Liège B),
S. Mares (Prague) et J. Mudry (Besançon)

autorise l'impression de la présente thèse.

Neuchâtel, le 3 octobre 2002

Le doyen:

F. Zwahlen

Shallow depth karst structure imaging with the Very Low Frequency-Electromagnetics GRADIENT (VLF-EM GRAD) method:

A new geophysical contribution to aquifer protection strategies compared with other near surface mapping geophysics

by

FRANK P. BOSCH

Doctoral dissertation at the University of Neuchâtel, Switzerland 2002

Abstract – In order to provide useful information relating to karst aquifer protection strategies, geophysical methods have to be capable of mapping heterogeneously distributed high permeability zones in carbonate rocks. High horizontal and vertical resolution of a method is as necessary as the ability to cover large areas.

Within this objective in mind, a Very Low Frequency-Electromagnetics GRADIENT device has been developed for high-resolution mapping at shallow depth. Joint surveys using different geophysical methods at different sites allowing in-situ validation demonstrate its efficiency and reliability. Apart from the particular focus on the gradient method, this work shows that the combination of electromagnetic methods provides an appropriate tool-set for obtaining integrated subsurface information necessary to characterise the high permeability zone distribution at local scale over large areas.

Moreover, this work indicates that the self-potential method is a promising tool for mapping hydrogeologically important aspects of karst structures.

The development and application of a null-array electrode configuration has demonstrated that the technique provides a significant sensitivity increase for geoelectrical methods to detect narrow, vertical structures at shallow depths.

Imagerie électromagnétique à très basse fréquence "GRADIENT" (VLF-EM GRAD) de structures karstiques peu profondes:

Comparaison avec d'autres méthodes géophysiques de surface appliquées à la stratégie de protection des aquifères

par

FRANK P. BOSCH

Thèse de doctorat de l'Université de Neuchâtel, Suisse, 2002

Résumé – Afin de fournir de l'information utile relative à la stratégie pour la protection des aquifères karstiques, les méthodes géophysiques doivent pouvoir prouver leur efficacité dans le profilage des zones hétérogènes hautement perméables que l'on rencontre dans les roches carbonatées. Deux conditions doivent être remplies simultanément : haute résolution horizontale et verticale, et grand rendement en termes de superficie explorée.

Avec ces deux objectifs à l'esprit, nous avons développé un appareil de type GRADIENT à très basse fréquence électromagnétique autorisant le profilage à haute résolution et faible profondeur. Son efficacité et sa fiabilité ont été vérifiées sur différents profils au moyen d'autres méthodes géophysiques. Le présent travail se concentre plus particulièrement sur la méthode du gradient. Mais il montre aussi que la combinaison de diverses méthodes géophysiques permet d'obtenir du sous-sol l'information nécessaire à caractériser sur de grandes étendues et à l'échelle locale la distribution des zones de haute perméabilité.

Ce travail indique également que la méthode du self potentiel est certainement un outil prometteur pour la cartographie des structures karstiques dans lesquelles l'hydrogéologie constitue un aspect important.

Le développement et l'application d'une configuration d'électrodes de mesure dite « null array » a montré que cette technique pouvait fournir aux méthodes géoélectriques un appréciable gain de sensibilité dans la détection superficielle de structures verticales étroites.

Kartierung oberflächennaher Karst Strukturen mit der Very Low Frequency-Electromagnetics GRADIENTEN Methode (VLF-EM GRAD):

Ein neuer geophysikalischer Beitrag zu Karst-Grundwasserschutz Konzepten im Vergleich mit anderen oberflächennahen geophysikalischen Methoden

by

FRANK P. BOSCH

Doktorarbeit an der Universität zu Neuenburg, Schweiz 2002

Zusammenfassung – Um zu Grundwasserschutz Konzepten von Karst Gebieten nützliche Information beitragen zu können, sollten geophysikalische Messverfahren speziell auf Karst in der Lage sein, die hier charakteristisch, herterogen verteilten Zonen hoher Permeabilität aufzuzeigen. Hierzu ist eine hohe räumliche Auflösung des Messverfahrens genauso wichtig wie die Möglichkeit, ein großes Messgelände mit geringem Zeitaufwand zu kartieren.

Im Hinblick auf diese Bedingungen wurde auf Grundlage der elektromagnetischen Induktion ein Gerät entwickelt, dass im langperiodischen Radiowellenbereich den vertikalen Gradient des induzierten, lokalen Magnetfeldes erfasst (Very Low Frequency Electromagnetics GRADIENT).

Um die Effizienz und Zuverlässigkeit des neuen Gerätes zu demonstrieren, wurde die Methode auf verschiedenen Messgebieten, teilweise mit in-situ Beobachtungsmöglichkeiten, immer im Vergleich mit weiteren geophysikalischen Messverfahren angewandt. Hier zeigt sich, dass neben der Gradienten Methode insbesondere die Kombination verschiedener elektromagnetischer Verfahren geeignet ist, die lokale Verteilung der Zonen hoher Permeabilität großflächig zu kartieren.

Abgesehen von den elektromagnetischen Verfahren zeigt die vorliegende Arbeit, dass auch das Eigenpotential Verfahren auf Karst Gebiete angewandt, ein vielversprechendes Werkzeug zur Kartierung wichtiger hydrogeologische Parameter darstellt. Zudem konnte gezeigt werden, dass die Anwendung der Null-Array Elektroden Konfiguration in der Geoelektrik auf Karst eine signifikante Verbesserung der Auflösung hinsichtlich schmaler vertikaler Strukturen im oberflächennahen Bereich ermöglicht.

Content

1 Introduction

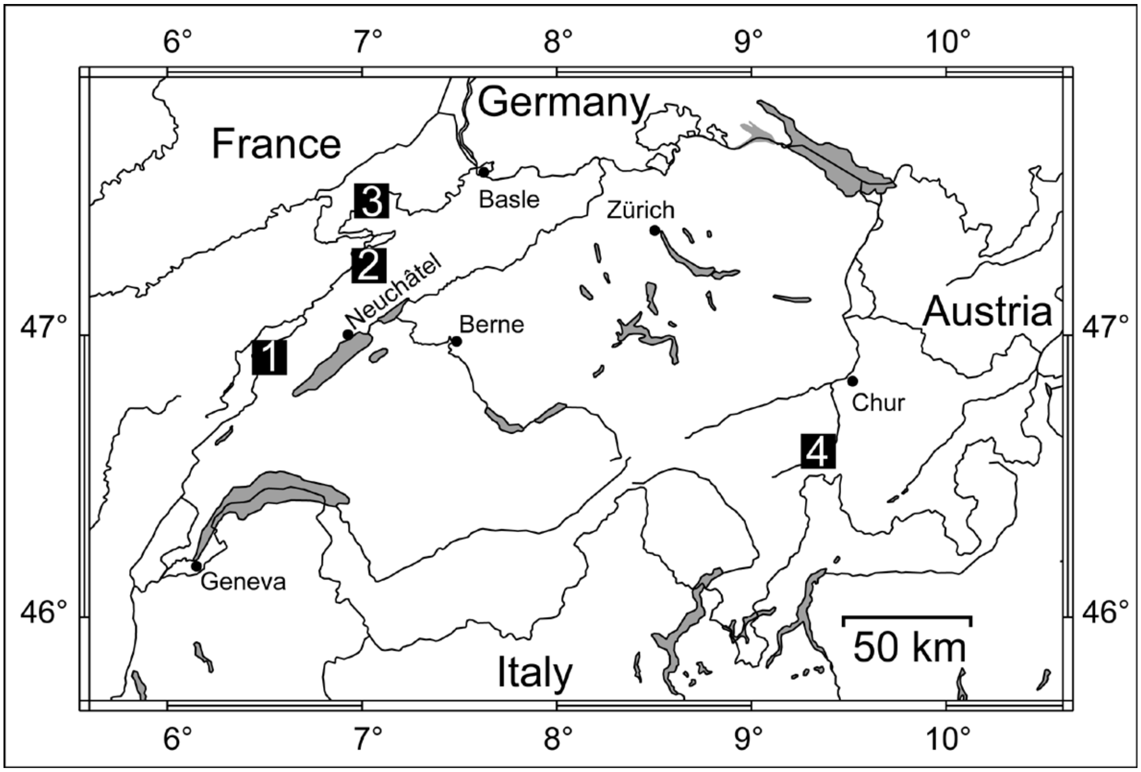

Figure 1 Map of Switzerland with survey area locations: 1 = "Chez les Brandt Cave" near Les Verrières, canton Neuchatel, (NE); 2 = Quarry of Les Breuleux, canton Jura (JU); 3 = Buix (JU); 4 = "Lai da Vons-lake" near Sufers, canton Graubünden (GR).

This doctoral dissertation consists of seven papers and one additional unpublished case study, which illustrate the development and application of some geophysical methods for shallow investigation depths. Figure 1 presents the survey area locations and Table 1 provides an overview about the applied methods and the included papers. The focus of this work lies in highlighting the efficiency and reliability of the latest electromagnetic device developed at the Centre of Hydrogeology Neuchâtel (CHYN). This is known as Very Low Frequency-Electromagnetic GRADIENT (VLF-EM GRAD) method and is used for mapping high permeability zones in karstic limestone (Bosch & Müller 2001a; Bosch & Müller 2001b; Bosch & Müller subm.).

In the framework of this PhD thesis, the VLF-EM GRAD equipment was developed in order to enhance the high-resolution mapping of electric resistivity contrasts of the ground in the epikarstic zone providing a fast, continuously measuring method without ground contact. Consequently, the method provides valuable information in the groundwater vulnerability assessment process and in protection strategy development of karst aquifers. The gradient method is compared with CHYN's former EM developments and with other common geophysical methods, such as seismics and geoelectric tomography. The methods have been applied at different investigation areas. These comparisons illustrate their advantages, limitations, and results that can be achieved by combined application.

Survey Area	Applied Methods	Paper
1. Chez les Brandt Cave (NE)	RMT RF-EM VLF-EM GRAD SP SPS	Paper 1: (Bosch & Gurk 2000) Paper 2: (Bosch & Müller 2001b) Paper 4: (Gurk & Bosch 2001)
2. Quarry of Les Breuleux (JU)	RF-EM VLF-EM GRAD Null-array geoelectrics	Paper 3: (Bosch & Müller 2001a) Paper 6: (Szalai et al. 2002)
3. Buix (JU)	RMT RF-EM VLF-EM GRAD Geoelectric Tomography Seismics Dye tracer test	Paper 7: (Bosch & Müller subm.)
Bure/ Le Maira (JU)	RMT VLF-EM GRAD Geoelectric Tomography	Thesis-Chapter 2.2
4. Sufers (GR)	Magnetics SP RF-EM	Paper 5: (Gurk et al. 2001)

Table 1 Overview of survey areas, applied methods and the contributing papers.

Apart from this focus, this work also includes approaches to near surface karst studies using the self-potential method (Bosch & Gurk 2000; Gurk & Bosch 2001) and null-coupling geoelectrics (Szalai et al. 2002).

The following introductory paragraphs illustrate the overall motivation for the application of geophysics to karst investigation. Consequently, the requirements of geophysical methods applied to karst research have been formulated. Furthermore, a historical view on geophysical karst research and methods is given, leading to the latest equipment developments at the CHYN to explain, in what context the development of VLF-EM GRAD stands. Although the theoretical background of the applied methods are explained in the included papers, the reader will find some of the basic principles of the methods in this mainly historical-orientated introduction with links to the corresponding papers for more detailed insights.

1.1 Geophysics for karst hydrogeology

Since carbonate aquifers cover a large part of Europe (35 %, i.e. approximately 3 million km^2), their investigation is of particular interest. According to the definition used here, the term "carbonate aquifers" includes fractured and karstified systems. Carbonate aquifers are prolific sources of groundwater because of their large catchment sizes and high transmissivity. Furthermore, they are particularly extensive in the areas surrounding the Mediterranean, where water demand is high. Consequently, it is reasonable to expect that sustainable water management in Europe and around the World will depend increasingly on water from carbonate aquifers. As a result, the understanding of carbonate aquifer hydraulics is of greatest interest in terms of both water exploration and water protection.

The application of geophysics for karst research can be used for both in terms of refining the conceptual models of karst used for the basic understanding of carbonate aquifers, and conversely contributing to water management by mapping underground structures with regard to the understood conceptual models.

1.1.1 Particularities of carbonate aquifers

Some particular properties of the karstic environment make water resource management and protection difficult and need to be considered in selecting/ developing appropriate geophysical methods. One important characteristic of karst aquifers in contrast to porous aquifers is the extremely heterogeneous nature of the medium schematically illustrated in Figure 2. Figure 3shows an example of karstified limestone from the Swiss Jura Mountains.

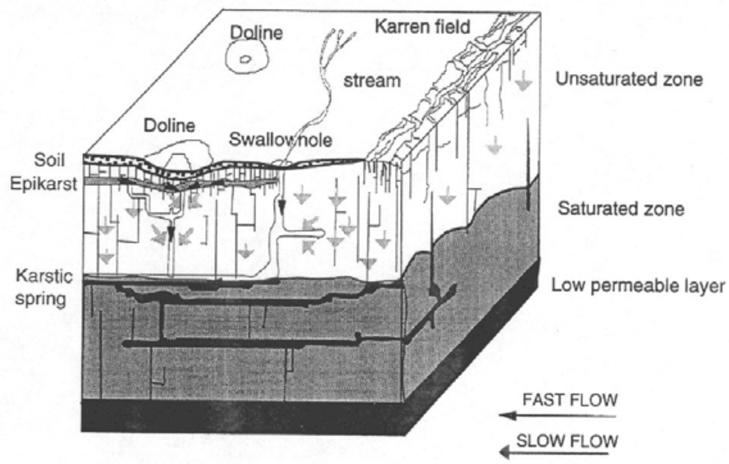

Figure 2 Conceptual model of karst aquifers (Doerfliger et al. 1999).

Figure 3 Example of karstified limestone at the quarry of Les Breuleux (JU), Switzerland.

The medium permeability can be considered as consisting of two extreme components, low permeability volumes of fissured rock and very high permeability conduits. Kiraly (1969, 1975) even avoids using the term "medium permeability". He emphasizes the "scale effect", which describes the observation of the distribution of permeability (strongly connected to fractures and conduits). On the small scale (m^3), random probes show extremely low permeability, while permeability is important on the regional scale (km^2) when considering the enormous discharges of karst springs. Thus motivates to speak of "high permeability singularities" in carbonate rocks, meaning that the parameter "high permeability" seldom occurs but in a concentrated manner.

Consequently, recharge is also considered as consisting of extreme cases (swallets or diffuse recharge). This is often referred to as the "duality of karst aquifers". Indeed, in such systems, a great part of the rainwater (diffuse phenomenon) is quickly collected and concentrated toward the conduits (highly permeable karstic network). This observed rapid flow can only be explained by the presence of a particularly porous and permeable layer at the system's surface. This zone was postulated as the epikarstic zone (Mangin 1973; Mangin 1975; Williams 1983) and is currently under investigation at the CHYN.

The epikarst forms the upper part of the limestone rock and consists of a layer, which has been exposed to intense weathering. This results in the development of a network of dissolution-enlarged fractures and conduits in the uppermost 10 meters at the top of the bulk limestone rock. Consequently, the epikarst has a greater porosity and permeability than the rest of the bulk mass in the depth. The presence or absence of epikarst is therefore an important aspect of water management and groundwater protection strategy.

1.1.2 Requirements on geophysics

Considering the properties of carbonate rocks and the resulting demands for water management, we can formulate some requirements that geophysical methods need to fulfil. If we focus on groundwater protection, geophysics should be able to provide information about the heterogeneous permeability distribution at groundwater catchment scale in order to detect these "high permeability singularities". Since permeability in fractured and karstified aquifers is essentially related to the density, orientation, depth extension, opening and filling of fractures and conduits, the horizontal and vertical resolution of geophysics applied to karst research has to be very high for shallow depth investigation in the range at zero meters to several tenths of meters depth. Furthermore, the properties of the cover layer, e.g. impermeable sediments or highly permeable epikarst, should be detectable. Finally, the methods must be able to cover large areas in short time.

Since the knowledge of fracture distribution and the properties of the cover layer are important aspects used by all recently developed water protection assessment strategies (e.g. Vrba & Zaporozec 1994; Doerfliger et al. 1999; Gogu & Dassargues 2000; Goldscheider et al. 2000; Daly et al. 2002) detailed information about the subsurface provided by geophysics is essential. Furthermore, the importance of the application of geophysics is emphasised by the fact that extensive mapping of fractures with direct methods is not possible when deposits cover these structures. Additionally, direct surface observations cannot provide information on the fracture distribution at greater depths.

1.1.3 History of research

Ever since geophysics was applied to the exploration of carbonate aquifers, it was used with the intention of locating high permeable fracture zones in order to enhance the successful positioning of boreholes for water exploitation. During the 1950s and 1960s, the development of geophysical methods was mainly focused on petroleum and mineral prospecting (e.g. seismics, geoelectrics). Coupled with the limitation of technical possibilities, the adaptation of methods towards the high resolution necessary for karst was neglected. Nevertheless, the first approaches on geophysical karst investigation were done with these conventional methods. First publications on this issue came from countries, where water was difficult to exploit from karst areas, e.g. Ex-Yugoslavia (Arandjelovic & Milosevic 1965; Kovaccic & Krulz 1967).

1.1.3.1 Geoelectrics

Geoelectrical approaches measure the voltage drop between ground-placed electrodes as a response to the electric currents injected into the ground (Figure 4 and Figure 5). Due to the large distances between the current electrodes (e.g. 400 m), one obtains average values of the galvanic resistivity of the rock. Consequently, this method is more applicable for a homogeneous, horizontally layered subsurface than for a heterogeneous medium like karst with vertical structures. However, geoelectrics were at least used to detect heterogeneities by testing particular geometric electrode configurations apart from the classical approaches used for petroleum and mineral prospection. Habberjam & Watkins (1967) proposed the application of the "square array configuration", which is sensitive to electric heterogeneities such as faults.

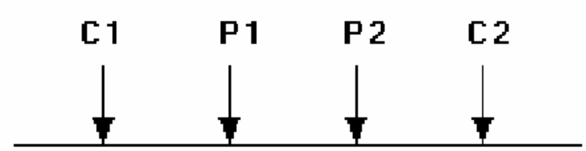

Figure 4 Four electrodes for subsurface resistivity measurement. C = current electrode, P = potential electrode

Another aspect for the geoelectrical application relates to the investigation of the electric anisotropy of the rock caused by fractures in order to define their orientation and intensity. The principle of multi-direction measurements was applied to obtain this information. Brion (1976) carried out Schlumberger soundings with a current electrode spacing of 400 m turning the measurement line around the line-centre at 30°-intervals. Carrington & Watson (1981) and Müller (1982b) reduced the electrode spacing in multi-direction measurements significantly for shallower depth investigation. Further array modifications were proposed and applied over several caves by Müller (1983). All these approaches provided important results, but suffered from both a high expenditure of human labour and a slow measuring progress. However, experiments are still undertaken to investigate anisotropy and to increase the resolution of geoelectrics in order to investigate near surface karst structures (Busby 2000; Szalai et al. 2002).

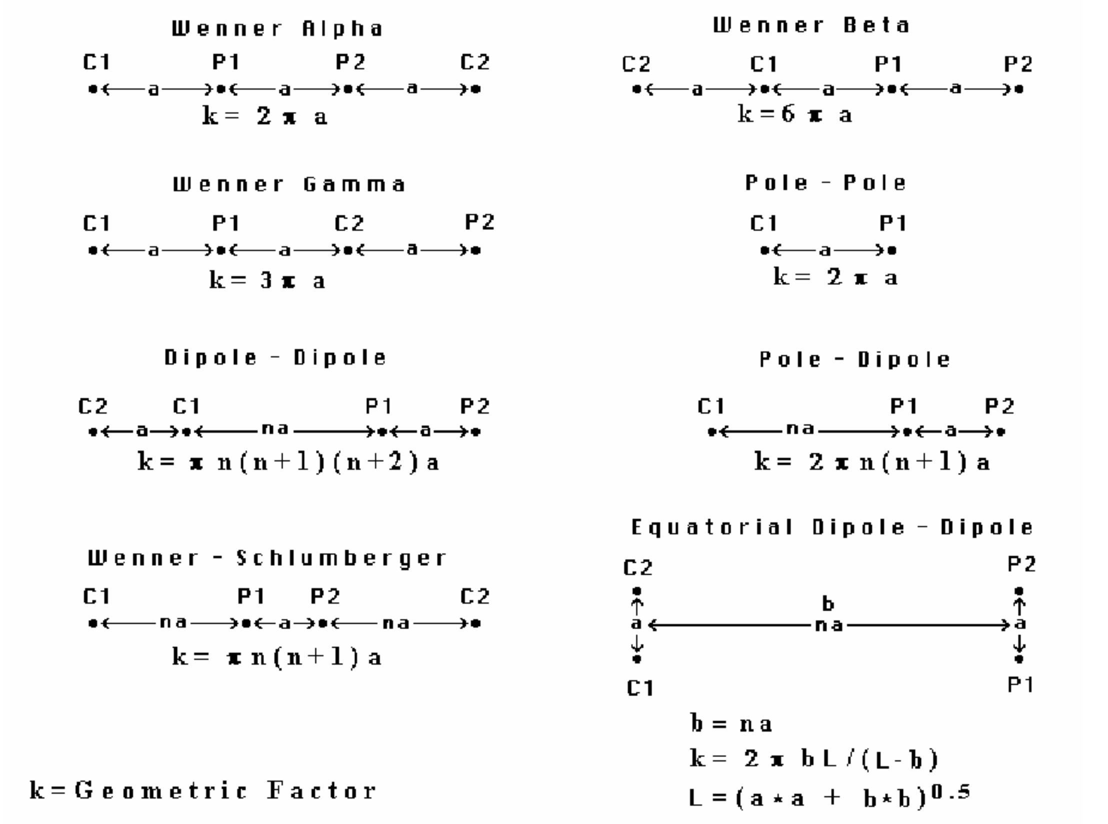

Figure 5 Common geoelectric arrays with their geometric factors k (Loke 1999).

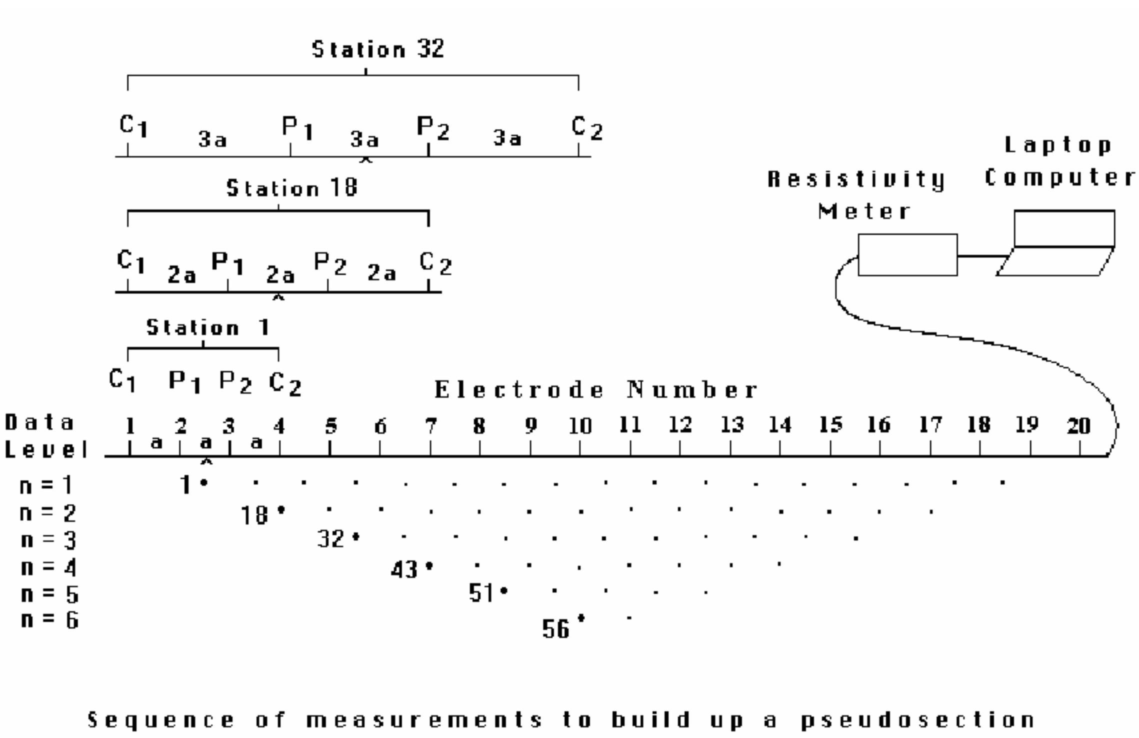

Figure 6 Geoelectrical Imaging: Arrangement of electrodes for a 2-D electrical survey and the sequence of measurements used to build up a pseudosection (Loke 1999).

As geophysical methods benefited generally from technical progress in instrumentation and computer science, also the performance of geoelectrics were enhanced significantly with the introduction of multi-electrode systems called Geoelectric Imaging System (also: Geoelectric Tomography) (Griffiths & Turnbull 1985; Griffiths et al. 1990; Barker 1992; Griffiths & Barker 1993). In contrast to traditional geoelectric soundings, a large number of electrodes connected to a multi-core cable and controlled by a computer are used for electrical imaging (Figure 6). This approach enables simultaneous, horizontal mapping and vertical sounding, providing resistivity pseudo-sections. Any array known from traditional surveys may be used. The method has become widely used for environmental and engineering geophysics (Loke 1999). An updated version of the Loke paper and further literature is downloadable at "http://www.geoelectrical.com".

Field equipment and inversion software is commercially available. However, the above-mentioned difficulties associated with geoelectrics in very heterogeneous media as karst remain a hindrance to appropriate interpretation (Zhou et al. 2000). Nevertheless, the method has been applied over carbonate rocks for fracture and cave-detection and its limitations have been reduced with data processing or coupling of additional information provided by accompanying methods (Piro et al. 2001).

1.1.3.2 Electromagnetic (EM) methods – The Very Low Frequency (VLF) technique

Since the 1980s, the CHYN has concentrated on the application and development of electromagnetic methods and equipment. These methods appeared to have the potential of being appropriate for investigating heterogeneous carbonate rocks. Instead of measuring a medium galvanic resistivity as a result of an electric current injected into the ground (geoelectrics), EM methods measure electric and magnetic fields of the ground, that are created by induction from external, natural or artificial EM fields. Before describing the equipment development at the CHYN, a brief overview of the application and adaptation of the Very Low Frequency method is provided in the next paragraph.

The **VLF method** was mainly developed for mineral exploration (Paal 1965). It uses radio-signals emitted by terrestrial transmitters distributed all around the world in the frequency range from 3 to 30 kHz. The VLF method measures the earth’s electromagnetic (EM) response induced by the EM fields emitted from these transmitters.

There are two ways of using these transmitter emissions with standard equipment:

- The VLF-Resistivity (VLF-R) method measures the relation between the horizontal *magnetic field* with an induction coil and the *electric field* using two electrodes placed in the ground. This method determines apparent resistivities at the penetration depth of the used transmitter-frequency. For further theoretical details, the reader is referred to (Bosch & Müller subm.).
- The VLF-Electromagnetics (VLF-EM) method measures the relationship between the *horizontal* and *vertical magnetic* field with two perpendicular induction coils. It determines resistivity contrasts. One advantage of this technique is that it has no ground contact. This allows for a fast measurement

and was used for airborn mineral exploration surveys (details also in Bosch & Müller (subm.)).

In mineral prospecting, the requirements on the sensitivity and resolution of VLF devices are not very high because the observed anomalies are very strong and the investigated targets are large. However, the principles of this method provided the possibility of rapid data acquisition and survey at a local scale. Consequently, electromagnetic methods have been adapted for engineering and environmental surveys and applied to hydrogeological investigations (Palacky et al. 1981; Meyer de Stadelhofen 1991; McNeill 1994). Theoretical studies on the behaviour of electromagnetic fields in fractured, heterogeneous media have been done by using analogue models and numerical calculations (Le Masne & Vasseur 1981; Schnegg et al. 1987; Telford et al. 1990). For recent commercially available and/or prototype equipment developments the reader is referred to the papers of Benderitter & Robin (1987), Telford et al. (1990), Tabbagh et al. (1991), DMT (1997), Geometrics (1997) and Pedersen et al. (1999).

1.2 EM developments at the Centre of Hydrogeology

The geophysical research at the CHYN focuses on karst research with particular emphasis on the hydraulic influence of the epikarstic zone in recent years. The geophysical investigations have been a part of an integrated approach including research on geomorphology, transport-processes, chemistry and numerical modelling of karst-hydrodynamics.

From the earliest stage, the requirements on geophysical methods for the application to carbonate aquifer investigation at shallow depth have been accounted for the choice of methods and their development. As indicated in previous paragraphs these needs are:

- High horizontal and vertical resolution at local scale until depths of 100 m
- Ability to cover areas at regional scale (e.g. water catchment scale)
- Rapid data collection
- Easy application in difficult terrain

1.2.1 Radiomagnetotelluric (RMT)

Since electromagnetic methods appeared to have the potential to fulfil the needed requirements for karst research, an initial approach was done by the construction of a Very Low Frequency-Resistivity (VLF-R) prototype equipment (Müller 1982a; Müller 1982c), that works in the 12 – 24 kHz frequency-range. A magnetic induction coil with a diameter of 40 cm was used to measure the *local horizontal magnetic field component* H_Y. With a pair of Al-electrodes placed into the ground the *horizontal, secondary electric field component* E_X is measured (see Figure 7). The signal-to-noise-ratio of the measured values is inversely proportional to the electrode spacing. An electrode spacing of 5 m was ascertained as a sufficient compromise between resolution and signal quality. For one polarization direction, this equipment provided from the measured values both

- apparent resisitivity ρ_a in Ωm

and

- *phase-shift* Ψ in degree

between the horizontal, magnetic and electric field component depending on the transmitter frequency.

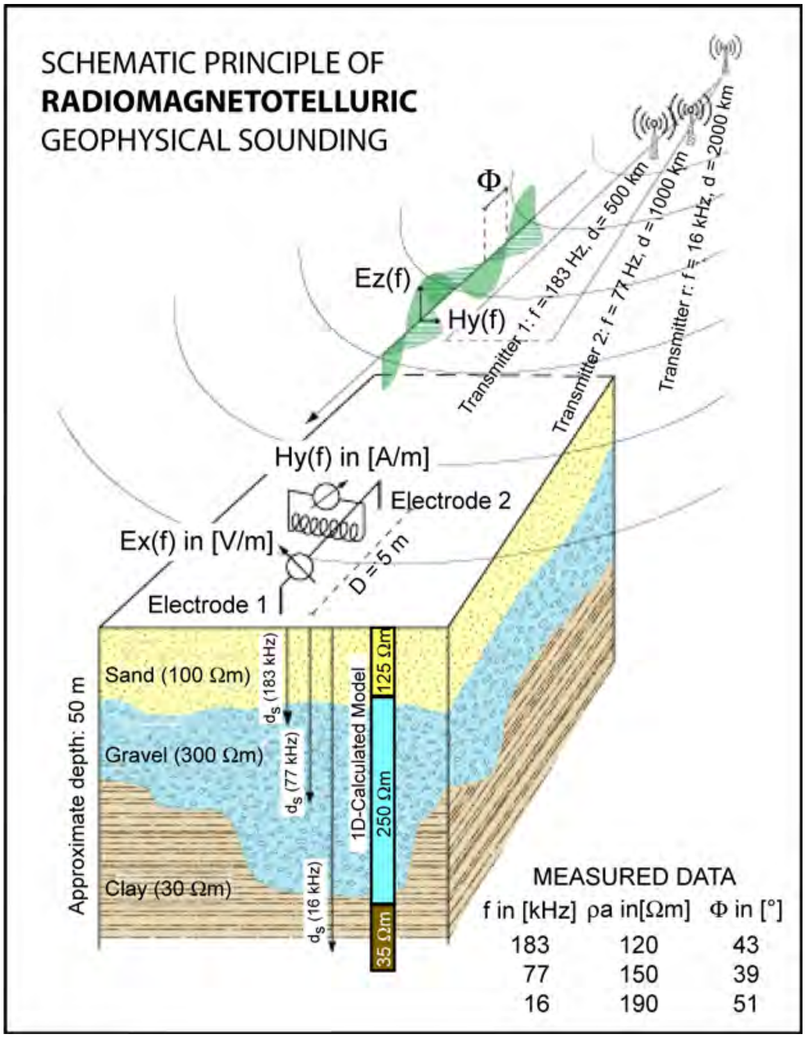

Figure 7 Schematic principle of VLF-R or RMT sounding. d_S(f) indicates the *penetration depth* of the *transmitter-frequency* f.

These two parameters allowed data interpretation based on magnetotellurics (MT) to calculate specific resistivity-depth-distribution (Fischer et al. 1981). With different frequencies and a fixed electrode spacing of 5 m VLF-R resistivity soundings are carried out several orders of magnitude faster, than with traditional geoelectric soundings using electrode-spacing variation. Moreover, to the increased measurement speed, the VLF-R significantly enhanced the horizontal resolution for vertical structures as fractures and faults. The vertical resolution of VLF-R was limited due to the small frequency range. Investigation depths for the frequency-range used and the typical electric resistivities of karstified and massive limestones of the Swiss Jura Mountains (100 to 3000 Ωm) vary between 40 m and 200 m. Consequently, the VLF-R method could detect major faults and fractures, but could not separate horizontal layers at very shallow depths. However, the presence of electrically conductive overburden (some tenth of Ωm) reduces the investigation depth, it remained to excessive for very shallow depths investigation.

A device extended to the Low Frequency range (LF) was subsequently constructed. This device works at between 12 and 240 kHz and was called RMT. Figure 7 summarises the principle of the RMT method and Figure 8 shows a photograph of the apparatus. The PhD work of Turberg (1994) provides a detailed overview of the RMT equipment, its theory, application and interpretation on the hydrogeology of fissured rocks. The penetration depths of the RMT device, varies between 10 to 200 m in karstified and massive limestone. Due to the provided parameters, *apparent resistivity* and *phase*, inversion algorithms calculate also specific resistivities at depths between 0 and 10 m, but these values are qualitative while working on karst. Single structures in the epikarst cannot be separated at that depth. However, in sedimentary environments with their significantly lower electric resistivities, the RMT also provides detailed information over the first 10 m depth (Turberg et al. 1994). The apparatus has been successfully applied to a variety of environmental, engineering and academic investigations in karstified, fissured and porous media. Examples include Turberg et al. (1994); Zacher et al. (1994); Tezkan et al. (1996); Turberg & Barker (1996); Zacher et al. (1996); Tezkan et al. (1997); Turberg & Müller (1997); Turberg & Persson (1997); Bosch & Gurk (2000); Pracser et al. (2000); Tezkan et al. (2000); Bosch & Müller (subm.).

Figure 8 The RMT equipment (12-240 kHz). Components from top to bottom and left to right: magnetic induction coil, battery, receiver-unit, headphones, electrodes.

Compared to geoelectrics, RMT significantly increased the speed for carrying out resistivity soundings. Two persons can perform at least 150 soundings per day. Thus, the method offers the possibility of covering large areas.

1.2.2 Radiofrequency-Electromagnetics (RF-EM)

Although RMT measurements increase the speed that resistivity soundings can be carried out, its horizontal resolution is limited due to its needs of ground-contact for measuring the electric field. If information on fracture density at the decametre scale needs to be

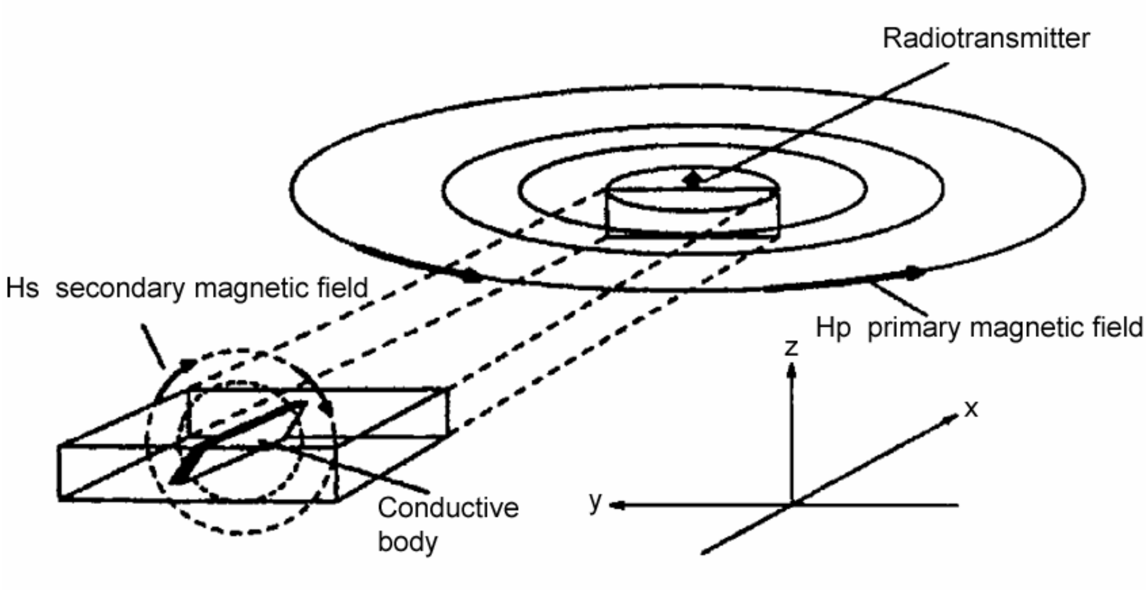

Figure 9 Distribution of primary, magnetic field component from radiotransmitter and induced, secondary magnetic field component.

investigated, the RMT station sample interval must be so small, that RMT survey is no longer reasonable except for academic research. A continuously data recording VLF-R apparatus was described in Tabbagh et al. (1991). However, continuous mapping of the apparent resistivity with this device with small spiked wheels was restricted to easily-accessible ground conditions. Consequently, a continuously measuring device without ground-contact would have been ideal.

With this intention, a continuously recording VLF-EM (12-28 kHz) prototype apparatus was constructed (Turberg & Müller 1992). The equipment simultaneously measured the *local horizontal* and *vertical magnetic field components* $H_Y(f)$ and $H_Z(f)$ for the used *transmitter frequency* f. A simple sketch of the magnetic field components distributions is presented in Figure 9. The stored parameters were:

the real-part $\mathrm{Re}\left(\frac{H_Z(f)}{H_Y(f)}\right)$, also called "inphase"

and the imaginary-part $\mathrm{Im}\left(\frac{H_Z(f)}{H_Y(f)}\right)$, also called "quadrature",

which indicate resistivity contrasts of the ground. Further theoretical details such as the typical signal shape over a narrow conductive dike can be found in Bosch & Müller (subm.). According to Wright (1988), the VLF-EM method is particularly sensitive to vertical, elongated, conductive structures as water bearing or clay filled fissures, fractures or faults, than VLF-R/ RMT is.

As with the VLF-R method subsequently with the VLF-EM method, the frequency range was extended to LF to adapt the method to shallow depth investigation. Therefore, a RF-EM device (15-300 kHz) was constructed (Stiefelhagen & Müller 1997). This system can be used with a handheld antenna or with a "towards the transmitter" self-orientating, shock absorbing antenna fixed to a vehicle (Figure 10). Data are recorded on a data-logger with 1 or 4 Hz sample-frequency and real-time-visualisation on a PC is

Figure 10 RF-EM system with selforientating antenna fixed behind a car.

possible as well as the implementation of Global Positioning System (GPS) data. Stiefelhagen (1998) gives an extensive description of the data-acquisition-device and -software. Extensive high resolution resistivity-contrast profiling became possible (Bosch & Gurk 2000). Case studies for karst investigation and landslide survey in Switzerland as well as groundwater prospecting in Niger are presented in Stiefelhagen (1998). The latter case study particularly demonstrated the advantage of a fast profiling tool for pre-surveying extended areas to locate anomalies, which can be investigated afterwards by resistivity methods. During the Niger project, e.g. the combination of RF-EM and Slingram was used.

Since the method did not provide apparent resistivity, Stiefelhagen (1998) proposed applying an adapted filter technique originally developed by Chouteau et al. (1996), that computes apparent resistivities from VLF-EM data to yield a quantitative parameter of the ground than the more qualitative one of resistivity-contrast. Also Gharibi & Pedersen (1999) and Radic & Becken (2000) contribute to that purpose. Even though the apparent resistivities calculated from pure magnetic transfer functions diverge from those values obtained with other resistivity-providing methods, they at least enhance the qualitative interpretation of data.

1.2.3 Very Low Frequency-Electromagnetic GRADIENT (VLF-EM GRAD)

The RF-EM could map fractures and faults in karstic terrain in the depth range from 10 to 100 m. The mapping of structures in the epikarstic zone (first 10 m depth), where a high density of little fractures and fissures is assumed, remained difficult due to two main problems with RF-EM measurements:

1. Limited discrimination of short-distance neighbouring structures, caused by their superimposed signals in the measured "in-phase" and "quadrature" curves.
2. Excessive penetration depths with the frequencies used over carbonate rocks.

A solution for these problems might have been a further extension of the frequency range used. The recently developed "ENVIRO MT" (Pedersen et al. 1999) uses frequencies up to 500 kHz. This enhances investigation depths to about 10 m in karstified limestones. However, this is not considered as significant progress in epikarst research. In addition, the problem of superimposed signals cannot be solved.

The utilization of even higher frequencies leads to the fact, that displacement currents cannot further be neglected as done in low-frequency diffusion representation of EM fields. Hence, both diffusion and wave propagation have to be considered. Song et al. (2002) very recently proposed a high-frequency electromagnetic impedance method for subsurface imaging by estimating the horizontal wavenumber. Subsequently they eliminate the effect of the wavenumber on the plane-wave impedance and present results for numerical models.

The proposition in this PhD work for enhancing the RF-EM method for near-surface-investigation of carbonate rocks benefited from the effects of measuring the gradient of a potential field instead of its total value. As with gravimetric and magnetic survey (Telford et al. 1990) the effects of gradient measurements, that are interesting for this purpose, are:

- Magnification of near surface features
- Enhanced discrimination of neighbouring anomalies.

Telford et al. (1990) describe the enhanced discrimination of neighbouring anomalies for magnetic vertical gradient survey. While gradient measurements yield two separated peaks for two poles at *depth* h separated by a *horizontal distance* h, total field measurements need a *horizontal pole distance* of 1.4 h to yield separated anomalies.

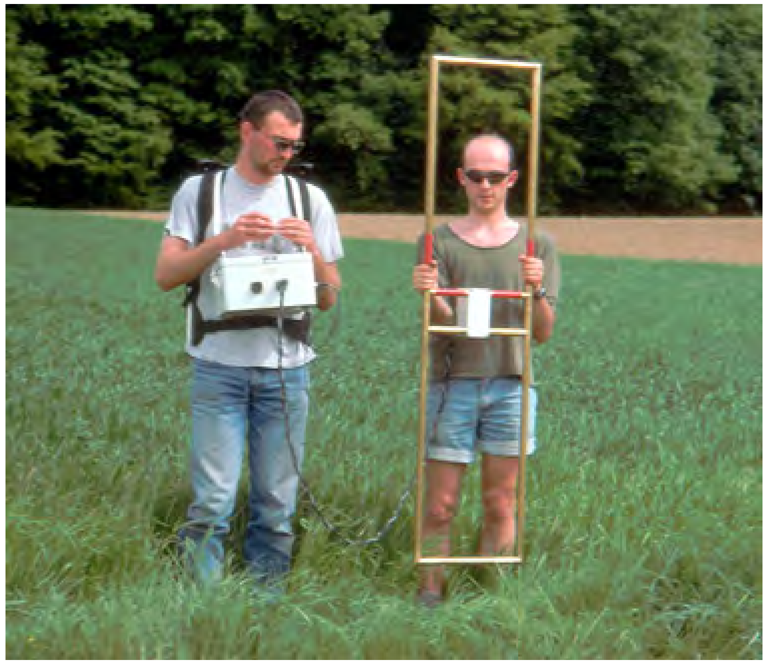

Figure 11 Profiling with the VLF-EM GRAD system. Left operator carries receiver, remote-control and both data-logger and battery inside backpack. Right operator holds the gradient antenna.

One expected advantage for enhanced signal discrimination compared to RF-EM, was that the vertical gradient of the local horizontal magnetic field component over a vertical narrow dike has the shape of a peak as illustrated in "Bosch & Müller (subm.) Fig. 1 and Fig. 2". The vertical magnetic field component used by the RF-EM method is instead of dipole shape with its inflection point over the structure location.

In order to investigate the applicability of such a device in karst environments, a prototype gradient antenna working in the frequency range from 15-25 kHz was constructed and described in Bosch & Müller (2001b). Even though the method was planned for very shallow investigation depths, the deeper penetrating VLF range was used for the first prototype to test gradient measurements generally.

This apparatus measures the local, horizontal, magnetic field components continuously and simultaneously at two altitudes above the ground with two magnetic induction coils. The coil-centres have a distance of about one meter (Figure 11 and "Fig.2 in Bosch & Müller (2001b)". The device stores real- and imaginary-part of the signal difference between the upper and lower coil, normalised by the medium signal from both coils and multiplied by a *device specific amplification factor* k to a data-logger operating at 1 or 4 kHz:

$$\mathrm{Re}\left(\frac{H(f,z_2)-H(f,z_1)}{\left(\frac{H(f,z_1)+H(f,z_2)}{2}\right)} \cdot k \right) = Inphase\left(\frac{\partial H_Y}{\partial z}\right) \equiv Inphase(\Delta H_Y)$$

$$\mathrm{Im}\left(\frac{H(f,z_2)-H(f,z_1)}{\left(\frac{H(f,z_1)+H(f,z_2)}{2}\right)} \cdot k \right) = Quadrature\left(\frac{\partial H_Y}{\partial z}\right) \equiv Quadrature(\Delta H_Y).$$

Further theoretical details are provided in Bosch & Müller (2001a, 2001b, subm.).

This equipment was tested at different sites in the Swiss Jura Mountains and compared with the other CHYN devices, as well as other geophysical methods (Bosch & Müller 2001a; 2001b; subm.).

1.3 Self-potential (SP) method

Apart from focusing on the development and the application of EM methods, this work also tests other methods, which may have the potential for the application on karst aquifer research. The self-potential (also called natural potential) method benefits from its simplicity and portability and permits high-measurement density and wide area coverage. Self-potential is the naturally occurring voltage at the ground surface resulting from ambient electrical currents within the earth.

The equipment deployed in these studies consisted of a pair of non-polarisable Cu-$CuSO_4$ electrodes arranged on spade sticks. A voltmeter measures the potential differences between the two electrodes (Figure 12). The base electrode was kept fixed whereas the second electrode was used to sample the potential field over a profile (Figure 13).

Figure 12 Self-potential field equipment "Type Münster" consisting out of two Cu-CuSO4 electrodes mounted on spade sticks, volt-meter, tape-meter, cable.

Some of the different SP anomaly-origins may exist in karstic environments. While electrochemical processes similar to those in a galvanic cell generate SP anomalies with magnitudes of several hundred millivolts (Sivenas & Beales 1982a), they can also be produced by thermoelectric and/or electrokinetic coupling processes (Fittermann 1979). In hydrogeological and hydrothermal studies, the self-potential caused by the streaming potential in porous media plays an important role and can be used to characterise the aquifer (Michel & Zlotnicki 1998; Ishido & Pritchett 1999; Revil et al. 1999a; Revil et al. 1999b). According to Aubert & Atangana (1996) and Wanfang et al. (1999), electrical potential gradients in karst terrains are generated by the water horizontally flowing along fractures or conduits and by the vertical infiltration of water into fractures or shafts. Consequently, accompanying SP profiles have been carried out on some case studies presented in this work (Bosch & Gurk 2000; Gurk et al. 2001).

Aubert & Atangana (1996) proposed using the self-potential surface (SPS) method in volcanic areas, where a linear correlation between the range of negative self-potential anomalies and the thickness of the unsaturated zone measured in borings is assumed.

According to Boubekraoui et al. (1998), the SPS surface represents the top of the water table when present, and/or the top of the conductive impermeable substratum. In the framework of the current work, Gurk & Bosch (2001) assumed similar conditions over a cave in the Jura Mountains (Switzerland) and showed the possibilities for detecting the cave with the SPS method in karstic terrain.

Figure 13 Application of self-potential method in difficult terrain over Suretta nappe at Sufers (GR).

1.4 Null-array geoelectrics

In cooperation with the Geodetic and Geophysical Research Institute of the Hungarian Academy of Sciences, Sopron, Hungary, a field study for the application of geoelectric null-arrays with short electrode-spacing was carried out on karstic terrain in the Jura Mountains (Switzerland) (Szalai et al. 2002). This technique was tested to study its nearsurface sensitivity for vertical karst structures rather than for its speed of measurement, which was quite slow for the actual prototype configuration.

The term "null-array" is used for those electrode configurations where the measured potential difference is zero above a homogeneous half-space, while using a small measuring dipole with the MN potential electrodes. This is the case, when using short MN potential electrode spacing perpendicular to the direction of the local earth current flow injected by the current electrodes AB (Figure 14). Passing heterogeneities as fractures should therefore result in a measurable potential difference unequally zero. For further details, the reader is referred to the included paper from Szalai et al. (2002).

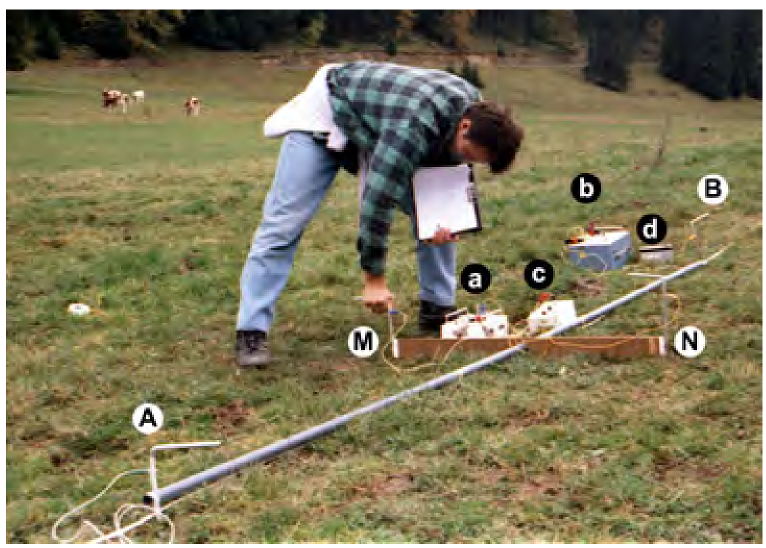

Figure 14 Schlumberger null-array at Les Breuleux (JU). A & B = current electrodes; M & N = potential electrodes; a = measurement device; b = current generator; c & d = batteries

The geoelectric device employed for this study was developed 20 years ago at the CHYN (Müller 1983). The device is a low weight, robust AC system that provides high precision measurements. The AC generator creates a rectangular impulse of 0.4 or 4 Hz to suppress polarisation effects at the electrodes. Signal stability and frequency has a precision of ±0.2%. The injected current can be varied between 0.25, 2.5, 25 or 250 mA. The voltage between the electrodes automatically adjusts between 0 and 500 Volts. The receiver has a sensitivity of 0.25 µV at maximum scale and displays directly the resistance as the ratio of the voltage drop between the potential electrodes and the injected current ΔU/I. Precision and repeatability of the measured values is ±0.2%. To avoid any electrode-disorientation a plastic-wood construction was used for the electrode array (Figure 14).

2 Case studies

The published papers presented in this cumulative dissertation provide examples of geophysical karst structure investigation from several locations in Switzerland. Furthermore, the reader will find an additional case study in Chapter 2.2. The different sites have one thing in common: They provide validation possibilities of the results either due to in-situ observations (e.g. caves, quarry walls) or due to the comparison of the results from several indirect methods. One paper (Gurk et al. 2001) is not focused on karst research, but on the application of some of the methods developed at the CHYN, particularly the RF-EM, for general near-surface investigations. The papers are presented in their chronological appearance order.

2.1 Published papers

Paper 1: **Bosch, F.P. & Gurk, M., 2000:**
Comparison of RF-EM, RMT and SP measurements on a karstic terrain in the Jura Mountains (Switzerland).
Proceed. of the Elektromagnetische Tiefenforschung, Altenberg, Germany, **18**, Deutsche Geophysikalische Gesellschaft: 51-59, ISSN 0946-7467.

Paper 2: **Bosch, F.P. & Müller, I., 2001b:**
Continuous gradient VLF measurements: A new possibility for high resolution mapping of karst structures.
First Break **19**(6): 343-350.

Paper 3 **Bosch, F. & Müller, I., 2001a:**
Nouveau développement dans la prospection géophysique électromagnétique. Le Very Low Frequency Electromagnetics - Gradient (VLF-EM-Grad), facilitant la cartographie des "zones sensibles" dans l'Epikarst et dans les aquifères fissurés.
Proceed. of the 7éme Colloque d'Hydrologie en Pays Calcaire et en milieu fissuré, Besançon, 20-22 Sept. 2001, Sci. Tech. Envir., Mém. H. S. n°13: 55-58, ISSN 0759-7517.

Paper 4 **Gurk, M. & Bosch, F., 2001:**
Cave detection using Self-Potential-Surface (SPS) technique on a karstic terrain in the Jura Mountains (Switzerland).
Proceed. of the Elektromagnetische Tiefenforschung, Burg Ludwigsstein, Germany, **19**, Deutsche Geophysikalische Gesellschaft: in press.

Paper 5 **Gurk, M., Bosch, F., Challandes, N. & Bigalke, J., 2001**:
Integration of geophysical methods to study the fold geometry of the Tschera nappe, eastern Switzerland.
Eclogae geologicae Helvetiae **94**: 329-338.

Paper 6 **Szalai, S., Szarka, L., Pracser, E., Bosch, F., Müller, I. & Turberg, P., 2002**:
Geoelectric mapping of near-surface karstic fractures by using null-arrays.
Geophysics **67**(6): in press.

Paper 7 **Bosch, F.P. & Müller, I., submitted**:
Contribution to karst groundwater vulnerability mapping by VLF-Gradient survey: Comparison with other geophysical methods.
European Journal of Environmental and Engineering Geophysics.

Paper 1

Reprint from

Deutsche
Geophysikalische
Gesellschaft e. V.

PROTOKOLL
über das 18. Kolloquium
<< ELEKTOMAGNETISCHE TIEFENFORSCHUNG >>
in Altenberg
vom 20.-24. März 2000
ISSN 0946 - 7467

COMPARISON OF RF-EM; RMT AND SP MEASUREMENTS ON A KARSTIC TERRAIN IN THE JURA MOUNTAINS (SWITZERLAND)

FRANK BOSCH
Centre d'Hydrogéologie, Université de Neuchâtel, Switzerland,
frank.bosch@unine.ch

MARCUS GURK
Groupe de Géomagnetisme, Institut de Géologie, Université de Neuchâtel,
Switzerland, marcus.gurk@unine.ch

Edited by

Andreas Hördt
Institut für Geophysik und
Meteorologie
Universität zu Köln
Albertus Magnus Platz
D-50933 Köln

Johannes B. Stoll
Institut für Geophysik
Herzberger Landstr. 180
D-37075 Göttingen

Comparison of RF-EM, RMT and SP measurements on a karstic terrain in the Jura mountains (Switzerland)

Frank Bosch[1], Marcus Gurk[2]

[1] Centre D'Hydrogéologie, Université de Neuchâtel, Switzerland, Frank.Bosch@unine.ch
[2] Groupe de Géomagnétisme, Institut de Géologie, Université de Neuchâtel, Switzerland, Marcus.Gurk@unine.ch

1 Introduction

The Centre of Hydrogeology Neuchâtel (CHYN) investigates and monitors karst aquifers, which are highly vulnerable to contamination. Knowledge of permeability distribution in carbonate aquifers is a

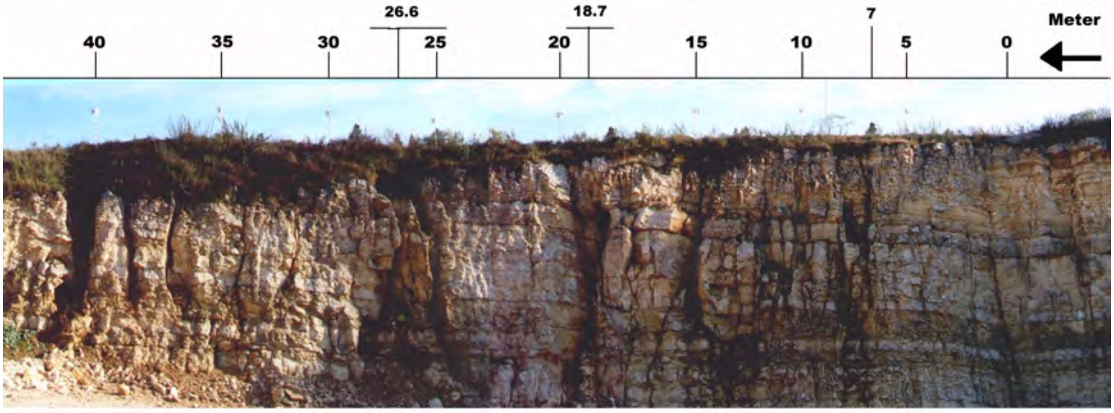

Figure 1: Example for karstified and tectonically influenced Kimmeridge Limestone in the Swiss Table Jura (Quarry of Les Breuleux, Cant. Jura, Switzerland)

fundamental condition for the understanding of water filtration processes. Permeability in fractured and karstified aquifers is essentially connected to density, orientation and opening of fractures/ conduits (Fig. 1). Extensive mapping of those fractures with direct methods is not possible when i. e. Quaternary deposits cover these structures. Additionally, direct surface observations can not provide information on the fracture distribution at greater depths. For the last 20 years several geophysical methods have been developed at the Centre of Hydrogeology Neuchâtel in order to locate the buried permeable fracture zones (depth range: 10-100 m) with "easy to handle" field equipment providing the possibility of mapping extensive areas (Bosch *et al.* 1999; Stiefelhagen 1998). The research mainly focuses on the development of electromagnetic (EM) methods (Radiomagneto-telluric = RMT; Radio Frequency-Electromagnetics = RF-EM) because they provide precise and fast measurements at a local scale.

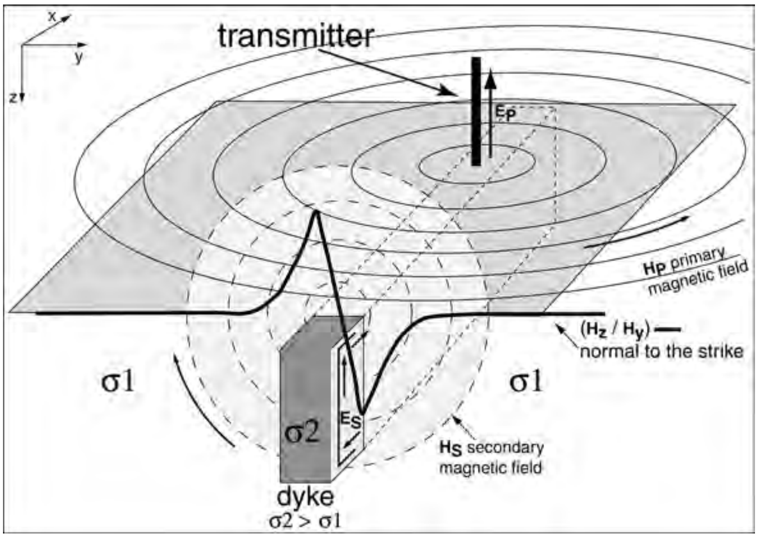

Figure 2: RF-EM-Field distribution and theoretical Outphase (Hz/ Hy) curve (after Wannamaker et al. 1985) for a thin, vertical low resistivity structure in the case of E-polarisation (redrawn after Turberg & Müller 1992).

In this case study we compare results from these EM methods, sensitive to the electric properties of the ground, with high resolution self-potential (SP) measurements. On karst, we suppose self-potential anomalies to be generated by various effects such as physiochemical processes, streaming potentials and water-table elevation. Among these we confine ourselves on SP anomalies caused by physiochemical processes that allows detecting clay deposits in fractured zones.

2 Radio Frequency (RF) method

The RF method uses terrestrial radio transmitters in the frequency range from 15-300 kHz (Very Low Frequency=VLF up to Low Frequency=LF). The transmitters are located at several positions around the world and are used for navigation, submarine communication, time signals or public radio transmissions. The emitted EM field penetrates into the ground and induces a secondary EM field related on the electrical conductivity properties of the ground. Depth penetration is depending on the chosen frequency (Skin Effect). EM field distributions are schematically shown in Fig. 2 for the case of E-polarisation and Cartesian co-ordinates.

2.1 Radiomagnetotellurics (RMT)

The RMT method uses a linear relation between magnetic and electric field component. It measures the resultant local horizontal magnetic field component H_{Ry} with an induction coil and the secondary horizontal electrical field component by the voltage drop between two electrodes placed into the ground. Assuming E-polarisation, the *apparent resistivity* ρ_a is given by:

$$\rho_a = \frac{1}{\omega\mu}\left|\frac{E_{Sx}}{H_{Ry}}\right|^2$$ (Cagniard 1953; Tikhonov 1950)

with *transmitter frequency* f = (ω/ 2π) and *magnetic permeability* μ.

Figure 3: CHYN's RMT equipment (12-240 kHz).

CHYN's RMT equipment (Fig. 3) works in the frequency range from 12-240 kHz. Provided that μ=1, the apparatus directly delivers values of ρ_a and its *phase* φ given in Ωm and degree. This enables the application of magnetotelluric inversion schemes published by Smith, Fisher and Wu (Fischer *et al.* 1981; Smith & Booker 1991; Wu *et al.* 1993).

Figure 4: CHYN's manual RF-EM (15-300 kHz)

2.2 Radiofrequency-Electromagnetics

The RF-EM method measures the horizontal and vertical component of the *resultant local magnetic field* $\mathbf{H_R}$ with two orthogonal induction coils. Due to far-field conditions and regarding, that *primary magnetic field* $\mathbf{H_P}$ << *secondary magnetic field* $\mathbf{H_S}$ (Parasnis 1986), the measured horizontal magnetic field component can be assumed as *primary magnetic field* $\mathbf{H_P}$, where the vertical component of $\mathbf{H_R}$ is only generated by the *secondary magnetic field* $\mathbf{H_S}$.
CHYN's manual RF-EM equipment (Fig. 4) measures continuously in the frequency range of 15-300 kHz with a sample frequency of 1Hz or 4Hz. *In-phase* of (Hz/ Hy) and *Out-of-phase* of (Hz/ Hy) in (%) are written to a datalogger. Results reflect resistivity contrasts.

Figure 5: Selfpotential equipment "Type Münster"

3 Selfpotential

The SP method measures the natural electric potential of the ground in mV caused by various effects (shale potential, water-table elevation, liquid junction potential, streaming potential,

mineralization potential). Hence, the self-potential method can be applied for the investigation of fractured zones in limestone filled with clay, which represent high permeability zones. For hydrogeological and hydrothermal demands, the self-potential caused by the streaming potential in porous media plays an important role and can be used to characterise the aquifer (Ishido & Pritchett 1999; Michel & Zlotnicki 1998; Revil *et al.* 1999a; Revil *et al.* 1999b).
The "Type Münster" equipment (Fig. 5) consists of saturated Cu-CuSO4 electrodes arranged on a spade stick

4 Survey Area

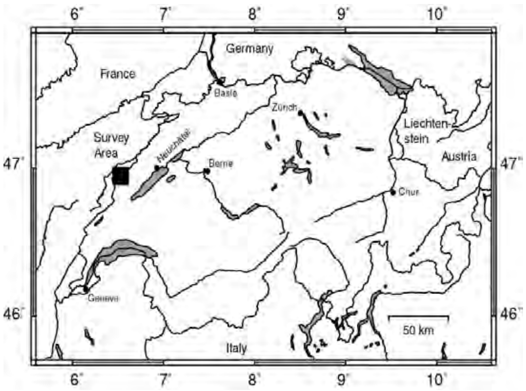

Figure 6: Map of Switzerland with survey area location

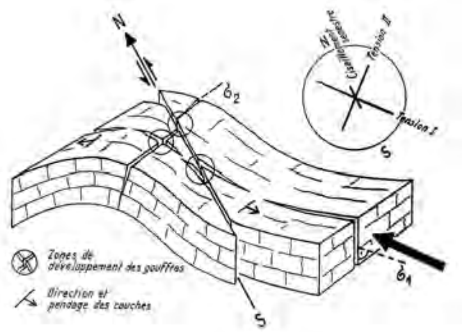

Figure 7: *Main karstification orientations in the folded Swiss Jura*: left shearing = N0°-N10°, σ_1 = N130°- N150°, σ_2 = N40°- N50° (after Müller, 1981)

The survey has been carried out over the cave of Chez-Le-Brandt near to France in the folded limestones of the Swiss Jura Mountains, canton Neuchâtel (Fig. 6). In this area Mesozoic limestone and marls crop out, covered by thin Quarternary deposits. The cave is developed in direction of about N140° in karstified limestone of the upper Sequanian/ Argovian (Fig.8) with a length of ca. 260 m. A marl layer of this sequence allowed the development of a small subterranean river. Tectonic features like faults are visible inside the cave. Another cave with an entrance in a doline has recently been detected in the centre of the profile-mesh (Fig.9, white cross). The new cave (a vertical shaft with a chamber in ca. 12 m depth) lies exactly at the position of a RF-EM anomaly measured before the cave has been discovered (profile 43.6 m, Fig 13). Inside the new cave two faults are visible with strike directions of ca. N150° & N176°. These strike directions coincide with the local stress parameters that controlled fracturing and karstification in the Swiss Folded Jura (left shearing = N0°-N10°, σ_1 = 130°-N150°, σ_2 = N40°- N50° ;Fig.7).

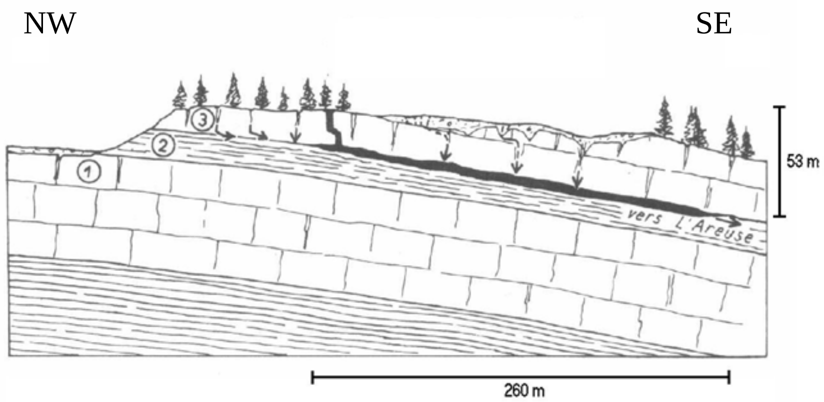

Figure 8: *Schematic geological cut of Chez le Brandt Cave area*: 1&3=karstified Sequanian/ Argovian Limestone; 2=Marl (after Müller, 1981)

5 Data

Table 1 shows the specifications for the different methods used in this case history. The main work of this survey area was focused on high resolution mapping of karst structures with RF-EM. The RMT

measurements were carried out on zones of particular interest for resistivity background information. The SP method was tested as an additional tool for karst structure mapping.
For the RF-EM and RMT data it must be taken into account, that in a geological complicated environment like karstified limestone, the assumed 2D case is not likely. Therefore signal deformations due to mode mixing effects can occur as well as superposition of neighbouring anomalies. Nevertheless the transmitters were chosen due to their availability and average direction of karstic and tectonic strike

	RF-EM	RMT	SP
Transmitter-Freq./Dir.	16kHz & 19.6kHz/ N-40° 234kHz/N3°	16kHz & 19.6kHz/ N-40° 162kHz/ N100° 234kHz/N3°	-----
Sample-Frequency	4 Hz (datalogger)	5m & 10m (Profile 43.6)	1m and less
Profile Spacing	5m	in general 10m	10m

Table 1: *Data collection specifications*

directions in the Swiss Jura Mountains. Parallel profiles offer the opportunity of grouping anomalies, which belong together and indicate geological structures. This is even possible, if the shape of the measured curves is deformed.
The contour plots (Figures 9-11) present all recorded data, whereas the single profile plots (Figures 12-14) concentrate on a few profiles around the doline in the centre of the survey area.

6 Results

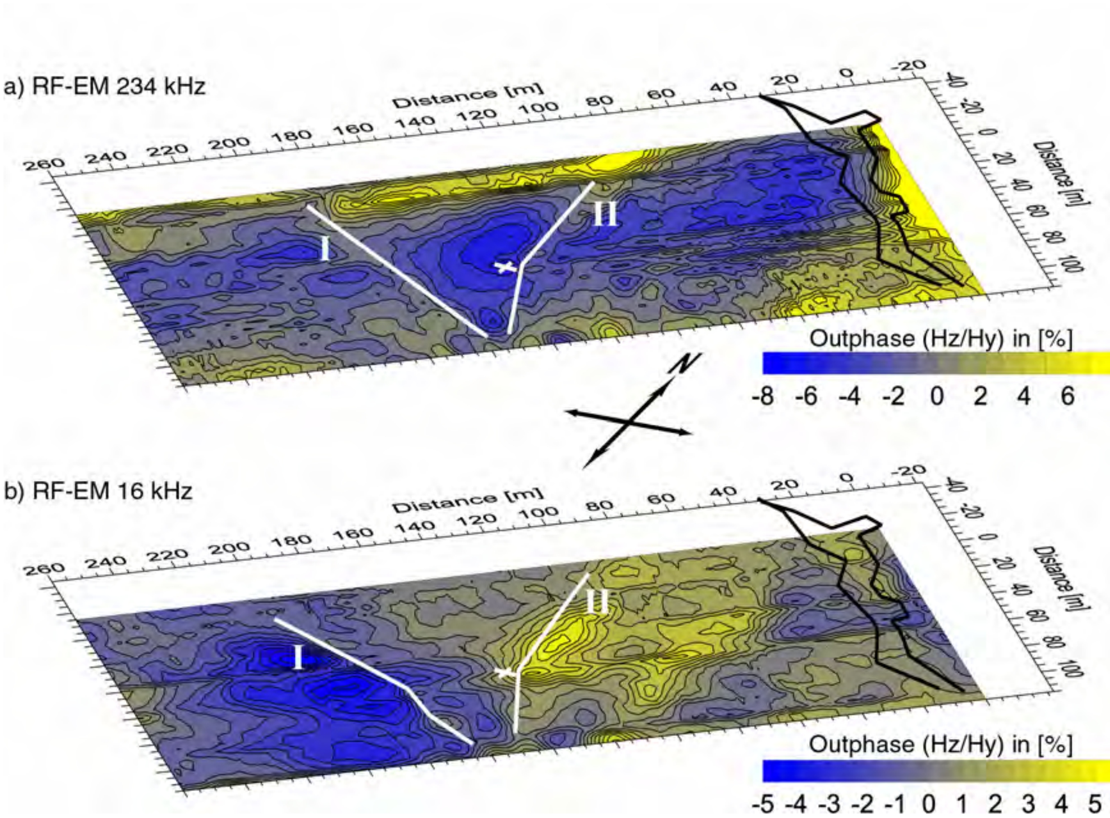

Figure 9: *Contour maps of RF-EM Data with Chez-le-Brandt cave position after speleo map.* White lines indicate two important anomalies dedicated from single profiles analysis. White cross = position of doline with entrance of new detected cave.

Generally, the contour plots of the electromagnetic results (RF-EM and RMT) enable to separate several units of different conductivity properties. In particular, the RF-EM anomalies I & II, as obtained from single profile analysis, have been graphically emphasised in the contour maps with white

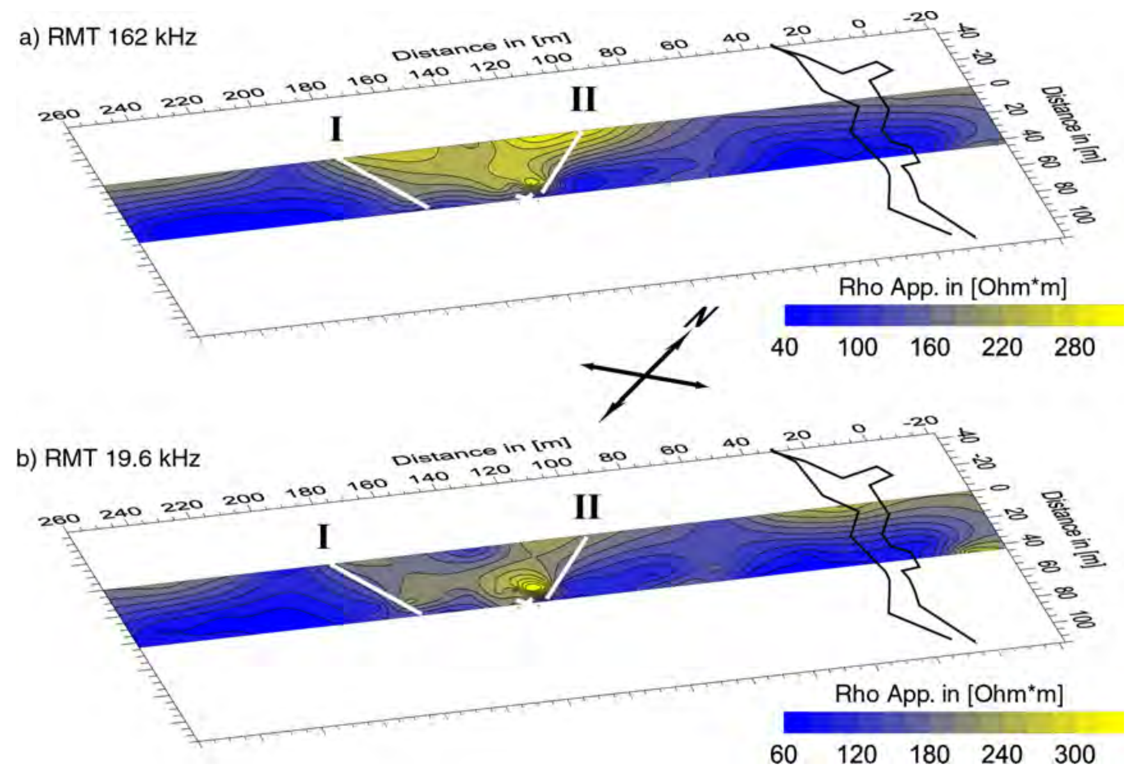

Figure 10: *Contour maps of RMT data.*

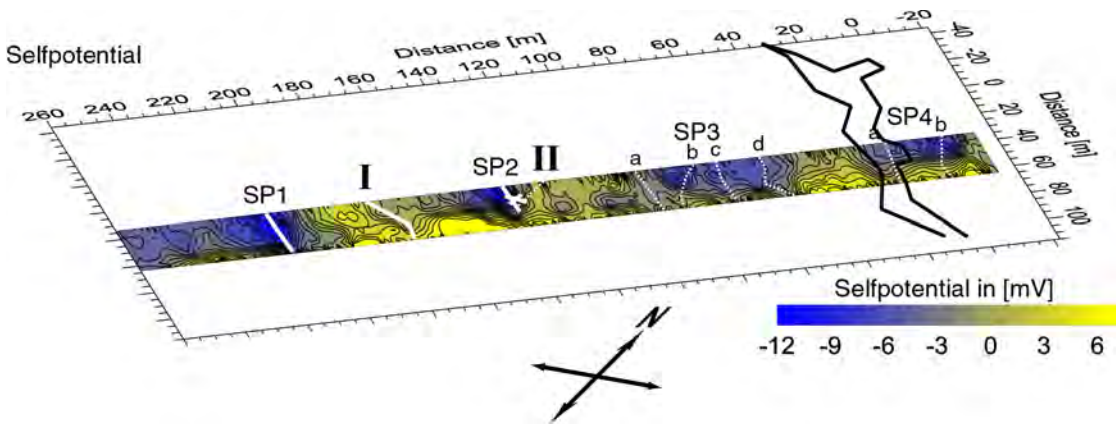

Figure 11: *Contour map of SP data.*

lines (Fig.9). Anomaly I and II are also visible in the RMT data (Fig. 10). They are thought to represent the limits of a block with slightly higher apparent resistivities (~200 Ωm) compared to the surrounding (~90 Ωm). The block between I and II might be interpreted as an uplifted unit due to tectonic activities (push of σ_1). The strike directions of I (~N120°) and II (~N175°, respectively south of doline ~N128°) follow the main karstification directions in the Swiss Jura Mountain as mentioned above. In particular, the strike direction of anomaly II is consistent with the two faults visible inside the new cave (white cross).
Regarding the single profiles (Figures. 13) on both sides of the "200 Ωm block", the RF-EM data show an almost equidistant series of smaller anomalies. They might be interpreted as second order fractures of anomaly I & II.

Comparing VLF and LF range, the apparent resistivities and phases in the centre of the survey area ("P33.6" & "P43.6") obtained with the RMT method show similar values. The apparent resistivity ρ_a varies between 80 Ωm and 300 Ωm and the phase φ is about 42° indicating a good conductor in the subsurface (Fig.12 & 13) followed by a more resistive halfspace. The conductor is likely formed by the

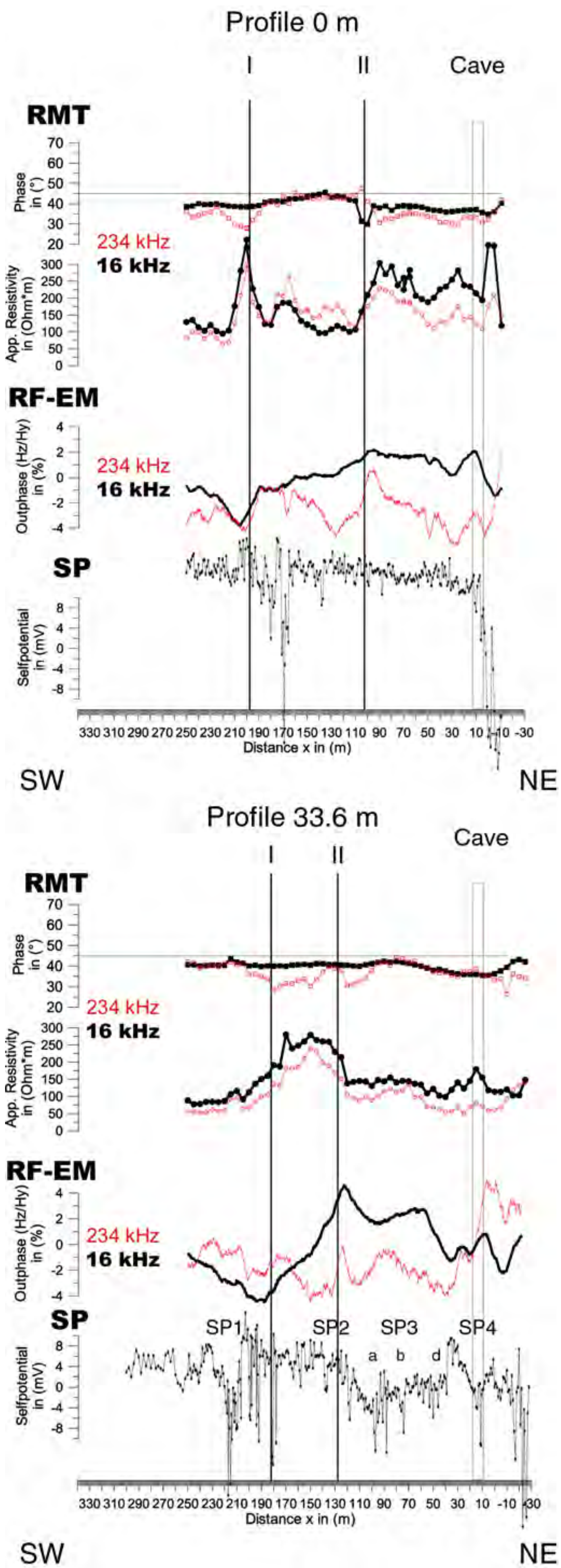

Figure 12: *Single Profile Data "Profiles 0 m & 33.6 m".*

low resistive marl layers embedded in the Sequanien/ Argovien limestone sequence. The following more resistive half-space is presumably caused by the decreasing degree of karstification and intrusion of Quarternary deposits into the fractures. An inversion of the RMT data to model the subsurface structure has not been done yet.

In contrast to the centred RMT profiles, the profile "P0" features more lateral changes in apparent resistivity and phase (Fig. 12). One of the most striking features of this line is the maximum in resistivity at ca. 200 m. Together with the decrease of the phase it may indicate a cavity. In fact, this resistivity maximum is suited a few meter aside of RF-EM anomaly I, which is likely to indicate a fault providing a cave development.

The data content can be checked in-situ with the locations of the "Cave of Chez le Brandt" and the small cave in the centre of the survey area. And in fact, the small cave is situated at a position where the RF-EM out-of-phase anomaly I changes its strike direction and where the out-of-phase amplitude reaches maximum values. Moreover, the RMT data feature with a slight increase of apparent resistivity and a slight decrease of phase.

The RF-EM and particular the RMT data (contour plot) do not show the position of the "Cave of Chez le Brandt" very clearly. Unfortunately, the RF-EM data were disturbed by a metallic fence at the right end of the survey area. The single profiles of Figures 12 to 14 have been repeated after removing this fence. On some profiles, we find anomalies directly at the supposed position of the cave as given by a speleological map (P33.6 & P43.6). On the other profiles, data anomalies and cave positions are not coherent. Either the map is incorrect or the anomalies do not show a cave itself. In the latter case, the anomalies indicate only geological features providing cave development due to fast water flow, such as fault zones and filled fractures.

Provided that SP anomalies are generated by clay deposits in fractures,

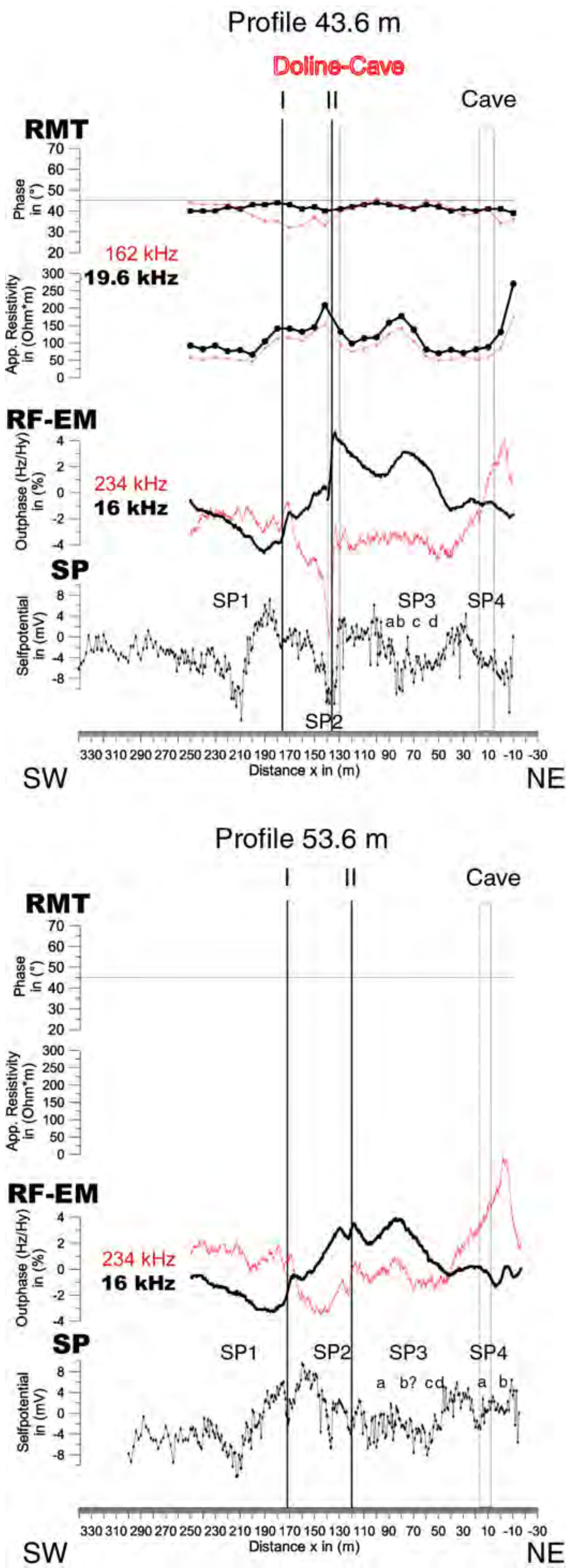

Figure 13: *Single Profile Data "Profiles 43.6 m & 63.6 m".*

the anomaly pattern confirms the results of the EM methods and gives even additional information. From SW to NE, the SP data show in all profiles a zone of low SP variations. With the beginning of SP1, the data are characterised by an equidistantly repeating series of anomalies (SP2-SP4), where SP3 and SP4 can be subdivided into smaller anomalies. In this part, the general variation pattern is overprinted by local variations in the fracture distribution. Obviously, the SP technique is sensitive to all the characteristic features of a karstic terrain like block structures separated by more fractured zones and strong spatial variation of fracture distribution. For example, the strong anomaly "SP1" seems to be connected with several small RF-EM anomalies in the LF range. This particular RF-EM anomaly pattern could indicate several fractures at shallow depths. The SP method may indicate this part of the profile as a permeable zone in general.

Some SP anomalies shown in this study may also be created by an electrokinetical effect when ground water moves through a porous medium. The possibilities of waterflow description provided by the SP method is recently discussed (Patella 1997; Sailhac *et al.* 2000) and make the use of this method on fractured hardrock very interesting for the future. Compared to the continuously measuring RF-EM, SP suffers from slow profiling, but is still cheap and relative fast compared to other methods.

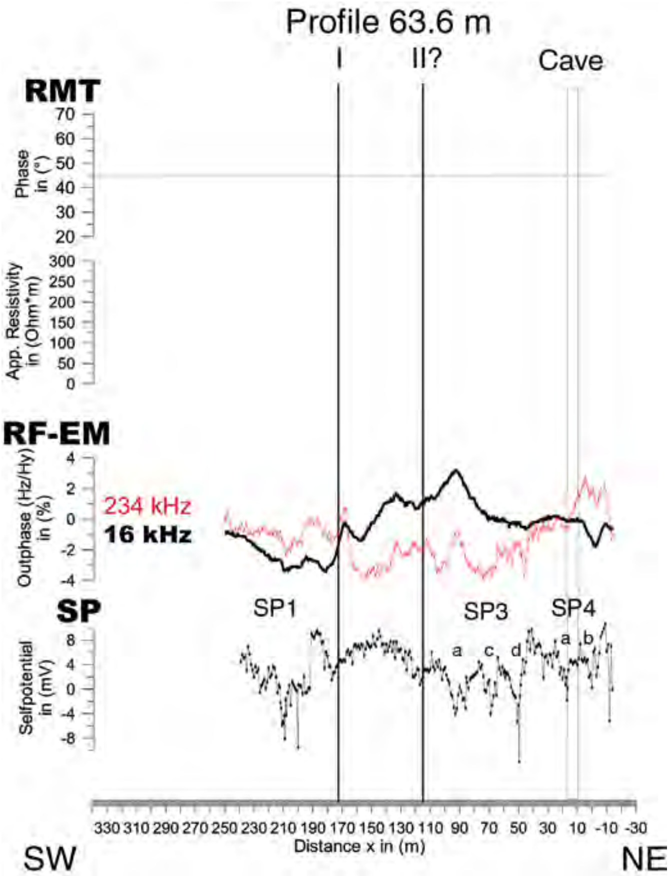

Figure 14: *Single Profile Data "Profile 63.6 m".*

7. References

Bosch, F.P., Szalai, S., Turberg, P. & Müller, I. [1999] Continuously recording radio-frequency electromagnetic (RF-EM) method (15-300 kHz) without ground contact: A powerful tool for groundwater vulnerability mapping in fissured rocks (Em4). *Proceed. of the 5th meeting of the Environmental and Engeneering Geophysical Society European Section*, Budapest 6 - 9 September 1999, Hungary, Environmental and Engeneering Geophysical Society European section.

Cagniard, L. [1953] Basic theory of the magnetotelluric method of geophysical prospecting. *Geophysics* **18**, 605-635.

Fischer, G., Schnegg, P.A., Peguiron, M. & Le Quang, B.V. [1981] An analytic one-dimensional magnetotelluric inversion scheme. *Geophysical Journal of the Royal Astronomical Society* **67**, 257-278.

Ishido, T. & Pritchett, J.W. [1999] Numerical simulation of elektrokinetic potentials associated with subsurface waterflow. *Journal of Geophysical Research* **104**(B7), 15247-15259.

Michel, S. & Zlotnicki, J. [1998] Self-Potential and magnetic surveying of la Fournaise volcano (Réunion Island): Correlation with faulting, fluid circulation and erruption. *Journal of Geophysical Research* **103**, 17845-17857.

Müller, I. [1981] La grotte de "Chez le Brandt" (Jura Neuchâtelois, Coord; 526 425/ 199 000). Essai de synthèse des donnees géologiques et hydroéologiques. *Cavernes (Neuchâtel)* **25**(1), 8-14.

Parasnis, D.S. [1986] *Principles of applied geophysics.*

Patella, D. [1997] Introduction to ground surface self-potential tomography. *Geophysical Prospecting* **45**, 653-681.

Revil, A., Pezard, P.A. & al., e. [1999a] Streaming potential in porous media, 1: Theory of the zeta potential. *Journal of Geophysical Research* **104**(B9), 20021-20031.

Revil, A., Schwaeger, H. & al., e. [1999b] Streaming potential in porous media, 2: Theory and application to geothermal systems. *Journal of Geophysical Research* **104**(B9), 20033-20048.

Sailhac, P., Marquis, G. & Aubert, M. [2000] A wavelet based technique applied to characterise subsurface fluid flow from SP data. *Proceed. of the 6th Meeting Environmental and Engeneering Geophysics - Explore Tomorrows Fundaments - Sept. 3-7 2000*, Bochum, Germany, EEGS-ES.

Smith, J.T. & Booker, J.R. [1991] Rapid Inversion of two- and three-dimensional magnetotelluric data. *J. Geophys. Res.* **96**, 3905-3922.

Stiefelhagen, W. [1998] Radio Frequency Electromagnetics (RF-EM): Kontinuierlich messendes Breitband-VLF, erweitert auf hydrogeologische Problemstellungen. *PhD thesis*, Centre of Hydrogeology, University of Neuchâtel, Neuchâtel, Switzerland, 243 pp.

Tikhonov, A.N. [1950] On determining the electric properties of deep layers of the earth's crust. *Proc (Doklady) Acad. Sci. USSR* **83-2**.

Turberg, P. & Müller, I. [1992] La méthode inductive VLF-EM pour la prospection hydrogéologique en continu du milieu fissuré. *Annales Scientifique de l' Université de Besancon, Mémoire hors série* **11**, 207-214.

Wannamaker, P.E., Stodt, J.A. & Rijo, L. [1985] PW2D - Finite element program for solution of magnetotelluric responses of two-dimensional earth resistivity structure, Earth Sciences Laboratory, University of Utah, Utah.

Wu, N., Booker, J.R. & Smith, J.T. [1993] Rapid two-dimensional inversion of COPROD2 Data. *J. Geomag. Geoelec.* **45**, 1073-1087.

Paper 2

Reprint from

EAGE
European
Association of
Geoscientists &
Engeneers

FIRST BREAK
(2001)
19(6), 343-350

CONTINUOUS GRADIENT VLF MEASUREMENTS: A NEW POSSIBILITY FOR HIGH RESOLUTION MAPPING OF KARST STRUCTURES

FRANK BOSCH
Centre d'Hydrogéologie, Université de Neuchâtel, Switzerland, frank.bosch@unine.ch

IMRE MÜLLER
Centre d'Hydrogéologie, Université de Neuchâtel, Switzerland, imre.müller@unine.ch

Edited by

The European Association of Geoscientists & Engineers *first break* volume 19.6 June 2001 **technical article**

Continuous gradient VLF measurements: a new possibility for high resolution mapping of karst structures

Frank P. Bosch[1] and Imre Müller[2]

1. Introduction

The Centre of Hydrogeology Neuchâtel (CHYN) investigates and monitors karst aquifers, which are highly vulnerable to contamination. One of our particular research tasks within this scope is the characterization and localization of the 'epikarstic zone' (0–20 m depth) (Mangin 1975; Kiraly 1995). Density, size and aperture of fractures that connect the water reservoir with the surface, are features which characterize the vulnerability of karst aquifers. Very local scale mapping of these types of high-permeability fracture zone over extensive areas is therefore of interest for karst hydrogeology.

In order to investigate this zone the very low frequency (VLF, 15–30 kHz) method has been adapted at CHYN for investigation at shallow depths with high lateral resolution. Geophysical surveying using VLF radio signals began in the 1960s as a tool for prospecting conductive minerals (McNeill & Labson 1991; Paal 1965). The CHYN equipment uses VLF and low frequency (LF, 30–300 kHz) radio transmitters, which are located at several positions around the world and are used principally for navigation and submarine communication. Consequently the CHYN has developed a radio frequency-resistivity device (RF-R), also called radio magnetotelluric (RMT, 12–240 kHz), and a continuously measuring radio frequency-electromagnetic (RF-EM, 15–300 kHz) device (Turberg *et al.* 1994; Turberg & Barker 1996; Stiefelhagen 1998). In fissured limestone with a resistivity of several hundreds of Ωm, the penetration depth for these frequencies is about 10–100 m. However, when investigating small structures at very shallow depths (0–10 m) in the epikarstic zone, these devices have limited use due to their excessive penetration depths and their poor horizontal resolution.

In this paper we introduce a method that is based on measuring the vertical gradient of the horizontal magnetic field component of VLF radio signals (VLF-EM-v$GRAD(H_y)$). According to our knowledge, such a technique has not been previously published. As with magnetic surveys (Telford *et al.* 1990), measuring the vertical gradient enhances the discrimination between neighbouring anomalies and the detection of small anomalies of near-surface origin (Millitzer & Weber 1984). We present results of our continuously measuring VLF-EM-v$GRAD(H_y)$ prototype device (abbreviated to: *GRAD* device) and compare it with RF-EM and RMT surveys in karstic terrain in the Swiss Jura mountains. The principles of VLF-R, VLF-EM, and in particular VLF-EM-v$GRAD(H_y)$, are explained in the following paragraphs.

2. Theoretical outlines

The primary electromagnetic (EM) field of a radio transmitter (vertical electric dipole), possesses a *vertical electric field component* E_{Pz} and a *horizontal magnetic field component* H_{Py} perpendicular to the propagation direction *x* (Fig. 1). At a distance greater than several free wavelengths from the transmitter, the primary EM field components can be assumed to be horizontally travelling waves. H_{Py} penetrates into the ground and induces a *secondary horizontal electric component* E_{Sx} with an associated magnetic field H_S. The secondary magnetic field has horizontal and vertical components. This secondary EM field has parts oscillating 'in-phase' and 'out-of-phase' (inphase and quadrature) with the primary field. The intensity

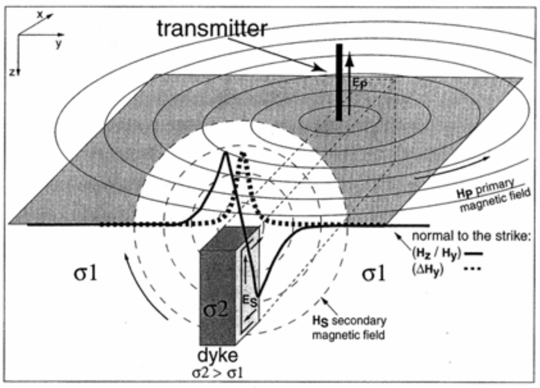

Figure 1 EM field distribution for the VLF method in E-polarization with theoretical signals over a vertical conductive dike; redrawn from Turberg & Müller (1992). H_z/H_y is taken from Wannamaker ***et al.*** (1985); ΔH_y calculated from Biot-Savart.

[1]Centre of Hydrogeology, University of Neuchâtel, Rue Emile Argand 11, CH-2007 Neuchâtel, Switzerland, E-mail: frank.bosch@unine.ch;
[2]Centre of Hydrogeology, University of Neuchâtel, Rue Emile Argand 11, CH-2007 Neuchâtel, Switzerland, E-mail: imre.muller@unine.ch

technical article *first break* volume 19.6 June 2001

of the secondary EM field depends on the conductivity of the ground. The two common methods of using these fields are briefly described in the next two paragraphs.

Very low frequency-resistivity (VLF-R) method

The VLF-R method measures the local *horizontal resultant magnetic field component* H_{Ry} with an induction coil and the *secondary horizontal electric field component* E_{Sx} by means of a voltage drop between two electrodes placed in the ground. Based on surface impedance, the measured parameters enable a calculation of the apparent resistivity (Tikhonov 1950; Cagniard 1953a; Cagniard 1953b; McNeill & Labson 1991) for a layered 1D case and a magnetic permeability of 1:

$$\rho_a = \frac{1}{\omega\mu}\left|\frac{E_{Sx}}{H_{Ry}}\right|^2 \quad (1)$$

with *transmitter frequency* $f = (\omega/2\pi)$ and *magnetic permeability* μ. Fischer *et al.* (1983) and McNeill & Labson (1991) have also demonstrated the applicability of VLF-R to 2D geological cases by considering the effects of *E*- and *H*-polarization.

Very low frequency-electromagnetic (VLF-EM) method

The (VLF-EM) method measures the resultant local horizontal and vertical magnetic field component with two orthogonal induction coils. As a consequence, no ground contact is necessary, which allows a higher speed of survey.

The *local resultant magnetic field* $\mathbf{H}_R$ is the superposition of the *primary field* $\mathbf{H}_P$ and *secondary field* $\mathbf{H}_S$, where $\mathbf{H}_P \gg \mathbf{H}_S$. $\mathbf{H}_S$ and therefore $\mathbf{H}_R$ depend on space, time and frequency. Because of the far field conditions, $\mathbf{H}_P$ is space independent (dependencies will not always be written explicitly in the following):

$$\mathbf{H}_R = \mathbf{H}_P + \mathbf{H}_S$$
$$\mathbf{H}_R = |\mathbf{H}_P|e^{i\omega t} + |\mathbf{H}_S|e^{i(\omega t-\varphi)} \quad (2)$$

with *transmitter frequency* $f = (\omega/2\pi)$ and *phase shift* φ between primary and secondary magnetic field component.

The magnetic field vectors have the following components:

$$\begin{pmatrix} 0 \\ H_{Ry} \\ H_{Rz} \end{pmatrix} = \begin{pmatrix} 0 \\ H_{Py} \\ 0 \end{pmatrix} + \begin{pmatrix} 0 \\ H_{Sy} \\ H_{Sz} \end{pmatrix} \quad (3)$$

Results of the VLF-EM method are the *inphase* and *quadrature* parts of the ratio (H_{Rz}/H_{Ry}) and reflect changes in the resistivity distribution of the ground.

Very low frequency-electromagnetic-vertical gradient (VLF-EM-v*GRAD*(H_y)) method

Because of far field conditions, the primary magnetic field is independent of the altitude z:

$$|H_{Py}| \neq f(z) \quad (4)$$

and one obtains the difference of the horizontal resultant magnetic field component H_{Ry} at two different altitudes:

$$\Delta H_{Ry} = H_{Ry}(z_2) - H_{Ry}(z_1) \quad (5)$$

with $H_{Ry}(z_1) < H_{Ry}(z_2)$ when $z_1 < z_2$ (z positive downwards). Together with equation 3 follows:

$$\Delta H_{Ry} = (H_{Py} + H_{Sy}(z_2)) - (H_{Py} + H_{Sy}(z_1))$$
$$\Leftrightarrow \quad \Delta H_{Ry} = H_{Sy}(z_2) - H_{Sy}(z_1) \quad (6)$$

From equation 6, ΔH_{Ry} is determined by the secondary magnetic field, which is caused by the conductivity properties of the subsurface alone.

3. Equipment

The results of our VLF-EM-*GRAD* are compared with those obtained with our RF-EM and RMT. For a chosen frequency, the RF-EM device directly determines the inphase and quadrature components of H_z/H_y in per cent and stores the data with a 1 Hz or 4 Hz sampling rate (Bosch *et al.* 1999; Stiefelhagen 1998). The RF-EM can be used in the so-called *manual mode* with a hand held antenna or in the *automatic mode* with an antenna, which orientates automatically towards the transmitter for use with a vehicle.

CHYN's RMT equipment directly displays apparent resistivity ρ_a and phase angle φ between the electric and magnetic field components. For further information concerning this equipment, the reader is referred to the papers by Turberg (1994) and Turberg & Barker (1996).

The VLF-EM-*GRAD* prototype device (Fig. 2) is based on our VLF/RF-EM devices. It continuously and simultaneously measures the horizontal component of the local magnetic field at two different altitudes above the ground with two induction coils with horizontal axes. The distance between the centres of the induction coils is 1 m. This device is a hand-held system and works in the frequency range from 15 to 25 kHz. Data output of the device is inphase and quadrature of the signal differences measured between the upper and lower induction coil ΔH_{Ry} (equation 5) in per cent of the average hori-

first break volume 19.6 June 2001 **technical article** fb

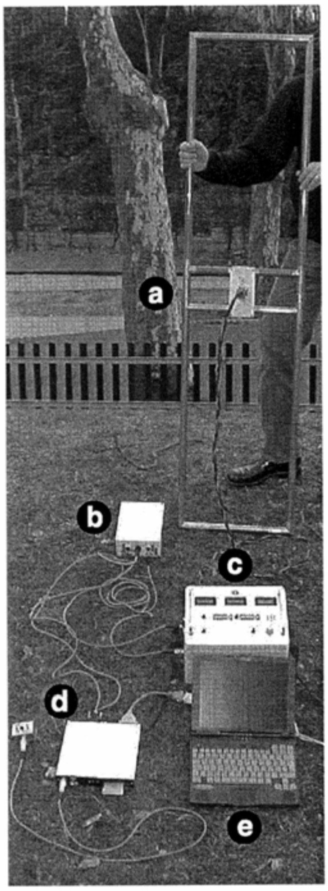

Figure 2 Photograph of VLF-EM-v*GRAD*(H_y) equipment: (a) receiving antenna, (b) power supply, (c) receiver, (d) datalogger with remote control, and (e) optional PC for online data visualization.

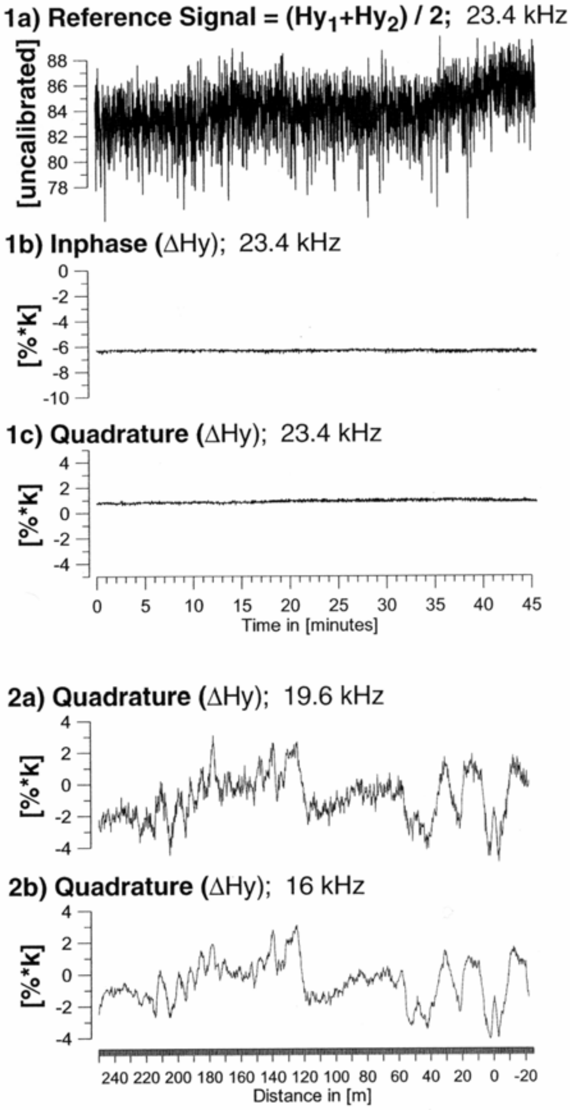

Figure 3 Data quality and repeatability of the VLF-EM-v*GRAD*(H_y) equipment: (1) Reference signal, Inphase and Quadrature stationary and simultaneously measured, (2) Two measurements over the same profile.

zontal field multiplied with a *device specific amplification factor k*. Signal quality over time and repeatability of the measurements over space are illustrated in Fig. 3.

4. Survey area

We carried out our first tests of the VLF-EM-*GRAD* device over the 'Chez-Le-Brandt' cave in the folded Jura mountains, Switzerland. In this area, Mesozoic (upper Sequonian/Argovian) karstified limestone and marls outcrop or are covered by thin Quaternary deposits (Muhlethaler 1931; Müller & Zötl 1980). The 'Chez-Le-Brandt' cave is situated in the eastern part of the survey area (Fig. 5). It is orientated in direction 140°N with a length of ≈ 260 m (Fig. 4). Tectonic features such as faults are visible inside the cave. Extensive RF-EM mapping (Bosch *et al.* 1999), as well as several other geophysical methods (Bosch & Gurk 2000) and hydrogeological experiments (Müller 1981), have been carried out at this site. They offer the opportunity to compare and validate the VLF-EM-v*GRAD*(H_y) measurements.

A new cave with an entrance in a doline has been detected in the centre of the survey area (Fig. 5, red cross) after completing the RF-EM measurements. The cave is a 12 m deep shaft. Two faults are visible inside the cave. They have geological strike directions of ≈ 150°N and 356°N, which are co-

Chapter 2 – Case Studies – Published Papers - **Paper 2** 33

technical article *first break* volume 19.6 June 2001

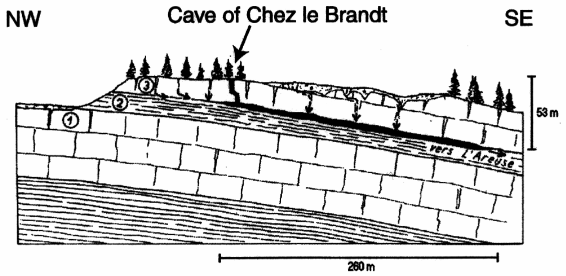

Figure 4 Schematic geological cross section of Chez le Brandt Cave and surrounding area: 1 and 3 = karstified Sequonian/Argovian Limestone; 2 = Marl, after Müller (1981).

incident with the main fracture orientations in the Swiss Folded Jura (left shearing = 0°N–10°N, σ_1 = 130°N–140°N, σ_2 = 40°N–50°N) (Kiraly & Simeoni 1971).

The area around the new cave was chosen for carrying out VLF-EM-*GRAD* profiles. All profiles also cross the 'Chez-Le-Brandt' cave.

5. Data

Table 1 shows the data collection specifications for the different methods presented in this case history. All profiles have a 225°N orientation.

The RF-EM data were collected with the hand-held antenna. We have completed profiles in an area of 130 m × 260 m with a parallel profile spacing of 5 m. The skin depths corresponding to the LF and VLF measurement frequencies are estimated from the RMT resistivity background information, as about 11 m and 42 m, respectively.

The RMT data were collected along six of the RF-EM profiles (P0 m, P23.6 m–P63.6 m) with an electrode spacing of 5 m.

The *GRAD* data were recorded on the same profiles as the RMT.

For all the methods applied, it must be taken into account that in a geological complicated environment like karstified limestone, the assumed 2D case is unlikely to occur. Therefore, signal deformations due to mode mixing effects can occur as well as the superposition of neighbouring anomalies. Nevertheless, the transmitters were chosen due to their availability and average direction of karstic and tectonic strike directions in the Swiss Jura mountains. Furthermore, parallel profiles offer the opportunity of grouping anomalies which belong together and indicate geological structures and strike directions, even if the shape of the measured curve is deformed.

6. Observations

Figure 5 presents contour plots of the quadrature components from: (a) RF-EM 234 kHz, (b) RF-EM 16 kHz, (c) ρ_A (243 kHz), (d) ρ_A (16 kHz) and (e) quadrature of VLF-EM-v*GRAD*(H_y) 16 kHz.

The RMT measurements show that the electrical apparent resistivity in this area is rather low. It varies for both frequency ranges (VLF and LF) from ≈ 50 to ≈ 350 Ωm. The phase values vary between ≈ 30° and 45° (Fig. 6) with greater variations in the LF range. The phases, generally below 45°, indicate that a conductive overburden overlies a more resistive halfspace. The conductive layer could be explained by a thin cover of Quaternary deposits that fill the fractures of the underlying karstified marl-limestone. The resistive halfspace is presumably caused by underlying limestone, with decreasing degrees of fracturing. This is consistent with ***in-situ*** observations made in the 'Chez-Le-Brandt' cave. In the centre of the survey area there is a zone with a slightly higher apparent resistivity (≈ 200 Ωm) than the surrounding area (80–100 Ωm).

In the RF-EM plots, the two large quadrature anomalies I and II are graphically emphasized by white lines. The lines represent a connection between the anomalies that is visible in single profile plots (inflection points). Obviously these two anomalies represent the borders of the high resistivity zone that is known from the RMT data. Anomaly I has a general strike direction of ≈ 120°N. Anomaly II strikes 177°N in the northern part of the survey area and turns to 128°N at the doline with the entrance to the new cave. The strike directions of anomaly II fit very well with the two faults detected inside the new cave (marked by the cross). Both anomalies are vis-

Table 1 Data collection specifications

	RF-EM	RMT	VLF-EM v*GRAD*(*Hy*)
Transmitter – frequency/direction	16 kHz and 19.6 kHz/40°N 234 kHz/3°N	16 kHz/40°N 234 kHz/3°N	16 kHz/40°N
Sample frequency	4 Hz (datalogger)	5 m	4 Hz (datalogger)
Profile spacing	5 m	23.6 m between profiles P0–P23.6 m 10 m between profiles P23.6–P63.6 m	23.6 m between profiles P0–P23.6 m 10 m between profiles P23.6–P63.6 m

first break volume 19.6 June 2001

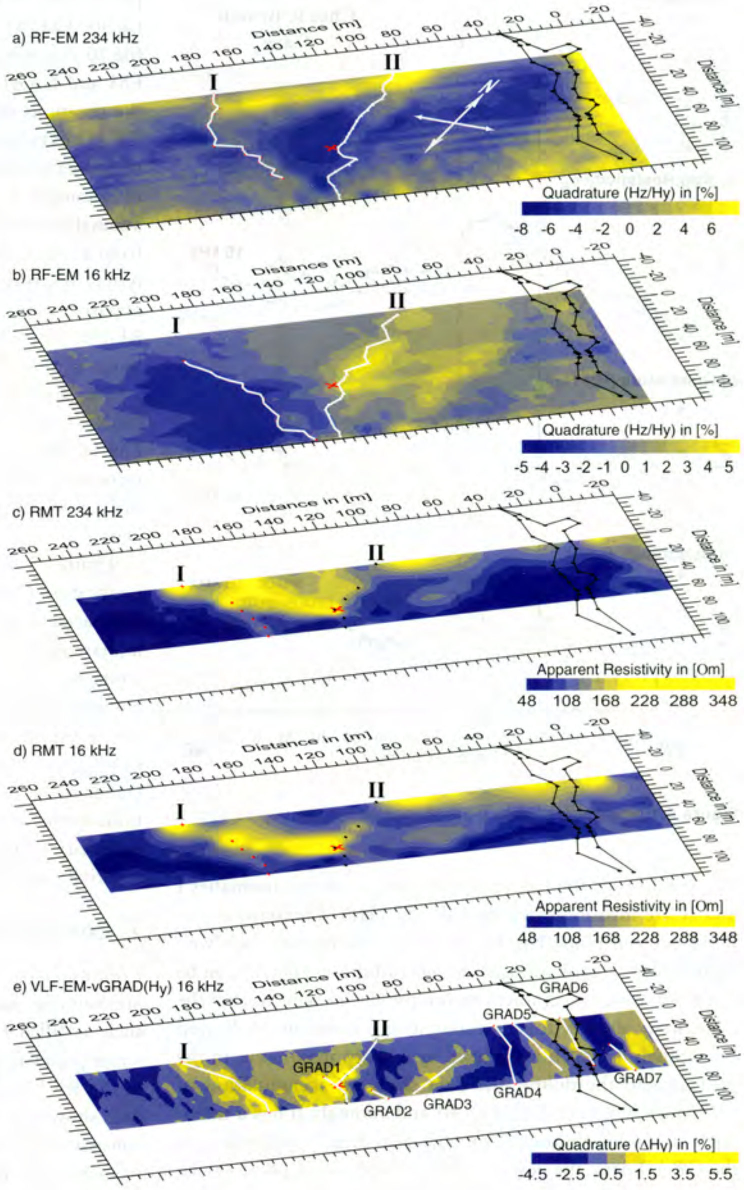

Figure 5 Contour maps of the geophysical data collected using the various survey techniques with Chez le Brandt Cave position. **x** indicates the position of the doline with new cave; black and red diamonds in the RMT plots indicate the positions of the ***GRAD*** quadrature peaks.

ible at 16 and 234 kHz and can therefore be interpreted as actual structures which extend from the near surface to the deeper ground.

Furthermore, due to the small 5 m distance between single RF-EM profiles, the data correctly illustrate the decomposition of these main fracture systems into the characteristic components of the regional tectonic fracture distribution pattern, such as the N-S orientated strike-slip faults and the compression fractures with a strike of 140°N–150°N, as previously mentioned in section 4.

The 'Chez-Le-Brandt' cave is not detectable in the RF-EM and particular RMT contour plots very clearly.

The *GRAD* quadrature contour plot (Fig. 5e) also shows anomalies I and II. In contrast to the RF-EM method, lateral resistivity contrasts are indicated by extremes rather than by inflection points, which illustrate the anomalies more clearly.

first break volume 19.6 June 2001 **technical article**

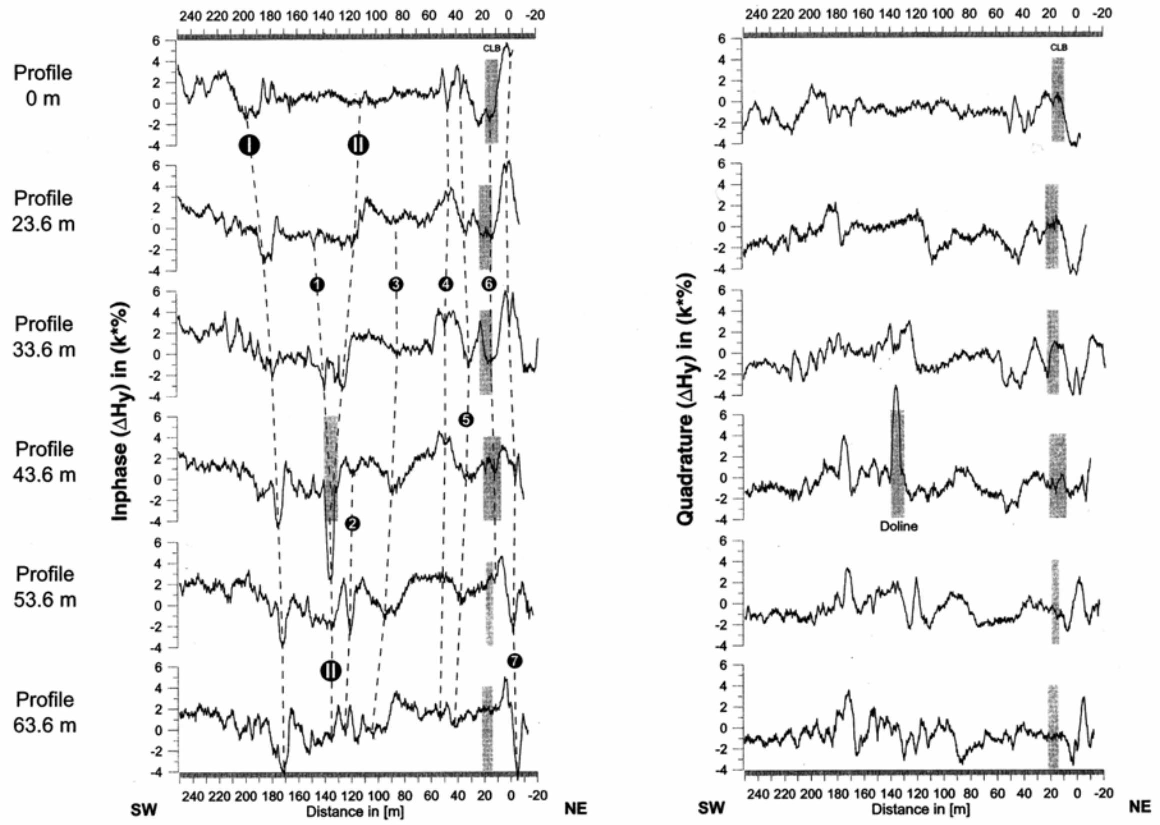

Figure 7 VLF-EM-v*GRAD*(*Hy*) single profiles: inphase and quadrature; light grey squares indicate the position of the Chez le Brandt cave and doline with new cave; Anomalies 1–7 are synonymous with the anomalies GRAD1–GRAD7 mentioned in the text and Figs 5 and 6.

not detect these structures at all. As a consequence, this method provides an improvement in the mapping of small near-surface fractures.

Combining VLF-EM-*GRAD* and RF-EM can give an improved overview of the horizontal and vertical distribution of structures from the unsaturated to the saturated zone of the ground. Further resolution enhancements can be expected from a gradient device in the LF-range.

Calculating model curves and further fieldwork will be helpful in understanding what kind of gradient signal response curve (i.e. polarity of peaks) is caused by different resistivity contrast models and geological structures (i.e. filled or open fractures, cavities).

8. Acknowledgements

This research was supported by grants from the Swiss National Science Foundation (Project No. FN20-53936.98). The authors are very indebted to Mr Jaques Duperrex who built the electromagnetic equipment used in this study.

References

Bosch, F.P. and Gurk, M. [2000] Comparison of RF-EM, RMT and SP measurements on a karstic terrain in the Jura Mountains (Switzerland). *Proceedings of the 18th Kolloquium Elektromagnetische Tiefenforschung 20–24.03.2000*, Altenberg, Germany 18. Deutsche Geophysikalische Gesellschaft, in press.

Bosch, F.P., Szalai, S., Turberg, P. and Müller, I. [1999] Continuously recording radio-frequency electromagnetic (RF-EM) method (15–300 kHz) without ground contact: A powerful tool for groundwater vulnerability mapping in fissured rocks. *Proceedings of the 5th Meeting of the Environmental and Engineering Geophysical Society European Section*, Budapest, 6–9 September 1999, Hungary. Environmental and Engineering Geophysical Society European section.

Cagniard, L. [1953a] Basic theory of the magnetotelluric method of geophysical prospecting. *Geophysics* **18**, 605–635.

Cagniard, L. [1953b] Principe de la méthode magnétotellurique, nouvelle méthode de prospection en géophysique. *Annales Géophysique* **9**, 95–125.

Fischer, G., Quang, B.V.L. and Müller, I. [1983] VLF ground surveys, a powerful tool for the study of shallow two-dimensional structures. *Geophysical Prospecting* **31**, 977–991.

Kiraly, L. [1995] Effect of the epikarst on the hydrograph of the karst springs. *Bulletin D'hydrogéologie* **14**, 199–220.

Kiraly, L. and Simeoni, G. [1971] Structure géologique et orientation des cavités karstiques: la Grotte de 'Chez le Brandt' (Jura neuch.). *Bulletin de la Société Neuchâteloise Des Sciences Naturelles* **94**, 91–97.

Mangin, A. [1975] Contribution à l'étude hydrodynamique des aquifères karstiques. *Annales de Spéléologie* **29**, 283–329.

McNeill, J.D. and Labson, V.F. [1991] Geological mapping using VLF radio fields. In: *Electromagnetic Methods in Applied Geophysics* (ed. M.N. Nabighian), pp. 521–640. Investigations in Geophysics no. 3, 2, Application, Parts A and B. Society of Exploration Geophysicists, Tulsa, Oklahoma, USA.

Millitzer, H. and Weber, F., eds. [1984] *Angewandte Geophysik Band 1 – Gravimetrie und Magnetik*. Springer Verlag Wien, New York and Akademie-Verlag, Berlin.

Muhlethaler, C. [1931] Étude Géologique de la région des Verrières (Canton de Neuchâtel). *Bulletin de la Société Neuchâteloise Des Sciences Naturelles* **56**, 123–300.

Müller, I. [1981] La grotte de 'Chez le Brandt' (Jura Neuchâtelois, Coord; 526, 425/199 000). Essai de synthèse des donnees géologiques et hydroéologiques. *Cavernes (Neuchâtel)* **25**(1), 8–14.

Müller, I. and Zötl, J. [1980] Karsthydrologische Untersuchungen mit natürlichen und künstlichen Tracern im Neuenburger Jura (Schweiz). *Steirische Beiträge Zur Hydrogeologie* **32**, 5–100.

Paal, G. [1965] Ore prospecting based on VLF-radio signals. *Geoexploration* **3**, 139–147.

Stiefelhagen, W. [1998] *Radio Frequency Electromagnetics (RF-EM): Kontinuierlich messendes Breitband-VLF, erweitert auf hydrogeologische Problemstellungen.* PhD Thesis, Centre of Hydrogeology, University of Neuchâtel, Neuchâtel, Switzerland.

Tchalenko, J.S. [1970] Similarities between shear zones of different magnitudes. *Geological Society of America Bulletin* **81**, 1625–1640.

Tchalenko, J.S. and Ambraseys, N.N. [1970] Structural analysis of the Dasht-e Bayaz (Iran) earthquake fractures. *Geological Society of America Bulletin* **81**, 41–60.

Telford, W.M., Geldart, L.P. and Sheriff, R.E. [1990] *Applied Geophysics*, 2nd edn. Cambridge University Press, Cambridge, UK.

Tikhonov, A.N. [1950] On determining the electric properties of deep layers of the earth's crust. *Proceedings of the (Doklady) Acad. Sci. USSR* 83-2.

Turberg, P. [1994] *Apport de la cartographie Radiomagnétotellurique a l'hydrogéologie des milieux fractures.* PhD Thesis, Centre d'Hydrogéologie de l'Institut de Géologie, Université de Neuchâtel, Neuchâtel, Switzerland.

Turberg, P. and Barker, R. [1996] Joint application of radiomagnetotelluric and electrical imaging surveys in complex subsurface environments. *First Break* **14**(3), 105–112.

Turberg, P. and Müller, I. [1992] La méthode inductive VLF-EM pour la prospection hydrogéologique en continu du milieu fissuré. *Annales Scientifique de L' Université de Besancon, Mémoire Hors Série* **11**, 207–214.

Turberg, P., Müller, I. and Flury, B. [1994] Hydrogeological investigation of porous environments by radio magnetotelluric-resistivity (RMT-R 12–240 kHz). *Journal of Applied Geophysics* **31**, 133–143.

Wannamaker, P.E., Stodt, J.A. and Rijo, L. [1985] PW2D – Finite element program for solution of magnetotelluric responses of two-dimensional earth resistivity structure. Earth Sciences Laboratory, University of Utah, Utah.

Paper 3

Reprint from

Université de Franche-Comté
Sciences & Techniques
de l'Environment

Proceedings of the
7th Conference on
<< Limestone Hydrogeology and Fissured Media >>
in Besancon (France)
20th – 22nd September, 2001

Sci. Tech. Envir., Mém. H.S.
(2001)
13, 55-58

NOUVEAU DÉVELOPPEMENT DANS LA PROSPECTION GÉOPHYSIQUE ÉLECTROMAGNÉTIQUE. LE VERY LOW FREQUENCY ELECTROMAGNETICS - GRADIENT (VLF-EM-GRAD), FACILITANT LA CARTOGRAPHIE DES "ZONES SENSIBLES" DANS L'EPIKARST ET DANS LES AQUIFÈRES FISSURÉS

FRANK BOSCH
Centre d'Hydrogéologie, Université de Neuchâtel, Switzerland,
frank.bosch@unine.ch

IMRE MÜLLER
Centre d'Hydrogéologie, Université de Neuchâtel, Switzerland,
imre.müller@unine.ch

Edited by

Jaques Mudry
Department of Geoscience
Université de Franche-Comte
16 Route de Gray
F-25030 Besancon

François Zwahlen
Université de Neuchâtel
Faculté des sciences
Centre d'Hydrogéologie
Case postale 2
CH-2007 Neuchâtel

Nouveau développement dans la prospection géophysique électromagnétique. Le Very Low Frequency Electromagnetics – Gradient (VLF-EM-Grad), facilitant la cartographie des “zones sensibles” dans l’Epikarst et dans les aquifères fissurés

Par Frank Bosch (1) & Imre Müller (1)

(1) Centre d’hydrogéologie de l’Université de Neuchâtel, 11 rue Emile-Argand, CH-2007 Neuchâtel, frank.bosch@.unine.ch

Résumé

L’établissement de la zone de protection des captages dans les aquifères karstiques nécessite une démarche particulière, basée sur l’évaluation multicritères des paramètres de la perméabilité en subsurface (Méthode EPIK). Les différentes approches proposées à ce jour pour la cartographie de la vulnérabilité ne recommande que modérément l’utilisation des méthodes géophysiques conventionnelles, car l’information est trop ponctuelle, les mesures sont trop longues à réaliser, donc trop coûteuses. Couvrir des grandes surfaces avec la géophysique et obtenir des informations instantanées sur la fracturation, ceci en continu, sans contact au sol, n’était guère possible avant la mise en œuvre des méthodes inductives électromagnétiques. L’une d'elles, mise au point à Neuchâtel, est connue aujourd’hui comme le “RF-EM” (Radio Frequency Electromagnetics). Elle utilise comme source d’énergie les antennes radio dans la gamme de fréquence LF et VLF et à l’aide de deux bobines orthogonales, elle compare le champ primaire de l'émetteur avec l’intensité d’un champ secondaire induit (en %) dans les fractures. Les courbes ainsi obtenues, par enregistrement en continu des paramètres de l’induction, grâce à un datalogger de 4 Hz, donnent une très bonne information sur la position et la dimension des fractures, mais ces “hétérogénéités conductrices” doivent encore être positionnées entre un pic positif et un pic négatif sur la courbe enregistrée. Théoriquement la fissure doit se trouver entre les deux pics, au milieu, mais sur des courbes complexes, cette interprétation n’est pas toujours aisée. Ce dilemme a été dissipé par la mise au point d’une nouvelle antenne sur l’instrument RF-EM: l’antenne à gradient. Celle-ci ne mesure que l’intensité du champ total (addition vectorielle du champ primaire et du champ secondaire) avec deux bobines à axe horizontal, mais superposées à différentes hauteurs. Cette nouvelle antenne à gradient facilite la localisation des fractures par un pic très net, juste à l’aplomb du conducteur, capable ainsi d'identifier et de séparer des fractures de faibles développements et très rapprochées l’une de l’autre. L’antenne a été testée sur plusieurs sites déjà fort bien documentés dans le karst, notamment derrière la paroi d’une carrière aux Breuleux (JU), où il a été possible de contrôler sur les affleurements de la carrière que la méthode VLF-EM-Grad est particulièrement bien adaptée pour la cartographie extensive des milieux fissurés.

Introduction

La démarche, actuellement en pleine mutation, pour appliquer une stratégie efficace de protection des aquifères fissurés karstiques suppose une bonne connaissance de la distribution des perméabilités au sein de ces réservoirs. Cela implique une vue synthétique sur la nature et l’épaisseur de la couverture meuble protectrice ainsi que sur la densité et l’organisation de la fracturation de la roche (DOERFLIGER *et al.* 1999). Pour des raisons économiques, on propose actuellement aux hydrogéologues des travaux basés essentiellement sur l’examen géomorphologique des cartes et sur la compilation des documents existants, notamment les résultats des essais de traçages. L’évaluation de l’épaisseur et la nature de la couverture meuble se fait par quelques sondages avec la tarière, même si on sait pertinemment que l’importante hétérogénéité spatiale de celle-ci rendra les conclusions quelque peu incertaines. Actuellement les méthodes d’investigations proposées concernant la protection des aquifères en milieu fissuré ne font que très rarement appel aux mesures géophysiques, car les hydrogéologues sont persuadés que ces investigations sont longues, coûteuses et semblables à des forages, ne renseignant que très ponctuellement sur les paramètres recherchés. Le but de cet article est d’attirer l’attention des praticiens de l’eau sur les récents développements des méthodes de prospections électromagnétiques, capables de couvrir très rapidement de grandes surfaces, sans contact au sol, et de localiser par l'enregistrement en continu l’état de la fracturation des roches à différentes profondeurs.

Le développement des méthodes de prospections électromagnétiques au Centre d’hydrogéologie de Neuchâtel

Encouragés par les résultats obtenus en prospection minière sur un filon conducteur avec les méthodes Very Low Frequency (VLF), nous avions également développé des instruments prototypes, dès 1982, en faisant l’hypothèse, que le comportement géophysique de la fissuration karstifiée serait comparable à celui d’un filon de minerais. Après avoir expérimenté avec succès le VLF-Résistivité sur le karst, la mise au point de la Radio-Magnétotellurique (RMT) a été l’étape suivante, qui a permis la mesure de la résistivité apparente et la phase entre 12 et 240 kHz. Dès lors, il est devenu possible d’effectuer des sondages de fréquence en quelques secondes et d'obtenir la résistivité électrique du milieu à différentes profondeurs et dans différentes directions (THIERRIN et MÜLLER 1988). La technique RMT a été testée et largement utilisée pour explorer le milieu karstique (TURBERG 1993), mais il nous manquait cependant une technique de prospection en continu, sans contact au sol, pour mettre en évidence à l’échelle métrique les changements de la propriété électrique de la roche engendrés par l’effet de la fracturation. Cette lacune a été en grande partie comblée par l’arrivée d’un nouveau prototype: le Radio-Frequency-Electromagnetics (RF-EM, 15-300 kHz), dont le principe du fonctionnement est illustré par la Fig. 1. STIEFELHAGEN (1998) avait bien mis en valeur la théorie et la pratique de cette technique sur le karst et en différents milieux fissurés en Afrique. Les antennes émettrices VLF et LF (E_P) diffusent un champ primaire (H_P) qui produit dans les fractures conductrices un petit courant électrique (E_S). Ce courant engendre à son tour un champ secondaire (H_S), qui aura la même fréquence que le champ primaire, mais il sera déphasé. Le composant vertical de ce champ secondaire est détectable par une bobine à axe vertical. Son intensité sera comparée en pourcentage à l’intensité du champ primaire, mesurée simultanément par une bobine à axe horizontal. En déplaçant les deux bobines le long des profils, il est possible de détecter la présence des fractures conductrices, par l'enregistrement en continu des paramètres de l’induction (inphase et la quadrature en % : H_Z / H_Y). Comme le montre la Fig.1, la fissure conductrice (σ_2) se situe au milieu, entre le pic positif et le pic négatif de la courbe enregistrée. Pour les situations complexes, il n'est pas toujours simple d’estimer exactement la position du conducteur et d'interpréter ces courbes sans ambiguïté.

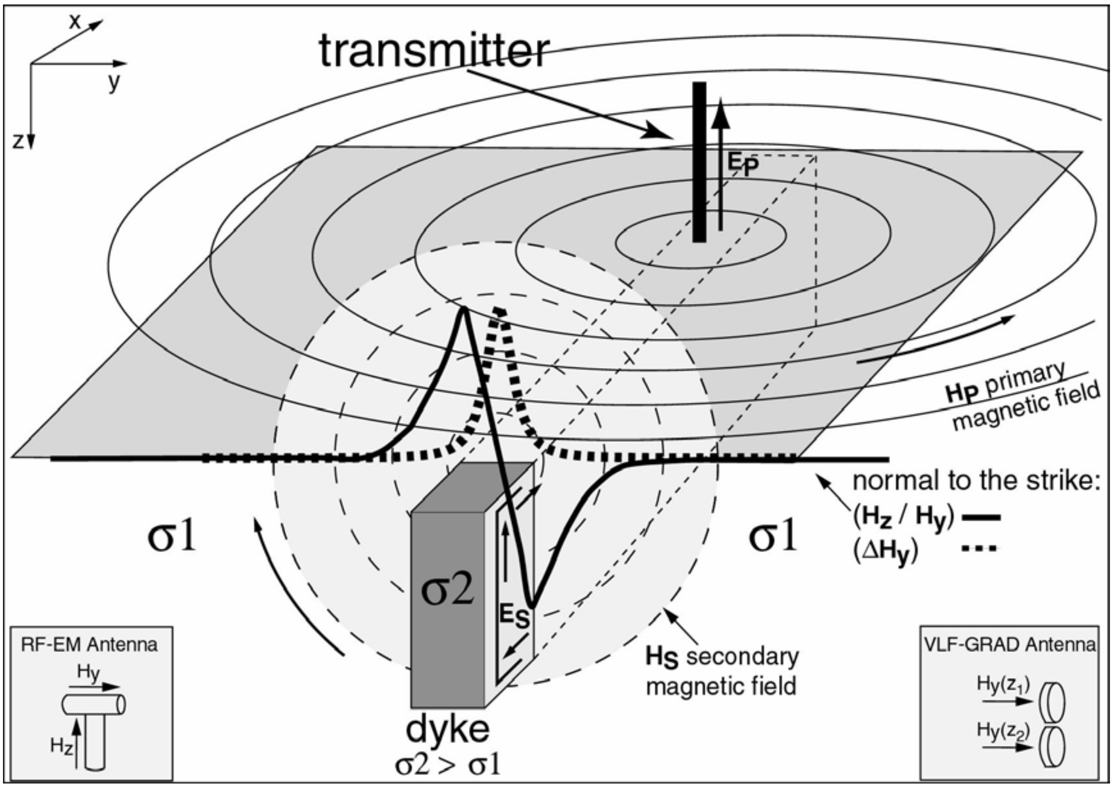

Figure 1 : Schéma comparatif entre la "réponse" obtenue sur une faille par un récepteur VLF muni d'une antenne à deux bobines orthogonales (VLF-EM) ou par une antenne à gradient (VLF-Grad).

Des expériences effectuées avec une nouvelle antenne, où les deux bobines à axe horizontal sont superposées à différentes hauteurs, ont finalement permis de mesurer le gradient du champ électromagnétique engendré par la fissure. Avec cette nouvelle technique, un pic apparaît sur l'enregistrement exactement à l’aplomb de la fracture karstifiée. Les premiers résultats avec le VLF-EM-Grad. sont très encourageants. La résolution spatiale très fine de la méthode et la rapidité d'exécution "en continu", permet une cartographie expéditive de la fracturation, avec une résolution inégalée et sans contact au sol.

Aperçu sommaire de la théorie du RF-EM-Gradient

Etant donné que l'antenne émettrice (E_P) se trouve très loin (far field), le composant horizontal du champ primaire (H_{Py}) n'est pas influencé par l'altitude de la mesure :

$$\left|\mathbf{H}_{Py}\right| \neq f(z) \qquad (1).$$

La mesure au sol porte cependant sur un champ résultant (H_{Ry}) qui est une addition vectorielle du champ primaire (horizontal) et du champ secondaire (horizontal + vertical)

$$\mathbf{H}_R = \mathbf{H}_P + \mathbf{H}_S \qquad (2).$$

Le champ résultant est constitué des vecteurs suivants:

$$\begin{pmatrix} 0 \\ H_{Ry} \\ H_{Rz} \end{pmatrix} = \begin{pmatrix} 0 \\ H_{Py} \\ 0 \end{pmatrix} + \begin{pmatrix} 0 \\ H_{Sy} \\ H_{Sz} \end{pmatrix} \qquad (3).$$

De ce fait ce champ résultant va décroître avec l'altitude et il sera d'autant plus faible qu'on s'éloigne du sol avec la bobine réceptrice. Si on utilise donc deux bobines (à axe horizontal) superposées, on va mesurer le gradient du composant horizontal du champ résultant et on aura:

$$\Delta H_{Ry} = H_{Ry}(z_2) - H_{Ry}(z_1) \qquad (4)$$

On peut déduire de l'équation (3):

$$\Delta H_{Ry} = (H_{Py} + H_{Sy}(z_2)) - (H_{Py} + H_{Sy}(z_1))$$

$$\Leftrightarrow \quad \Delta H_{Ry} = H_{Sy}(z_2) - H_{Sy}(z_1) \qquad (5).$$

L'équation (5) illustre que le gradient mesuré ne dépend plus que du champ secondaire et celui-ci est intiment lié aux propriétés électriques de la roche.
Puisque le champ résultant est essentiellement lié à la présence d'un conducteur (fracture) en subsurface, le maximum de différence du champ résultant (ΔH_{Ry}) entre les deux bobines superposées se produira à l'aplomb du conducteur, comme illustré par la Fig. 1.
Le même instrument électronique (RF-EM) peut être équipé alternativement par les deux types d'antennes de réception. Un ou deux opérateurs peuvent ensuite parcourir le terrain à pied ou en voiture avec l'instrument et un "datalogger" (4 Hz), pour effectuer des profils parallèles et enregistrer les courbes d'inphase et de quadrature.

Résultats obtenus sur le karst jurassien

Nous présentons quelques profils parallèles et comparatifs dans la région des Breuleux (JU) où, non loin d'une paroi dans une carrière, il est possible de contrôler les résultats des mesures grâce aux fractures bien visibles à l'affleurement. La Fig. 2 compare la résolution d'un système de mesures RF-EM avec les résultats obtenus par le VLF-EM-Grad.

Conclusions

Les récents développements des méthodes d'investigations géophysiques électromagnétiques, notamment le RF-EM et le VLF-EM-Grad, nous obligent à réviser fondamentalement la stratégie d'utilisation de la géophysique dans l'élaboration des méthodologies pluridisciplinaires pour la protection des aquifères fissurés. Ces nouvelles techniques géophysiques incisives et expéditives, car très légères et mobiles même sur un terrain difficile, ont leurs places parmi les autres approches, telles la géomorphologie ou la télédétection. Certes, on ne peut pas encore obtenir des informations fiables et quantifiables sur la nature et l'épaisseur de la couverture meuble sur la roche en place avec ces techniques, mais l'état de la fracturation peut être relevé en continu, sans contact au sol et à grande vitesse (5 à 20 km/h). Le pouvoir de résolution métrique, voire décimétrique du système de prospection proposé, appliqué à la cartographie expéditive de la fracturation sur l'épikarst est très supérieur à toutes les autres méthodes géophysiques proposées jusqu'ici. Les profils parallèles VLF-EM-Grad conviendront très bien pour une représentation 2D ou 3D des anomalies et aideront à visualiser les "zones sensibles", qui pourront être explorées ensuite, si nécessaire, par des méthodes plus "lourdes" et plus coûteuses.

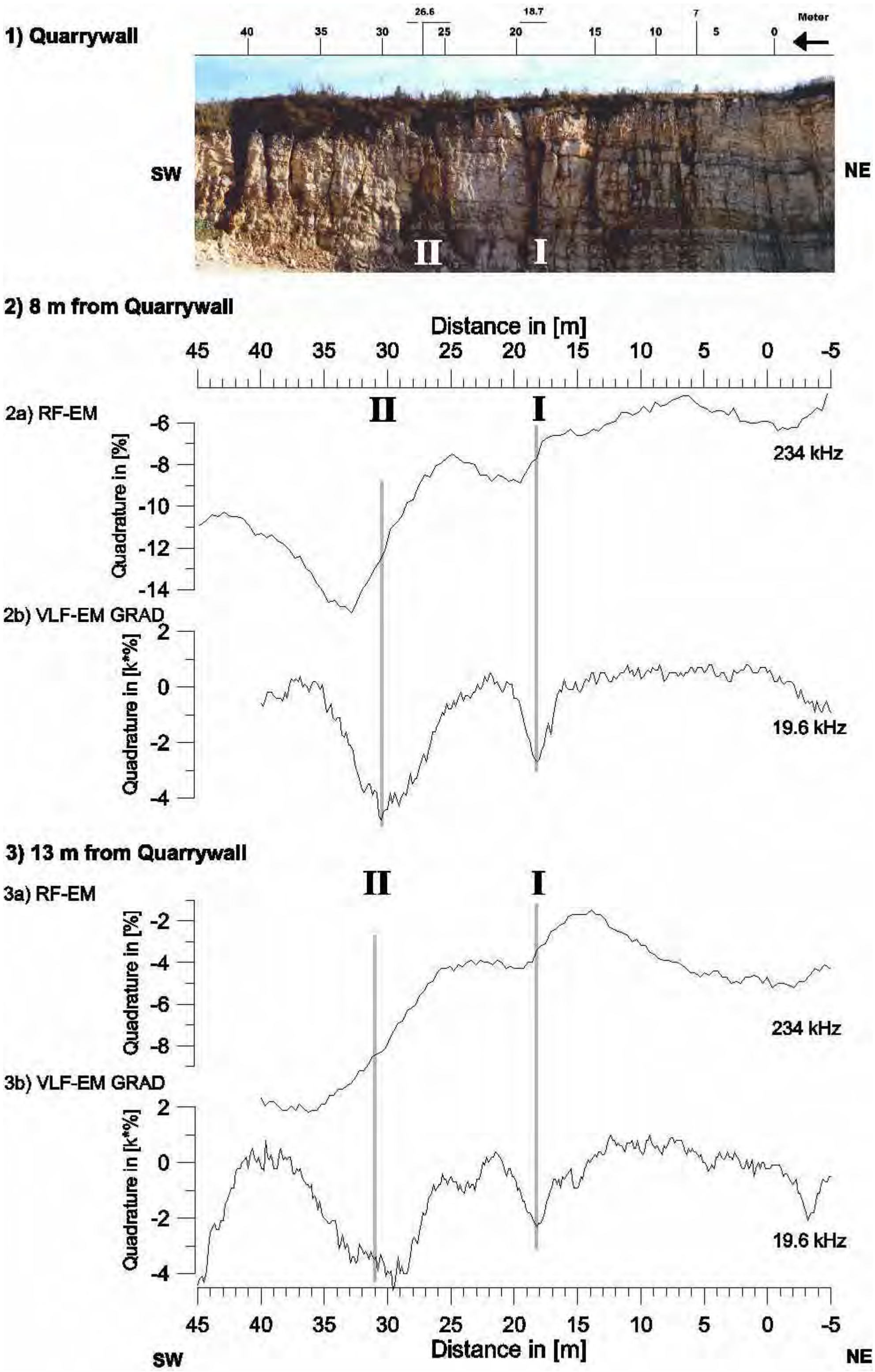

Figure 2 : Comparaison entre les courbes enregistrées en continu par VLF-EM et VLF-Grad derrière les parois fracturées d'une carrière aux Breuleux (JU).

Bibliographie

DOERFLIGER, N., JEANNIN, P.-Y., ZWAHLEN, F. 1999. Water vulnerability assessment in karst environments : a new method of defining protection areas using a multi-attribute approach and GIS tools (EPIK method). - Environmental Geology 39(2) 165- 176.

BOSCH, F.P. & MÜLLER, I. 2001. Continuous gradient VLF measurements : Anew possibility for high resolution mapping of karst structures. - First Break (In press).

STIEFELHAGEN, W. 1998. Radio Frequency Electromagnetics (RF-EM) : Kontinuierlich messendes Breiband-VLF, erweitert auf hydrologische Problemstellungen. – PhD, Univ. Neuchâtel 243 p.

THIERRIN, J. & MÜLLER, I. 1988. La méthode VLF-Résistivité multifréquence, un exemple d'exploration hydrogéologique dans un synclinal crétacé à la Brévine (Jura neuchâtelois). – Quatrième Coll. Hydrol. En Pays calcaire et en milieu fissuré, Besançon, 29.9-1.10.1988. Ann. Sci. Univ. Besançon Mém. H.S. 6 : 17-24

TURBERG, P. 1993. Apport de la cartographie Radiomagnétotellurique à l'hydrogéologie des milieux fracturés. - PhD Univ. Neuchâtel 132 p.

Paper 4

Reprint from

Deutsche
Geophysikalische
Gesellschaft e. V.

PROTOKOLL
über das 19. Kolloquium
<< ELEKTOMAGNETISCHE TIEFENFORSCHUNG >>
in Burg Ludwigsstein
vom 01.-05. Oktober 2001
ISSN 0946 - 7467

CAVE DETECTION USING THE SELF-POTENTIAL-SURFACE (SPS) TECHNIQUE ON A KARSTIC TERRAIN IN THE JURA MOUNTAINS (SWITZERLAND)

MARCUS GURK
Groupe de Géomagnetisme, Institut de Géologie, Université de Neuchâtel, Switzerland, marcus.gurk@unine.ch

FRANK BOSCH
Centre d'Hydrogéologie, Institut de Géologie, Université de Neuchâtel, Switzerland, frank.bosch@unine.ch

Edited by

Andreas Hördt
Institut für Geophysik und Meteorologie
Universität zu Köln
Albertus Magnus Platz
D-50933 Köln

Johannes B. Stoll
Institut für Geophysik
Herzberger Landstr. 180
D-37075 Göttingen

Cave detection using the Self-Potential-Surface (SPS) technique on a karstic terrain in the Jura mountains (Switzerland)

Marcus Gurk[1,3], Frank Bosch[2]

[1] Groupe de Géomagnétisme, Université de Neuchâtel, Switzerland, marcus.gurk@unine.ch
[2] Centre D'Hydrogéologie, Université de Neuchâtel, Switzerland, frank.bosch@unine.ch

1 Introduction

Originally, Aubert & Atangana (1996) developed the Self-Potential-Surface (SPS) technique for hydrogeological exploration of volcanic areas. Provided that two conditions are satisfied, they experimentally found a linear relation between the range of negative Self-Potential (SP) anomalies and the thickness of the unsaturated zone. The first condition is a strong contrast between the resistivity of the unsaturated zone and the resistivity of the substratum and the water-saturated zone. The second condition is the homogeneity of the unsaturated zone. The qualitative interpretation of SP maps indicates that the lines of maximum negative values correspond to the drainage axes and the lines of minimum negative values to the boundaries between two watersheds (Jackson & Kauahikaua (1987)).

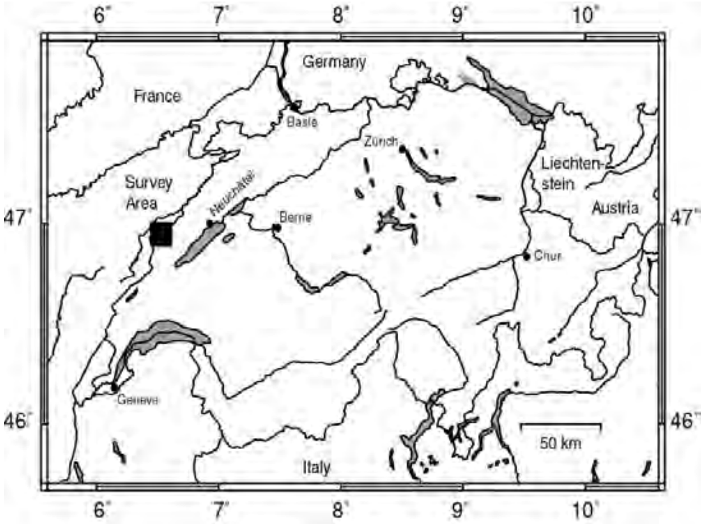

Figure 1: Map of Switzerland with survey area location

We expected similar conditions to be valid in carbonate aquifers. Especially in a karstic cave, the resistivity contrast created by the air-layer must be significant, so that the SPS technique can be used to detect these structures.

Motivated by this hypothesis, an experiment was conducted in co-work with the Centre of Hydrogeology Neuchâtel (CHYN).

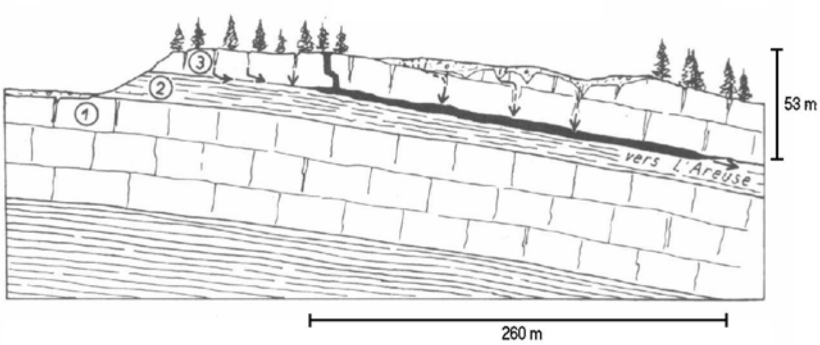

Figure 2: Schematic geological cut of the Chez le Brandt Cave area; 1&3=karstified Sequanian/ Argovian Limestone; 2=Marl (after Müller, 1981)

2 Survey area

The field experiment has been carried out over the cave of Vers-Chez-Le-Brandt (Bosch & Gurk, 2000) near to France in the folded limestone of the Swiss Jura Mountains, canton Neuchâtel (Fig. 1). In this area Mesozoic limestone and marl crop out, covered by thin Quarternary deposits. The cave is developed in direction of about N140° in karstified limestone of the upper Sequanian/ Argovian (Fig.2) with a length of about 260m. A marl layer of this sequence allowed the development of a small subterranean river. Tectonic features like faults are visible inside the cave (Müller, 1981). These strike directions coincide with the local stress parameters that controlled fracturing and karstification in the Swiss Folded Jura (main shearing = N0°,σ_1 = N130°-N150°, σ_2 = N40°- N50°).

3 SPS method

Figure 3a represents the SPS model for a subhorizontal layered structure in karst. According to Aubert et al. (1990) and Aubert & Atangana (1996), three specific conditions shall be satisfied in this model:

1) A high ratio between the resistivity of the unsaturated zone (A) and the resistivity of the impermeable zone (B)
2) Zone (A) is composed out of porous and homogenous medium
3) The resistivity distribution of zone (A) is homogenous

The interface (C) is the contact between zone (A) and zone (B). Under the above mentioned conditions, Aubert et al. (1990) and Aubert & Atangana (1996) give the following experimental linear relation:

$$d_{(x,y)} = \frac{V_{(x,y)}}{K} + d° \qquad (1)$$

$d_{(x,y)}$ is the thickness of the unsaturated zone (A) and $V_{(x,y)}$ is the range of SP anomaly measured at the surface.

K is a coefficient in Volt/Meter, $d°$ is the known thickness of zone (A) below the SP reference point R, where $V_{(R)} = 0$ Volt by convention.

The interface (C) would then be an equipotential surface, called the Self-Potential-Surface (SPS).

K is a function of various parameters including the average resistivity of zone (A) and the resistivity of zone (B). When the SPS is sub-horizontal, K defines the topographic effect in SP and we can derive K by:

$$K = \frac{dV}{dh}, \qquad (2)$$

i.e. by the vertical SP gradient from the reference point R down to the surface of zone (B):

$$K = \frac{dV_{(R)}}{d°}, \qquad (3)$$

K can be determined from borehole information or laboratory measurements of rock samples of zone (A).

If the field topography $h_{(x,y)}$ and the SP mapping $V_{(x,y)}$ are known, we can then calculate the topography of the SPS:

$$H_{(x,y)} = h_{(x,y)} - d° - \frac{V_{(x,y)}}{K} \qquad (4)$$

The SPS topography will give the topography of the impermeable zone (B).

A cave will significantly change the potential distribution in the structure and therefore the SP mapping at surface. In our working model for the field experiment (Fig. 3b), a possible equipotential surface is thought to align with the bottom of the cave. Another possible equipotential surface can be considered to follow the roof of the cave.

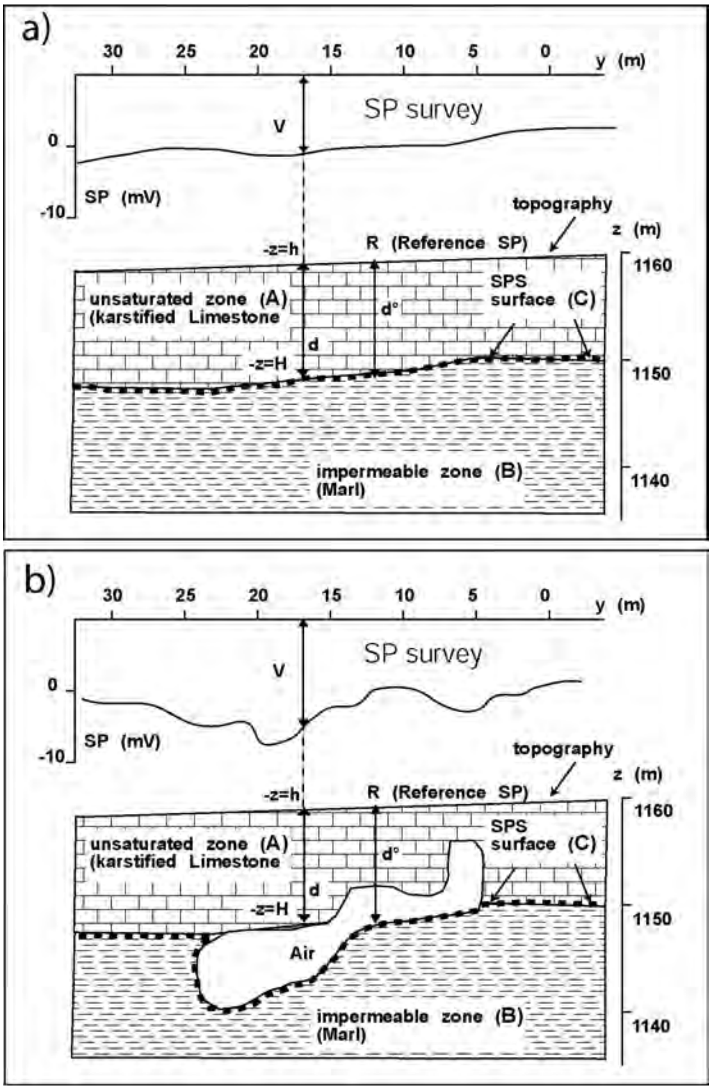

Figure 3a: SPS model for a sub-horizontal layered structure in karst
Figure 3b: SPS model for a sub-horizontal layered structure in karst with a cave

4 Field experiment

The experiment was carried out over a shallow part (depth between 5 to 12 m) of the cave (Fig. 5).

Positioning of the reference Electrode
Besides the careful sampling of the SP anomalies, the accurate estimate of K is crucial for the method. One of the main problems in a cave is to determine $E°$ and the plumb line between the SP reference point R to the vertical electrode inside the cave. $d°$ must be taken from maps and crosscuts.
To delineate the projection of the position of the vertical electrode (placed inside the cave) to the surface we now use a triangulation method:
At the chosen position of the vertical electrode in the cave we set up a portable VLF transmitter of 13.5 kHz (Fig. 6) and triangulating its projection to the surface with the RMT (RadiofrequencyMagnetoTelluric) equipment (Fig. 7) developed at CHYN. This method will give the position R for the reference electrode of the SP mapping at the surface (Fig. 3a and 3b).

Figure 4: Self-Potential equipment "Type Münster"

Vertical SP gradient (K)
Estimates of K were obtained by placing an electrode in the bottom of the cave (zone (B)) beneath reference point R and sampling the vertical SP gradient between this electrode and the reference electrode at the surface.

K was found in this experiment to be –10.3 mV/15m.

Topography and SP mapping at the surface
We sampled topographic and SP data at the surface in a 10m x 20m area (x -> East, y-> South). SP data were collected every meter using saturated Cu-$CuSO_4$ electrodes arranged on a spade stick (Fig. 4). All SP values are sampled in addiction to the surface reference electrode at position R.

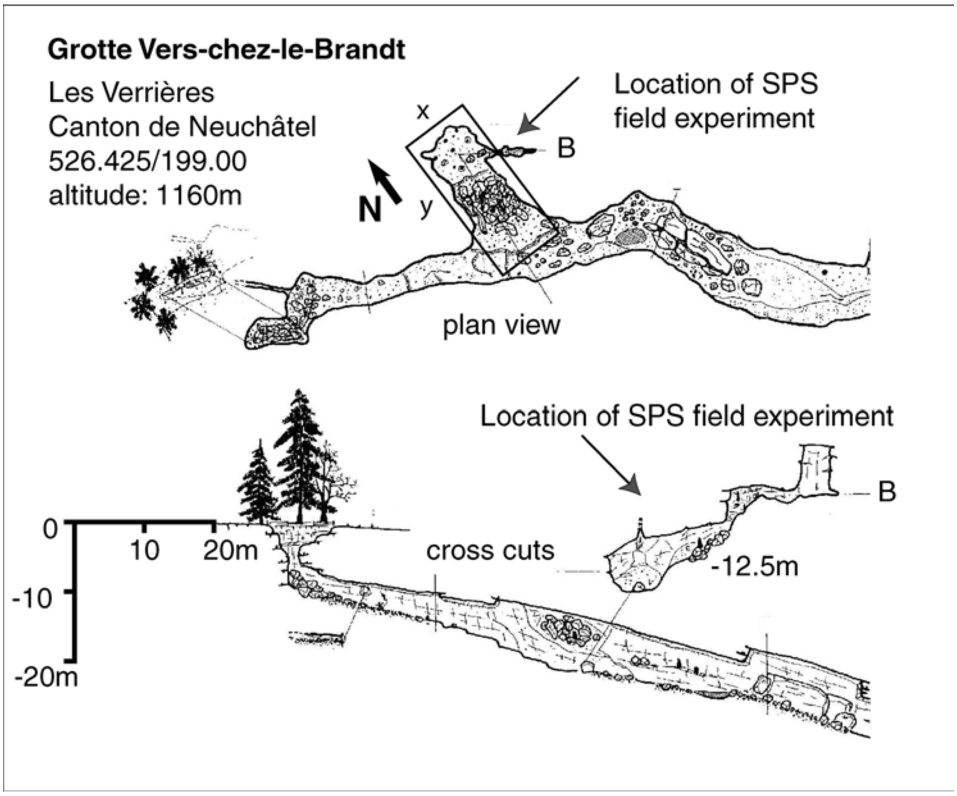

Figure 5: The experiment site and part of the cave Vers-Chez-Le-Brandt

Figure 6 (left): Portable VLF transmitter (grey box) of 13.5 kHz on the bottom of the cave, the vertical electrode will be placed in the centre of the rectangular coil
Figure 7 (right): CHYN's RMT receiver and horizontal coil above the cave to triangulate the projection of the transmitter position to the surface. This will give the SP reference point R .

5 Results

The findings of the experiment are presented in Figure 8. First of all we find that the SP-mapping is de-coupled from the surface topography, indicating that the SP is created by internal features of the subsoil. The SP data varies between values of –8 to +4 mV, which is found to be a typical range for SP data on karst areas in the Jura mountain (Bosch & Gurk, 2000). The SP mapping itself allows drawing conclusion about the position of the cave: Maximum negative SP values at y = 20-28m are indicating the main cave and main drainage axis to be East – Southeast with a branch (minimum negative values) that leads towards the North.
However, the valence of the SP data with the topographic information and the vertical SP gradient (K) gives a detailed view insight the cave's topography. The estimate of $d°$ and K was sufficient to give a comparable topography of the bottom of the cave (Fig. 9).

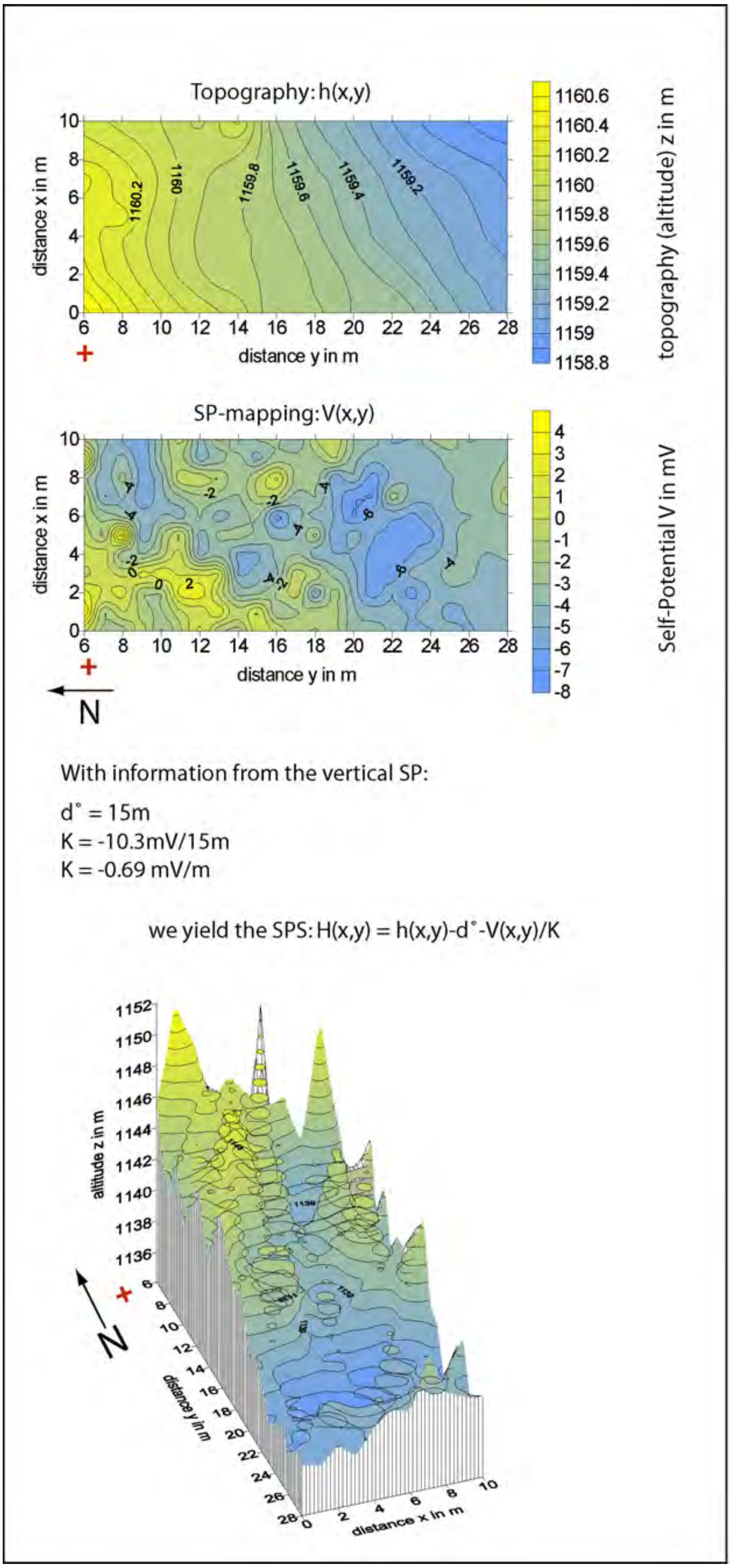

Figure 8: Topography, SP-mapping and the resulting SPS over the cave Vers-Chez-Le-Brandt. For spatial position of the survey see Fig. 5 (x-> East, y -> South).

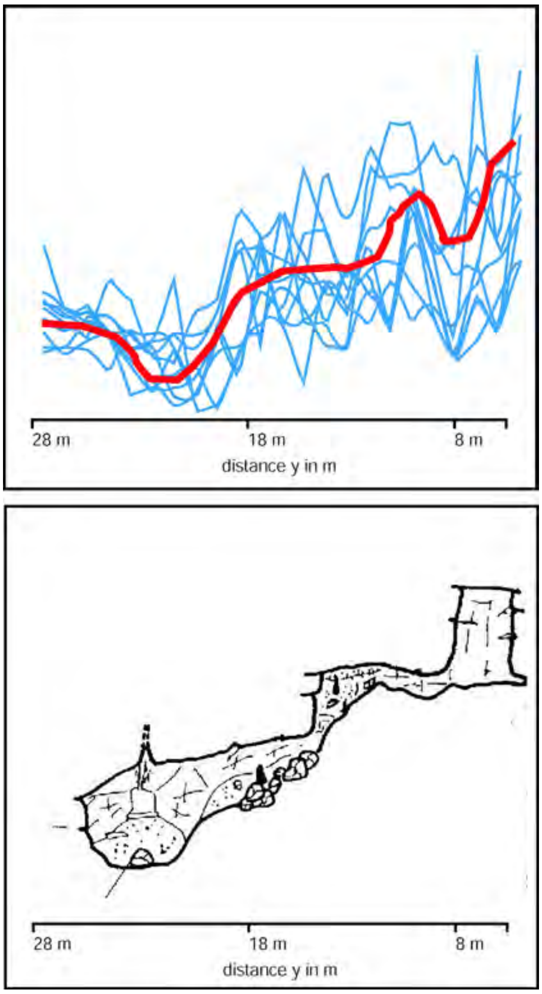

Figure 9: Comparison of SPS slices of Fig 8 (x= 1,2, …,10, blue, respectively thin lines) and its visual average (red, respectively thick line) with the crosscut based on speological data of the cave taken from Fig. 5.

6 Discussion

By definition, the SPS technique does not account for any inhomogeneities, such as a cave. Theoretically, the method should have failed. However, to explain our experimental observation at surface we divide the problem into an active and static part. The active part comprises the mechanism that creates a charge accumulation along the SPS, whereas the passive part explains how this charge distribution is mirrored to the surface. The latter question can be qualitatively explained in terms of a capacitor with various dielectric media:

Static model for a subhorizontal layered structure without a cave

We state that the K factor, as defined in the original idea by Aubert et al. (1990) and Aubert & Atangana (1996) for a subhorizontal layered structure of homogenious media, is similar to the electric field strength in a capacitor (Fig. 10 a)):

$$E_F \cong K \,. \qquad (5)$$

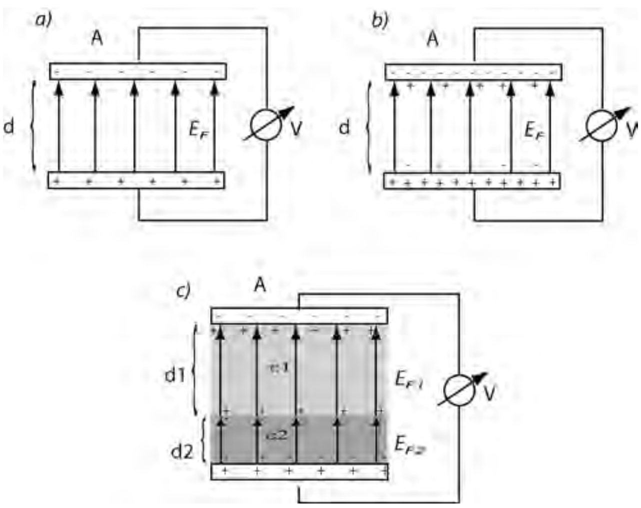

E_F electrical field strength
A area
Q charge
D displacement of charge
d distance
ε_0 electrical permittivity of vacuum
$(\frac{1}{36\pi}10^{-9}\frac{As}{Vm})$
ε_r relative electrical permittivity
$(\varepsilon_{limestone} = 8-12,\ \varepsilon_{water} = 80,\ \varepsilon_{air} = 1)$
V potential
(Values taken from Landolt & Börnstein (1952))

Figure 10: a) Capacitor without and b) capacitor with a dielectric media. c) Capacitor with a series of dielectric media.

For a given charge distribution

$$\frac{Q}{A} = D = \varepsilon_0 \varepsilon_r E_F \, , \tag{6}$$

the electric field strength is defined as:

$$E_F = \frac{V_{(x,y)}}{d_{(x,y)}} \tag{7}$$

From this equation we obtain the potential:

$$V_{(x,y)} = E_F \cdot d_{(x,y)}, \text{ respectively } V_{(x,y)} = K \cdot d_{(x,y)} . \tag{8}$$

Similar to a capacitor, the charge on its boundaries is depending on the polarisation effect in a given dielectric medium between these boundaries. In a carbonate aquifer, the electrical permittivity of limestone enhances the charge by a factor 8 – 12:

$$\frac{Q}{A} = D = \varepsilon_0 \varepsilon_{limestone} K \tag{9}$$

With $K = \frac{D}{\varepsilon_0 \varepsilon_{limestone}}$ we get a measure for the thickness of the structure:

$$d_{(x,y)} = \frac{V_{(x,y)}}{D} \varepsilon_0 \varepsilon_{limestone} \, . \tag{10}$$

And the potential is given by:

$$V_{(x,y)} = \frac{d_{(x,y)}}{\varepsilon_0 \varepsilon_{limestone}} D \, . \tag{11}$$

Static model for a subhorizontal layered structure with a cave and water
This model is characterised by a series of capacitors with different dielectric media:

$$D_1 = \varepsilon_0 \varepsilon_1 E_{F\,1}, D_2 = \varepsilon_0 \varepsilon_2 E_{F\,2}, \ldots, \; D_i = \varepsilon_0 \varepsilon_{i2} E_{F\,i} \tag{12}$$

Since the charge distribution at the boundaries are equal:

$$D_1 = D_2 = \ldots D_i = D \, . \tag{13}$$

The resulting potential of a multiple layered structure is:

$$V'_{(x,y)} = \frac{D}{\varepsilon_0} \left(\frac{d_1}{\varepsilon_1} + \frac{d_2}{\varepsilon_2} + \ldots + \frac{d_i}{\varepsilon_i} \right) = \frac{D}{\varepsilon_0} \sum \frac{d_i}{\varepsilon_i} \, . \tag{14}$$

To estimate the effect of these structures on our field experiment, we calculate the resulting potential for three specific models (Figure 11):

Model A: *limestone*

$$V'_{(x,y)} = \frac{D}{\varepsilon_0} \left(\frac{d_1}{\varepsilon_1} \right), \; \varepsilon_1 = 8 \, , \tag{15}$$

Model B: *limestone and air*

$$V'_{(x,y)} = \frac{D}{\varepsilon_0}\left(\frac{d_1}{\varepsilon_1} + \frac{d_2}{\varepsilon_2}\right),\ \varepsilon_1 = 8, d_1 = 5m, \varepsilon_2 = 1, \quad (16)$$

Model C: *limestone, air and water*

$$V'_{(x,y)} = \frac{D}{\varepsilon_0}\left(\frac{d_1}{\varepsilon_1} + \frac{d_2}{\varepsilon_2} + \frac{d_3}{\varepsilon_3}\right), \varepsilon_1 = 8, d_1 = 5m, \varepsilon_2 = 1, d_2 = 10m, \varepsilon_3 = 80\,. \quad (17)$$

For the calculation we used the experimental estimate of the electric displacement $D = K\varepsilon_0\varepsilon_{\lim estone}$.

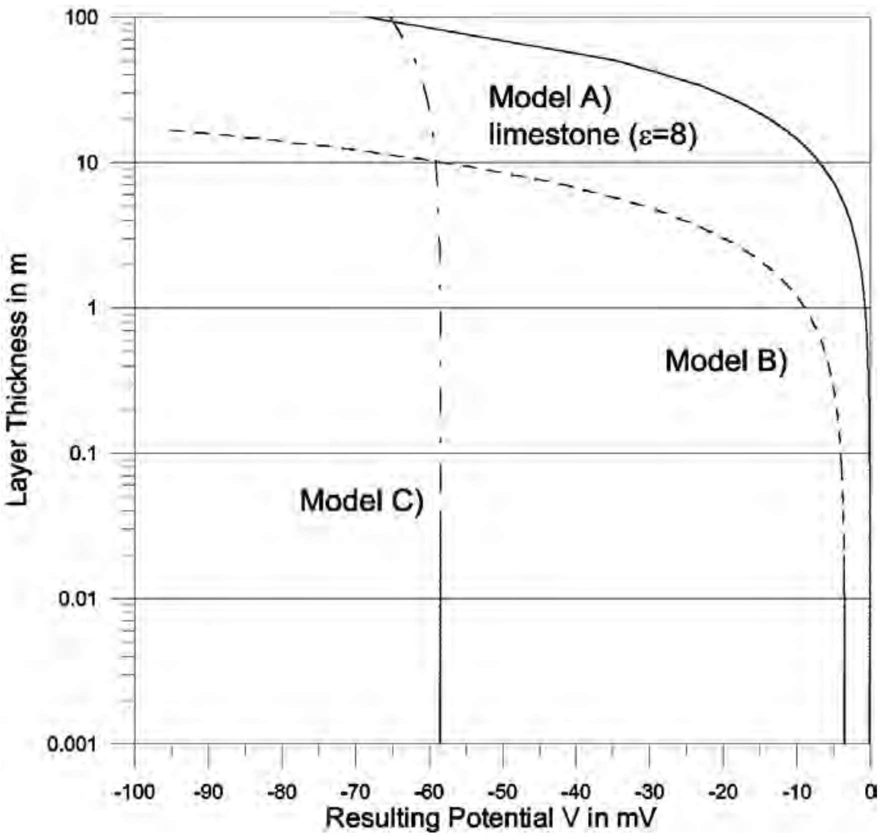

Figure 11: The resulting potential V for three specific layered capacitor models.

Model A is a one-layer structure consisting solely of limestone with increasing thickness. Figure 11 shows that this limestone layer will have a measurable effect on the potential distribution at surface with a beginning thickness of some meters.

In Model B, we kept the thickness of the limestone roof constant (5m) and inserted a cavity (air) of varying thickness. This will enhance the measurable effect on the potential distribution at surface.

The strongest effect on the potential distribution is shown in Model C. Here, we studied the wetting effect of a (thin) water layer at the bottom or at the roof of a given cave (roof out of limestone 5m thick, cavity (air) 10m thick). As Figure 11 shows, a thin water layer affects the measurable potential distribution at surface enormously.

From these simple models we can conclude, that an air layer and the wetting effect of water will locally affect the SP values at the surface. Hence, the cave is detectable with the SP technique.

Compared to the model by Aubert et al. (1990) and Aubert & Atangana (1996) our capacitor model is independent from the resistivities of Zone (A) and (B). In analogy to the geo-battery model for large SP anomalies created by geochemical processes (Bigalke & Grabner, 1997) we term our static model a geo-capacitor model.

Active model
Superimposed on the static charge distribution we assume an active charge separation that is controlled by the (micro) climatic conditions in the cave. For shallow cavities, heat and water transport by oscillatory convection plays an important role (Morat et al., 1999). Periodical variations of the temperature, relatively humidity, air pressure and the Self-Potential (at the roof of the cave !) are interpreted as manifestations of oscillatory convection motions of the air inside the cave, driven by the geothermal gradient and transporting water as well as heat from the bottom to the roof.
Morat (1999) state that convection is a much more efficient mechanism of heat transport than conduction through the air of the cavity. The air will convect and transport heat, but, at the same time, it will entrain upward the water vapour released at the floor of the cave by evaporation. The vapour will condense on the roof and the upper part of the pillars. In general, the condensed water enters the rock by capillarity, and the relative humidity of the air remains constant in the cave. This aspect together with the streaming potential in the porous media of zone (A) (Revil et al., 1999a, Revil et al., 1999b) plays an important role in our observations.

7 Conclusion

We showed that a shallow cave in karst is detectable with the SP technique. Nevertheless, we expect that the effect of a potential distribution in a deeper structure will be soon attenuated towards the surface and the method will fail. It remains unknown whether the SPS follows the bottom or the roof of the cave. However, from the findings in the field experiment (Fig. 8 and Fig. 9) we can conclude that the SPS technique gives the relief of the bottom of the cave. To answer this question, it is planned to study the potential distribution along a crosscut inside the cave.

[3] New mailing address: Institut für experimentelle Biomechanik, WWU Münster, Germany, marcus.gurk@uni-muenster.de

8 References

Aubert, M., I. N. Dana, M. Livet (1990): Vérification des limites de nappes aquifères en terrain volcanique par la méthode de polarisation spontanée, C.R.Ac.Sc. Paris, **311**, 999-1004.

Aubert, M. & Q. Atangana (1996): Self-Potential Method in Hydrogeological Exploration of Volcanic Areas, Ground Water, **34**, 1010-1016.

Bigalke, J. & E.W. Grabner (1997): The Geobattery Model: A contribution to large scale Electrochemistry, Electrochimic Acta, **42**, 23-24.

Bosch, F. & M. Gurk (2000): Comaprison of RF-EM, RMT and SP measurements on a karstic terrain in the Jura mountains (Switzerland), in A. Hoerdt & J. Stoll (eds.): Kolloquium Elektromagnetische Tiefenforschung in Altenberge/Bergisches Land vom 20.-24. April 2000, **18**, 51-59.

Jackson, D. B. & J: Kauahikaua (1987): Regional SP anomalies on Kilauea Volc. in Hawaii, U.S. Geol. Surv. Prof. Paper. , **40**, 947-959.

Landolt, Börnstein (1952): Zahlenwerte und Funktionen aus Physik, Chemie, Astronomie, Geophysik und Technik, Springer Verlag, Heidelberg, pp. 795.

Morat, P., J.-L. LeMouel, J.-P. Poirier, V. Kossobokov (1999): Heat and water transport by oscillatory convection in an underground cavity, C.R. Acad. Sci. Paris, Sciences de la terre et des planètes, **328**, 1-8.

Müller, I. (1981): La Grotte de "Chez-le-Brandt" (Jura Neuchâtelois, Coord. 526 425/ 199 000). Essai de synthèse des données géologiques et hydrogéologiques. Cavernes (Neuchâtel), **25** (1), 8-14.

Revil, A., P.A. Pezard, et al. (1999a): Streaming potential in porous media, 1: Theory of the zeta potential, Journal of Geophysical Research, **104**, 20021-20031.

Revil, A., H. Schwaeger, et al. (1999b): Streaming potential in porous media, 1: Theory and application to geothermal systems, Journal of Geophysical Research, **104**, 20033-20048.

Paper 5

Reprint from

**Schweizerische
Geologische
Gesellschaft**

ECLOGAE GEOLOGICAE HELVETIAE
(2001)
94, 329-338

INTEGRATION OF GEOPHYSICAL METHODS TO STUDY THE FOLD GEOMETRY OF THE TSCHERA NAPPE, EASTERN SWITZERLAND

MARCUS GURK
Groupe de Géeomagnetisme, Institut de Géologie, Université de Neuchâtel, Switzerland,
marcus.gurk@unine.ch

FRANK BOSCH
Centre d'Hydrogéologie, Université de Neuchâtel, Switzerland, frank.bosch@unine.ch

NATHALIE CHALLANDES
Institut de Géologie, Université de Neuchâtel, Switzerland, nathalie.challandes@unine.ch

Jürgen Bigalke
Institute of Meteorology and Geophysics, University of Frankfurt, Germany,
bigalke@geophysik.uni-frankfurt.de

Edited by

Schweizerische Geologische Gesellschaft

0012-9402/01/030329-10 $1.50 + 0.20/0
Birkhäuser Verlag, Basel, 2001

Eclogae geol. Helv. 94 (2001) 329–338

Integration of geophysical methods to study the fold geometry of the Tschera nappe, eastern Switzerland

MARCUS GURK[1], FRANK BOSCH[2], NATHALIE CHALLANDES[3] & JÜRGEN BIGALKE[4]

Keywords: Self-potential, magnetic method, VLF, RF-EM, induction arrows, graphite

ABSTRACT

A combined survey using the self-potential (SP), magnetic profiling and continuously measuring Radio Frequency-Electromagnetic (RF-EM) method has been carried out to study the fold geometry and the lithostratigraphy of the Tschera nappe. The Schams nappe sub-unit is located between the steep structural contact of the Mesozoic sediments (Bündnerschiefer) and the crystalline Penninic Suretta nappe (Rofna Porphyr) in Graubünden, eastern Switzerland.

Originally, the measurements have been initiated to give evidence for the existence or the absence of a presumed electrical high conductivity zone of large lateral extent within this major contact. If the conductivity anomaly exists, the zone can contribute to the directional dualism of the real parts of induction arrows observed in the magnetotelluric (MT) and geomagnetic deep sounding (GDS) survey of Graubünden. Contrarily the absence of such a high conductive zone supports the magnetic distortion hypothesis for magnetic transfer function in Graubünden. This major contact is therefore an important key for the understanding of electromagnetic induction processes in the central Alps. The change of direction of the real induction arrows occurs over the entire period range (T= 1-300 s) between two MT/GDS sites over a 400 m distance on the Tschera/Gelbhorn nappe. This implies that a major contrast in conductivity with considerable lateral and vertical extent is present in this contact zone.

The first analysis of the order of a set of self-potential and magnetic anomalies images a tight fold. Since the symmetry of the anomalies allows for a north or a south vergent fold, the self-potential anomalies have been modelled to determine the most reliable geometry within the nappe.

The RF-EM method confirms the SP and magnetic anomalies and detects the structural contact on both sides of the sub-unit. Finally, the geophysical findings have been well documented by a geological survey, showing the presence of graphite in the Tschera nappe. However, the assumed presence of a super-regional conductivity zone with the required lateral and vertical extension cannot be confirmed.

ZUSAMMENFASSUNG

Die Geometrie und die Lithostratigraphie der ostschweizerischen Tscheradecke waren das Ziel einer kombinierten geophysikalischen Messreihe unter Verwendung von Eigenpotential (SP), magnetischen und kontinuierlichen Radio Frequenz-Elektromagnetischen (RF-EM) Verfahren. Die Tscheradecke ist eine Untereinheit der Schamser Decke und markiert in Graubünden den strukturellen Kontakt zwischen den mesozoischen Sedimenten (Bündnerschiefern) im Norden und der penninischen Kristallindecke Suretta (Rofna Porphyr) im Süden. Flächendeckende magnetotellurische (MT) Messungen und geomagnetische Tiefensondierungen (GDS) zeigen in Graubünden einen Richtungswechsel der reellen Induktionspfeile (T= 1-300 s). Dieser periodenunabhängige Richtungswechsel stellt sich zwischen zwei Messpunkten über eine Distanz von ca. 400 m auf der Tschera/Gelbhorn Decke ein, und weist somit auf eine grossräumige gutleitende Störzone innerhalb des Kontaktes hin.

Falls diese leitfähige Störzone existiert, kann sie eine Erklärung für das beobachtete Verhalten der Induktionspfeile liefern. Dementgegen deutet das Ausbleiben einer angenommenen grossräumigen elektrisch gutleitenden Zone in diesem Kontakt auf eine magnetische Verzerrung der Magnetfelddaten.

Die vorläufige Analyse einer Reihe von Eigenpotential- und magnetischen Anomalien zeigt eine steile Falte mit unbestimmtem Einfallsinn. Um einen genaueren Aufschluss über die Geometrie innerhalb der Tscheradecke zu erhalten, wurden die SP Daten modelliert. Die RF-EM-Messungen belegen die SP und magnetischen Ergebnisse und zeigen zusätzlich zu beiden Seiten den strukturellen Kontakt zwischen der Tscheradecke und den umliegenden Einheiten. Alle geophysikalischen Beobachtungen wurden durch eine anschliessende geologische Begehung des Messgebietes bestätigt, wie z.B. das Vorhandensein einer graphitisierten Störzone.

Die Existenz einer überregionalen elektrisch leitfähigen Störzone entlang des strukturellen Kontakts kann jedoch nicht bestätigt werden.

1 Introduction

Few case histories exist where simple geophysical methods can help the geologist to understand complex tectonic structural settings and changes in lithostratigraphy in the absence of sufficient outcrop data. In this paper, we present an approach using the combination of self-potential (SP) and magnetic method responses as lithostratigraphic markers. Additional Radio Frequency-Electromagnetic (RF-EM) soundings were performed to support the magnetic and SP techniques and to

[1] Marcus Gurk, Groupe de Géomagnétisme, Institut de Géologie, Université de Neuchâtel, Rue Emile-Argand 11, CH-2007 Neuchâtel, Switzerland. E-Mail: marcus.gurk@unine.ch

[2] Frank Bosch, Centre d'Hydrogéologie, Institut de Géologie, Université de Neuchâtel, Rue Emile-Argand 11, CH-2007 Neuchâtel, Switzerland. E-Mail: frank.bosch@unine.ch, corresponding author

[3] Nathalie Challandes, Institut de Géologie, Rue Emile-Argand 11, Université de Neuchâtel, CH-2007 Neuchâtel, Switzerland. E-Mail: nathalie.challandes@unine.ch

[4] Jürgen Bigalke, Institute of Meteorology and Geophysics, University of Frankfurt, Feldbergstrasse 47, D-60323 Frankfurt, am Main, Germany. E-mail: bigalke@geophysik.uni-frankfurt.de

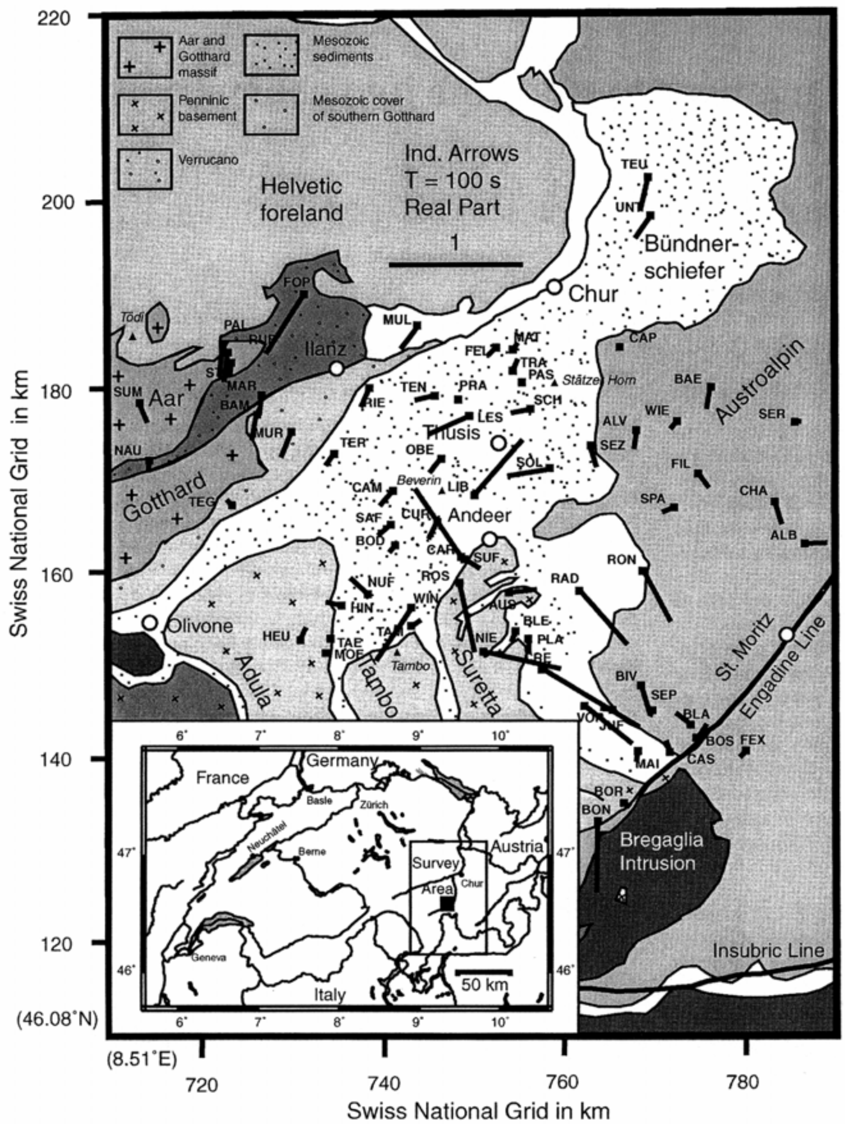

Fig. 1. Location of the investigation area (inlet) and real induction arrows in Graubünden for the 64 MT/GDS sites (filled squares) for the period T= 100 s. The lower left corner refers to coordinate: (λ= 8.51°E / ϕ= 46.08°N).

identify the Tschera nappe limits. These light weighted shallow depth high-resolution investigation techniques are ideally suited for the rugged alpine region of eastern Switzerland (Fig.1).

In contrast to the survey findings in the western Swiss Alps (Schnegg 1998), data collected in eastern Switzerland using the MT/GDS methods (Gurk 1999) revealed a change of direction in the real part of the induction arrows over the entire period range (T= 1-300 s). Induction arrows are a parameter of the induced magnetic field used to map lateral changes in the electrical conductivity distribution in the subsurface. Their change in direction in Graubünden coincides with the structural contact (SW-NE) between the Mesozoic Bündnerschiefer and the Penninic basement slices (Fig. 1). As the induction arrows point towards a region of lower electrical conductivity (Wiese 1962) a highly conductive zone was anticipated within this structural discontinuity. This major contact is therefore an important marker for understanding electromagnetic induction processes in the Central Alps. The notable change in the induction arrows direction between the two MT/GDS sites called CAR and SUF over the Tschera unit (Fig. 1) prompted further detailed investigations between these two locations using the above mentioned additional geophysical methods.

2 Survey area

2.1 Geological outline

The Tschera and Gelbhorn nappe (Fig. 2) are sub-units of the Schams nappe. The Schams nappe is the allochthonous part of the Mesozoic sedimentary cover of the imbricated Tambo/

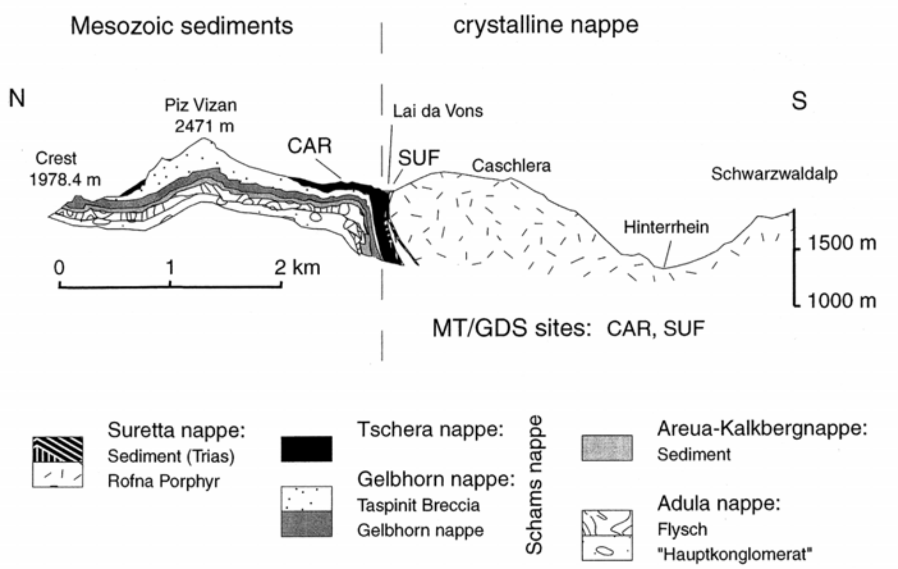

Fig. 2. Cross-section through the investigation area showing the steep sedimentary bands of the Schams unit in front of the hangingwall of the Suretta nappe. Redrawn from J. Neher in: Streiff et al. (1976).

Suretta basement slices. The structural contact with the Bündnerschiefer farther to the North and with the crystalline Suretta nappe to the South, is characterised by the presence of various sediments including Plattensandstein, anoxic black shales and various Triassic carbonates. The rocks form a compressed series of steep and deep reaching (detached) sedimentary bands divided by thrusts. The black shales exhibit a high organic carbon content (Schmid et al. 1990). The alteration of competent and incompetent layers creates an eroded, smoothly varying morphology without any remarkable outcrops. Consequently, detailed geological mapping of the units is difficult.

Figure 3 provides an overview of the survey area as well as the induction arrows for T = 100 s period of the two MT/GDS investigation sites CAR and SUF (Gurk 1999). Since the change of direction of the induction arrows in Graubünden is almost independent of the signal period (Gurk 1999), this change supports an initial hypothesis that a major lateral variation in conductivity might exist over these narrow sequences. As the induction arrows indicate a high conductivity zone, the following section deals with the different general mechanisms, which can explain the origin of such zones and the kind of conductive zone that might be likely in our survey area.

2.2 *Origin of electric conductive zones*

Structural discontinuities are promising candidates to create electrically conductive zones. Apart from high conductive structures caused by partial melts (Schmeling 1986; Shankland & Waff 1977), there are two other principal conductivity mechanisms producing low resistivity zones:

On one hand, elevated conductivities can result from electronically conducting ores such as interconnected graphite (ELEKTB-Gruppe 1994) or pyrite minerals. Alternatively, increased conductivities can also arise from an ionic current flow

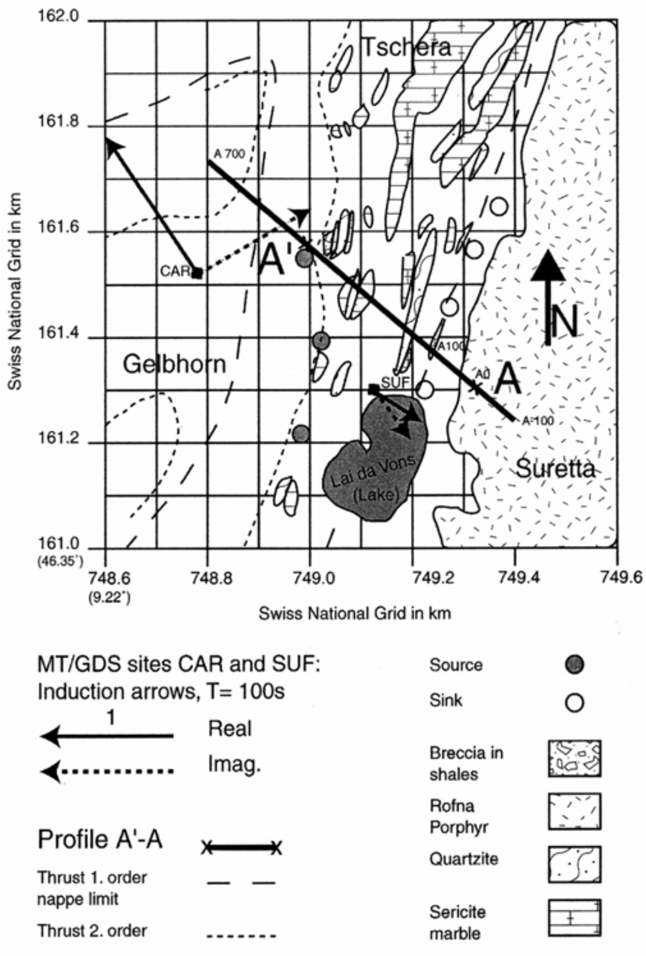

Fig. 3. Map of the investigation area. Redrawn from Streiff et al. (1971). The lower left corner refers to coordinate: (λ= 9.22°E / ϕ= 46.35°N).

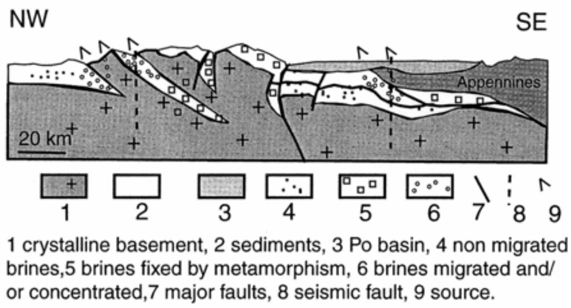

Fig. 4. Simplified section of the alpine arc showing a general model of fluid traps and fluid escape along deep reaching thrusts (Arthaud & Dazy 1989).

caused by fluids (Jödicke 1992). A general hydrological model for fluid transport and escape of brines in the Western Alps is summarised in Fig. 4 (Arthaud & Dazy 1989). The Arthaud & Dazy model reflects the tectonic setting of the stacked Penninic basement slices orientated either N-S or E-W. The expected enhanced electric conductivity along deep reaching thrusts in the studied contact zone could then be caused by brines migrating from the lower crust.

Figure 3 suggests that both conductivity mechanisms are feasible in the area of interest. Several springs and swallow holes are aligned along the major thrusts. However, the water in these springs has an electrical conductivity of up to 200 μS/cm (T= 26°C). These values contrast with conductivities in excess of 15000 μS/cm at T= 5.6°C (ca. 0.65 Ωm) measured in the Inn valley, 50 km to the East (Bissig 1997). The Scuol-Tarasp/Inn valley mineral springs isotopic CO_2 significance is typical for thermo-metamorphic reactions with carbonates (Wexsteen et al. 1988).

Beside the existence of springs and swallow holes in the survey area, metamorphic organic matter up to a coal rank of semi-graphite is present in Graubünden (Erdelbrock 1994; Mählmann 1995; Mählmann 1996). Weh et al. (1996) state, that in many cases, structural and metamorphic discontinuities coincide. Hence, due to the enhanced organic carbon content of the black shales in the Tschera unit, we expect, in analogy with the MT/GDS survey in the Valais Alps (Schnegg 1998) to find a graphite conductivity anomaly.

Apart from the non-linear induced polarisation method (Bigalke & Junge 1999), standard resistivity field surveys do not allow the difference between these two conductance mechanisms to be distinguished. However, SP-anomalies, for example, with magnitudes of several hundreds of millivolts provide strong evidence for the existence of electrically conducting ore minerals (Sato & Mooney 1960).

3 Geophysical survey methods and equipment

According to the initial hypothesis of a major lateral change in electrical conductivity in the survey area, as well as the previously mentioned different possibilities of its origin, different geophysical high resolution investigation methods for shallow depths were chosen to ascertain, which of the above mentioned hypotheses was most probable. The methods were:

- Self-potential,
- Magnetics and
- Radio Frequency-Electromagnetics.

The measurements were carried out along profile A (length: 800 m, orientation: 309° N, see Fig. 3) from the Suretta nappe to the Gelbhorn unit crossing the Tschera nappe nearly perpendicular to the fault boundaries.

The following sections explain the motivation for the application of these particular methods in this case history. Their main principles including particular sensitivities as well as data acquisition and equipment specifications are described briefly.

3.1 Self-potential

Ore mineralisation often produces a natural negative electrical potential along the earth's surface. SP-anomalies are nearly invariant in time and can have magnitudes of up to -1.8 V (Gay 1967). Thermoelectric and/or electrokinetic coupling processes

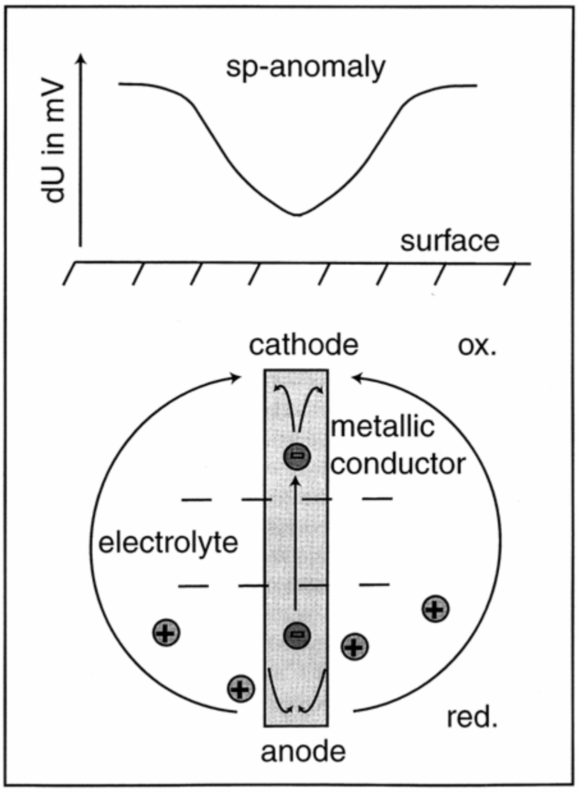

Fig. 5. A steeply inclined electronic conductor connects regions of different redox potential (ox: oxidation zone, red: reduction zone) and forms a "geobattery". The redox potential difference corresponds to an electron flow from the formation into the lower end of the electron conductor (anode). The electrons move to the upper end (cathode) and are transferred to the environment, (Sato & Mooney 1960).

can generate SP anomalies (Fittermann 1979), but they can also be produced by electrochemical processes similar to those in a galvanic cell. Geological structures showing such processes are called geobatteries (Sivenas & Beales 1982). The conceptual model of a self-potential anomaly caused by a geobattery is shown in Fig. 5. According to Sato & Mooney (1960) a steeply inclined metallic conductor (graphite, pyrite, ores, etc.) connects the oxidising country rock with the reducing environment at depth. Due to the chemical energy of the redox potential gradient, electrons flow within the conductor from its lower end – the anode of the battery – upwards to the cathode. The charge conservation is provided by a simultaneous flow of ions in the formation and the voltage drop at the surface can be measured as SP anomaly. Geobatteries may produce SP signals with magnitudes of several hundred millivolts and provide a strong indication for interconnected electronically conducting minerals (Bigalke & Grabner 1997; Stoll et al. 1995).

The self-potential measuring equipment consists of a pair of non-polarisable Cu-$CuSO_4$ electrodes arranged on a spade stick, and a voltmeter to measure the potential differences between the two electrodes. One electrode (the base) is kept fixed whereas the second electrode is used to sample the field every 20 m. On the anomalies the step is reduced to 1.0 m or less.

3.2 Magnetics

Due to the existence of magnetite in the Plattensandstein of the survey area, magnetics offered a promising means of obtaining information about the stratigraphy of the structural contact between the Bündnerschiefer and the crystalline Suretta nappe. The total magnetic field was measured using a Geometrics G 816 proton precession magnetometer. An initial 10 m sampling interval identified the main anomalies and the magnetic background. Over anomalies, the measuring interval is reduced to 1.0 or 0.2 m. All values were corrected for time variations using data of the Neuchâtel Geomagnetic Observatory.

3.3 Radio Frequency-Electromagnetic (RF-EM) method

The RF-EM method is an enhancement of the traditional VLF-EM (Very Low Frequency-Electromagnetic) method. It uses electromagnetic signals from permanently transmitting remote sources provided by terrestrial radio broadcasting antennas in the extended frequency range of 15–300 kHz.

The instrumentation used was developed at the Hydrogeology Centre of Neuchâtel (Stiefelhagen 1998; Turberg & Müller 1992; Turberg et al. 1994; Bosch & Müller 2001) with focus on the investigation of karst structures (Bosch & Gurk 2000) at shallow depths (10–100m). The instrument continuously measures the local horizontal and vertical magnetic field components with two orthogonal induction coils. For a chosen frequency, the device determines directly the "in-phase" and "out-of-phase" (also called "quadrature") components of the secondary to primary magnetic field's ratio, i.e. the real and imaginary part of the magnetic transfer function. Datalogging with 1 Hz or 4 Hz sampling rate can be chosen. Data obtained on a profile yield lateral resistivity contrasts in the subsurface that directly reflect geological features such as fractures, faults or facies/permeability variations. Due to the skin effect, profiling with various transmitter frequencies provides lateral resistivity contrast information for different penetration depths of the electromagnetic fields.

A handheld system was used for this survey. Compared to the imaginary parts, the real parts of the transfer function are much more affected by antenna deviations from the vertical caused by the continuously walking process. Consequently the real part data are of minor quality and are not subject of this paper. Some particular aspects of the method should be considered:

The RF-EM technique is a true 2D method and very sensitive for vertical structures. It obtains the magnetic transfer functions over a profile assuming E-polarisation. Therefore, the instrument actually yields the magnetic field components: $B_z/B_{y'}$, with y' normal to the strike of the structure. Vertical structures are indicated by the inflection points of the measured $B_z/B_{y'}$ curve (McNeill & Labson 1991). Due to transmitter availability and the nature of complicated geological structures, the precise E-polarisation case is not very likely. Consequently, a mixture of polarisation results in a distorted sounding curve. Additionally the dip of a buried conductor will deform the RF-EM response (McNeill & Labson 1991). These facts do severely impede the RF-EM interpretation. According to the main strike directions in the survey area and the chosen profile A-A' (Fig. 3), the 216 kHz transmitter fulfils quite well the case of E-polarisation. 20.3 kHz is unfortunately close to the H-polarisation case as listed in Table 1. 216 kHz was recorded with 4 Hz sampling rate and 20.3 kHz with 1 Hz. According to subsurface apparent resistivities of about 1000–3000 Ωm obtained in previous geoelectric mapping and soundings along the profile (not discussed in this paper), these frequencies provide estimated penetration depths δ shown in Table 1.

4. Observations Part I: Self-potential and Magnetics

A preliminary survey showed that all kinds of magnetic and SP anomalies are found with stable background values in the profile interval 0–320 m (A-A'). Hence, we restrict our presentation to this 320 m-long part of the profile. The results of

Tab. 1: Estimated *skin–depths* δ against *apparent resistivities* ρ_a of the subsoil and *signal frequency* f of the RF-EM technique (and direction of transmitter against North)

	ρ_a = 1000 Ωm	ρ_a = 3000 Ωm
f=216 kHz, 221° N	δ= 30 m	δ= 60 m
f=20.3 kHz, 144° N	δ= 110 m	δ= 192 m

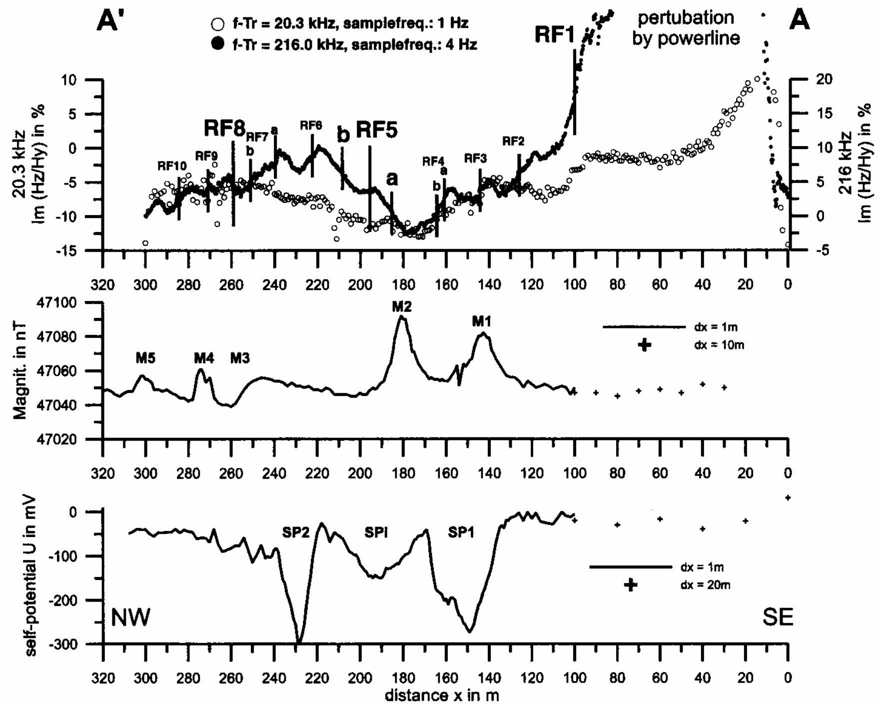

Fig. 6. RF-EM, total intensity of the magnetic field and self-potential measurements along the profile section A'-A.

the three applied profiling methods are presented in Fig. 6. The self-potential and the magnetic data show some sharp anomalies, whereas the RF-EM curve features a complex series of responses with superimposed signals. In the next sections, we confine ourselves on the description and interpretation of the self-potential and magnetic data. The modelling of the SP data then leads to a preliminary interpretation of the SP and magnetic anomalies series. Finally a description and interpretation of the RF-EM data are given and are used to confirm the results.

4.1 The series of SP and magnetic anomalies

The magnetic and SP values create an ordered series of anomalies:

Starting from SE the series begins with magnetic anomaly **M1** at 143 m, which is directly followed by a broad self-potential anomaly **SP1** with its minimum of about –270 mV at 149 m.

The series continues with the sharp magnetic anomaly **M2** at 181 m and the self-potential anomaly **SP2** measuring about –300 mV at 229 m. The intermediate self-potential anomaly **SPi** (190 m) between **SP1** and **SP2** reaches only -150 mV. Beyond 200 m the magnetic data show a smooth trend towards higher values which ends with a sudden step (**M3**) to lower magnitudes at 250–260 m. Two small anomalies **M4** and **M5** (274 m, 300 m) occur in the western part of the profile. Focussing on the magnitudes of the magnetic anomaly pairs (**M1/M2**), (**M4/M5**), we find that this series starts with a low amplitude anomaly (**M1**) followed by the high amplitude **M2** anomaly. The pair on the NW side of the profile shows the inverse pattern.

4.2 The shape of the self-potential anomalies

The dip of a buried conductor, ideally a dyke with infinite lateral extension, can be estimated from the shape of the anomaly. A vertical dyke, as shown in Fig. 5, produces a symmetric SP anomaly, whereas a dyke with a certain dip distorts the anomaly shape. Anomaly **SP2** is distorted such that the NW shoulder is lower than the SE shoulder. This behaviour corresponds to the model of a right dipping dyke (Telford et al. 1990). It is difficult to draw the same conclusion for **SP1**. This anomaly cannot be described by a simple dyke model. Nevertheless, a predominant right dipping feature seems to be present in the data for **SP1**. The **SPi** anomaly exhibits a small distortion effect implying a NW dipping structure.

4.3 The shape of the magnetic anomalies

Similar estimation about the dip of a buried dyke can be made for magnetic anomalies (Telford et al. 1990). But unfortunately, both magnetic anomaly pairs (**M1/M2**) and (**M4/M5**) are too close to each other. Therefore, no magnetic background values can be found between the anomalies and the analysis of their shape will be misleading. However, the sudden step (**M3**) to lower magnetic values, as mentioned above, is typical for a contact between two blocks of different susceptibilities (Telford et al. 1990).

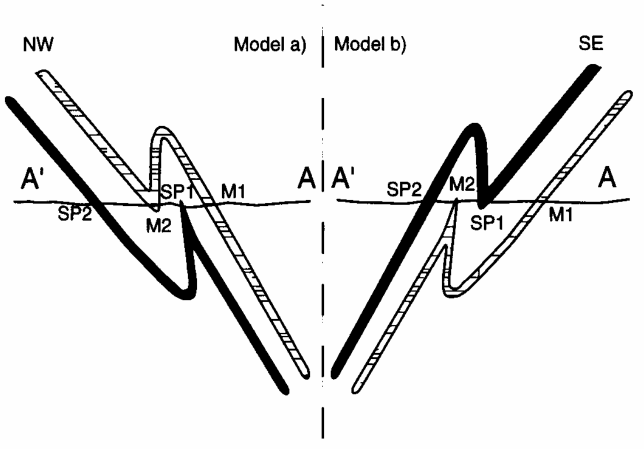

Fig. 7. Two equivalent explanations for the observed series of magnetic and self-potential anomalies **SP2 – M2 – SP1 – M1.**

5 Preliminary interpretation of the SP and magnetic anomalies series

The sequence of magnetic and SP anomalies:

SP2-M2-SP1-M1

may be interpreted in stratigraphical and tectonic terms. According to the geological map (Fig. 3, Streiff et al. (1971)) we can assume that both types of anomaly in this series are caused by the same lithology. Fig.7 shows that this series then can be interpreted as tight folds, which are dipping either (a) SE or (b) NW.

Model (b) is less probable since the analysis of the shape of anomaly **SP2** reflects a south dipping structure. However, the dip angle and the extension with depth of the strata remain uncertain. The SP data may be modelled to delineate the most realistic fold geometry (Fig. 8).

5.1 Self-Potential Model

The modelling has been performed at the University of Frankfurt/Main using the approach method of Bigalke & Grabner (1997) which includes an electrochemical model of the redox potential distribution. It was necessary to split the self-potential data into two branches and to limit the sample interval to 3.5 m. The intermediate anomaly **SPi** was excluded from the modelling. Each branch has been treated separately.

The most striking feature is the good match of both models. The first conductor, responsible for anomaly **SP2**, plunges southwards down to a depth of 40 m and with a dip of about 45°. If extrapolated, the conductor finds its continuation in the 80° northwards and 62° southwards dipping limbs of the anticline structure of the second conductor. Although we did not take the **SPi** anomaly into account, the model fits the field data sufficiently well. Generally, the model confirms our former analysis of the ordered anomaly series. Yet, the origin of the **SPi** anomaly is still unknown.

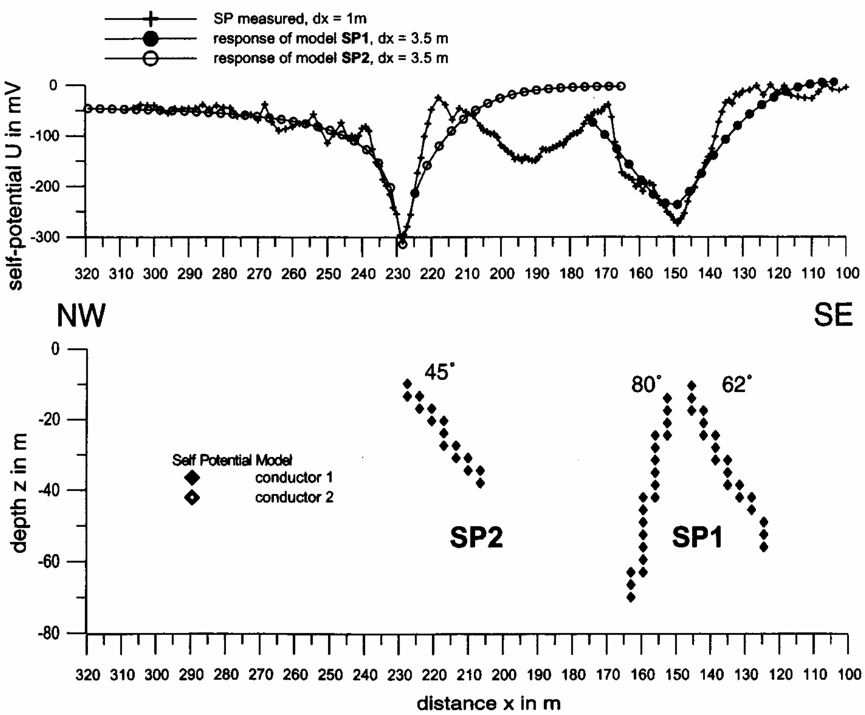

Fig. 8. Model of the self-potential data and its response.

6 Observations Part II and interpretation of RF-EM sounding curves

In this section the RF-EM data are described and interpreted in comparison with the results from SP and magnetic data.

The RF-EM curves of the imaginary part of the B_Z/B_Y ratio show superimposed anomalies (Fig. 6), which indicate lateral resistivity contrasts at the specific penetration depths. The 216 kHz curve shows more variations with higher amplitudes than the 20.3 kHz curve, which is of poorer quality. It is likely that the missing variations in the 20.3 kHz quadrature curve are a result of the H-polarisation case for this frequency. Therefore, we focus on the 216 kHz curve. An electric powerline crosses the profile at 0 m and influences the RF-EM measurements for 216 kHz up to ca. 80 m and up to ca. 40 m for 20.3 kHz. The different anomalies are named **RF1** to **RF10,** from SE to NW (Fig. 6).

The most striking resistivity contrasts are indicated by **RF1** (visible for both frequencies) at 100 m and by **RF5**. The latter is a superposition of two signals (**RF5a** at 185 m & **RF5b** at 209 m) which are far away enough from each other to be separated by the 216 kHz band. The centre of **RF5** lies at 90 m and is therefore at the same position as **SPi**, whereas it's eastern edge is at 180 m, the same position as **M2**. These two big RF-EM anomalies show amplitude variations of up to 15 % indicating strong geological discontinuity zones. The geological map in Figure 3 shows that anomaly **RF1** coincides with a 1st order thrust, the structural contact between the Rofna Porphyr and the Tschera nappe. The intensity of anomaly **RF5** supports the argument for a thrust producing **SPi**. Anomaly **RF2** at 134 m also has a remarkable change in amplitude of 7.5 %, but magnetic and SP data show only very small variations at this position. The series of the anomalies **RF6** (221 m) / **RF7a** (239 m) lies at the edges of **SP2**. These two RF-EM anomalies may therefore indicate the edges of a conductive dyke, which shows up as **SP2**. This situation is similar for the sequence **RF3** (144 m) / **RF4a** (161 m) / **RF4b** (165 m) compared with **SP1**. **RF3** coincides with **M1**, whereas **RF8** coincides with **M3** at 260 m confirming the conclusion of an almost vertical contact between two blocks drawn from the magnetic curve shape. **RF9** at 271 m coincides with **M4**. The RF-EM anomaly pattern confirms the anomalies from SP and magnetic data quite well, but cannot explain their origin as stand-alone information.

7 Geological survey and synoptic model along the profile

We investigated the anomalies along the profile A'-A by coring and rock sampling. The main findings are listed in Table 2. The magnetic and RF-EM anomalies (**M1/ RF3, M2**) and (**M4/ RF9, M5**) are generated by the (exposed) magnetite bearing Plattensandstein.

Black shale with a high graphite content corresponds to the **SP1** and **SP2** anomalies, whereas the **SPi** anomaly occurs where only strongly weathered gneiss was found. From this observation and from the findings of the previous section, we conclude that the **SPi** anomaly and the strong gradient in the 216 kHz RF-EM data (**RF5**) are caused by a thrust. It extends, dipping slightly to the NW, down to a maximum depth of 30-110 m. This conclusion leads to the synoptic model presented in Fig. 9: Compression of the isoclinal folds (see Fig. 9c) leads to a detachment along the most incompetent series (black shale) of the folded Tschera nappe. The projected effective direction of the magnetisation in the Plattensandstein onto the profile will then create the observed change in the amplitudes of the magnetic anomaly pairs (**M1/M2**) and (**M4/M5**).

Tab. 2. Type of geophysical anomaly, lithology after Streiff et al. (1971) and strike and dip values along the profile section A'-A.

x in m	Anomaly	Lithology
100	**RF1**	thrust (structural contact Tschera/Rofna porphyr)
143	**M1 / RF3**	exposed Plattensandstein ("Gault") with magnetite (285° N / 68°)
149	**SP1**	exposed graphitic blackshale (285° N/ 79°)
161	**RF4a**	
165	**RF4b**	
179		exposed sericite marble (302° N / 67°)
181	**M2**	Plattensandstein ("Gault") with magnetite
185	**RF5a**	
192	**SPi / RF5**	strongly weathered gneiss, dip to NW, thrust
209	**RF5b**	
221	**RF6**	
229	**SP2**	Graphitic blackshale (ca. 2 m overburden by strongly weathered gneiss)
239	**RF7a**	
250	**RF7b**	
260	**M3 / RF8**	thrust, contact between two units of different susceptibility
274	**M4 / RF9**	(123° N / 69°) Plattensandstein ("Gault")
284	**RF10**	
290	**M5**	(123° N / 78°) Plattensandstein ("Gault")

8 Conclusion

A case history for an integrated geophysical survey has been presented to separate magnetic and self-potential anomalies over a narrow sequence of detached sedimentary bands. The combination of self-potential, RF-EM and magnetic measurements provides a high-resolution technique to investigate structural contacts in the absence of reliable outcrops. The synoptic model explains the combined results of applied geophysical methods and geological in-situ information. The RF-EM method is the most rapid technique and detects resistivity contrasts with the highest lateral resolution, but does not identify their origin because of its sensitivity for resistivity contrasts caused by different mechanisms. The geophysical findings and the modelling of the SP data agree well with the geological analysis of the sequence. Moreover, the survey was able to confirm the known geology at this locality and could detect two additional thrust faults in the Tschera unit. The presence of interconnected graphite is confirmed by the SP method.

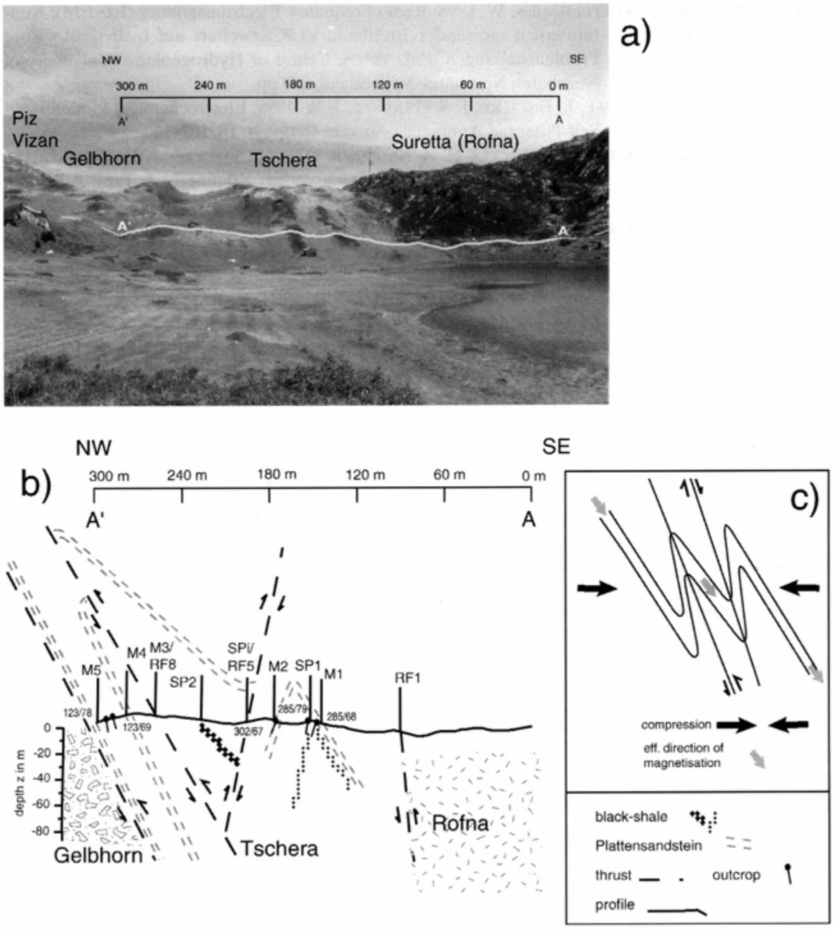

Fig. 9. (a) View parallel to the structural contact and (b & c) synoptic model of the fold geometry of the Tschera nappe along the profile section A'-A together with geophysical anomaly positions.

On a more regional scale, the electrical properties offered by the Tschera nappe are not sufficient to create a large conductive zone which could be responsible for the directional dualism of the GDS real induction arrows observed in Graubünden over long periods (T > 10 s). Consequently, the direction change of the real part of the induction arrows is more likely the result of a current channelling (Gurk 1999).

Acknowledgements

The Swiss National Foundation financially supported the research presented in this paper. The authors are very indebted to Mr Jaques Duperrex who built the electromagnetic equipment used in this study.

REFERENCES

Arthaud, F. & Dazy, J. 1989: Migration des saumures au front des chevauchements de l'arc alpin occidental. C. R. Acad. Sci. Paris. 309 (Sér. 2), 1425–1430.

Bigalke, J. & Grabner, E.W. 1997: The Geobattery Model: A contribution to large scale Electrochemistry. Electrochimica Acta 42 (23–24), 3443–3452.

Bigalke, J. & Junge, A. 1999: Using evidence of non-linear induced polarization for detecting extended ore mineralisations. Geophys. J. int. 137, 516–520.

Bissig, P. 1997: Hydrogeologische Untersuchung der CO2-reichen Mineralquellen von Scoul-Tarasp (GR, Schweiz). Diploma thesis, Centre de Hydrogéologie, Neuchâtel, Neuchâtel, 91 pp.

Bosch, F.P. & Gurk, M. 2000: Comparison of RF-EM, RMT and SP measurements on a karstic terrain in the Jura Mountains (Switzerland). Proceed. of the Kolloq. elektromagnet. Tiefenforsch., Altenberg/Bergisches Land, Germany, Mitt. Dtsch. geophys Ges. 18, 51–59.

Bosch, F.P. & Müller, I. 2001: Continuous gradient VLF measurements: A new possibility for high resolution mapping of karst structures. First Break 19 (6), 343–350.

ELEKTB-Gruppe: Bahr, K., Bigalke, J., Eisel, M., Haak, V., Harms, U., Hirschmann, G., Huenges, F., Jödicke, H., Kotny, A., Kücke, J., Nover, G., Rauen, A., Stoll, J., Walther, J., Winter, H. & Zulauf, G. 1994: Untersuchungen zur elektrischen Leitfähigkeit in der Kontinentalen Tiefbohrung und ihrem Umfeld – was bringt sie uns Neues? Mitt. dtsch. geophys. Ges. 4, 2–40.

Erdelbrock, K. 1994: Diagenese und schwache Metamorphose im Helvetikum der Ostschweiz (Inkohlung und Illit-"Kristallinität"). PhD thesis, Fakultät für Bergbau, Hüttenwesen und Geowissenschaften, Rheinisch-Westfälische Technische Hochschule Aachen, Aachen, 220 pp.

Fittermann, D.V. 1979: Calculation of self-potential anomalies near vertical contacts. Geophysics 44, 195–205.

Gay, S.P. 1967: A 1800 Millivolt Self-Potential Anomaly near Hualgayoc, Peru. Geophys. Prosp. 15, 236–245.

Chapter 2 – Case Studies – Published Papers – **Paper 5** 63

GURK, M. 1999: Magnetic Distortion of GDS Transfer Functions: An Example from the Penninic Alps of Eastern Switzerland Revealing a Crustal Conductor. Earth Planets Space 51, 1023–1034.

JÖDICKE, H. 1992: Water and graphite in the earth's crust – an approach to interpretation of conductivity models. Surv. in Geophys. 13, 381–407.

MÄHLMANN, R.F. 1995: Das Diagenese-Metamorphose-Muster von Vitrinitreflexion und Illit-"Kristallinität" in Mittelbünden und im Oberhalbstein Teil 1: Bezüge zur Stockwerkstektonik. Schweiz. mineral. petrogr. Mitt 75. 85–122.

MÄHLMANN, R.F. 1996: Das Diagenese-Metamorphose-Muster von Vitrinitreflexion und Illit-"Kristallinität" in Mittelbünden und im Oberhalbstein Teil 2: Korrelation kohlenpetrographischer und mineralogischer Parameter. Schweiz. mineral. petrogr. Mitt. 76, 23–46.

MCNEILL, J.D. & LABSON, V.F. 1991: Geological mapping using VLF radio fields. In: Electromagnetic Methods in Applied Geophysics Volume 2, Application, Parts A and B (Ed. by M.N. NABIGHIAN). Investigations in Geophysics, 3, Society of Exploration Geophysicists, Tulsa Oklahoma, Tulsa, 521–640.

SATO, M. & MOONEY, H.M. 1960: The Electrochemical Mechanism of Sulfide Self-Potentials. Geophysics XXV(1), 226–249.

SCHMELING, H. 1986: Numerical models on the influence of partial melt on elastic, anelastic and electrical properties of rocks. Part II, electrical conductivity. Phys. Earth Planet. Inter. 43, 123–135.

SCHMID, S.M., RÜCK, P. & SCHREURS, G. 1990: The significance of the Schams nappes for the reconstruction of the paleotectonic and orogenic evolution of the Penninic zone along the NFP-20 East traverse (Grisons, eastern Switzerland). Mém. Soc. géol. France 156, 263–287.

SCHNEGG, P.-A. 1998: The magnetotelluric survey of the Penninic Alps of Valais. Matériaux pour la Géologie de la Suisse – Geophysique 32, Swiss Geophysical Commission, Bern, 76 pp.

SHANKLAND, T.J. & WAFF, H.S. 1977: Partial melting and conductivity anomalies in the upper mantle. J. geophys. Res. 82, 5409–5417.

SIVENAS, P. & BEALES, F.W. 1982: Natural geobatteries associated with sulphide ore deposits, I. Theoretical Studies. J. geochem. Explor. 17, 123–144.

STIEFELHAGEN, W. 1998: Radio Frequency Electromagnetics (RF-EM): Kontinuierlich messendes Breitband-VLF, erweitert auf hydrogeologische Problemstellungen. PhD thesis, Centre of Hydrogeology, University of Neuchâtel, Neuchâtel, Switzerland, 243 pp.

STOLL, J., BIGALKE, J. & GRABNER, E.W. 1995: Electrochemical Modelling of Self-Potential Anomalies. Surv. in Geophys. 16, 107–120.

STREIFF, V., JÄCKLI, H. & NEHER, J. 1971: Geologischer Atlas der Schweiz, Blatt: 1235 Andeer. Kommissionsverlag: Kümmerly & Frey AG Geographischer Verlag Bern, Bern, 1:25 000.

STREIFF, V., JÄCKLI, H. & NEHER, J. 1976: Erläuterungen zu Blatt: 1235 Andeer, Kommissionsverlag: Kümmerly & Frey AG. Geographischer Verlag Bern, Bern, 106 pp.

TELFORD, W.M., GELDART, L.P. & SHERIFF, R.E. 1990: Applied Geophysics, Cambridge University Press, Cambridge, 770 pp.

TURBERG, P. & MÜLLER, I. 1992: La méthode inductive VLF-EM pour la prospection en continu de milieu fissuré. Proceed. of the Cinquième Coll. d'Hydrol. en Pays calcaire, Neuchâtel, 16–18.10, Ann. Sci Univ. Besançon Géologie, 207–214.

TURBERG, P., MÜLLER, I. & FLURY, B. 1994: Hydrogeological investigation of porous environments by radio magnetotelluric-resistivity (RMT-R 12–240 kHz). J. appl. Geophys. 31, 133–143.

WEH, M., MÄHLMANN, R.F. & FROITZHEIM, N. 1996: Strukturelle und metamorphe Diskontinuitäten im Penninikum am Westrand der Ostalpen. Proceed. Tektonik und Strukturgeologisches Kolloqium.

WEXSTEEN, P., JAFFÉ, F.C. & MAZOR, E. 1988: Geochemistry of cold CO2 –rich springs of the Scuol-Tarasp region, Lower Engadine, Swiss Alps. J. Hydrol. 104, 77–92.

WIESE, H. 1962: Geomagnetische Tiefentellurik Teil II: Die Streichrichtung der Untergrundsstrukturen des elektrischen Widerstandes, erschlossen aus geomagnetischen Variationen. Geofis. pura Appl. 52, 83–102.

Manuscript received November 24, 1999
Revision accepted July 25, 2001

Paper 6

Reprint from

SEG
Society of Exploration Geophysicists

GEOPHYSICS
(2002)
67(6), in press

GEOELECTRIC MAPPING OF NEAR-SURFACE KARSTIC FRACTURES BY USING NULL ARRAYS

SÁNDOR SZALAI
Geodetic and Geophysical Research Institute of the Hungarian Academy of Sciences, Sopron, Hungary, szalai@ggki.hu.

LÁSZLO SZARKA
Geodetic and Geophysical Research Institute of the Hungarian Academy of Sciences, Sopron, Hungary, szarka@ggki.hu

ERNÖ PRÁCSER
Eötvös Loránd Geophysical Institute, Kolumbusz u. 17–23, H–1145 Budapest, Hungary, E-mail: pracser@elgi.hu.

FRANK BOSCH
Centre d'Hydrogéologie, Université de Neuchâtel, Switzerland,
frank.bosch@unine.ch

IMRE MÜLLER
Centre d'Hydrogéologie, Université de Neuchâtel, Switzerland,
imre.muller@unine.ch

PASCAL TURBERG
Swiss Federal Institute of Technology Lausanne (EPFL), Department of Civil Engineering (DGC), Laboratory of Geology, Ecublens, Lausanne, Switzerland,
pascal.turberg@epfl.ch.

Edited by

Society of Exploration Geophysicists

GEOPHYSICS, VOL. 67 NO. 6 (NOVEMBER-DECEMBER 2002); P.1-10, 13 FIGS., 1 TABLE

Geoelectric mapping of near-surface karstic fractures by using null-arrays

Sándor Szalai*, Lászlo Szarka*, Ernö Prácser‡, Frank Bosch**,
Imre Müller**, Pascal Turberg§

ABSTRACT

The term "null-array" is introduced for those electrode configurations where the measured potential difference is zero above a homogeneous half-space, while using a small measuring dipole M^0N^0. Different types of null-arrays (three-electrode, Schlumberger and dipole axial/ equatorial null-arrays) and their corresponding traditional ones are studied. It was shown in a field study carried out in a karstified limestone area covered by thin sediments that it is possible to obtain geologically meaningful results with null-array techniques. The main features of the null-array data are as follows. (1) Null-array data appear to be more spatially variable than the classical data. The spatial variability provides information about the presence of karstic fractures in the subsurface; (2) The null-array anomalies caused by nearly vertical karstic fractures in the limestone basement do not decay with depth as quickly as the classical array anomalies; (3) The strike direction of the fractures is much less ambiguous than that found by using classical arrays. Nevertheless, the depth variation of the basement is more reliably observed in geoelectric anomalies obtained using traditional arrays. Therefore a joint use of classical arrays and their corresponding null methods is recommended, because the combined methods provide more information about the subsurface structure.

INTRODUCTION

If current electrodes A, B and potential electrodes M, N lie on the surface of a homogeneous half-space, depending on the mutual positions of A, B, M, and N, the measured potential difference may be zero in many places. Such configurations can be defined as "null-arrays". In this paper we discuss null arrays with small-size MN. In such cases, null-arrays are those configurations where the measuring dipole is perpendicular to the direction of the local earth current flowline.

Although there have been some occasional studies using such configurations in the 1960s–1970s (e.g. Jakosky, 1960; Gupta and Bhattacharya, 1963; Habberjam and Watkins, 1967; Militzer et al., 1979; Brizzolari and Bernabini, 1979), in addition to related studies that were carried out later (Mathias and Habberjam, 1984; Tsokas et al., 1997), the null-arrays we propose in this paper have not been previously investigated. These arrays are closely related to the classical AMNB approaches differing only in that the small-size measuring dipole MN is rotated by 90° (denoted in this new position as M^0N^0), and that any small variations in potential difference $\Delta U_{M^0N^0}$ are due to lateral conductivity inhomogeneities. The field application of this idea emerged for first time following analog modeling experiments in Hungary (Szalai, 1993; Szarka, 1994).

Szalai (1993) first considered geoelectric null-arrays when studying the geoelectric effect of leakages in waste-disposal-site lining using a multielectrode configuration. Szarka (1994) proposed incorporating electromagnetic configurations into the geophysical interpretation that provide zero response over a homogeneous half-space, but concrete results have been published only for different non-DC situations (Szarka, 1991; Szarka and Nagy, 1992; Szarka and Menvielle, 1999).

We are not aware of any field application of our proposed null-array technique. We believe this may be because null-array data require a completely different interpretation compared to data from traditional arrays. For example, a good

Manuscript received by the Editor December 20, 2000; revised manuscript received Feburary 6, 2002
*Geodetic and Geophysical Research Institute of the Hungarian Academy of Sciences, POB 5, H–9401 Sopron, Hungary, E-mail: szarka@ggki.hu; szalai@ggki.hu.
‡Eötvös Loránd Geophysical Institute, Kolumbusz u. 17–23, H–1145 Budapest, Hungary, E-mail: pracser@elgi.hu.
**University of Neuchâtel, Centre d'Hydrogéologie, 11, rue Emile Argand, CH– 2007 Neuchâtel, Switzerland, E-mail: frank.bosch@unine.ch; imre.muller@unine.ch.
§Swiss Federal Institute of Technology Lausanne (EPFL), Department of Civil Engineering (DGC), Laboratory of Geology, Ecublens, CH–1015 Lausanne, Switzerland, E-mail: pascal.turberg@epfl.ch.

understanding of parameter-sensitivity maps is required. These maps are described in detail by Barker (1979) and by Spitzer (1998).

In this paper we initially provide a simple classification of possible geometrical null-arrays, which bring together traditional and non-traditional array pairs. The results of a case study in the Swiss Jura mountains are then presented.

NULL-ARRAY AND TRADITIONAL ARRAY PAIRS

The potential difference is zero wherever the small measuring dipole M^0N^0 is at right angles to the local direction of the earth current flow line. Among the infinite number of arrangements, we discuss here only null-arrays having corresponding configurations with the family of traditional arrays. These pairs are presented in Figure 1.

In case (I), MN (M^0N^0) is close to one of the current electrodes. In this case, the current lines are nearly radial around the current electrode. According to the similarity with the classical three-electrode (pole-dipole) configuration AMN, the AM^0N^0 configuration is called the “three-electrode null-array”.

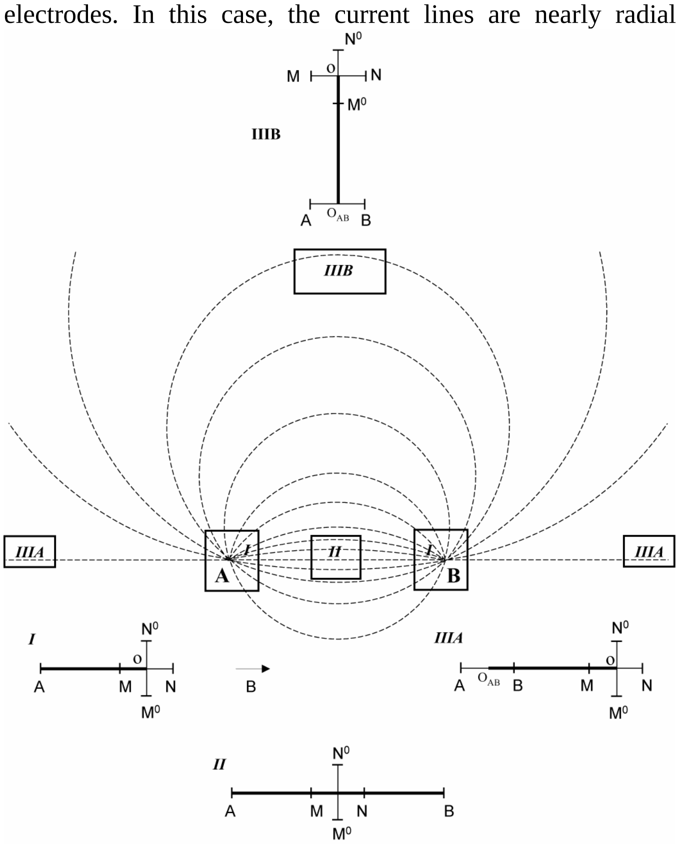

FIG. 1. Three characteristic traditional arrays and the corresponding null-arrays. The potential electrodes MN (M^0N^0) are placed (I) close to one of the current electrodes, so that the Earth currents flow lines are nearly radial, II) between the two current electrodes, so that the Earth current flow lines are nearly parallel, III) far from the current electrodes, so that the current source may be considered as a dipole. The traditional dipole axial and equatorial arrays produce the respective null ones by rotation of the potential dipole. However, the two dipole null-arrays (IIIA and IIIB) are equivalent due to the reciprocity theorem.

In case (II), MN (M^0N^0) is located between the two current electrodes. Here, the current lines are nearly parallel. A special situation in this group is the Schlumberger (or AM^0N^0B) null-array, when the center of M^0N^0 is on the line between A and B at an equal distance from both current electrodes;

In case (III), MN (M^0N^0) is far from the current electrodes. In this case, the current source may be considered as a dipole. Two null-arrays can be easily constructed from well-known traditional configurations: (IIIA) the dipole axial null-array and (IIIB) the dipole equatorial null-array. Due to the reciprocity theorem these last two null-arrays are equivalent, whereas the traditional dipole-equatorial and dipole-axial configurations would give different responses.

Figure 2 shows a parameter sensitivity map for the dipole axial null-array. It was calculated using the analytical approach of Szalai and Szarka (2000). The values of isolines in Figure 2 are the percentage of effect caused by a small cube in the given place (at a depth of one tenth of the dipole-dipole distance) by this null-array with respect to the homogeneous half-space value in the field of the corresponding traditional array. The antisymmetry about the y = 0 axis indicates that any

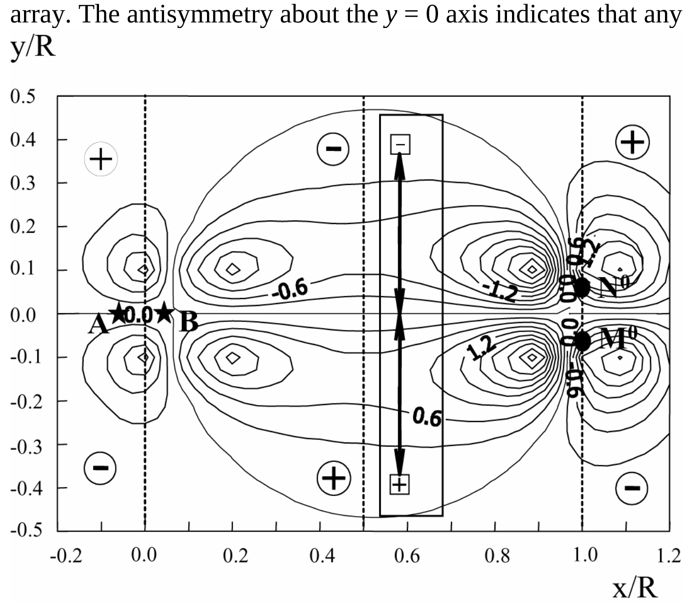

FIG. 2. Parameter sensitivity map of the dipole-axial null-array (IIIb in Figure 1). In this map, the effect is shown of a small anomalous cube placed at various x and y positions in a horizontal plane (at a depth of one-tenth the value of the dipole-dipole distance) in percentage of the response in dipole-axial array over a homogeneous half-space. Isoline units are in percents. Due to the antisymmetric sensitivity about the y = 0 line, symmetrical bodies do not produce any null-array response. The circled + and – signs merely emphasize the antisymmetric character of this parameter sensitivity map.

anomalous body which is symmetrical over this axis has zero effect on the null-array response. In case of a symmetrical body, the effects of pairs due to related small portions (those at distances $+y/R$ and $-y/R$) are mutually cancelled out. This holds true for all one-dimensional bodies (layers), two-dimensional bodies whose dip direction coincides with the $y = 0$ axis, and three-dimensional bodies having a symmetry axis coincident with $y = 0$.

THE TEST AREA AND THE TECHNICAL PARAMETERS

The test area is situated in the folded part of the Swiss Jura in the vicinity of a quarry near the village Les Breuleux in the northwestern part of Switzerland. In this region, Kimmeridgian limestone with a thickness of several hundred meters is covered by a thin (0.2 - 1.5 m) layer of Quarternary clay and silt. The limestone is karstified and tectonically influenced by a combination of faults and overthrusts (Zwahlen and Doerfliger, 1995). Karstification and tectonics have generated a system of fractures and fissures. In the test area, the fractures are nearly vertical, and the fracture planes are perpendicular to the wall of the quarry. Neither the ground surface nor the limestone's top surface is horizontal.

Table 1. Characteristic distances in null array and traditional array pairs I, II, IIIA, and IIIB. O_{AB} is the center of the transmitting dipole AB; O is the common center of MN and M^0N^0.

Array	Charactaristic Distance (m)	M^0N^0(MN) Distance (m)
I	AO = 2	1
II	AB = 4	1
IIIA and IIIB	OABO = 2.5	1

Measurements were carried out along three profiles (1, 2 and 3) parallel to the wall (at distances of 2, 8 and 16 m from the wall, respectively). The results obtained along profile 2 are presented in this paper. This particular distance was close enough to the wall to allow a direct comparison between the visible fractures and the obtained anomalies. On the other hand, it was far enough from the wall not to be greatly influenced by the void space. Furthermore, the profile has a gentle topography. (Even in profile 1, the data were found to be more disturbed by the rugged topography than by the proximity of the wall.) The parameters of the four arrays used are shown in Table 1.

In order to avoid any mispositioning of the electrodes, a special tool (a wooden lattice fixed on a tube) was prepared (shown in Figure 3), allowing the geometric error to be

reduced to a value of less than 1 cm. Its weight was less than 4 kg, and the cables run through the tube, thereby facilitating rapid measurements in the field.

NULL-ARRAY PROFILES AND THEIR INTERPRETATION

A major objective of this study is to determine whether it is possible to obtain information about fractures by using non-traditional null-arrays. In order to avoid the possibility of misinterpretation, test measurements were carried out to study repeatability. Since the test produced coherent results (that is, the main features of null-array profiles consistently remained the same), we proceeded to the detailed study.

FIG. 3. Geoelectric null-array measurement (Schlumberger null-array) in the field. A plastic tube with a proper length and a wooden lattice fixed on it serves to reduce geometrical errors.

Main features of null-array anomalies

Figures 4 presents typical apparent resistivity profiles (measured along profile 2 with the dipole-axial null-array and with the traditional dipole-axial array). The depth to the limestone's top surface (as determined by boreholes along profile 2) is also indicated. Both apparent resistivity profiles seem to be a superposition of a slowly varying trend and many small, localized undulations. For the traditional arrays, it is evident that the trend is due to the nonparallelism between the nearly flat ground surface and the top of the high-resistivity limestone basement. (See the basement depth values shown in Figures 4.) It is our hypothesis that the local variations are due to fractures in the limestone. Such an interpretation is possible also for the null-arrays, as it is demonstrated by a simple logical approach summarized in Figure 5. The observed null-array anomaly is composed of steps A, B, C and D as follows.

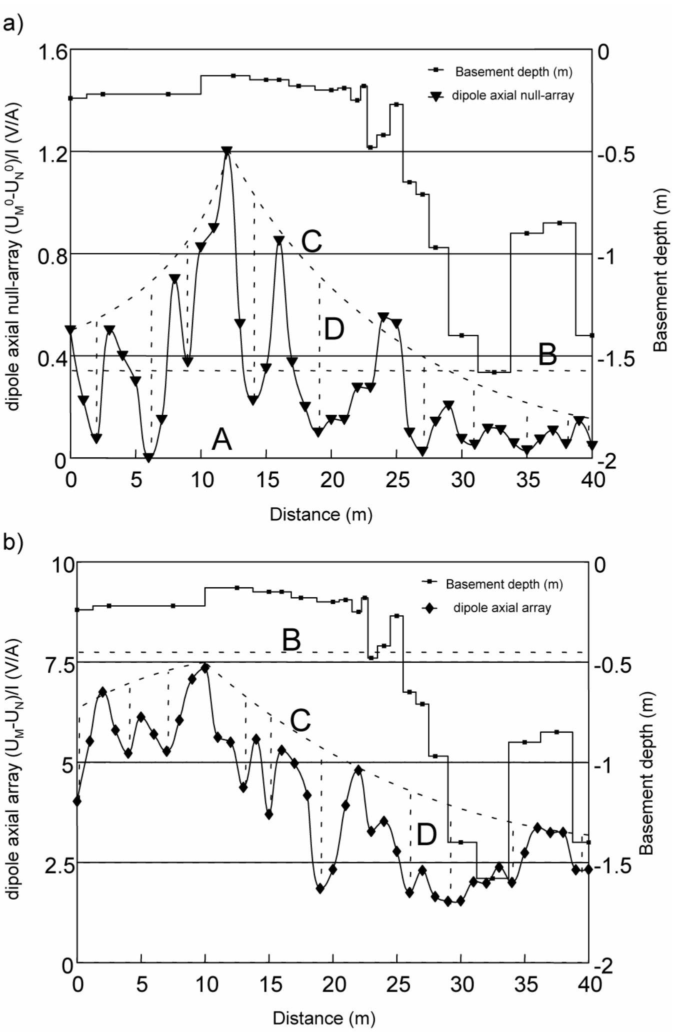

FIG. 4. (a) Dipole-axial null-array and (b) classical dipole-axial array response, measured in the field. The basement depth values (as known from boreholes) are shown in both figures. Letters A, B, C and D indicate effects of features explained in Figure 5.

Step A) In case of a simple one-dimensional earth (e.g., a horizontal interface between a homogeneous high-resistivity basement and the sediment; see Figure 5a), the null-array response on the ground surface should be zero (See A also in Figure 4a).

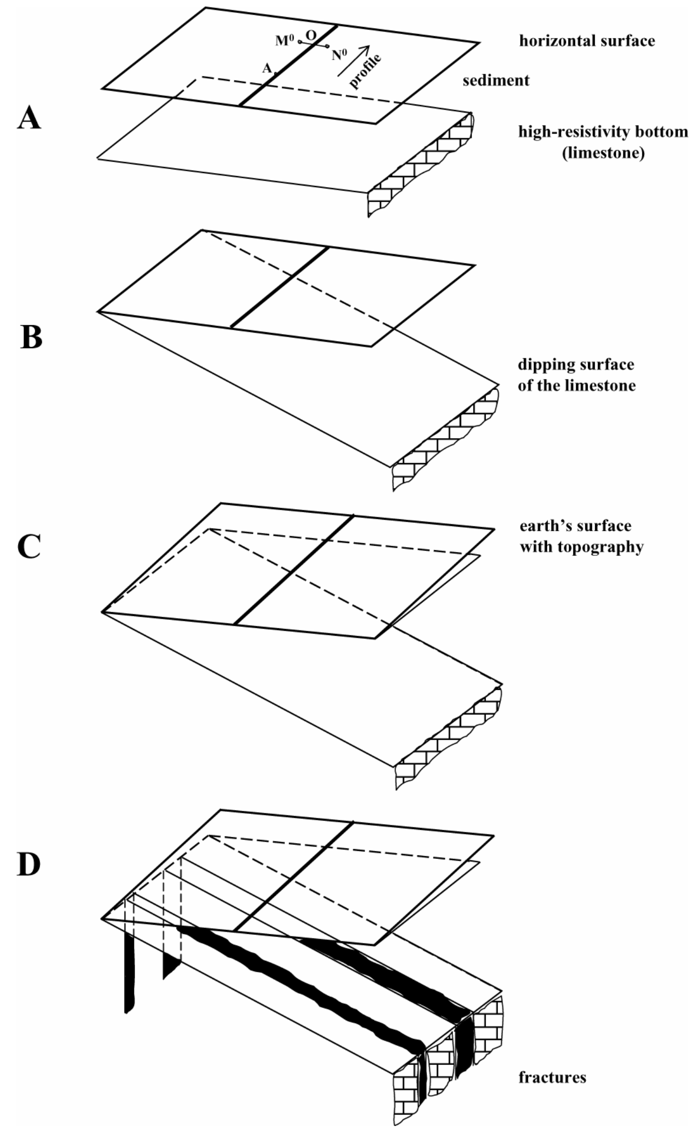

FIG. 5. Analysis of the main features of the anomaly profiles in Figure 4. The measuring profile is shown by the bold line on the horizontal surface. (a) In one-dimensional situation (e.g., over a two-layered half-space with high-resistivity basement), the null-array response is zero everywhere. (b) In the case of a dipping high-resistivity basement, the null-array response is a constant nonzero value along the profile. (c) In the case of non-horizontal topography, the null-array response is not constant. It is decreasing when going upwards on the ground surface (resulting in a trend). (d) In the case of high-conductivity fractures in the basement, the null-array response is the superposition of the trend and the local anomalies (minima) due to the fractures.

Step B) In case of a dipping basement (see Figure 5b), when AO is in the strike direction, a constant ΔU_{M0N0} value is measured due to the perfect two dimensionality of the problem. (See B also in Figure 4a.) This ΔU_{M0N0} value — due to the asymmetry about line AO — differs from zero.

Step C) If the thickness between the ground surface and the dipping high-resistivity basement increases due to a gently sloping surface (Figure 5c), the measured ΔU_{M0N0} will diminish progressively, because the response is less and less influenced by the basement. In other words, the half-space seems to be more and more homogeneous for an observer at the surface. It is the case in Figure 4a (shown by curve C) in the direction of increasing distances starting at about 10 m. From this point towards zero (towards left), another decrease is seen. Without doubt, the limestone surface is closest to the surface at the distance of 10 m. (This particular feature is not shown in Figure 5.)

Step D) The local variations (denoted as D in Figure 4a) are assumed to be a result of fractures as shown in Figure 5d. This was later verified by numerical modeling.

The anomalies obtained by the traditional arrays are straightforward; thus, no detailed comments will be made. Nevertheless, one can identify the features B, C, D for traditional array profile as well (see B, C, D in Figure 4b; A would be a non-zero constant).

Numerical modeling results

If vertical fractures are laterally extensive and have a horizontal upper surface, they would not have any effect on the null-array response. In our case, the roof of the vertical fractures coincides with the roof of the basement. An individual fracture is modeled by a thin and long (0.2 m x 10 m) low-resistivity (10 ohm-m) body. Because of the restriction of our three-dimensional numerical modeling software (Prácser, 1999; based on the approach of Dey and Morrison, 1979; for details see Appendix A), the dipping-plane upper surface was approached by staircase. The bedrock resistivity was set to 1000 ohm-m. The model is shown in Figure 6; the numerical modeling results are shown in Figure 7.

In Figure 7, the response of the body is given in millivolts/amp for both the traditional array (left side) and the corresponding null-array (right side). The zero horizontal distance (directly above the center of the anomalous body) is the reference point of each array, indicated by the filled star in Figures 7a-d. Note the sharper response of the body when using the null-arrays I, IIIA and IIIB, and the antisymmetric response relative to the traditional one using null-array II (the Schlumberger null-array).

Such high-conductivity fractures are indicated with null-arrays I, IIIA and IIIB by minima in the null-array response. In the two latter cases the theoretical responses are equivalent, due to the reciprocity theorem (see again Figures 7c and 7d).

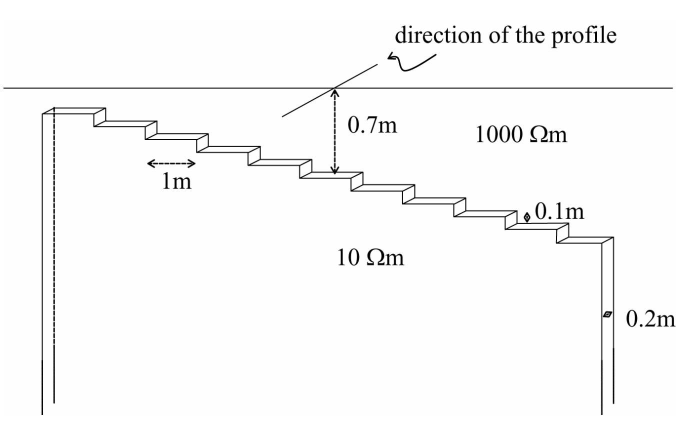

FIG. 6. A simplified fracture model used for interpretation of array responses. The anomalous body is elongated and highly conducting; it has an infinite depth extent and a stepped upper surface. The direction of the profile is at right angles to the long axis of the body. The body is embedded in a homogeneous half-space.

INTERPRETATION OF FIELD RESULTS

Comparison of geoelectric results with the photo of the quarry wall

The measured data along profile 2 are shown in Figure 8 for the three-electrode and Schlumberger arrays and in Figure 9 for the axial and equatorial dipole-dipole arrays. The quarry wall is shown at the bottom of both figures. (Note that the depth to the limestone roof along profile 2 is shown in Figure 4.)

The slowly varying trend in the responses is due to the relative dipping of the ground surface with respect to the limestone bed: the depth to the basement increases to the right, which shown as “basement depth” in the Figure 4. (This variation of the basement depth is only partly visible in the photo).

By a visual comparison of the fractures on the photo with the measured profiles we infer that the minima of the three-electrode null-arrays data give a picture of the presence of karstic fractures (e.g. at 18, 26-27, and 38 m). The Schlumberger null-array in Figure 8 also seems to indicate the fractures by the minima instead of the inflection points shown by numerical results in Figure 7b. For the type of structures modeled, the distance between the inflection point and the minimum is only about 1 meter, so this phenomenon, at least in this field study, is not a source of confusion.

The dipole-equatorial anomalies are slightly shifted. The dipole-axial null-array again gives a poorer result than the three-electrode or the Schlumberger null-array, but remains better than its corresponding traditional array, mainly on the right side of the profile.

The reason for the large peak at distance about 10 m in case of the Schlumberger null-array (and for a somewhat similar peak with the dipole axial null-array) is associated with the shallowest depth to the limestone roof. The enhanced position of the limestone surface is evident from handmade drillings along profile 2 (shown in Figures 4a and 4b). At the same time, this enhanced position is not seen on the photo but is hidden by the irregular wall edge.

The similarity between the dipole-equatorial and the dipole-axial null-array anomalies measured in the field (Figure 10) is apparent. This is expected due to their reciprocity relationship. Of course, the two curves are no longer identical as they were previously in the synthetic model (shown in Figures 7c and 7d) because of measuring (positional) errors.

Without doubt, the null-array data are spatially more variable than the classical data. Nevertheless, we should emphasize that they are not artifacts: they reflect the physical response from a heterogeneous ground. (They are repeatable in time, and furthermore, most minima are shown by at least two measured values.) Of course, not all of the minima could be identified as fractures, but this increased spatial variability

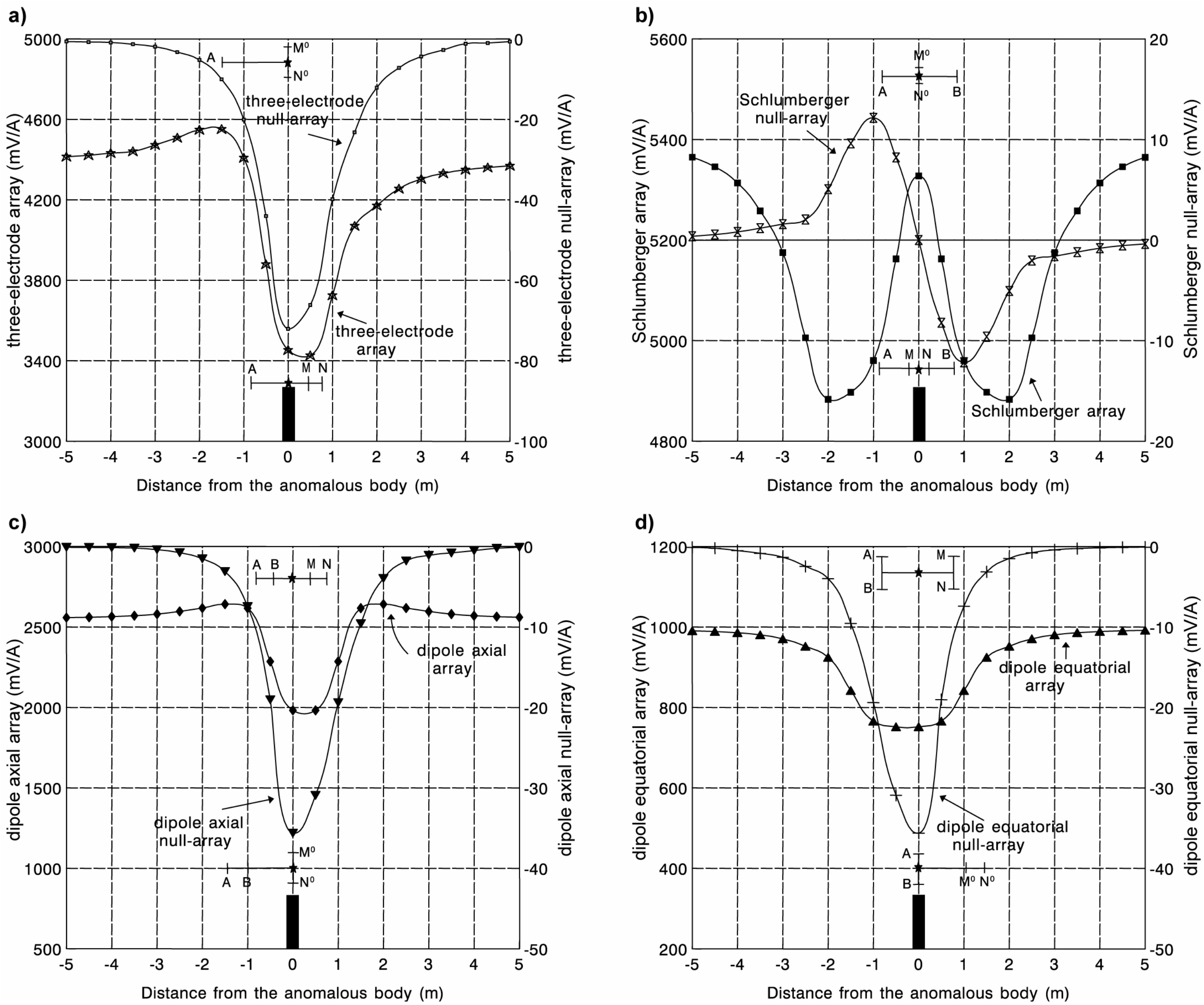

FIG. 7. Numerical modeling results for the classical arrays and their corresponding null arrays I, II and IIIA and IIIB. The MN and M^0N^0 potential differences (for the traditional and the null array accordingly) are plotted as a function of the distance from the anomalous body. Note the difference of points of reference between the traditional and null-arrays, which are indicted by stars. (a) I, (b) a special case of II (the traditional Schlumberger array and the Schlumberger null-array), (c) IIIA, (d) IIIB (its null-array version is in a reciprocity relation with that of IIIA).

(provided the sampling distance is small enough) may be a result of the possible presence of smaller fractures. At the same time, the increased spatial variability may obscure long-range trends in the depth-variation of the limestone roof.

As the figures show, the null-array provides useful information about the presence of karstic fractures. It must be emphasized that the null-array anomalies due to the fractures do not decay with depth as quickly as the classical array anomalies do. At the same time, the classical arrays better describe the basement depth. Consequently, the joint use of the null-arrays and their classical array pairs is recommended.

Determination of the fracture direction by using null-arrays

In order to be able to determine the fracture direction, an analogue modeling experiment was carried out.

Assume an elongated horizontal and tabular low-resistivity anomalous body in the subsurface with an undetermined

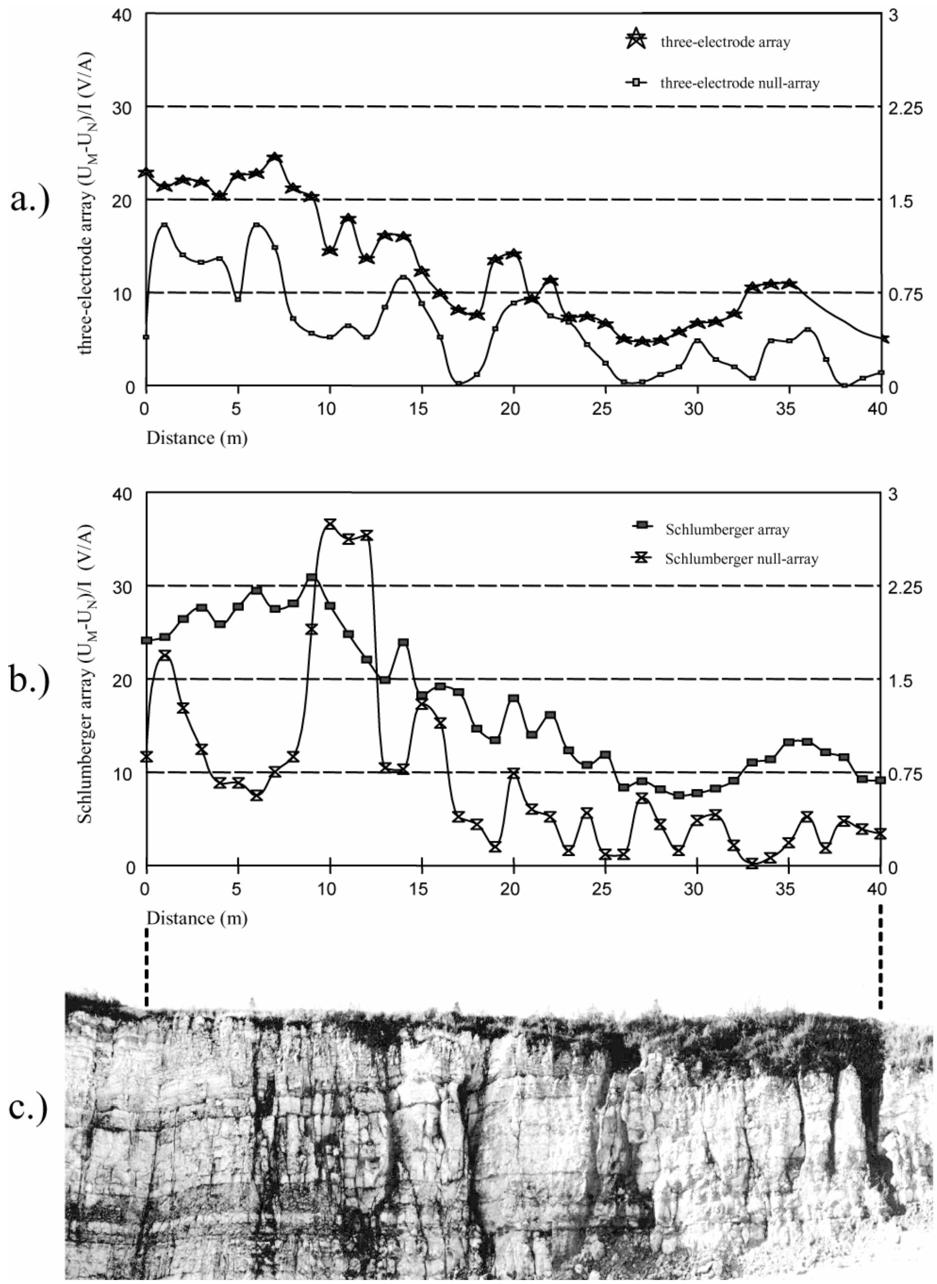

FIG. 8. Comparison of the null and classical array responses by an actual example: (a) three-electrode null-array and three-electrode traditional array, (b) Schlumberger null-array and Schlumberger array, (c) the wall of the quarry. The limestone roof is under the soil covered by grass. (Its topography along profile 2 is better seen in the drillhole values shown in Figure 4.).

Geoelectric Null Arrays

a.)

b.)

c.)

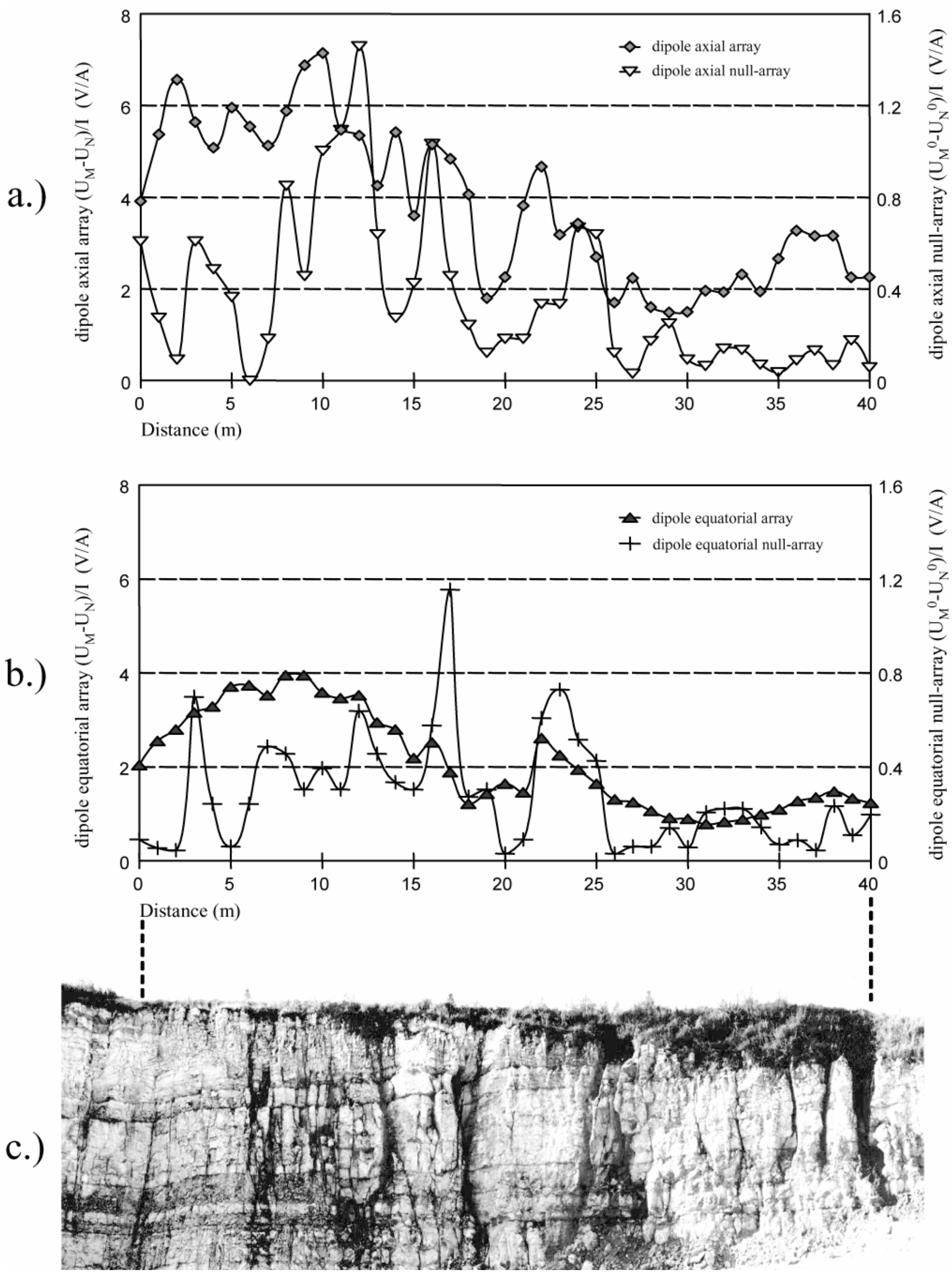

FIG. 9. Comparison of the null and classical array responses by an actual example: (a) dipole-axial null-array and dipole-axial array, (b) dipole-equatorial null-array and classical dipole-equatorial array, (c) the wall of the quarry.

orientation. In Figure 11, azimuthal response profiles for the classical Schlumberger array and for the Schlumberger null-array are shown for two different offsets that is the distance *d* between the profile and the center of the body. The diagrams are results of analogue modeling experiments. Rotating the array through 360° on the surface (equivalently, rotating the body in the host medium) produces, in the case of the classical array, two minima in the azimuthal response profile, whereas the null-array has four minima. In the special case of zero offset, the direction of the body unambiguously can be determined by using the classical Schlumberger array. In the case of the Schlumberger null-array, the number of minima is doubled, depending on whether AB or M^0N^0 is parallel to the strike. Fortunately, this feature (according to the modeling results) will be preserved in case of nonzero offsets (that is if we are not exactly over the center of the body). Note that in case of nonzero offset, the direction of the body can no longer be determined by using the classical array because the minimum zones of the azimuthal response profiles become

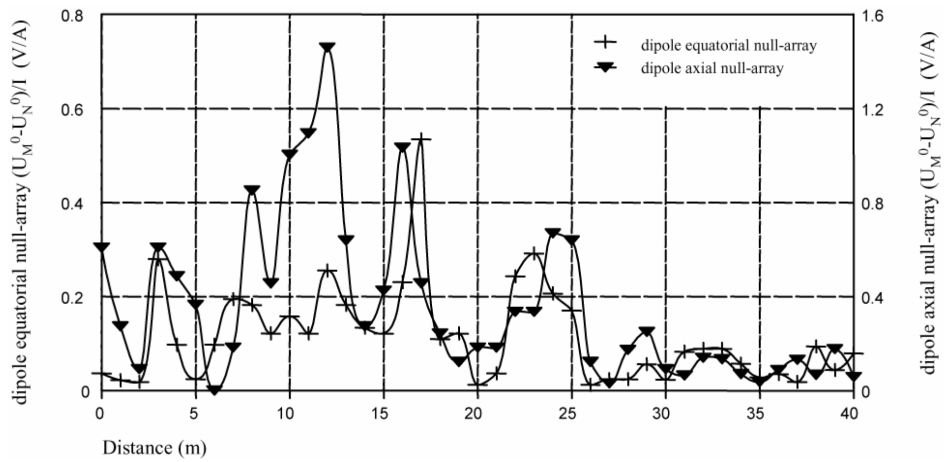

FIG. 10. The dipole-equarorial and the dipole-axial null-array responses along profile2. The patterns are similar because of the power of the reciprocity theorem.

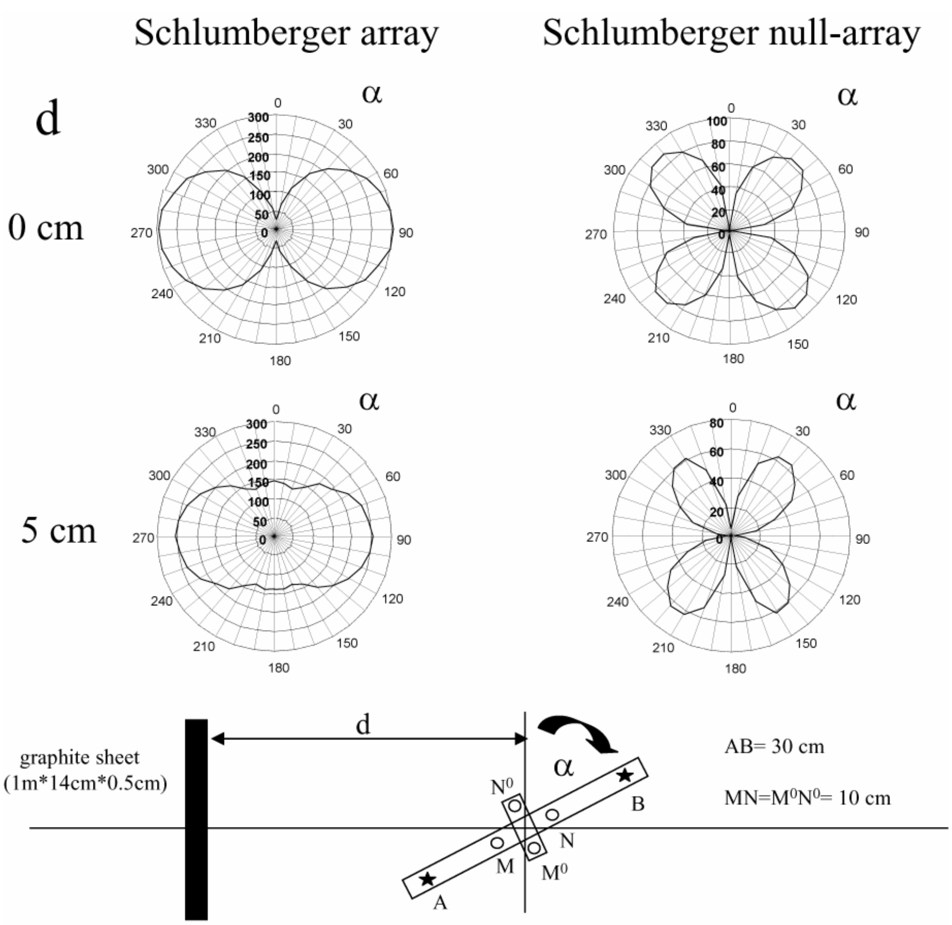

FIG. 11. Master diagrams for the determination of the strike direction by using a Schlumberger array (left) and a Schlumberger null-array (right) obtained from analog modeling experiments carried out for two different offsets d = 0 and d = 5 cm.

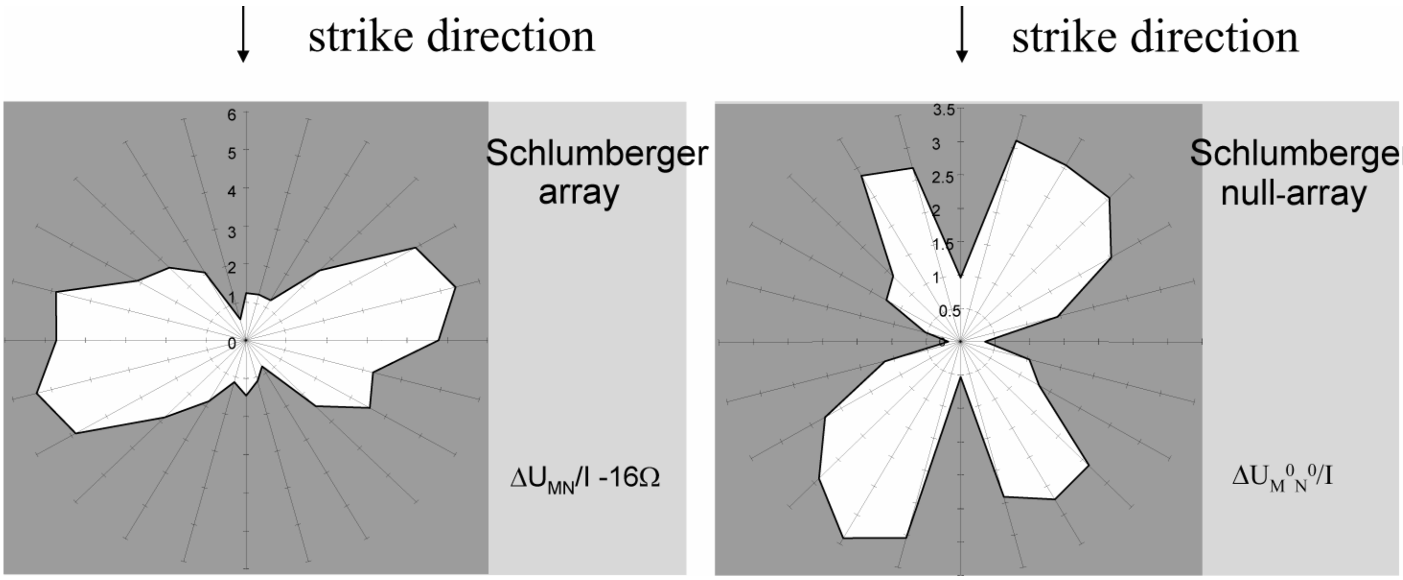

FIG. 12. Azimuthal diagrams for the determining of the strike direction in the field by using a classical Schlumberger array (left) and a Schlumberger null-array (right). In case of the classical Schlumberger array a special value ($\Delta U_{MN}/I$)-16 ohm is shown. In this way of representation, the minimum resistance value approaches zero.

too wide. Although some information about the direction of the body can still be obtained from the relatively narrower maximum zone, the determination of the strike direction is ambiguous. At the same time, the direction can be still reliably determined from the null-array measurements, due to the very narrow minimum zone. The remaining uncertainty of 90° is resolved with the aid of the classical Schlumberger-array measurements, which provide orientation.

The field results obtained at 17 m along profile 2 are shown in Figure 12. The elongated bodies in this case are the nearly vertical karstic fractures in the limestone. In case of the classical Schlumberger-array, instead of ΔU_{MN}, the transformed quantity ($\Delta U_{MN}/I$)-16 ohm is shown. (In this way, the maximum and minimum values are seen more clearly.) As in the analogue modeling experiment, the strike direction can be determined relatively unambiguously from the maximum, resulting in an estimate of –15° to 165°. For the Schlumberger null-array within 360° again two minimum pairs are obtained: 0°-180° and 90°-270°. The true fracture direction can be easily selected from the two possible ones, in spite of the slight (15°) discrepancy between the classical and the null-array strike-direction determination results. As expected, direct fracture direction determination in the field agreed with the null-array estimation.

In Figure 13, the fracture directions as observed on the quarry wall and as determined along profile 2 by using this combined traditional/null-array resistivity technique, are presented. A good correlation was found between the observed and the measured strike directions. See especially the characteristic direction of 20° on the left side and roughly 0° elsewhere.

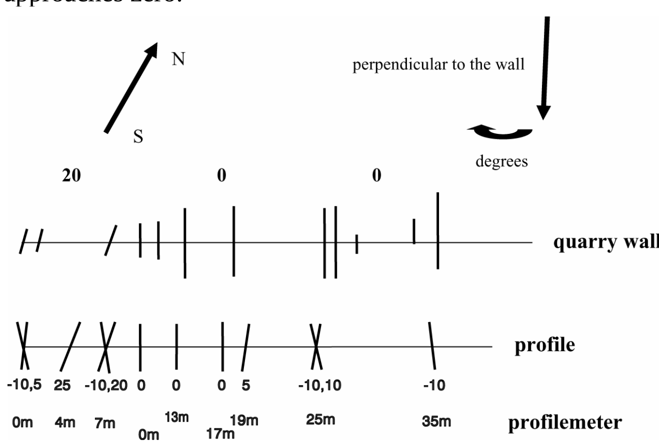

FIG. 13. Comparison of strike directions of the fractures, as observed directly on the wall and as inferred from the data along profile 2 by using the Schlumberger null-array. The length of the lines denote the significance of the fracture.

SUMMARY

Different pairs of geoelectric null-arrays and their classical counterparts were tested. Systematic field measurements were carried out in a karstic area. It has been shown that it is possible to get geologically meaningful results using null-arrays. The null-array anomalies, because of their physically meaningful spatial variability, provide useful information in finding vertical fractures in limestone basement. It is especially worth emphasizing that the null-array anomalies do not decay with depth as quickly as the classical array anomalies do. At the same time, by using null-arrays the strike direction of the fractures is given by sharper and narrower minimum zones with azimuthal response profiles than are obtained using classical arrays. Therefore, joint use of classic arrays and their corresponding null arrays provides complementary information about subsurface structure.

ACKNOWLEDGEMENTS

The field test was made within the framework of bilateral co-operation between the Geodetic and Geophysical Research Institute at Sopron (Hungary) and the Centre of Hydrogeology Neuchâtel (Switzerland), supported by the Swiss National Research Foundation under the title "Developments in electromagnetic geophysics" (1995–1998). The authors are grateful to the referees, among them Gregory N. Tsokas and to Associate Editor Mark Everett who improved the quality of the paper.

REFERENCES

Barker, R. D., 1979, Signal contribution sections and their use in resistivity studies, Geophys. J. Roy. Astr. Soc., 39, 123–129.

Brizzolari, E., and Bernabini, M., 1979, Comparison between Schlumberger electrode arrangement and some focused electrode arrangements in resistivity profiles, Geophys. Prosp., 27, 233–244.

Dey, A., and Morrison, H.F., 1979, Resistivity modelling for arbitrary shaped three-dimensional structures, Geophysics, 44, 753–780.

Gupta, R. N., and Bhattacharya, P. K., 1963, Unipole method of electrical profiling, Geophysics, 28, 608–616.

Habberjam, G. M., and Watkins, G. E., 1967, The use of a square configuration in resistivity prospecting, Geophys. Prosp., 15, 445–467.

Jakosky, J. J., 1960, Exploration geophysics, Newport Beach, California Mathias, M. J. S., and Habberjam, G. M., 1984, A field example of the use of anisotropy parameters derived from resistivity soundings, Geophys. Prosp., 32, 725–739.f

Militzer, H., Rsler, R., and Lsch, W., 1979, Theoretical and experimental investigations for cavity research with geoelectrical resistivity methods, Geophys. Prosp., 27, 640–652.

Pracser, E., 1999, Annual report about the activity of the geoelectric laboratory in 1988. 3D d.c. modeling, Internal report, Etvs Lornd Geophysical Institute, Budapest (in Hungarian)

Spitzer, K., 1998, The three-dimensional DC sensistivity for surface and subsurface sources, Geophys. J. Int., 134, 736–746.

Szalai, S., 1993, Multielectrode DC measurements for leakage monitoring. Diplom work. Etvs Lornd University, Budapest (in Hungarian)

Szalai, S., and Szarka, L., 2000, An approximate analytical approach to compute geoelectric dipole-dipole responses due to a small burried cube. Geophys. Prosp., 48, 871–885.

Szarka, L., 1991, Detectability of high-conductivity plates by the CSAMT method on basis of analogue modelling results. - An interesting analogue modelling experince, Acta Geod. Geoph. Mont. Hung., 26, 273–285.

Szarka, L., 1994, Three-dimensional electromagnetic imaging. Dissertation for the degree Doctor of the Academy. Geodetic and Geophysical Research Institute of the Hungarian Academy of Sciences, Sopron, Hungary (in Hungarian)

Szarka, L., and Menvielle, M., 1999, A possibility for an enhanced 3D parameter-sensitivity - the keyhole imaging, Geophys. Prosp., 47, 59–71.

Szarka, L., and Nagy, Z., 1992, A possibility of an electromagnetic technique to locate oil reservoir boundaries on basis of analogue modelling experiments, Acta Geod. Geoph. Mont. Hung., 27, 131–138.

Tsokas, G. N., Tsuorlos, P. I., and Szymanski, J. E., 1997, Square array resistivity anomalies and inhomogeneity ratio calculated by the finite element method, Geophysics, 62, 426–435.

Zwahlen F., and Doerfliger, N., 1995, Swiss report, COST 65 Action, Hydrogeological aspects of groundwater protection in karstic areas, in: Final report of the COST 65 action (European Comission, Directorate General Science, Research and Development).

APPENDIX A
OUR NUMERICAL MODELING SOFTWARE

The software developed by Prácser (1999) is based on the approach by Dey and Morrison (1979).

The differential equation describing the potential U (x,y,z) due to a point source in three-dimensional case is:

$$div\left[\sigma(x,y,z)\,\mathrm{grad}U(x,y,z)\right] = -I\delta(x_0,y_0,z_0)\,. \qquad \text{(A-1)}$$

This equation is solved for the nodes of a three-dimensional grid. Among a node and its the six neighboring nodes there is a linear relationship (Dey and Morrison 1979) as follows:

$$\iiint_{V_{i,j,k}} div(\sigma\,\mathrm{grad}U)\,dx\,dy\,dz = \iint_{S_{i,j,k}} \sigma\,\mathrm{grad}U\,ds\,\cdot \qquad \text{(A-2)}$$

The surface planes of the body $V_{i;j;k}$ are the median planes of distances connecting the node (*i*; *j*; *k*) with its neighbours, and $S_{i;j;k}$ is the total surface of this body. As boundary conditions the well-known boundary condition for the surface and the boundary condition for the domain boundaries is applied as

$$\alpha U + \beta \mathbf{n} \operatorname{grad} U = \gamma , \qquad \text{(A-3)}$$

where **n** is a unit vector, perpendicular to the domain boundary, the values of α, β and γ can be determined from value of U in case of homogeneous half-space. Equations (A-2) and (A-3) yield a system of linear equations, and the elements of its solution vector are the values of the potential function in the nodes.

The FORTRAN code is solved in iterations, by using the preconditioned conjugated gradient method.

Paper 7

Environmental and Engineering Geophysical Society European Section Editor-In-Chief

Technical University Berlin
Prof: Dr: Ugur Yaramanci
Dept. of Applied Geophysics
Ackerstr.: 71-76, 13355 Berlin, Germany
Tel.: +49-30-314 72599, Fax: +49-30-314 72597
E-mail: yaramanci@/u-berlin.de

Angewandte Geophysik. TU Berlin
Sekr. ACK 2 . Ackerstraße 71 - 76 D - 13355 Berlin

Frank Bosch
Centre of Hydrogeology, University of Neuchâtel
Rue Emile Argand 11
CH-2000 Neuchâtel, Switzerland

☎ (030) 314 72599 ☎ (030) 314-72627 (Secr.)
FAX (030) 314 72597 e-mail yaramanci@tu-berlin.de Az.: EJEEG-118-rec.doc

10.07.2002

Paper submission to EJEEG

Dear Frank Bosch,

herewith I would like to confirm the submission of your paper

BOSCH, F.P., MÜLLER, I.

CONTRIBUTION TO KARST GROUNDWATER VULNERABILITY MAPPING BY VLF-EM-GRADIENT SURVEY: COMPARISON WITH OTHER GEOPHYSICAL METHODS

to the "European Journal of Environmental and Engineering Geophysics". It has been given the reference number EJEEG-118 which you are asked to use in further correspondence.

We put your paper immediately into the reviewing process by at least 2 reviewers. We hope for a quick reviewing and will send you the reviewer comments very soon.

Thank you very much für your interest and submission by EJEEG.

Best regards

Ugur Yaramanci

Manuscript

Submitted to EJEEG 09.07.2002 via e-mail

Entrance confirmed on 10.07.2002

Reference-#: EJEEG-118

Contribution to karst groundwater vulnerability mapping by VLF-EM-Gradient survey:

Comparison with other geophysical methods

by F.P. Bosch[1] & I. Müller[2]

[1,2]Centre of Hydrogeology, University of Neuchâtel, Rue Emile Argand 11, CH-2000 Neuchâtel, Switzerland

[1]e-mail: frank.bosch@unine.ch

[2]e-mail: imre.muller@unine.ch

Abstract - The knowledge of the size, density and both orientation and vertical distribution of fractures as well as the opening and filling material or overburden thickness is a valuable contribution to estimate hydraulic conductivity and to evaluate vulnerability assessment and protection strategy of karst aquifers.

To obtain some of these parameters and to ascertain high permeability zones the Very Low Frequency-Electromagnetic Gradient (VLF-EM GRAD) method was applied together with Radio Frequency-Electromagnetics (RF-EM), Radiomagnetotellurics (RMT), Geoelectrical Tomography and refraction seismics over a karstic terrain in the Swiss Jura Mountains. In this area, karst springs infiltrate into a porous aquifer. This survey investigated the highly permeable karst structures, which provide fast water infiltration pathways into the karstic flow network. A dye tracer test validated the geophysical results. The results show particularly the efficiency and reliability of the VLF-EM GRAD method for high-resolution investigation at shallow depths and its potential for fast data acquisition over large surfaces at catchment area scale without ground contact.

KEYWORDS: Very Low Frequency-Electromagnetic Gradient method, environmental geophysics, fracture mapping, Karst aquifer vulnerability

1 INTRODUCTION

In Switzerland, many porous aquifers are in hydraulic connection with karst groundwater. Therefore, the investigation of permeable near surface karst structures is a contribution to both the vulnerability to contamination of karst as well as of porous aquifers. In the presence of overburden, direct methods do not allow extensive mapping of the orientation and density of karst structures from the surface. Even if some outcrops exist, direct surface observations do not provide information on layer thickness and fracture distribution at greater depths. Geophysical surveys may help solving this problem. Considering both the very heterogeneous nature of karst and particularly of epikarst (0 -20 m depth) (Mangin 1975; Kiraly 1995) as well as the requirements of hydrogeologists, geophysical methods applied to karst water research must fulfil certain criteria. The methods have to be appropriate for high-resolution investigation at shallow depths with fast data acquisition over large surfaces at catchment area scale. The geophysical research applied to karst aquifers at the Centre of Hydrogeology Neuchâtel (CHYN) is focused on the development of electromagnetic (EM) methods, which fulfil these criteria (Turberg 1994; Turberg & Barker 1996; Stiefelhagen 1998; Bosch & Gurk 2000; Szalai et al. xxxx).

In this paper, we present a case study from the Swiss Jura Mountains, where karst springs infiltrate into a porous aquifer used for the water supply of the village Buix (JU, Switzerland). We compare results from several near surface geophysical methods in order to describe their possibilities. We emphasize the new Very Low Frequency-Electromagnetic Gradient (VLF-EM GRAD, short: VLF-GRAD) method (Bosch & Müller 2001b) and compare the results with Radio Frequency-Electromagnetics (RF-EM), both being fast, ground-contactless mapping methods, sensitive to horizontal resistivity changes. Further comparison is made with the light weighted Radiomagnetotelluric (RMT) equipment and the Geoelectrical Tomography (also called: Geoelectrical Imaging method) being well-known resistivity methods and with refraction seismics. Finally, the survey results are validated by means of a hydrogeological dye tracer test. Two infiltration sites where chosen. According to the geophysical results, one site was forecasted as highly permeable and the other one as not particularly permeable.

2 THEORY & EQUIPMENT

In the following paragraphs, we give a brief theoretical background of the methods and equipment used in this case study starting with outlines of the principles of remote transmitter electromagnetics leading to the specific developments at CHYN. For the well-known methods like electrical imaging and refraction seismic, we mainly restrict ourselves to the explication of the equipment used.

2.1 Electromagnetic methods developed at CHYN

The electromagnetic (EM) methods developed at CHYN are enhancements of the traditional VLF technique (3-30 kHz), which uses signals of terrestrial radio transmitters, distributed around the world and mainly used for navigation purposes. Figure 1 illustrates the EM field distribution over a vertical conductive dike with transmitter direction parallel to the

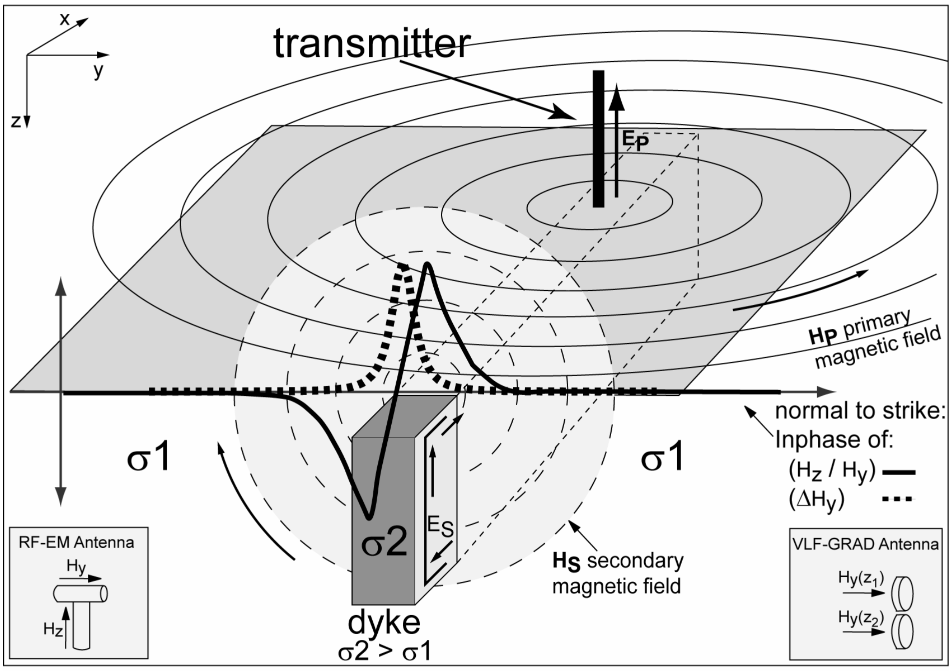

Figure 1 EM field distribution for VLF method in E-polarisation with theoretical signals over a vertical conductive dike; redrawn after Turberg & Müller (1992). Hz/ Hy according to Wannamaker et al. (1985); ΔHy calculated after Biot-Savart.

strike of the dike (E-polarisation). The transmitted, primary EM field consists of a *vertical electric field component* E_{Pz} and a *horizontal magnetic field component* H_{Py} perpendicular to the propagation direction x. At a distance of several wavelengths away from the source, the primary EM field components can be considered as horizontally travelling plane waves. While penetrating into the earth, the primary EM field induces a far smaller secondary EM field whose intensity depends on the ground's electric resistivity. The secondary EM field consists of a *horizontal electric field component* E_{Sx} and an associated magnetic field H_S which can be subdivided into a horizontal and a vertical component. One part of the secondary field oscillates "in-phase" and another part "out-of-phase" with respect to the primary field. The penetration depth of the primary field depends on the transmitter frequency and the electric resistivity of the ground. It can be estimated by the *skin depth* δ_{Skin} at which an electromagnetic wave is attenuated by a factor 1/e.

The different use of the various EM field components results in different geophysical methods. The CHYN electromagnetic equipment was developed with the intention to increase the horizontal and vertical resolution of the traditional VLF technique while benefiting from its advantage of light weighted devices for shallow-depth investigations. As a consequence, we focused on the additional use of the low frequency range (LF, 30-300 kHz) and continuous data recording and also introduced the measuring of the vertical gradient of the horizontal magnetic field components (Bosch & Müller 2001b).

2.1.1 Radiomagnetotellurics (RMT)

2.1.1.1 Resistivity soundings

CHYN's RMT device works within the frequency range of 12 to 240 kHz. It measures the local *horizontal resultant magnetic field component* H_{Ry} with an induction coil and the *secondary horizontal electric field component* E_{Sx} by means of a voltage drop between to electrodes placed in the ground. For a chosen *transmitter frequency* $f = (\omega/2\pi)$ with the *angular frequency* ω, it displays directly the *apparent resistivity* ρ_a of the ground and the *apparent phase* ψ_a between magnetic and electric field according to Tikhonov (1950) and Cagniard (1953) based on the *surface impedance tensor* **Z** for a layered 1D case and a *magnetic permeability* μ of 1:

$$\rho_{axy} = \frac{1}{\omega\mu}\left|\frac{E_{Sx}}{H_{Ry}}\right|^2 \qquad \text{with angular frequency:} \qquad \omega = 2\pi f \qquad (1)$$

and

$$\Psi_{axy} = \arctan\left(\frac{\operatorname{Im} Z_{xy}}{\operatorname{Re} Z_{xy}}\right) \qquad (2)$$

with surface impedance tensor element:

$$Z_{xy} = \frac{E_{Sx}}{H_{Ry}} \quad . \qquad (3)$$

By considering the effects of H- and E-polarisation cases, Fischer et al. (1983) and McNeill & Labson (1991) revealed the applicability of the VLF-R method to 2-D geological settings. The knowledge of apparent resistivity and phase enables the calculation of inversion models with magnetotelluric inversion codes. For further information concerning the RMT equipment, the reader is referred to the papers of Turberg et al. (1994) and Turberg & Barker (1996).

2.1.1.2 Resistivity Anisotropy

Besides resistivity soundings using different frequencies from transmitters sending from approximately the same direction, anisotropy information can also be gathered by using transmitters of similar frequencies sending from different orientations. The multi-direction RMT results are used for calculating anisotropy arrows according to Turberg (1994). For each sampling station an arrow is calculated with the value $\Delta\psi = \psi_{MAX} - \psi_{MIN}$ and the orientation of of the transmitter with ψ_{MIN}.

2.1.2 Radio Frequency-Electromagnetics (RF-EM)

2.1.2.1 Principle

The RF-EM method enables continuous profiling of resistivity contrasts at the *skin depth* δ_S without ground contact with two orthogonal induction coils as it only measures magnetic field components. The investigated parameters are the horizontal and vertical local resultant magnetic field components for a chosen *transmitter frequency* f. The *resultant field* H_R is the superposition of the *primary field* H_P and the *secondary field* H_S:

$$\mathbf{H}_R = \mathbf{H}_P + \mathbf{H}_S$$
$$\mathbf{H}_R = \left|\mathbf{H}_P\right| e^{i\omega t} + \left|\mathbf{H}_S\right| e^{i(\omega t - \varphi)} \quad (4)$$

with $\mathbf{H}_P >> \mathbf{H}_S$, $\omega = 2\pi f$ and *phase shift* φ between the primary and secondary field. Due to far field conditions, H_P is considered as space-independent, while H_S forces H_R to depend on space, time and frequency. The magnetic field vectors possess the following components:

$$\begin{pmatrix} 0 \\ H_{Ry} \\ H_{Rz} \end{pmatrix} = \begin{pmatrix} 0 \\ H_{Py} \\ 0 \end{pmatrix} + \begin{pmatrix} 0 \\ H_{Sy} \\ H_{Sz} \end{pmatrix} \quad (5)$$

Because of $H_P >> H_S$, H_{Sy} is neglected and the measured local, horizontal component is simplified as primary field, while only the secondary field, dependent on the electrical properties of the ground, contributes to the vertical component.

With (4) and (5), the vertical component of the time invariant part of the measured resultant field is as follows:

$$H_{Rz} = H_{Sz} = \left|H_{Sz}\right| e^{i\varphi} = \left|H_{Sz}\right| \cos\varphi + i\left|H_{Sz}\right| \sin\varphi \quad (6)$$

where the real part of equation (6) describes the component of the secondary field oscillating "in-phase" with the primary field (called inphase) and the imaginary part the component oscillating "out-of-phase" (called quadrature). The typical inphase signal over a vertical conductive structure in E-polarisation is illustrated in Fig. 1 where the inflection point of the curve indicates the horizontal dike position.

2.1.2.2 Equipment

CHYN's RF-EM equipment works in the frequency range from 15 – 300 kHz. It stores the inphase and quadrature of the ratio of (H_Z/H_Y) on a data-logger with a sampling frequency of 1 or 4 Hz. Real time visualization on a PC is possible. The mathematical sign of the signals behaves according to the coordinate system definition used by Wannamaker et al. (1986), and Steiner et al. (1992). The RF-EM system can be used with a handheld antenna as well as with a self-orientating automatic antenna for application with a vehicle (Stiefelhagen 1998).

In karstified limestone with its typical resistivity of several hundred Ωm, the frequencies used by our RMT and RF-EM devices have skin depths of about 10-100 m.

2.1.3 Very Low Frequency-Electromagnetic Gradient (VLF-EM GRAD)

In order to enhance the resolution of the RF-EM device, in particular for investigating small structures of the epikarstic zone (0-20 m depth), we developed an antenna, which measures the vertical gradient of the local horizontal magnetic field component. As known from magnetics and gravimetry, gradient measurements enhance the discrimination of neighbouring anomalies, magnify near-surface features and reduce noise (Millitzer & Weber 1984; Telford et al. 1990). Spitzer et al. (2000) illustrate an example where magnetic field gradient measurements in a borehole are applied to magnetotellurics in order to avoid measuring the generally disturbed electric field. Sattel & Macnae (2001) showed both theoretically and in a case study the resolution increasing and noise reducing advantages of gradient measurements applied to transient electromagnetic surveys.

2.1.3.1 Principle

Generally, for the RF-EM method H_{Sy} is neglected in equation (5). For the gradient method, this is quite the contrary. There we are particularly interested in that parameter. The difference of the local, resultant horizontal magnetic field component at two different altitudes above the ground is:

$$\Delta H_{Ry} = H_{Ry}(z_2) - H_{Ry}(z_1) \qquad (7)$$

According to the chosen coordinate system in Fig. 1 (z positive downwards), it is:

$$H_{Ry}(z_1) < H_{Ry}(z_2) \qquad (8)$$

Furthermore, due to far field conditions the primary magnetic field is independent of the altitude z:

$$\left|H_{Py}\right| \neq f(z) \qquad (9)$$

This yields together with equation (5) and (7) to:

$$\Delta H_{Ry} = (H_{Py} + H_{Sy}(z_2)) - (H_{Py} + H_{Sy}(z_1))$$

$$\Leftrightarrow \qquad \Delta H_{Ry} = H_{Sy}(z_2) - H_{Sy}(z_1) \qquad (10)$$

From equation (10) ΔH_{Ry} is determined exclusively by the secondary magnetic field, which is caused by the conductivity properties of the ground.

As in equation (6) the time-invariant part of the measured gradient can be separated into a real and an imaginary part with the *phase* φ between the primary and secondary field:

$$\Delta H_{Ry} = \left|H_{Sy}(z_2) - H_{Sy}(z_1)\right| \cos\varphi + i\left|H_{Sy}(z_2) - H_{Sy}(z_1)\right| \sin\varphi \qquad (11)$$

with Re{ΔH_{Ry}} = Inphase and Im{ΔH_{Ry}} = Quadrature.

Fig. 1 shows schematically the ΔH_{Ry} inphase signal over a conductive dike. Fig. 2 presents calculated EM responses to a line current, as a simple approximation of the effect from a conductive dike, for (a) the quadrature of (H_z/H_y) and (b) H_y and dz(H_y(z)). As known e.g. from McNeill (1990), the vertical H_z component has a dipole-like signal with its inflection point over the conductor, while the horizontal H_y component features a peak over the structure. Furthermore, the signal width of the gradient is much narrower than of (H_z/H_y). This increases the resolution of neighbouring anomalies and the separation of their superimposed signals. Following the defined coordinate system used in Wannamaker et al. (1986), in E-polarisation the gradient inphase peak should be a local maximum over a vertical electric conductive structure and a local minimum over a resistive one. Since the quadrature signal shape is influenced by a variety of factors, e.g. just a thin conductive overburden resulting in an inverted signal (McNeill 1990; Chouteau et al. 1996), it is difficult to draw the same general conclusions from quadrature curves. Furthermore, the strength of a resistivity contrast as well as a strong deviation from E-polarisation case and 3D structures have a strong influence on the curve shape.

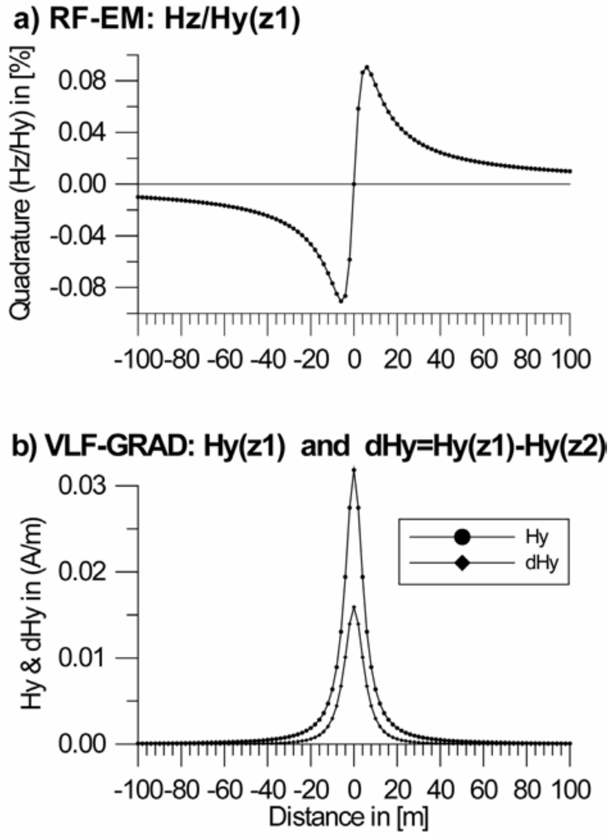

Figure 3 EM responses to a line current of 1 Ampere: a) line current approximation of RF-EM quadrature data calculated with rational polynomials; b) $H_y(z_1)$ and $dH_y=H_y(z_1)-H_y(z_2)$ after Biot-Savart with z_1=5m and z_2=10m.

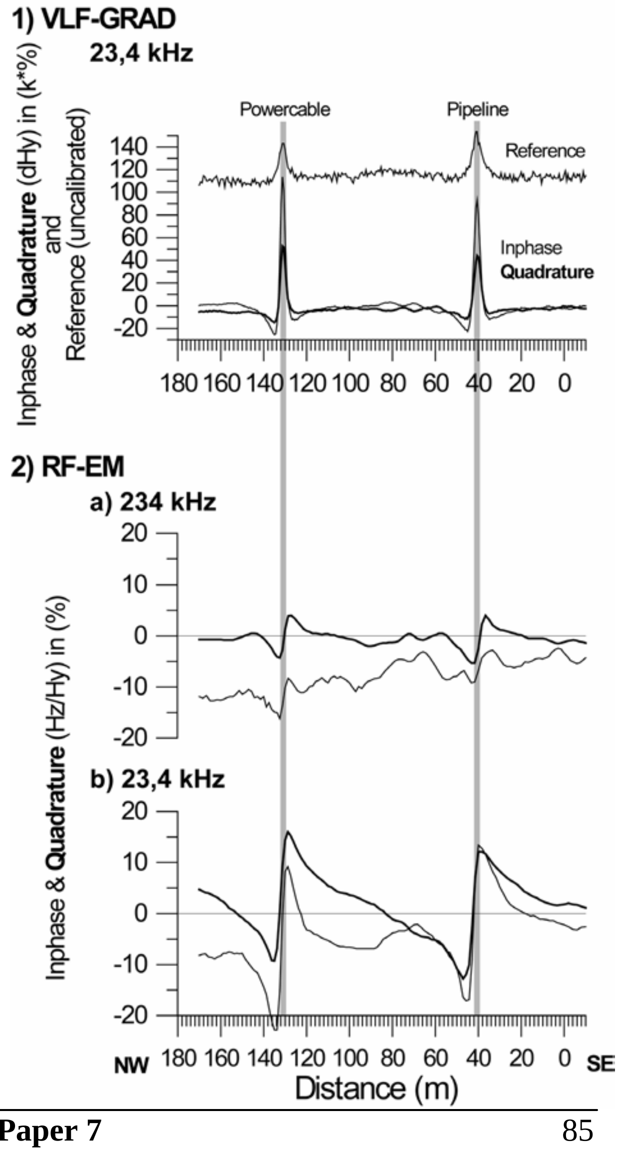

Figure 3 Comparison of VLF-EM GRAD and RF-EM over a buried powercable and a pipeline. 1) VLF-GRAD reference, inphase and quadrature signal, transmitter-frequency (Tr-f): 23.4 kHz, transmitter-direction (Tr-Dir): 5°N and data-logger-sample-frequency (DLS-f): 1 Hz. 2) RF-EM inphase and quadrature signals measured with automatic antenna: 2a) Tr-f: 234 kHz, Tr-Dir: -3°N, DLS-f: 1 Hz; 2b) Tr-f: 23,4 kHz, Tr-Dir: 5°N, DLS-f: 1 Hz

2.1.3.2 Equipment

The first VLF-EM-GRAD prototype device is based on the RF-EM equipment and measures continuously and simultaneously for a chosen frequency between 15-25 kHz the local, horizontal magnetic field component at two different altitudes above the ground with two induction coils (Bosch & Müller 2001b). The centres of the coils are separated by 1 meter. Inphase and quadrature of the signal differences between upper and lower induction coil (equation 11) is stored to a datalogger with 1 or 4 Hz sample rate in percent of the average horizontal field multiplied with a *device specific amplification factor* k. Further specifications may be found in Bosch & Müller (2001a) and Bosch & Müller (2001b).

Measured data of an approximation of the above-mentioned synthetic line current case are presented in Fig. 3. VLF-GRAD data (23.4 kHz; 5°N) are compared with RF-EM data (23.4 kHz; 5°N and 234 kHz; -3°N) sampled on a profile (orientation 124°N) crossing a buried power cable (orientation 57°N) and a pipeline (orientation 43°N). The GRAD data show sharp peaks with their maxima exactly at the position of these artificial structures at 40 and 131 m. The asymmetric deformation may result from the slight deviation from E-polarisation. Although the distance between cable and pipeline amounts 90 m, the two RF-EM signals in the VLF range are still superimposed, while the VLF-GRAD signals are obviously separated just like the RF-EM signals in LF range.

2.2 Electrical Imaging

2-D electrical imaging (or tomography) surveys for mapping the resistivity of areas with moderately complex geology has become more and more popular during the last years (Griffiths et al. 1990; Barker 1992; Griffiths & Barker 1993). Therefore, a deeper theoretical insight is not given here.

As opposed to traditional geo-electric soundings, a large number of electrodes connected to a multi-core cable and controlled by a computer are used for electrical imaging. This enables horizontal mapping and vertical sounding at the same time, providing resistivity pseudo-sections. Any array known from traditional surveys may be used. Field equipment and inversion software is commercially available and offered by a variety of companies.

For the imaging survey presented in this paper, we used the GEOPULSE TIGRE RESISTIVITY METER (Campus International Products Ltd.) with a 32-electrode multi-core cable with 5 m unit electrode spacing. The 2-D inversions have been calculated with the program RES2DINV (Loke & Barker 1996).

2.3 Seismics

For the seismic measurements, we used the 24-channel "OYO-McSeis170" with 40 Hz geophones and a geophone spacing of 5 m together with a seis-gun as seismic source. In this survey area the seismic velocities of the reached underlying layers are generally higher than of the upper ones (cover, epikarst, massive limestone). Therefore refraction seismics were applied.

2.4 Dye Tracer Test

Dye tracer tests are a common method in hydrogeology to investigate ground water flow directions and velocities and to determine aquifer properties. These information help e.g. delineating water protection zones. Tracers are injected at one or several locations of the investigation area (Käss 1998). Water samples are taken manually, with automated bottle samplers, or recently with flow-through field fluorometers at natural springs, boreholes or catchworks to measure the time variation of tracer concentration (breakthrough curve) as response to the injection.

Three tracers at two infiltration sites were used: Uranine (Na fluorescein), Tinopal CBS-X and Amidorhodamine G extra. According to Käss (1998), Uranine is a very conservative tracer among dye tracers due to its small sorptivity in neutral and alkaline media. Sulforhodamine B has a low sorptivity, while Tinopal is more sorptive. The used Amidorhodamine G extra is slightly more conservative than Sulforhodamine B (Wenger 2001). Therefore, Uranine is characterised by high recovery in karst and porous aquifers. Tinopal and Amidorhodamine G are good in karst but have low recovery in porous media. Tracer concentrations were measured at a spring with the high precision flow-through field fluorometer "GGUN-FL02" developed at the Institute of Geology Neuchâtel. Detailed description of the working principles can be found in Schnegg & Bossy (2001). A ray of bandpass filtered light excites the fluorescence of the dye and a detector yields an electric voltage of amplitude proportional to the fluorescence and therefore to the dye concentration. The used device is able to measure 2 dye tracers of different spectral characteristics continuously and simultaneously and stores the data on a data-logger with the operator-chosen sampling interval.

Additionally, an automatic bottle sampler was used at the spring in order to analyse the samples for all three dyes with the "Perkin-Elmer LS 50B" spectrofluorometer in the lab.

3 SURVEY AREA

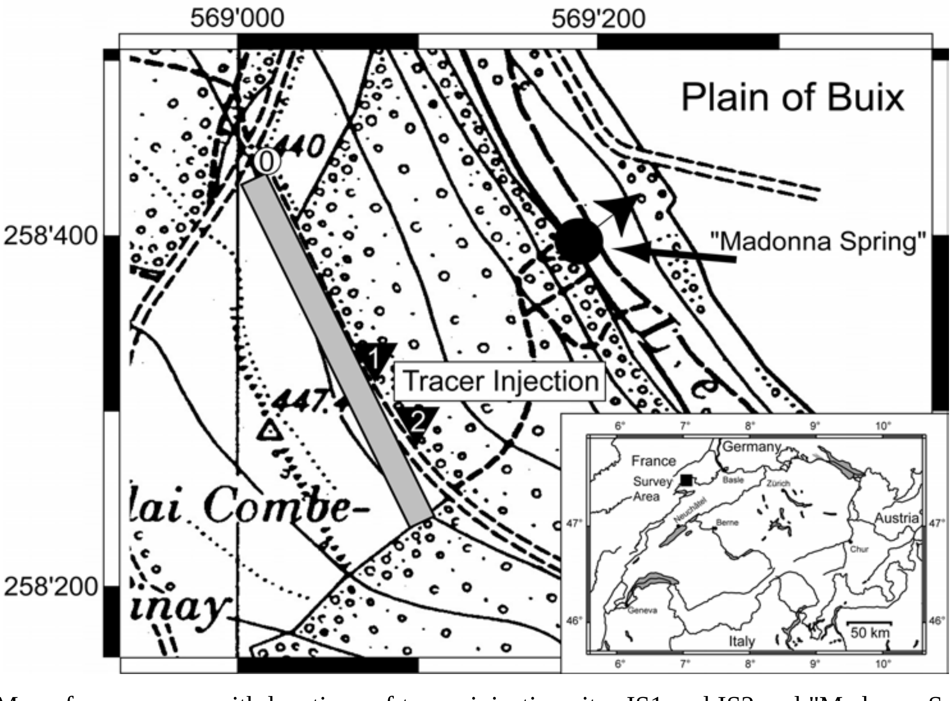

Figure 4 Map of survey area with locations of tracer injection sites IS1 and IS2 and "Madonna Spring". Grey rectangle indicates geophysical investigation area. Coordinates of Switzerland map in degrees North and East, coordinates of survey area map in Swiss Military Coordinates (metric coordinates in the Swiss system CH1903; Berne: 600'000 km / 200'000 km).

The survey area is located near the village Buix (Cant. Jura, Switzerland) in the Ajoie area of the Swiss Table Jura Mountains (Fig. 4). Fig. 5 shows a schematic geological cross section. The geophysical profiles and tracer infiltration sites are on top of the plateau in the west of the Allaine river valley, where Malm limestones (middle Oxfordian) with an average thickness of about 30 - 40 m are found. They overlie an up to 80 m thick marl sequence (lower Oxfordian). The upper 8 to 10 m of the limestone show up a strong degree of karstification (Liniger 1969; Liniger 1970). At the contact between limestone and marls, several springs discharge karst groundwater into the alluvial sediments of the Allaine river valley.

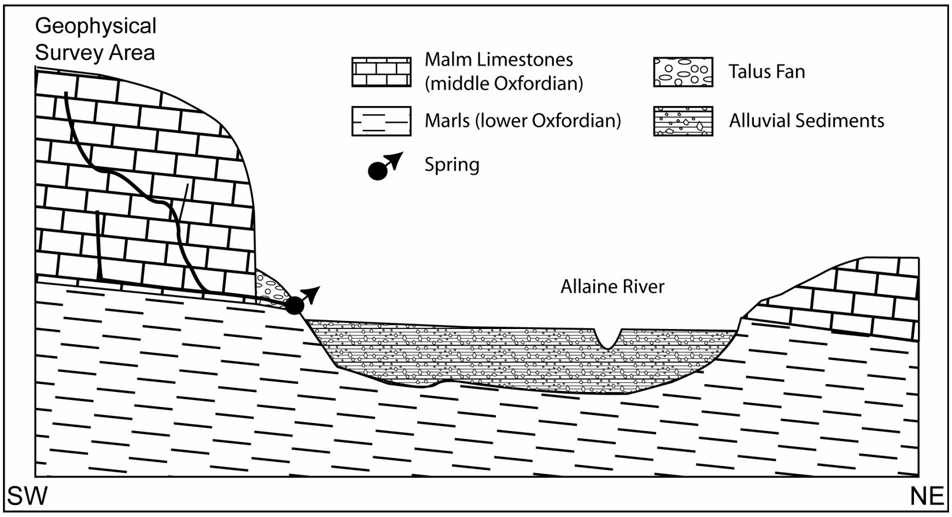

Figure 5… Schematic geological cut of Allaine River area without scale.

Three tectonic joint systems created a fracture grid, which separates the Ajoie region into narrow clods. These three fracture systems strike N-S (most important system), NW-SE and NE-SW (Liniger 1969; Liniger 1970) and correspond to the tectonic stress parameters and main strike directions of highly permeable karst structures in the Swiss Jura according to Kiraly & Simeoni (1971) illustrated in Fig. 6: sinistral shearing = 0°-10°N, σ1 = 130°-140°N and σ2 = 40°-50°N.

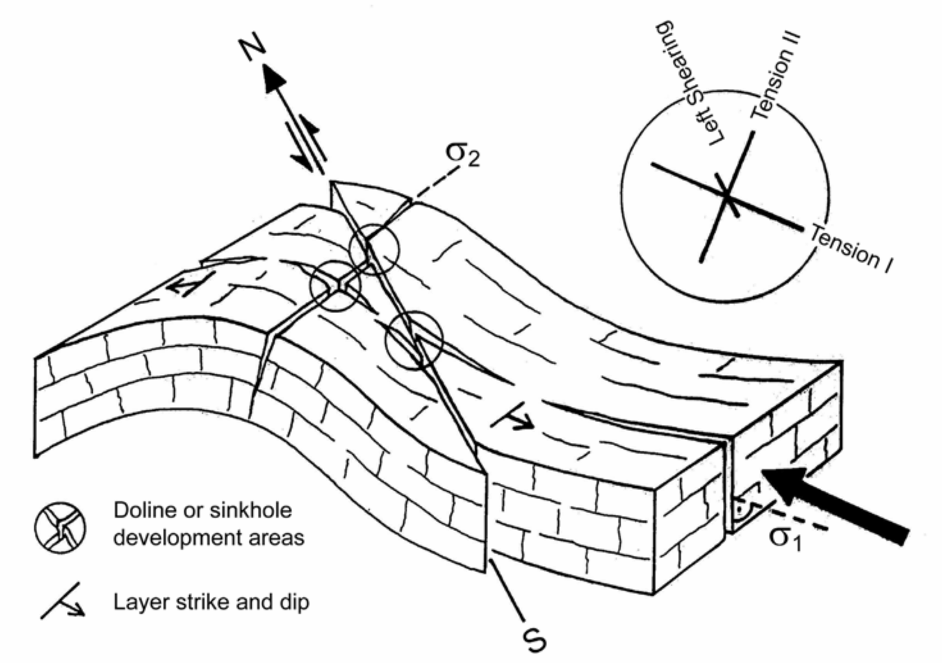

Figure 6 Main karstification orientations in the folded Swiss Jura following the tectonical stress parameters: sinistral shearing = N0°-N10°, σ_1 = N130°- N150°, σ_2 = N40°- N50° (redrawn after Müller (1981)).

4 DATA

The data were collected on a 230 m vs. 15 m surface on four parallel profiles with an orientation of about 155°N indicated by the grey rectangle in Fig. 4. The 0-point of the measurement coordinate system lies in the NE corner of the rectangle. "Profile 0m" is the eastern-most profile and mainly follows an agriculture path. The other three profiles are situated on a field with a profile distance of each 5 m.

4.1 VLF-EM GRAD

The VLF-GRAD data were collected over all four profiles with a data-logger frequency of 4 Hz. In order to have at least two polarisation directions, a "N-S transmitter" (23.4 kHz, 8°N) and a "NW-SE transmitter" (24.0 kHz, 114°N) were used.

4.2 RF-EM

As the VLF-GRAD data also the RF-EM data were collected over all four profiles with a data-logger frequency of 4 Hz. Two "N-S transmitters" in LF and VLF range (234 kHz, -8°N and 23.4 kHz, 8°N) were used. The measurements on "Profile 0m" were carried out with the automatic antenna system (good inphase signal quality), whereas the measurements along the other profiles were done with the hand-held antenna (noisy inphase signal).

4.3 RMT

4.3.1 Resistivity soundings

RMT resistivity soundings were performed over the reference profile "Profile -5m" every 5 m with three "N-S transmitter" frequencies from LF to VLF range (183 kHz, -10°N; 77.5 kHz, 36°N; 23.4 kHz, 8°N) with an electrode spacing of 5 m. The chosen frequencies have skin depths of respectively 17, 25 and 46 m for a ground resistivity of about 200 Ωm and about 52, 80 and 146 m for a resistivity of about 2000 Ωm. 1-D inversions were calculated for each sounding according to Fischer et al. (1981) and put together to a pseudo section.

4.3.2 Resistivity anisotropy

To obtain information on anisotropy, three frequencies of different directions in the LF range (183 kHz, -10°N; 171 kHz, 40°N; 162 kHz, 102°N) were measured at the RMT stations between 80 m and 200 m along "Profile -5m".

4.4 Geoelectrical tomography

The Electrical Imaging system was used with a 32-electrode cable over the central part of "Profile -5m" (50 to 205 m) with electrode spacing of 5 m. Wenner-Schlumberger, Schlumberger and Dipol-Dipol arrays were applied. In this paper, we only present the Dipol-Dipol results. Wenner-Schlumberger and Schlumberger results were of minor quality as a consequence of their poorer sensitivity for vertical inhomogenities.

4.5 Refraction seismics

Shooting points for the refraction seismics were located at 65 m and 190 m on "Profile -5m" with 24 geophones separated by 5 m. First arrivals were picked manually.

4.6 Dye tracer experiment

The two infiltration sites (IS1 and IS2, Fig. 4) for the dye tracer experiment have been chosen on "Profile 0m" according to the geophysical results at 127 m (IS1) and 180 m (IS2). At 127 m 200 g Uranine and 50 g Tinopal CBS-X and at 180 m 50 g Amidorhodamine G extra were injected. Additionally 3 m^3 of water were used for flushing. The injections took place at IS1 on 01.05.2001 14:20 h and at IS2 on 14:35 h. Sampling at "Madonna Spring" with the flow-through field fluorometer began about one hour prior to the injection at 13:30 h and continued for three days until 04.05.2001 15:18 h. The bottle sampler worked from 01.05.2001 14:01 until 03.05.2001 1:01 h. The flow-through field fluorometer sampled in a 4-minute interval for Uranine and Tinopal. The bottle sampler took samples once an hour.

5 OBSERVATIONS

5.1 VLF-EM GRAD surface / contour map

As we would like to emphasise the mapping possibilities of the new VLF-GRAD method for near surface structures in karstic terrain, surface and contour plots of the quadrature component of 23.4 kHz (Tr-Dir: 8°N) measured on the four profiles are shown in Fig. 7.

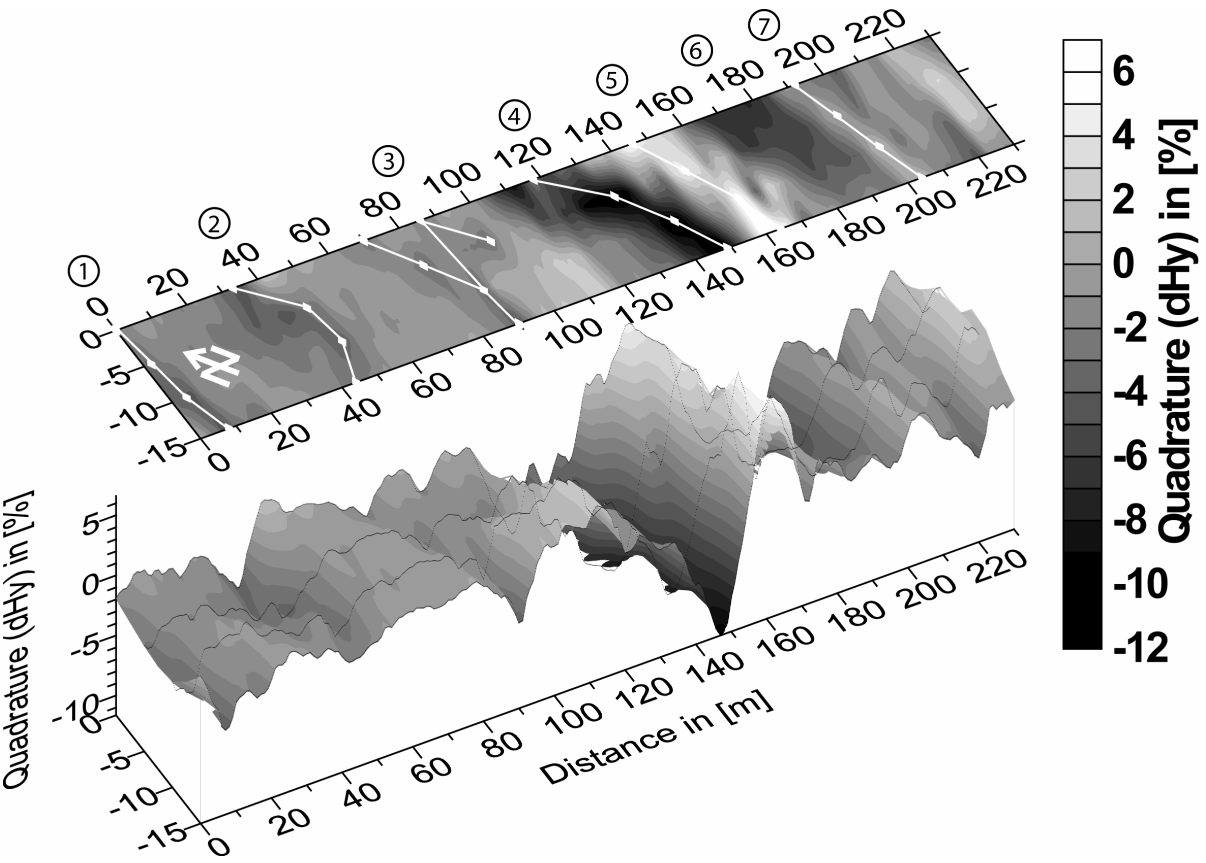

Figure 7 VLF-EM GRAD data: Contour- and surface maps of the Quadrature from 23.4 kHz radio transmitter sending from 8°N. White diamond-shaped symbols indicate quadrature-peaks connected by white lines. Most prominent anomalies are labelled.

Several lineamentic anomalies are visible. The most prominent ones are labled in Fig. 7 and will be called "GRAD#" in the following text. To visually emphasise the strike directions of the lineaments we indicated the quadrature peak positions with white diamond symbols and connected them with white lines. The most important anomalies are the quadrature minimum (=inphase maximum, GRAD4) followed by a maximum (GRAD5) in the centre of the survey area. GRAD4 e.g. crosses the area from 149 m on "Profile -15m" to 118 m on "Profile 0m" with a strike direction varying between 4°N in the SW part and -8°N in the NE part. This coincides with the strike direction of sinistral shearing in the Swiss Jura Mountains (Kiraly & Meia 1967), which is the strike direction of the most important fracture system according to Liniger (1970). The frequency of anomalies is about 40 m, with a general N-S orientation in the NW area of the main anomaly, and 20°N to 26°N orientation southeast of it. Additionally to these generally different orientations on both sides of the main anomaly zone, we also find sudden orientation changes or crossing points of anomalies. GRAD2 for instance, changes orientation from 24°N to -2°N, while GRAD3a and b strike with 2°N and 48°N (≈ σ_2) and cross each other at about 89 m of "Profile -10m". After anomaly GRAD7 we find 5 equidistant minima and maxima with an appearance frequency of about 10 m indicating an important amount of resistivity contrasts within a small area. This may indicate the presence of epikarst.

This particular strike direction pattern of the VLF-GRAD anomalies follows the main orientation of karstification in the Swiss Jura, as shown in Fig. 6. This suggests that the VLF-GRAD method is a powerful, ground-contactless method for detecting high permeability zones in karstic limestone at shallow depths. In the following paragraphs the gardient results are compared with the other methods with a detailed view on single profile data in order to confirm this hypothesis.

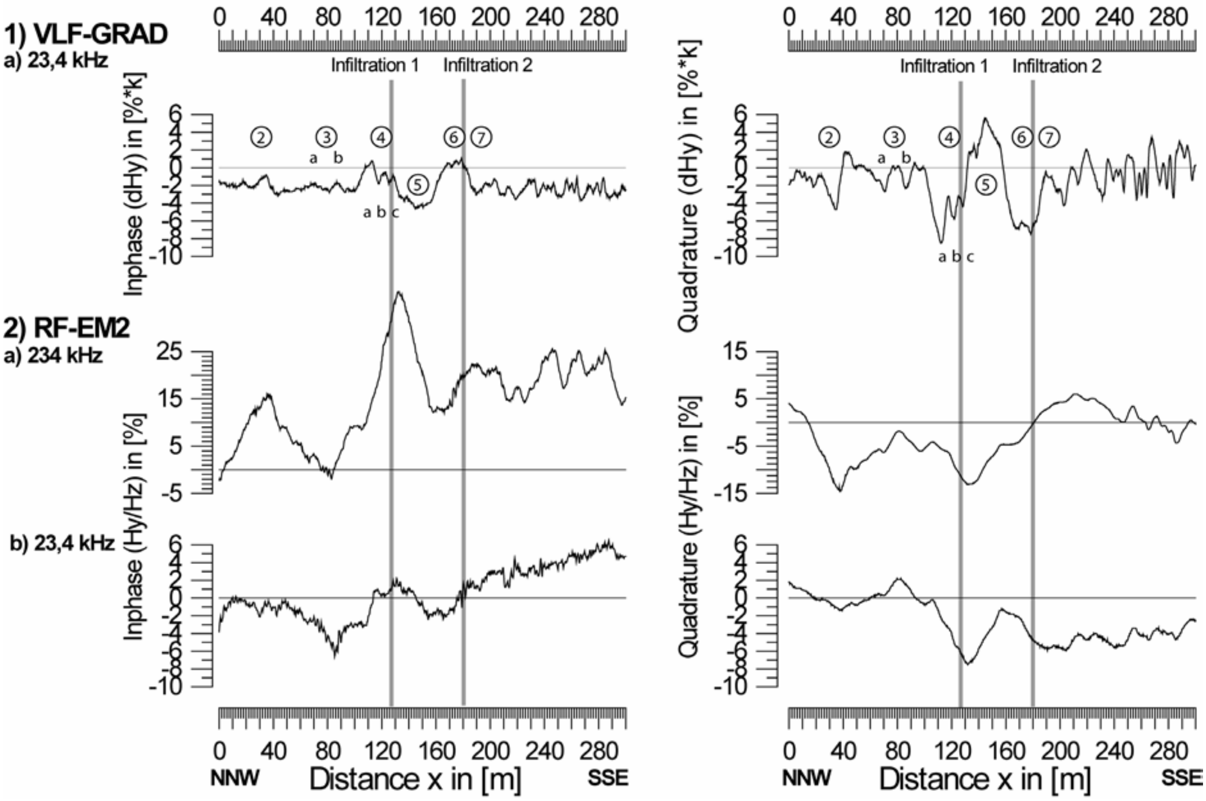

Figure 8 Comparison of VLF-EM GRAD and RF-EM data on "Profile 0m" with "N-S" orientated radio transmitters. Left side: inphase signals; right side: quadrature signals.

5.2 VLF-EM GRAD and RF-EM on "Profile 0m"

Fig. 8 compares inphase and quadrature of VLF-GRAD with RF-EM data in the LF and VLF range on "Profile 0m". This profile was easily to access by car, which enabled us to record the RF-EM data with the automatic RF-EM system. Therefore, even the inphase component of Hz/Hy is of high quality. The VLF-GRAD system even provides good quality data for inphase and quadrature with a handheld antenna. For both methods inphase and quadrature curves are inverse. This is commonly the effect of a conductive overburden (McNeill & Labson 1991).

More detailed than in Fig. 7, the single profile data in Fig. 8 represent the complex series of anomalies with positive and negative peaks in the gradient curves and their corresponding inflection points in the RF-EM curves. The anomaly pattern implies a rather complicated geological setting with a huge number of resistivity contrasts as can be assumed in karstified limestone. The anomaly labelling corresponds to Fig. 7. The GRAD data subdivide the major anomaly 4 (= wide inphase maximum/ quadrature minimum) with its centre at about 122 m into three peaks a to c. The RF-EM signals are superimposed and therefore an internal subdivision cannot be clearly distinguished. This shows the improved resolution of the GRAD data compared to RF-EM. Particularly from about 200 m until 290 m a harmonious series of quite narrow and sharp GRAD peaks is visible over a distance of 100 m. The appearance frequency is about 2 to 4 m in this zone. Such a high density of resistivity contrasts would fit well to the conceptual model of epikarst. As a matter of fact, epikarst crops out in this area along the profile. This anomaly pattern is more distinctive in the LF range of the RF-EM data than in its VLF range indicating the improved sensitivity of the gradient method for near surface structures. Obviously, the GRAD curves feature more details and facilitate the separation of anomalies compared to RF-EM.

When crossing dike-like geological structures in the case of E-polarisation, the mathematical sign of the inphase peaks may give a hint on the type of resistivity contrast (resistive or conductive structure). GRAD anomalies 4, 5 and 6 have almost a NS orientation according to Fig. 7. The 23.4 kHz transmitter, sending from 8°N, should therefore fulfil the E-polarisation case well enough. According to this, the GRAD inphase maximum of the major anomaly GRAD4 may indicate a relatively more conductive zone from about 100 m to 130 m. We assume that this zone is a high permeable fractured fault zone. From about 130 to 160 m a resistive zone (GRAD5) may follow, followed by another conductive zone until about 190 m (GRAD6). Since we do not cross these resistivity contrasts perpendicularly, the GRAD peaks are quite wide.

These assumptions are cross-validated in the following paragraphs by comparison with electrical resistivity distributions, as provided from methods such as RMT and Electrical Imaging as well as by refraction seismics and a hydrogeological tracer test.

5.3 VLF-EM GRAD, RMT and Electrical Imaging on "Profile -5m"

Fig. 9 compares inphase and quadrature of VLF-GRAD (23.4 kHz) with RMT and Electrical Imaging Data on "Profile -5m". The two tracer infiltration sites are indicated although they are situated on "Profile 0m".

5.3.1 VLF-EM GRAD

Compared to "Profile 0m" in Fig. 8 all gradient anomalies are moved to the east in Fig. 9. The main peak of anomaly "GRAD4" can be found at 133 m while it is at about 118 m on "Profile 0m".

5.3.2 RMT

We present the RMT raw field-data (apparent resistivity and phase) as well as a pseudosection of 1-D inversions. The three chosen radio transmitters (183 kHz, 77.5 kHz and 23.4 kHz) are approximately north-south orientated.

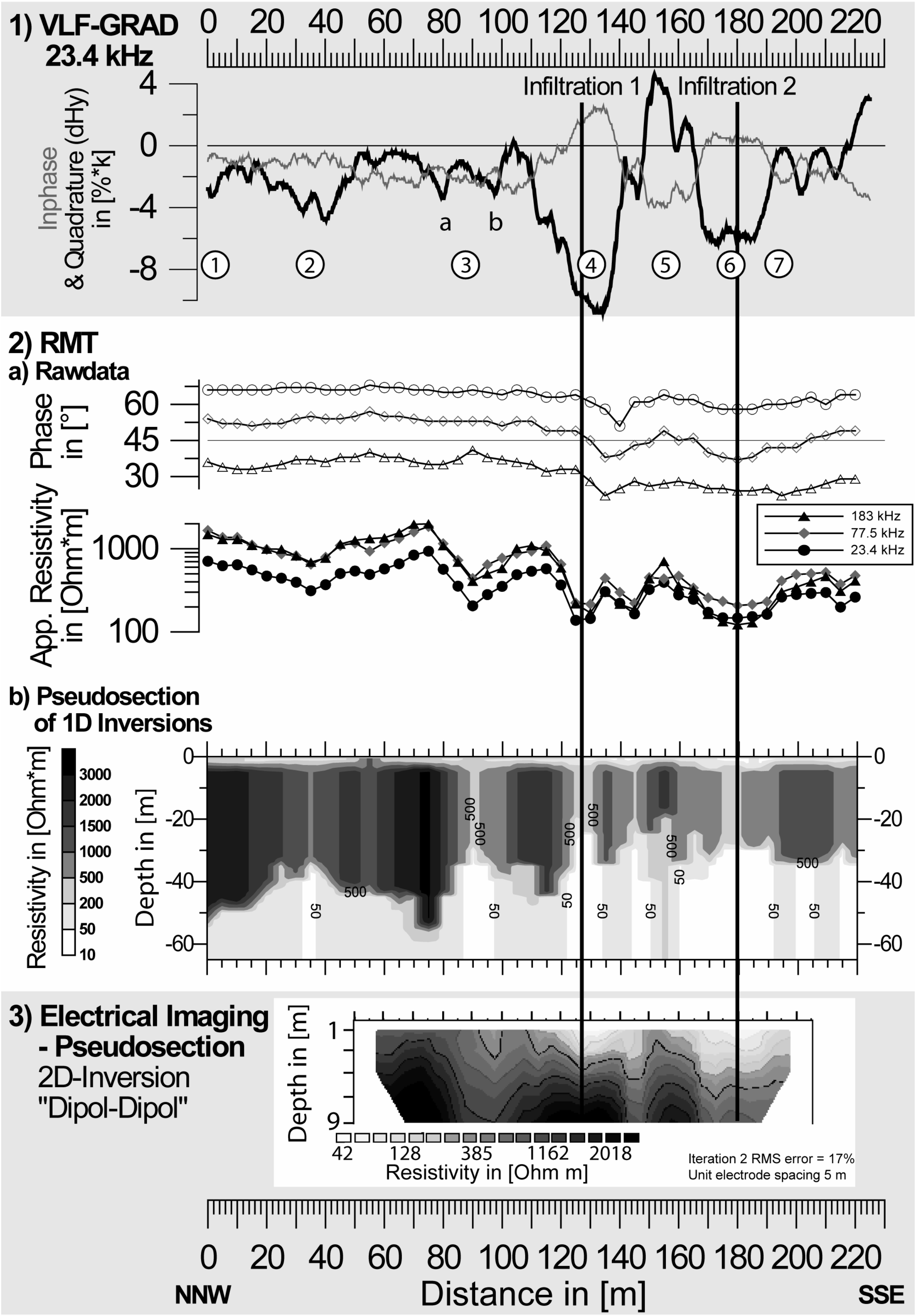

Figure 9 Data comparison on "Profile -5m": 1) VLF-EM GRAD inphase and quadrature of 23.4 kHz, 2a) RMT rawdata, 2b) Pseudosections of 1D Inversions after Fischer et al. (1981) and 3) Geo-Electric Tomographie 2-D inversion after Loke & Barker (1996) for Dipole-Dipole configuration with 5 m unit electrode spacing; IS1 and IS2 locations from "Profile 0m" are also indicated.

Already the raw data indicate a rather complicated geological situation featuring 2-D and 3-D structures. Therefore, the RMT pseudosection based on 1-D inversions should be more regarded as qualitative result than used for detailed conclusions.

The most important RMT anomaly was found between 120 and 150 m. The apparent resistivity of this zone is for all frequencies reduced and reaches a minimum value of 150 Ωm for the lowest frequency compared to the surrounding values of 1000 to 2000 Ωm. At the same time, a remarkable decrease in phase of about 10° is observed for all three frequencies. This behaviour of apparent resistivity and phase indicates E-polarisation for the chosen frequencies and therefore a mainly N-S orientation of this low resistivity structure. This confirms the conclusions drawn from the VLF-GRAD 23.4 kHz inphase maximum (GRAD4) at this position. It is interesting to observe the delayed position for the phase minimum, which occurs at 135 m for 183 kHz, 137 m for 77.5 kHz and finally 140 m for 23.4 kHz. This shows that the low resistivity structure is dipping to the SSE. Furthermore, the apparent resistivity slightly increases in the centre of this low resistivity zone and reaches the highest value of about 500 Ωm for the intermediate frequency used at 135 m. This may be the result of encapsulated air in a karst cavity. The following resistivity maximum at 155 m with the highest values for the highest used frequency is conform with GRAD5.

The other important RMT apparent resistivity decrease at 90 m is not obviously visible in the GRAD data. This may be explained by the fact that the RMT intermediate frequency 77.5 kHz indicates with its increasing phase a H-polarisation situation.

Generally the RMT data show a conductive overburden (about 50 Ωm) over a resistive layer (1000 to 3000 Ωm) followed by a low resistive half space (10- 200 Ωm). This data set is interpreted as quarternary sediments, limestone / karstified limestone and marls respectively. The presence of a conductive overburden explains the fact that all inphase and quadrature signals for both VLF-GRAD and RF-EM are inverse. The resistivity values are generally higher to the NNW of the main anomaly between 120 and 150 m than to the SSE. Furthermore, this anomaly indicates a vertical displacement step. The inversion results indicate the contact between limestone and marls at about 40 m depth NNW of the anomaly and at only 25 m depth SSE of it.

Worthwhile noticing is the low resistivity zone between 165 m and 195 m further on, coinciding with the wide anomaly GRAD6. While we assume a permeable fracture zone at GRAD4 the RMT and imaging data suggest an impermeable zone in the area of GRAD6. This may be interpreted as clay-filled epikarst. The gradient data alone do not help to distinguish the nature of these two anomalies.

5.3.3 Geoelectrical tomography

The dipole-dipole configuration Electrical Imaging data are represented by a 2-D inversion. These data provide near surface information from 0 m to a depth of up to 8.5 m.

As the RMT data, also the 2-D inversion of the Electrical Imaging data shows strong variations of true resistivities in the upper 10 m. The root mean square error after two iteration steps is with 17 % still quite high but more iterations leaded to unreasonable high resistivity values.

While the imaging data generally confirms the resistivity distribution found with RMT, it suffers from its poor penetration depths and from its inability to follow vertical structures to greater depths. Particularly the RMT-inversion resistivity minimum (200 Ωm) of the main anomaly at 125 m reaching down to 25 m depth, is reflected by very low Imaging resistivities of only 40 Ωm for the first 3 m depth, but already 2000 Ωm at 8.5 m. The high resistivity values on both sides of this narrow vertical conductive zone may disable geo-electrics from following it to greater depths.

According to the working time required the RMT survey seems to offer more information than Electrical Imaging and is more appropriate for mapping vertical heterogeneities.

5.4 VLF-EM GRAD and Seismic on "Profile -5m"

Fig. 10 shows the first arrival times of the two seismic shots at 65 and 190 m on "Profile -5m" compared with the 23.4 kHz GRAD data. The information from seismics are conform

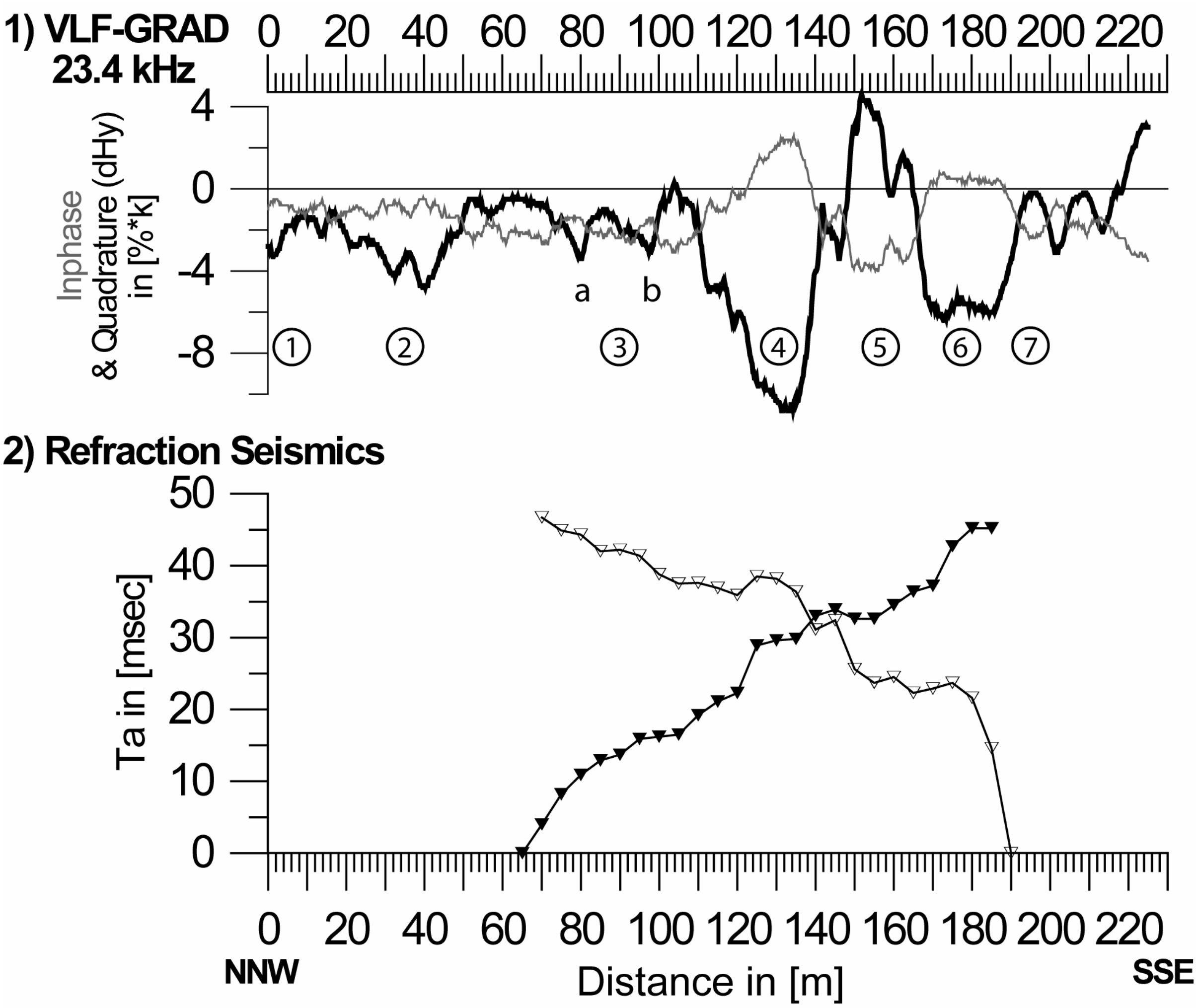

Figure 10 Comparison of (1) VLF-EM GRAD and (2) Refraction Seismics (Ta = first arrival time) on "Profile -5m". Filled triangles belong to shot 1 at 65 m, unfilled triangle to shot 2 at 190 m.

with those from the resistivity methods. The whole area seems to be subdivided into different blocks, separated by fractures as indicated by seismic travel time retardations. Seismic velocities are generally higher in the western part of the profile than in the eastern part, coinciding with higher electric resistivities in the west and lower resistivities in the east. In the central part of the profile, where we assume the main discontinuity zone to be due to the results from electromagnetic methods, the seismic data also show an increase in travel time. In detail we find two prominent travel time delays at 125 m and between 140 and 145 m which fit very well with the anomalies detected with the other methods. Another block border may be indicated by the travel time delay between 90 and 95 m, where RMT and Electrical Imaging also found decreased electrical resistivities.

5.4 Strike direction analysis with VLF-EM GRAD and RMT-Anisotropy

While the 23.4 kHz GRAD data showed mainly N-S strike directions, particularly for the main anomaly GRAD4, the RMT data also gave indications for W-E directions e.g. at 90 m on "Profile -5m". This is of particular interest because the "Madonna Spring" is situated east of our profiles. If the tracer is supposed to arrive at the spring, East-West connections within the karstic network should exist.

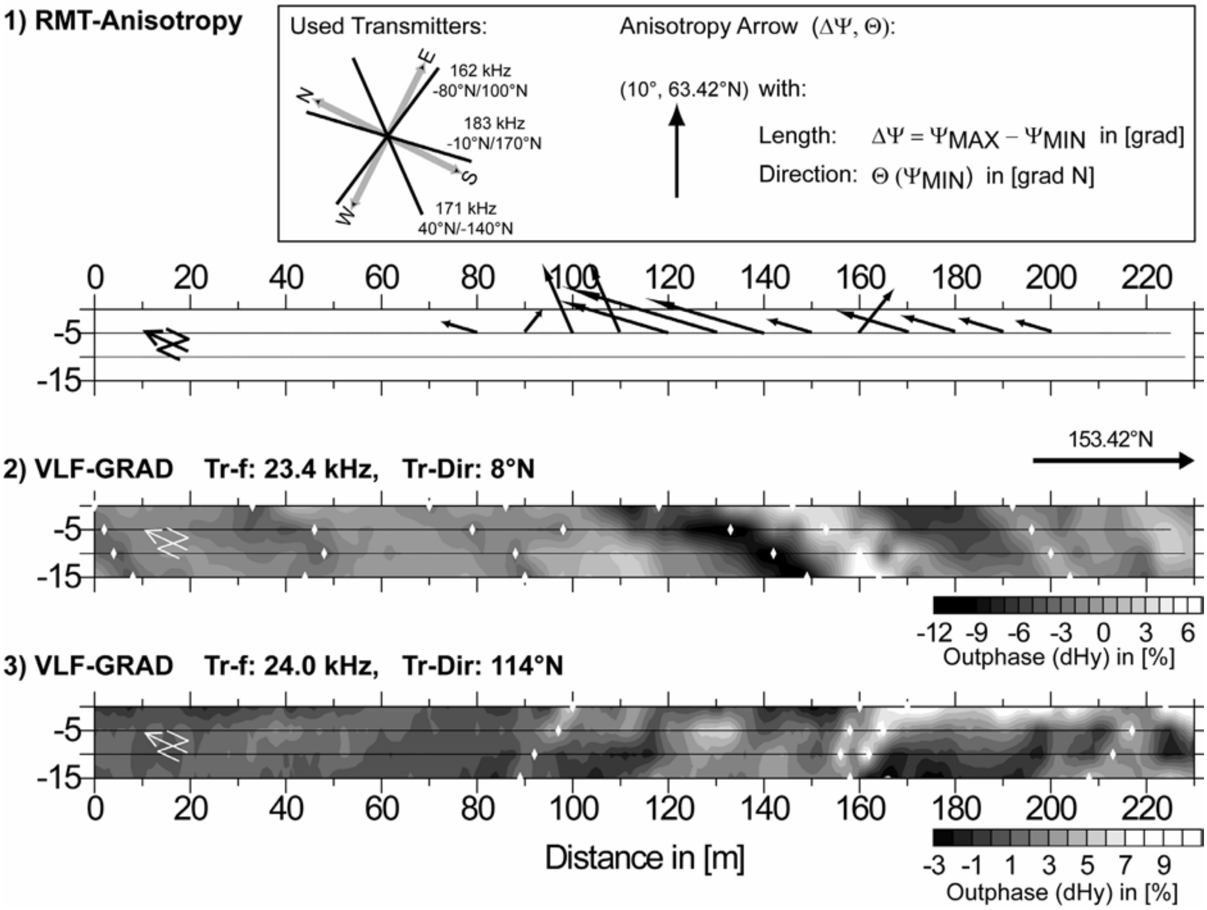

Figure 11 Strike direction analysis: (1) RMT-Anisotropy Arrows calculated according to Turberg (1994) and VLF-EM GRAD Quadrature contour plots of (2) 23.4 kHz / 8°N and (3) 24.0 kHz / 114°N radio transmitters.

To proof this, we carried out additional VLF-GRAD measurements along all profiles with the 24.0 kHz transmitter sending from 114°N. Contour plots of the outphases from 23.4 kHz and 24.0 kHz results are presented in Fig. 11 together with RMT anisotropy arrows on "Profile -5m". Lineamentic anomalies with strike directions varying between 88°N and 110°N are visible in the 24.0 kHz GRAD contour plot. They fit well with the anisotropy arrows at 90 m and 160 m deviating from the general N-S orientation. This explains that the 23.4 kHz GRAD measurements do not show any particular anomaly at the low resistitvity zones at 90 m, which was detected by the RMT and Electrical Imaging system. The orientation of this structure deviates too much from the E-Polarisation of the 23.4 kHz transmitter.

5.6 Dye Tracer Experiment

According to the geophysical results, we chose the two locations on "Profile 0m" at 127 m and 180 m as infiltration sites (IS1 and IS2) for the dye tracer experiment with sampling at the "Madonna Spring" (Fig. 4). IS1 is situated, where the geophysics located a major fault zone (GRAD4, Fig. 7 & 9). IS2 lies in a 30 m wide zone where the electric resistivity is between 50 and 200 Ωm up to a depth of 30 m (Fig. 9). This zone was interpreted as clay-filled low permeable epikarst and therefore the tracer should not arrive as

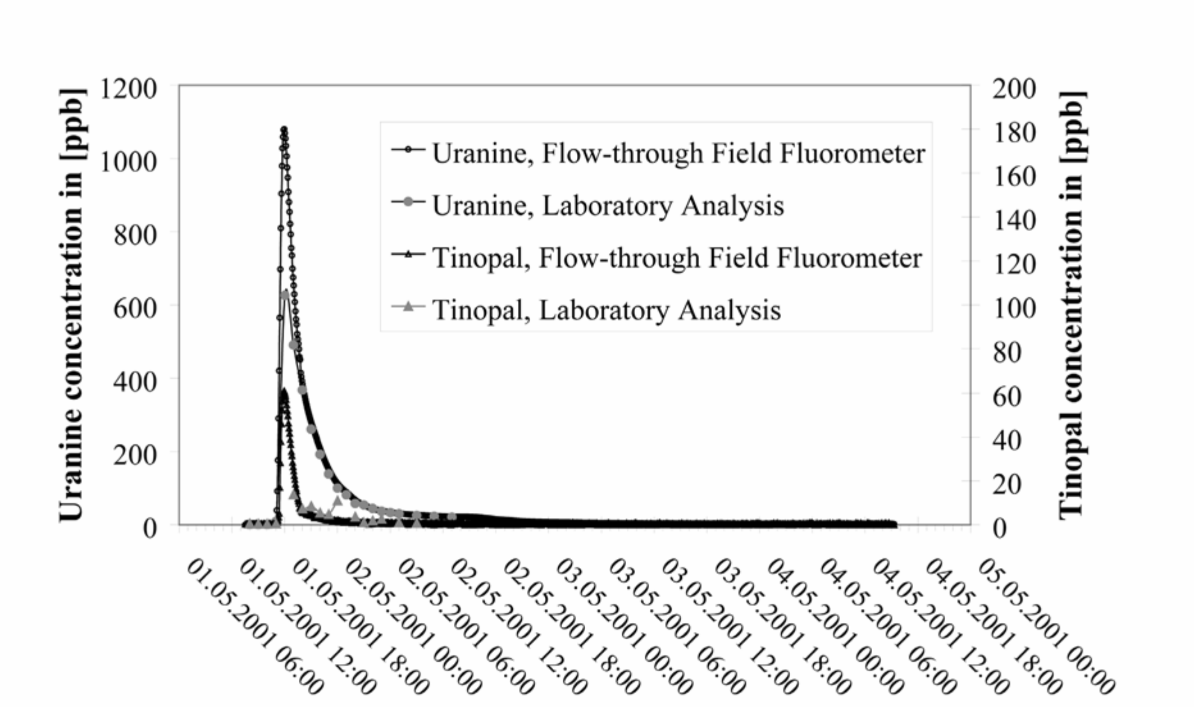

Figure 12 Breakthrough curves of dye tracer experiment sampled at "Madonna Spring".

fast as from IS1. Fig. 12 shows the break-through curves. Uranine and Tinopal injected at IS1 arrived 154 and 170 minutes respectively after injection. These times yield rather high maximum flow velocities of 55 m/h for Uranine and 50 m/h for Tinopal. Both tracers have sharp peaks and the concentrations decrease quite fast down to their background values. This behaviour is typical for fast flow paths in karst networks. The break-through curves derived from the sampled water, which was analysed in the laboratory, generally follow the curves of the field flow-through fluorometer, but they are noisier and the measured concentration maximum for Uranine is only half the concentration measured by the field fluorometer. For Tinopal the peak maximum was not even found. This demonstrates well the advantage of field flow-through fluorometers compared to bottle samplers. Amidorhodamine G extra injected at IS2 was not detected in any of the samples analysed in the laboratory.

6. CONCLUSIONS

The combined geophysical survey, verified by a tracer test, detected the most fractured and permeable zones at shallow depths, which contribute to fast infiltration into the karst flow channel network. It was possible to map a fault with vertical displacement and its accompanying fractures.

Particularly the RF-EM and VLF-GRAD method are able to collect fast resistivity contrast data over large areas. With its improved horizontal resolution, the VLF-GRAD method seems to be the best method to locate narrow-spaced fracture pattern. Crossing points of fractures and changes of strike direction are likely to be the most permeable locations (Fig. 6) and were detected by VLF-GRAD (Fig. 7 & 11). By using two perpendicularly orientated radio transmitters, the VLF-GRAD method detected the major N-S structures as well as the approximately E-W orientated second order structures in this survey area. The presence of the latter, provide the potential flow paths of the tracer down to the "Madonna Spring".

That measuring the gradient enhances the sensitivity for near surface targets, was clearly indicated by the fact, that the narrow-spaced structures were detected by the gradient method with VLF transmitters. The RF-EM method instead, detected these structures only in the LF range and even there not as obvious. To make use of the LF range also for the gradient method could therefore be promising for more detailed, very shallow depths investigation.

Since VLF-GRAD and RF-EM are only sensitive for resistivity contrasts, complementary information, allowing the estimation of the nature of the contrasts, is sometimes necessary. This information can be provided by RMT or Electrical Imaging. RMT is more appropriate for karst survey than Electrical Imaging for two reasons: The first reason is that the light weighted RMT equipment enables coverage of large areas with resistivity soundings several times faster than with the Geo-Electric Tomography, particularly in rough terrains with difficult access. The second reason is the high resolution of RMT for vertical conductive heterogeneities like fractures, faults or vertical contacts. A major problem for geo-electrics is the poor sensitivity to vertical heterogeneities. Dipol-Dipol electrode configuration can be used in this case, but it extremely reduces the investigation depths. Therefore, information of RMT and Imaging data can be combined in order to get information from near surface to greater depth, but Imaging remains too slow to perform extensive and fast surveys, which are possible with RMT.

That geophysical investigations can detect high permeability zones in karst was validated by the tracer injection at the infiltration site IS1 ("Profile 0m", 127 m). With IS2 ("Profile 0m", 180 m) we wanted to show an example for an impermeable zone and as a matter of fact the dye Amidorhodamine G extra (ARGe) injected at IS2 was not recovered at the spring within the sampling period. However, the missing of ARGe may have several reasons. According to the quite low electric resistivity values around IS2 (Fig. 9) from surface to circa 30 m depths over 35 m horizontal distance we interpret this zone as clay filled and therefore low permeable zone without any fast connection to the karst network. This explains particular the zero recovery at the spring according to the sorptive properties of ARGe. Tinopal instead, which is even more sorptive and was infiltrated at IS1, arrived at the spring because it had been quickly transported to the network. Another possibility might be that the fault zone represents a water catchment border and that there is simply no connection from IS2 to the network feeding the "Madonna Spring". To validate this hypothesis sampling at more springs would need to be done.

The ability of mapping highly permeable fracture zones in limestone is a valuable contribution to karst and porous groundwater vulnerability mapping and protection strategy. Particularly the continuously and ground-contactless measuring VLF-EM-GRAD method enables to quickly get information about fracture density, size of fractures and their orientation with high resolution over large areas.

7 ACKNOWLEDGEMENTS

This research was supported by grants from the Swiss National Science Foundation (Project No. FN20-53936.98). The authors are very indebted to Mr Jaques Duperrex (Chateau d'Oex, Switzerland) who built the electromagnetic equipment used in this study as well as Dr. Pierre Schnegg (Geological Institut of the University of Neuchâtel, Switzerland) who developed the flow-through field fluorometer.

8 REFERENCES

Barker, R.D., 1992. A simple algorithm for electrical imaging of the subsurface. First Break 10: 53-62.

Bosch, F. & Müller, I., 2001a. Nouveau développement dans la prospection géophysique électromagnétique. Le Very Low Frequency Electromagnetics - Gradient (VLF-EM-Grad), facilitant la cartographie des "zones sensibles" dans l'Epikarst et dans les aquifères fissurés. Proceed. of the 7éme Colloque d'Hydrologie en Pays Calcaire et en milieu fissuré, Besançon, 20.-22. Sept. 2001, Sci. Tech. Envir., Mém. H. S. n°13: 55-58, ISSN 0759-7517.

Bosch, F.P. & Gurk, M., 2000. Comparison of RF-EM, RMT and SP measurements on a karstic terrain in the Jura Mountains (Switzerland). Proceed. of the Elektromagnetische Tiefenforschung, Altenberg, Germany, 18, Deutsche Geophysikalische Gesellschaft: 51-59, ISSN 0946-7467.

Bosch, F.P. & Müller, I., 2001b. Continuous gradient VLF measurements: A new possibility for high resolution mapping of karst structures. First Break 19(6): 343-350.

Cagniard, L., 1953. Basic theory of the magnetotelluric method of geophysical prospecting. Geophysics 18: 605-635.

Chouteau, M., Zhang, P. & Chapellier, D., 1996. Computation of apparent resistivity profiles from VLF-EM data using linear filtering. Geophysical Prospecting 44: 215-232.

Fischer, G., Quang, B.V.L. & Müller, I., 1983. VLF ground surveys, a powerful tool for the study of shallow two-dimensional structures. Geophysical Prospecting 31: 977-991.

Fischer, G., Schnegg, P.A., Peguiron, M. & Le Quang, B.V., 1981. An analytic one-dimensional magnetotelluric inversion scheme. Geophysical Journal of the Royal Astronomical Society 67: 257-278.

Griffiths, D.H. & Barker, R.D., 1993. Two-dimensional resistivity imaging and modelling in areas of complex geology. Journal of Applied Geophysics 29: 211-226.

Griffiths, D.H., Turnbull, J. & A.I.Olayinka, 1990. Two-dimensional resistivity mapping with a computer-controlled array. First Break 8: 121-129.

Käss, W., 1998. Tracing Technique in Geohydrology. A.A.Balkema, Rotterdam, Netherlands.

Kiraly, L., 1995. Effect of the epikarst on the hydrograph of the karst springs. Bulletin d'hydrogéologie 14: 199-220.

Kiraly, L. & Meia, J., 1967. Observations tectoniques dans une carrière de Chaumont (Jura Neuchâtelois, Suisse). Société Neuchâteloise des Sciences Naturelles 90: 276-283.

Kiraly, L. & Simeoni, G., 1971. Structure géologique et orientation des cavités karstiques: la Grotte de "Chez le Brandt" (Jura neuch.). Bulletin de la Société neuchâteloise des Sciences naturelles 94: 91-97.

Liniger, H., 1969. Geologischer Atlas der Schweiz - Blatt 1065 Bonfol (Atlasblatt 55), Schweizerische Geologische Kommission, Bern.

Liniger, H., 1970. Erläuterungen zu Geologischer Atlas der Schweiz - Blatt: 1065 Bonfol (Attlasblatt 55), Schweizerische Geologische Kommission, Bern.

Loke, M.H. & Barker, R.D., 1996. Rapid least-squares inversion of apparent resistivity pseudosections using a quasi-Newton method. Geophysical Prospecting 44: 131-152.

Mangin, A., 1975. Contribution à l'étude hydrodynamique des aquifères karstiques. Annales de spéléologie 29: 283-329.

McNeill, J.D., 1990. Use of electromagnetic methods for groundwater studies. in Geotechnical and environmental geophysics, edited by S.H. Ward, Investigations in Geophysics, Volume 5, I: Review and tutorial, Society of Exploration Geophysicists, Tulsa, Oklahoma, USA: 191-218.

McNeill, J.D. & Labson, V.F., 1991. Geological mapping using VLF radio fields. in Electromagnetic Methods in Applied Geophysics,Volume 2, Application, Parts A and B, edited by M.N. Nabighian, Investigations in Geophysics No. 3, 3, Society of Exploration Geophysicists, Tulsa, Oklahoma, USA: 521-640.

Millitzer, H. & Weber, F. (Eds.), 1984. Angewandte Geophysik Band 1 - Gravimetrie und Magnetik. Springer Verlag Wien - New York & Akademie Verlag Berlin, 353 pp.

Müller, I., 1981. La grotte de "Chez le Brandt" (Jura Neuchâtelois, Coord; 526 425/ 199 000). Essai de synthèse des donnees géologiques et hydroéologiques. Cavernes (Neuchâtel) 25(1): 8-14.

Sattel, D. & Macnae, J., 2001. The feasibility of electromagnetic gradiometer measurements. Geophysical Prospecting 49: 309-320.

Schnegg, P.A. & Bossy, F., 2001. Sonde for downhole measurement of water turbidity and dye tracer concentration. Swets & Zeitlinger Lisse, 795-798 pp.

Spitzer, K., Fluche, B. & Storz, W., 2000. Investigating the near-surface conductance with an integrated EM experiment in Bad Königshofen. Proceed. of the Elektromagnetische Tiefenforschung, Altenberg, Germany, 18, Deutsche Geophysikalische Gesellschaft: 70-80, ISSN 0946-7467.

Steiner, T., de Carvalho Dill, A., Szarka, L. & Müller, I., 1992. Comparative studies of VLF-R and VLF-EM geophysical methods; 1-D and 2-D numerical modelling at the tracer test-field Wilerwald (BE, Switzerland). Bull. du Centre d'Hydrogéologie de l'Université de Neuchatel 11.

Stiefelhagen, W., 1998. Radio Frequency Electromagnetics (RF-EM): Kontinuierlich messendes Breitband-VLF, erweitert auf hydrogeologische Problemstellungen. PhD thesis, Centre of Hydrogeology, University of Neuchâtel, Neuchâtel, Switzerland, 243 pp.

Szalai, S., Szarka, L., Pracser, E., Bosch, F., Müller, I. & Turberg, P., xxxx. Geoelectric mapping of near-surface karstic fractures by using null-arrays. Geophysics: accepted.

Telford, W.M., Geldart, L.P. & Sheriff, R.E., 1990. Applied Geophysics Second Edition. Cambridge University Press, Cambridge, UK, 770 pp.

Tikhonov, A.N., 1950. On determining the electric properties of deep layers of the earth's crust. Proc (Doklady) Acad. Sci. USSR 83-2.

Turberg, P., 1994. Apport de la cartographie Radiomagnétotellurique a l'hydrogéologie des milieux fractures. PhD thesis, Centre d'Hydrogéologie de l'Institut de Géologie, Université de Neuchâtel, Neuchâtel, Switzerland, 132 pp.

Turberg, P. & Barker, R., 1996. Joint application of radio-magnetotelluric and electrical imaging surveys in complex subsurface environments. First Break 14(3): 105-112.

Turberg, P. & Müller, I., 1992. La méthode inductive VLF-EM pour la prospection hydrogéologique en continu du milieu fissuré. Annales Scientifique de l' Université de Besancon, Mémoire hors série 11: 207-214.

Turberg, P., Müller, I. & Flury, B., 1994. Hydrogeological investigation of porous environments by radio magnetotelluric-resistivity (RMT-R 12-240 kHz). Journal of Applied Geophysics 31: 133-143.

Wannamaker, P.E., Stodt, J.A. & Rijo, L., 1985. PW2D - Finite element program for solution of magnetotelluric responses of two-dimensional earth resistivity structure, Earth Sciences Laboratory, University of Utah, Utah.

Wannamaker, P.E., Stodt, J.A. & Rijo, L., 1986. Two dimensional topographic responses in magnetotellurics modeled using finite elements. Geophysics 51: 2131-2144.

Wannamaker, P.E., Stodt, J.A. & Rijo, L., 1987. A stable finite element solution for two-dimensional megnetotelluric modelling. Geophysical Journal of the Royal Astronomical Society 88: 227-296.

Wenger, B., 2001. Traceurs fluorescents en hydrogéologie: Description des propriétés optiques, de la conservativité, la toxicité et le prix des principaux colorants utilisés pour le traçage des eaux souterraines., Centre of Hydrogeology, University of Neuchâtel, Switzerland, pers.com.

2.2 Method comparison at Bure / Le Maira (JU, Switzerland)

This section focuses on the problematic of the interpretation of Geoelectric Tomography data in karstic areas. Results from different Geoelectric Tomography electrode configurations are compared with results from RMT, VLF-EM GRAD and borehole data.

2.2.1 Study Area

The study area is situated between the two villages of Le Maira and Bure (Cant. Jura, Switzerland) in the Ajoie area of the Swiss Table Jura Mountains (Figure 15), where Malm limestones (Sequanian, Rauracian) overlay Oxfordian marls. This area features a regional N-S orientated discontinuity zone and the "Milandre Cave" network. It is one of the important test sites of the CHYN. An important number of former and actual hydrogeological and geophysical experiments have been carried out (RMT by Turberg (1994) and RF-EM by Stiefelhagen (1998)). Furthermore, several boreholes exist along "Profile1" (Figure 15and Figure 16).

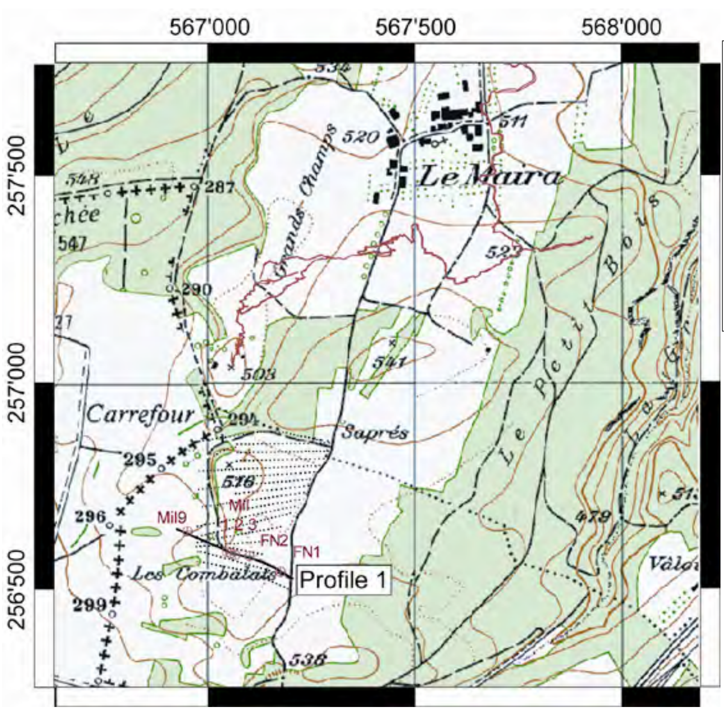

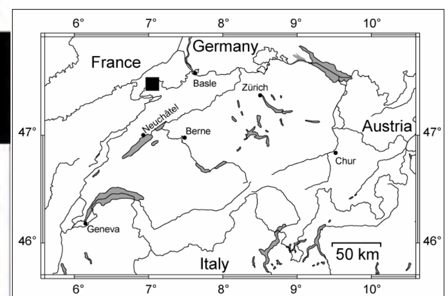

Figure 15: Map of Switzerland (right) and of study area (left). The black dots in the North and South of "Profile1" indicate the RMT stations from Turberg (1994). The red line indicates the "Milandre Cave". MIL 1,2,3 and FN1,2 are the locations of boreholes.

Profile 1 crosses a trench. Stiefelhagen (1998) assumed that the Milandre Cave may follow this trench. But neither geophysical results nor drillings confirmed that hypothesis. Maybe this trench arose from a collapse of the assumed cave. The boreholes in Figure 16 indicate compact limestone in the eastern part of "Profile 1" (FN1 and FN2) and clay filled limestone from the top up to 50 m depth in the area of the trench (MIL1,2,3) as well as at the western end of the profile (MIL9).

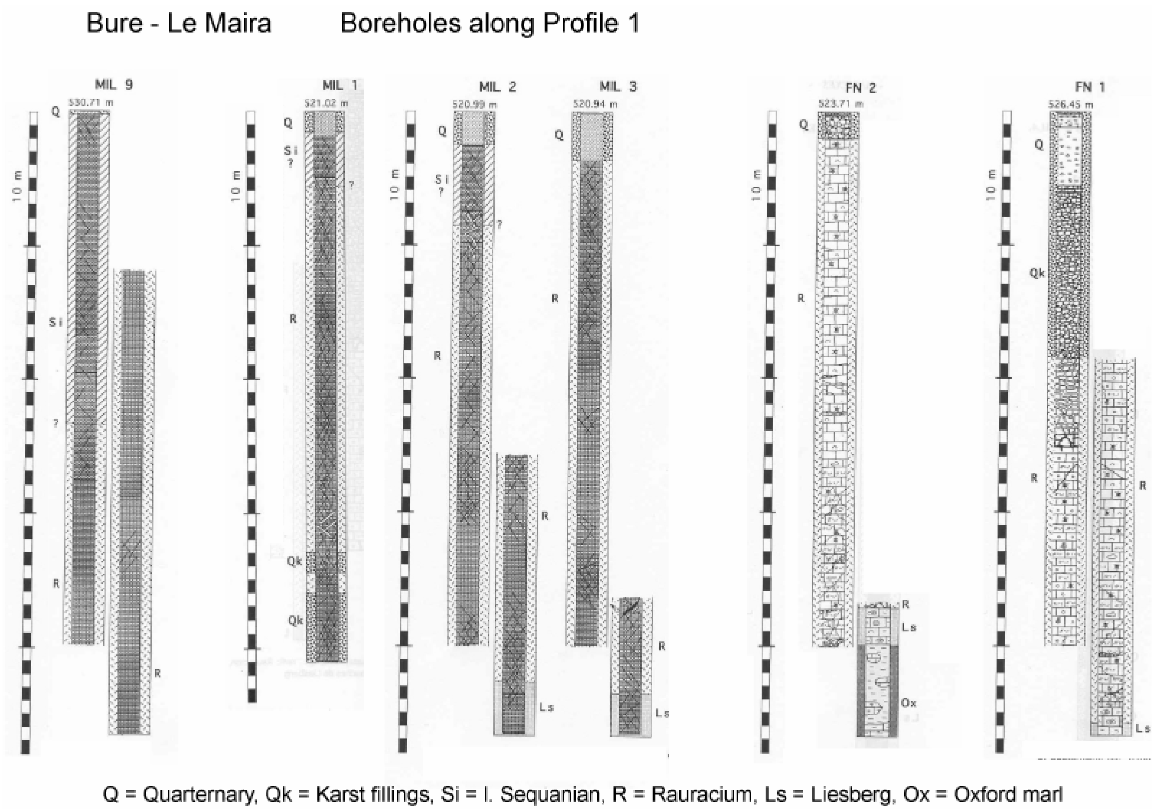

Figure 16 Boreholes along "Profile1".

2.2.2 Data and observations

Figure 17 compares results from RMT measurements (apparent resistivity and phase) carried out by Turberg (1994) with Geoelectric Tomography and VLF-EM GRAD data.

2.2.2.1 RMT

The two RMT profiles "N^{o}14" and "N^{o}15" are parallel to "Profile1". The latter is the profile where the GRAD and tomography data were collected. The distance between "N^{o}14" and "Profile1" measures 10 m and between "Profile1" and "N^{o}15" about 20 m.

In order to obtain sharp resistivity and phase contrasts to map both the boarders of the trench as well as possible internal discontinuities, Turberg (1994) chose W-E orientated transmitters (162 kHz and 63.8 kHz) to measure in H-polarization. The station spacing was 10 m, the electrode spacing 5 m.

The RMT data delineate the trench on both profiles as a zone of low apparent resistivity (80 to 100 Ωm) and increased phase, while on the northern profile "N^{o}14" additional internal variations are visible. The data along the profile coincide with the information from the boreholes.

2.2.2.2 VLF-EM GRAD

The GRADIENT data were recorded with 4 Hz datalogger sample frequency and the 23.4 kHz (orientation 8° N) radio transmitter on "Profile1". Inphase and quadrature

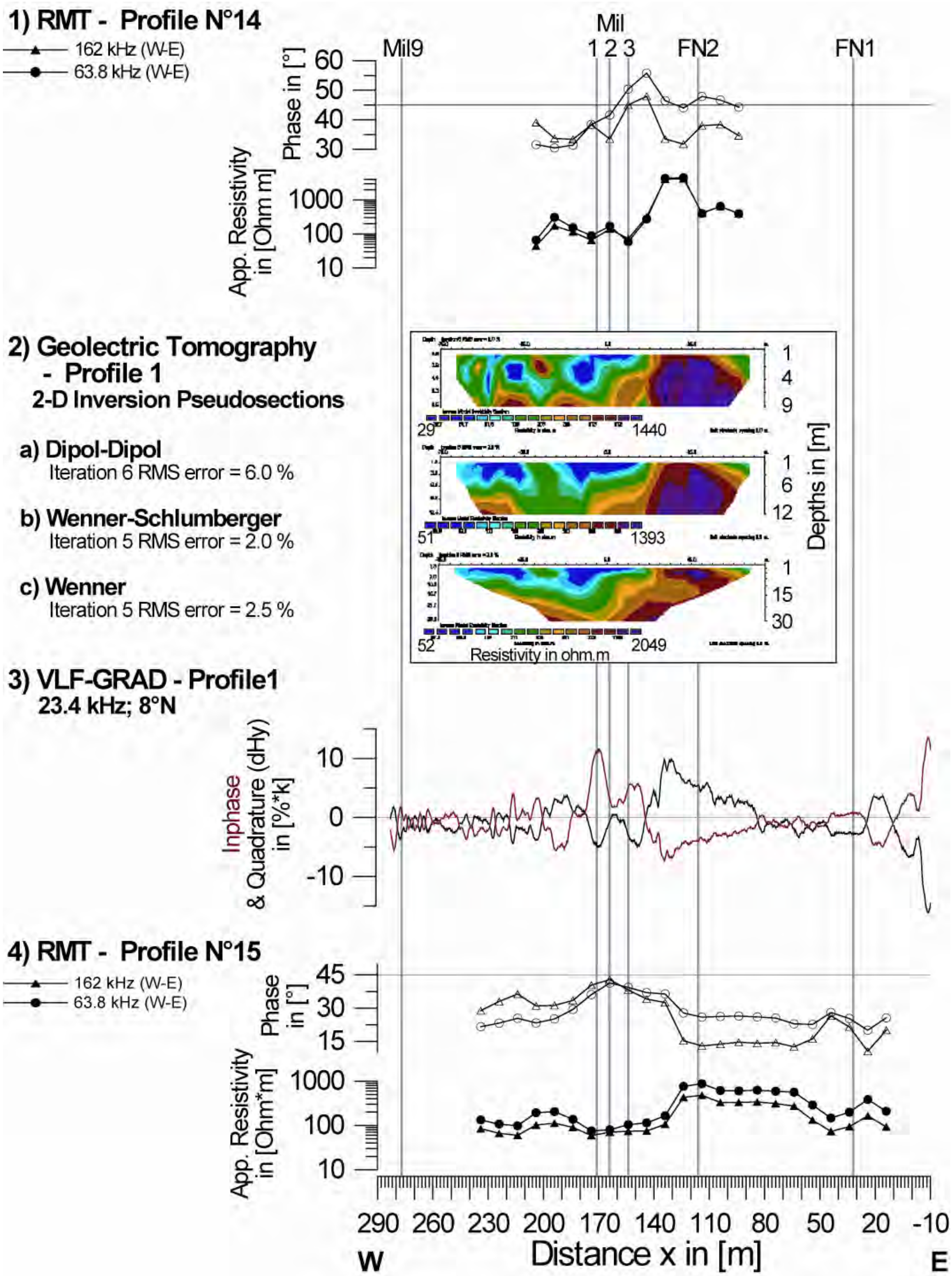

Figure 17: Comparison of RMT, Geoelectric Tomography and RMT data over a profile crossing a trench in karstified limestone of the Swiss Table Jura Mountains.

show numerous resistivity contrasts. The most important one is at the borehole MIL1. The data delineate the trench edges and internal structures. The inphase peak orientation is coherent with the resistivity information from RMT and Geoelectric Tomography. Particularly the resistivity distribution of the dipole-dipole configuration at about 8 m depth coincides with the GRAD peaks. This provides valuable information about the depth range of the VLF-EM GRAD measurements.

2.2.2.3 Geoelectric Tomography

The Geoelectric Tomography data were recorded along "Profile1" with 32 electrodes and a unit electrode spacing of 5 m. Three electrode configurations were used: Dipole-Dipole, Schlumberger-Wenner and Wenner. These three configurations have decreasing sensitivity for vertical structures and increasing penetration depth respectively in the order of mentioning. Figure 17 shows 2D inversion resistivity pseudosections calculated with the program RES2DINV (Loke & Barker 1996).

All configurations show resistivities typical for compact limestone in the eastern part of the profile conform to RMT and borehole data (FN2). Generally lower resistivities are found in the central part, where the profile crosses the trench, and in the eastern part. This coincides with the former observations from the other methods and boreholes.

However, a detailed look at the resistivity distribution pattern shows:

- Data from different electrode configurations are not coherent to each other.
  - Example: The relatively high resistivities of about 800 Ωm in the dipole-dipole data around profile meters 220 and 180 at 8 to 9 m depth can not be found in the results of the two other electrode configurations.
- The resistivity data do not correlate with the geological borehole information.
  - MIL1,2,3 indicate clay filled fissured limestone up to 50 m depth and more. The resistivity values of the tomography give the impression of compact limestone starting at 6 m depth!
- The pseudosections do not provide the image of karstified rock.
  - Instead of sharp, vertical elongated resistivity changes as can be assumed for dike boarders or fractures, the tomography rather gives the impression of a limestone host rock with varying thickness of overburden.

2.2.3 Discussion

Since the efficiency of the RMT and the VLF-EM GRAD methods were already discussed in the previous case studies of the published papers, here the results of the Geoelectric Tomography data are emphasized.

The main reasons of the inconsistent tomography data is the fact that this method tends to present sudden changes of the electric resistivity as gradual changes (Zhou *et al.* 2000). Moreover, the sensitivity for vertical structures as assumed appearing in karst is generally poor for geoelectric methods. Only the dipole-dipole configuration is able to detect sudden resistivity changes of small extension in this case study, but suffers from poor penetration depth, because the "signal to noise ratio" decreases remarkably at greater depths (Loke 1999). It may be that the increased resistivity values at 4 to 9 m depth around the boreholes MIL 1, 2, and 3 are produced by air filled fractures, as MIL1 showed open fractures at 30 m and MIL2 at 10 m depth (Stiefelhagen 1998). However, if this should be the case, at least the inversion results of the Schlumberger-Wenner and the Wenner configuration lead to wrong interpretations of these increased resistivity values.

3 Conclusions

The case studies presented in this work show, that geophysical methods are now able to provide valuable information of the subsurface, which can be used for the various aspects of karst groundwater vulnerability assessment. They provide information about overburden thickness and consistency and can map fractures and fault zones and their fillings from the near-surface to depth.

3.1 Electromagnetic methods

Particularly the presented electromagnetic methods RMT, RF-EM and VLF-EM GRAD are fully adapted for imaging the "high-permeability-singularities" of carbonate rocks.

Advantages of the RMT, RF-EM and VLF-EM GRAD method:

- They have the necessary resolution.
- Their measurement speed enables covering of large areas at groundwater catchment scale.
- The amount of work force required is reduced compared to other common methods. A minimum of two operators is sufficient.
- The methods are applicable in difficult terrain.
- The ground-contactless methods RF-EM and VLF-EM GRAD can be used with a vehicle.
- While repeating a profile with different transmitter frequencies, the dip of resistivity contrasts can be estimated with RF-EM.
- RMT offers horizontal and vertical resistivity distribution
    - to proof the nature of RF-EM/VLF-GRAD anomalies
    - to detect the underlying impermeable zone (e.g. marls under limestone)

Particular advantages of the VLF-EM GRAD method:

- Distinguishes clearly heterogeneous from homogeneous zones.
    - Indirect approach to permeability distribution imaging.
- The VLF-EM GRAD method increases the possibilities for imaging neighbouring near-surface structures on large areas:
    - Paper 5 highlights the issue of superimposed RF-EM anomalies. Paper 2 and Paper 7 in contrast demonstrate the efficiency of VLF-EM GRAD to detect internal structures of larger discontinuity zones.
    - Fig. 8 in Paper 7 indicates a horizontal resolution of the VLF-EM GRAD of a resistivity contrast frequency of about 2 m (RF-EM: 7-10 m).
- It offers a qualitative indication of the presence of epikarst:
    - huge number of low-amplitude anomalies

- It increases data quality and stability compared to RF-EM. Moreover, "inphase" signals are stable.
    - This is important because in the E-Polarisation case, the inphase-polarity can determine whether an anomaly is conductive or resistive (see "Paper 2", Fig. 7: signals over CLB and Doline and "Paper 7", Fig. 9).
- It offers the highest "horizontal resolution"/"measurement speed" ratio of all methods presented in this study.

The gradient method enhances the detection of near-surface structures. Another illustration from the "Les Breuleux" survey (Paper 3 and 6) with in-situ validation

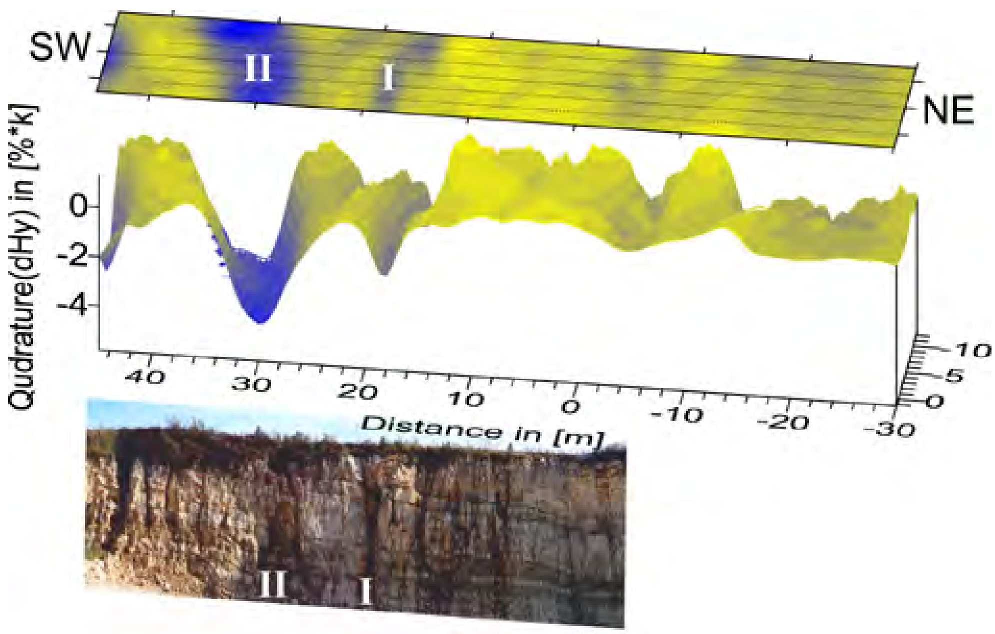

Figure 18 VLF-EM GRAD 19.6 kHz quadrature contour and surface plots with photo of "Les Breuleux Quarry" (JU). The transmitter is sending from orientation -40°N. The parallel lines in the contour map indicate the profiles. "Profile 2.5m" is ca. 8m behind the quarry wall. Anomalies I and II coincide with the fractures I and II at the quarry wall. The filled "shaft" at ca. 43 m is also visible in the data.

possibilities at the quarry wall is given in Figure 18. However, to quantitatively identify the contributing depths is not possible. For RMT and RF-EM, the depth of information can be estimated by the skin depth for a chosen frequency and a given resistivity of the ground. From the comparison of VLF-EM GRAD results with results from RF-EM we can at least qualitatively say that the VLF-EM GRAD detects structures, which are at or above the skindepth of about 230 kHz. In terms of karstified limestone the detected structures are located in the first 15 meters depth. The comparison with dipole-dipole Geoelectric Imaging in Figure 17 in Chapter 2.2 demonstrates, that the GRADIENT method already detects structures at about 8 m depth in that case history. This indicates that a gradient device utilizing frequencies from the LF range shows significant potential as a tool for very shallow depths subsurface mapping.

Limitations of the EM methods:

- The presence of a thick conductive overburden limits the penetration depth.
- Dependency on remote transmitters:
    - Not all frequencies and directions are available all over the world.
- Sensitivity to electromagnetic noise (current power cables, metallic fences, tubes, etc.):
    - Responses from these artificial structures superimpose the signals from geological structures. The VLF-EM GRAD method is less affected from that (e.g.: 5 m distance from a metallic fence is sufficient)
- Scalar instead of tensor measurements:
    - Measuring only one polarisation direction as a compromise for easy field application prohibits the full data interpretation possibilities known from the Magnetotelluric and Geomagnetic Deep Sounding (GDS) method.

3.2 Self-potential

The application of the self-potential method to karst was interesting because of the simplicity of the equipment and the relative rapid progress of measurements. Moreover, considering that streaming potentials are one origin of the self-potential the method holds some promise for hydrogeological investigations in the sense of mapping the high permeability zones in karst.

Overall, the SP profiling results over the "Chez le Brandt cave" area presented in "Paper 1", confirm the anomaly pattern of the EM methods, which have been shown to be capable of detecting high permeability zones. However, while comparing the anomalies of the different methods, one can see that sometimes SP anomalies with important amplitudes coincide with moderate EM anomalies (e.g. SP1 in "Paper 1") and vice versa. One explication for this phenomenon may be that the EM methods only detect the geological discontinuity structures, which may transport water. The SP method may be more sensitive for the existence or absence of flowing water (see anomalies over "Chez le Brandt Cave" and "Doline Cave" in Fig. 13 of Paper 1). Consequently, further investigation on this issue might hold some promise for hydrogeological studies. As a tool for mapping on the water catchment scale, the method might be a bit too slow. Otherwise, the chosen sample interval of 1 m and less in "Paper 1" may not be necessary.

Paper 4 illustrated the "imaging" of the "Chez le Brandt Cave"generated by using the self-potential surface (SPS) method. If the method has detected the bottom of the cave, namely the contact between the unsaturated zone (karstified limestone) and the underlying impermeable zone (marls) or the top (contact of karstified limestone/ air) is not sure yet. However, the calculated potential surface qualitatively coincides very well with the geological cross-section of the cave. Nevertheless, this example showed that SP anomalies are linked to hydrogeological parameters. However, detection of the cave topography on the surface using the SPS method can only be achieved, if the estimation of the vertical self-potential gradient with depth is possible. For this purpose, the cave needs to be accessible or information from boreholes must be available.

3.3 Geoelectric methods

According to the results presented in "Paper 7" and the additional Bure case study in Chapter 2.2, the common geoelectric mapping method "geoelectric tomography" is not an appropriate approach to integrated large-scale carbonate aquifer investigation. It cannot resolve the heterogeneous nature of carbonate rocks but at near surface. The field application is quite cumbersome even though the method improved the traditional geoelectrics. The disadvantages of the method in heterogeneous rock systems are recently compensated with further data processing and the application of electrode-arrays particularly sensitive for narrow and vertical elongated resistivity anomalies like fractures and faults. The geoelectric null-array configuration e.g. provides significantly more accurate data in high-resolution fracture detection at very shallow depth ("Paper 6") and is therefore a promising array for tomography.

Even though geoelectrics can provide high-resolution data at shallow depths and the research in this work was focused on near surface geophysics concerning the epikarst, the geoelectric methods are considered as an unsuitable tool for mapping large areas compared to the EM methods presented. Due to their relative expensive field application and rather slow profiling speed, they are more appropriate for detailed studies at local scale.

3.4 Summary

- The EM methods presented provide integrated information concerning the density and the horizontal and vertical distribution of karst structures as fractures and faults. Consequently, they indirectly provide the distribution of high-permeability zones in carbonate rocks at the water-catchment scale from shallow to greater depths. Thus, they provide valuable parameters for karst groundwater protection concepts.
- The continuously measuring, VLF-EM GRAD method enables the imaging of carbonate rock structures with an appearance frequency of 2 m within the first 15 m depth without further data-processing. This approach makes mapping of epikarst possible.
- The self-potential method is suitable for karst structure mapping. Its ability to detect the presence or absence of water-flow should be considered for further research.
- Geoelectric Tomography is not an appropriate approach to integrated large-scale carbonate aquifer investigation as a stand-alone method.
- The integrated application of the reconnaissance EM mapping methods together with additional methods for detailed local scale investigation, such as electrical tomography, provides a detailed image of the subsurface.

4 Outlook

The results of this PhD work encourage proposing the following ideas for further research regarding the VLF-EM GRAD method:

- **2D forward modeling of the VLF-EM GRAD response of simple resistivity distributions and karst structures**
- **Extension of the frequency range of the VLF-EM GRAD method to the LF range**
    - This will enable the gradient method for detailed small scale structure detection at very shallow depth (0-10 m).
- **Calculation of apparent resistivities from VLF-EM GRAD data**
    - The measured parameters of the VLF-GRAD method offers the possibility for the application of the Vertical Gradient Magnetometry (VGM) method (Jones 1983; Meyer 1965; Radic 1994; Schmucker 1986; Spitzer *et al.* 2000). Different from Cagniard (1953a) the VGM method estimates the surface impedance only from magnetic measurements based on Ampere's flux law, where the vertical gradient of the horizontal magnetic field component is proportional to the horizontal electric field component.
- **Construction of a portable radio transmitter**
    - A portable transmitter could fill the gap of missing frequencies and transmitter directions

5 Acknowledgements

I wish to thank Prof. **François Zwahlen** and Prof. **Imre Müller** for initiating and supporting my studies in any way.

Furthermore, I would like to thank Prof. **Alain Dassargues**, Prof. **Stanislav Mares** and Prof. **Jaques Mudry** for being in the doctorial jury.

I am very indebted to Mr. **Jaques Duperrex** who has built the electromagnetic equipment used in these studies.

Special thanks go to Dr. **Pierre-André Schnegg** and Dr. **Marcus Gurk**. Without you I would not have come to Neuchâtel. I thank Pierre for all the discussions and particular for providing the PUCH. A big thank you goes out to Marcus for being together with you "the team". This will continue.

Furthermore, I thank **Roberto Costa** for maintaining and upgrading the datalogger system.

Ray Flynn, **Rachel Hosein** and **Ellen Milnes**, I thank you for checking the English.

A very special thank you goes to **Vincent Puech** and, in memory, to **Katia Lauber**. Because of you, I felt at home at Neuchâtel.

The same goes to all the friends inside and outside CHYN, particularly **Carolin Banasek-Richter**, **Bernd Eilrich**, **Ray Flynn**, **Attila Kovacs** and **Michael Sinreich**.

Für Euch auf Deutsch: Besonders bedanke ich mich bei meinen **Eltern**. Ich danke Euch für all Eure Liebe und dafür, daß Ihr mein Interesse für die Naturwissenschaften gefördert und unterstützt habt.

Thank you **Birgitta**, my beloved, for staying patient!

Most of all I thank **the creator** of all the things we try to discover.

This thesis was supported by the Swiss National Science Foundation grants: FN2028-047175.96/1, FN2000-053936.98/1 and FN2000-061717.00/1.

6 Complete References

Arandjelovic, D. & Milosevic, L., 1965. Hydrogeological investigation in Yugoslavian karst by the application of geophysical methods. Mémoire de l'Association International des Hydrogéologue.

Arthaud, F. & Dazy, J., 1989. Migration des saumures au front des chevauchements de l'arc alpin occidental. C.R. Acad. Sci. Paris. **309**(2): 1425-1430.

Aubert, M. & Atangana, Q.Y., 1996. Self-potential method in hydrogeological exploration of volcanic areas. Ground Water **34**(6): 1010-1016.

Aubert, M., Dana, I.N. & M.Livet, 1990. Vérification des limites de nappes aquiféres en terrain volcanique par la méthode de polarisation spontanée. C.R.Ac.Sc Paris **311**: 999-1004.

Barker, R.D., 1979. Signal contribution sections and their use in resistivity studies. Geophys. J. Roy. Astr. Soc. **39**: 123-129.

Barker, R.D., 1992. A simple algorithm for electrical imaging of the subsurface. First Break **10**: 53-62.

Benderitter, Y. & Robin, G., 1987. Approche singulière des discontinuités de perméabilité en milieu carbonaté. Hydrogéologie **3**: 161-168.

Bigalke, J. & Grabner, E.W., 1997. The geobattery model: A contribution to large scale electrochemistry. Electrochimic Acta **42**: 23-24.

Bigalke, J. & Junge, A., 1999. Using evidence of non-linear induced polarization for detecting extended ore mineralisations. Geophysical Journal International **137**: 516-520.

Bissig, P., 1997. Hydrogeologische Untersuchung der CO2-reichen Mineralquellen von Scoul-Tarasp (GR, Schweiz). Diploma thesis, Centre d'Hydrogéologie, Université de Neuchâtel, Neuchâtel, 91 pp.

Bosch, F. & Müller, I., 2001a. Nouveau développement dans la prospection géophysique électromagnétique. Le Very Low Frequency Electromagnetics - Gradient (VLF-EM-Grad), facilitant la cartographie des "zones sensibles" dans l'Epikarst et dans les aquifères fissurés. Proceed. of the 7éme Colloque d'Hydrologie en Pays Calcaire et en milieu fissuré, Besançon, 20.-22. Sept. 2001, Sci. Tech. Envir., Mém. H. S. n°13: 55-58, ISSN 0759-7517.

Bosch, F.P. & Gurk, M., 2000. Comparison of RF-EM, RMT and SP measurements on a karstic terrain in the Jura Mountains (Switzerland). Proceed. of the Elektromagnetische Tiefenforschung, Altenberg, Germany, **18**, Deutsche Geophysikalische Gesellschaft: 51-59, ISSN 0946-7467.

Bosch, F.P. & Müller, I., 2001b. Continuous gradient VLF measurements: A new possibility for high resolution mapping of karst structures. First Break **19**(6): 343-350.

Bosch, F.P. & Müller, I., submitted. Contribution to karst groundwater vulnerability mapping by VLF-Gradient survey: Comparison with other geophysical methods. European Journal of Environmental and Engineering Geophysics: submitted.

Bosch, F.P., Szalai, S., Turberg, P. & Müller, I., 1999. Continuously recording radio-frequency electromagnetic (RF-EM) method (15-300 kHz) without ground contact: A powerful tool for groundwater vulnerability mapping in fissured rocks. Proceed. of the 5th meeting of the Environmental and Engineering Geophysical Society European Section, Budapest 6 - 9 September 1999, Hungary, Environmental and Engineering Geophysical Society European section: (Em4).

Boubekraoui, S., Courteaud, M., Aubert, M., Albouy, Y. & Coudray, J., 1998. New insights into the hydrogeology of a basaltic shield volcano from a comparison between self-potential and electromagnetic data: Piton de la Fournaise, Indian ocean. Journal of applied geophysics **40**.

Brion, M., 1976. L'etude du phénomène de l'anisotropie électrique appliquée au milieu carbonaté fracturé. PhD thesis, Université des Sciences et Technique du Languedoc, France.

Brizzolari, E. & Barnabini, M., 1979. Comparison between Schlumberger electrode arrangement and some focused electrode arrangements in resistivity profiles. Geophysical Prospecting **27**: 233-244.

Busby, J.P., 2000. The effectiveness of azimuthal apparent-resistivity measurements as a method for determining fracture strike orientations. Geophysical Prospecting **48**: 677-695.

Cagniard, L., 1953a. Basic theory of the magnetotelluric method of geophysical prospecting. Geophysics **18**: 605-635.

Cagniard, L., 1953b. Principe de la méthode magnétotellurique, nouvelle méthode de prospection en géophysique. Ann. Géophysique **9**: 95-125.

Carrington, T.J. & Watson, D.A., 1981. Preliminary evaluation of alternate electrode array for use in shallow subsurface electrical resistivity studies. Groundwater **19**(1): 48-57.

Chouteau, M., Zhang, P. & Chapellier, D., 1996. Computation of apparent resistivity profiles from VLF-EM data using linear filtering. Geophysical Prospecting **44**: 215-232.

Daly, D., Dassargues, A., Drew, D., Dunne, S., Goldscheider, N., Neale, S., Popescu, I.C. & Zwahlen, F., 2002. Main concepts of the "European approach" to karst-groundwater-vulnerability assessment and mapping. Hydrogeology Journal **10**: 340-345.

Dey, A. & Morrison, H.F., 1979. Resistivity modelling for arbitrary shaped three-dimensional structures. Geophysics **44**: 753-780.

DMT, 1997. COMTRAN Computer controlled transceiver and analyzer, DMT-Institute of Deposits, Surveying and Applied Geophysics.

Doerfliger, N., Jeannin, P.-Y. & Zwahlen, F., 1999. Water vulnerability assessment in karst environments: a new method of defining protection areas using a multi-attribute approach and GIS tools (EPIK method). Environmental Geology **39**(2): 165-176.

ELEKTB-Gruppe, Bahr, K., Bigalke, J., Eisel, M., Haak, V., Harms, U., Hirschmann, G., Huenges, F., Jödicke, H., Kotny, A., Kücke, J., Nover, G., Rauen, A., Stoll, J., Walther, J., Winter, H. & Zulauf, G., 1994. Untersuchungen zur elektrischen Leitfähigkeit in der Kontinentalen Tiefbohrung und ihrem Umfeld - was bringt sie uns Neues? Mitteilungen der Deutschen Geophysikalischen Gesellschaft **4/1994**: 2-40.

Erdelbrock, K., 1994. Diagenese und schwache Metamorphose im Helvetikum der Ostschweiz (Inkohlung und Illit-"Kristallinität"). , Fakultät für Bergbau, Hüttenwesen und Geowissenschaften, Rheinisch-Westfälische Technische Hochschule Aachen, Aachen, 220 pp.

Fischer, G., Quang, B.V.L. & Müller, I., 1983. VLF ground surveys, a powerful tool for the study of shallow two-dimensional structures. Geophysical Prospecting **31**: 977-991.

Fischer, G., Schnegg, P.A., Peguiron, M. & Le Quang, B.V., 1981. An analytic one-dimensional magnetotelluric inversion scheme. Geophysical Journal of the Royal Astronomical Society **67**: 257-278.

Fittermann, D.V., 1979. Calculation of self-potential anomalies near vertical contacts. Geophysics **44**: 195-205.

Gay, S.P., 1967. A 1800 Millivolt Self-Potential Anomaly near Hualgayoc, Peru. Geophys. Prosp. **15**: 236-245.

Geometrics, 1997. Strategem EH-4: Electrical Conductivity Imaging Systems - Hybrid-Source Magnetotellurics. Geometrics.

Gharibi, M. & Pedersen, L., 1999. Transformation of VLF data into apparent resistivities and phases. Geophysics **64**(5): 1393-1402.

Gogu, R.C. & Dassargues, A., 2000. Current trends and future challanges in groundwater vulnerability assessment using overlay and index methods. Environmental Geology **39**(6): 549-559.

Goldscheider, N., Klute, M., Sturm, S. & Hötzl, H., 2000. The PI method - a GIS-based approach to mapping groundwater vulnerability with special consideration of karst aquifers. Zeitschrift für angewandte Geologie **46**(3): 157-166.

Griffiths, D.H. & Barker, R.D., 1993. Two-dimensional resistivity imaging and modelling in areas of complex geology. Journal of Applied Geophysics **29**: 211-226.

Griffiths, D.H. & Turnbull, J., 1985. A multi-electrode array for resistivity surveying. First Break **3**(7): 16-20.

Griffiths, D.H., Turnbull, J. & A.I.Olayinka, 1990. Two-dimensional resistivity mapping with a computer-controlled array. First Break **8**: 121-129.

Gupta, R.N. & Bhattacharya, P.K., 1963. Unipole method of electrical profiling. Geophysics **28**: 608-616.

Gurk, M., 1999. Magnetic Distortion of GDS Transfer Functions: An Example from the Penninic Alps of Eastern Switzerland Revealing a Crustal Conductor. Earth Planets Space **51**: 1023-1034.

Gurk, M. & Bosch, F., 2001. Cave detection using Self-Potential-Surface (SPS) technique on a karstic terrain in the Jura Mountains (Switzerland). Proceed. of the Elektromagnetische Tiefenforschung, Burg Ludwigsstein, Germany, **19**, Deutsche Geophysikalische Gesellschaft: in press.

Gurk, M., Bosch, F., Challandes, N. & Bigalke, J., 2001. Integration of geophysical methods to study the fold geometry of the Tschera nappe, eastern Switzerland. Eclogae geologicae Helvetiae **94**: 329-338.

Habberjam, G.M. & Watkins, G.E., 1967. The use of the square array configuration in resitivity prospecting. Geophysical Prospecting **15**: 445-467.

Ishido, T. & Pritchett, J.W., 1999. Numerical simulation of elektrokinetic potentials associated with subsurface waterflow. Journal of Geophysical Research **104**(B7): 15247-15259.

Jackson, D.B. & Kauahikaua, J., 1987. Regional SP anomalies on Kilauea Volc. in Hawaii. U.S. Geol. Surv. Prof. Paper **40**: 947-959.

Jakosky, J.J., 1960. Exploration geophysics, Newport Beach, California.

Jödicke, H., 1992. Water and graphite in the earth's crust - an approach to interpretation of conductivity models. Surveys in Geophysics **13**: 381-407.

Jones, A.G., 1983. A passive natural- source twin-purpose borehole technique: Vertical Gradient Magnetometry (VGM). Journal of Geomagnetism and Geoelectricity **35**: 473-490.

Käss, W., 1998. Tracing Technique in Geohydrology. A.A.Balkema, Rotterdam, Netherlands.

Kiraly, L., 1969. Statistical analyses of fractures (orientation and density). Geologische Rundschau **59**: 125-151.

Kiraly, L., 1975. Rapport sur l'état des connaissance dans le domaine des caractères physiques des roches karstiques. in Hydrogeology of karstic terrains, **B 3**, International Union of Geology Science: 53-67.

Kiraly, L., 1995. Effect of the epikarst on the hydrograph of the karst springs. Bulletin d'hydrogéologie **14**: 199-220.

Kiraly, L. & Meia, J., 1967. Observations tectoniques dans une carrière de Chaumont (Jura Neuchâtelois, Suisse). Société Neuchâteloise des Sciences Naturelles **90**: 276-283.

Kiraly, L. & Simeoni, G., 1971. Structure géologique et orientation des cavités karstiques: la Grotte de "Chez le Brandt" (Jura neuch.). Bulletin de la Société neuchâteloise des Sciences naturelles **94**: 91-97.

Kovaccic, S. & Krulz, Z., 1967. Some aspects of geoelectrical investigation for ground water in the Yugoslavian karst region. Mémoire de l'Association Internatinal des Hydrogéeologues **7**(8): 463-474.

Le Masne, D. & Vasseur, G., 1981. Electromagnetic field of sources at the surface of a homogenous conducting halfspace with horizontal anisotropy: Application to fissured media. Geophysical Prospecting **29**: 803-821.

Liniger, H., 1969. Geologischer Atlas der Schweiz - Blatt 1065 Bonfol (Atlasblatt 55), Schweizerische Geologische Kommission, Bern.

Liniger, H., 1970. Erläuterungen zu Geologischer Atlas der Schweiz - Blatt: 1065 Bonfol (Attlasblatt 55), Schweizerische Geologische Kommission, Bern.

Loke, M.H., 1999. Electrical imaging surveys for environmental and engineering studies. A practical guide to 2-D and 3-D surveys. Pre-conference workshop notes W2, The theory and practice of electrical imaging, 5th meeting of the Environmental and Engineering Geophysical Society European Section, Budapest, Hungary.

Loke, M.H. & Barker, R.D., 1996. Rapid least-squares inversion of apparent resistivity pseudosections using a quasi-Newton method. Geophysical Prospecting **44**: 131-152.

Mählmann, R.F., 1995. Das Diagenese-Metamorphose-Muster von Vitrinitreflexion und Illit-"Kristallinität" in Mittelbünden und im Oberhalbstein Teil 1: Bezüge zur Stockwerkstektonik. Schweiz. Mineral. Petrogr. Mitt **75**: 85-122.

Mählmann, R.F., 1996. Das Diagenese-Metamorphose-Muster von Vitrinitreflexion und Illit-"Kristallinität" in Mittelbünden und im Oberhalbstein Teil 2: Korrelation kohlenpetrographischer und mineralogischer Parameter. Schweiz. Mineral. Petrogr. Mitt. **76**: 23-46.

Mangin, A., 1973. Sur la dynamique des transferts en aquifères karstiques. Proceed. of the 6th intern. conf. of Spéléol., Olomouc, **4**: 157-162.

Mangin, A., 1975. Contribution à l'étude hydrodynamique des aquifères karstiques. Annales de spéléologie **29**: 283-329.

Mathias, M.J.S. & Habberjam, G.M., 1984. A field example of the use of anisotropy parameters derived from resistivity soundings. Geophysical Prospecting **32**: 725-739.

McNeill, J.D., 1994. Use of electromagnetic methods for groundwater studies. in Geotechnical and Environmental Geophysics, edited by S.H. Ward, **1**, Society of Exploration Geophysics, Tulsa, Band 1: 191-218, dritte Ausgabe.

McNeill, J.D. & Labson, V.F., 1991. Geological mapping using VLF radio fields. in Electromagnetic Methods in Applied Geophysics,Volume 2, Application, Parts A and B, edited by M.N. Nabighian, Investigations in Geophysics No. 3, **3**, Society of Exploration Geophysicists, Tulsa, Oklahoma, USA: 521-640.

Meyer de Stadelhofen, C., 1991. Applications de la géophysique aux recherches d' eau. Lavoisier, Paris.

Meyer, J., 1965. Übertragung des Cagniard'schen Verfahrens auf den Fall der Beobachtung nur magnetischer Größen. Proceed. of the Elektromagnetische Tiefensondierung, Goslar, Germany: 133 pp.

Michel, S. & Zlotnicki, J., 1998. Self-Potential and magnetic surveying of la Fournaise volcano (Réunion Island): Correlation with faulting, fluid circulation and erruption. Journal of Geophysical Research **103**: 17845-17857.

Militzer, H., Rösler, R. & Lösch, W., 1979. Theoretical and experimental investigations for cavity research with geoelectrical resistivity methods. Geophysical Prospecting **27**: 640-652.

Millitzer, H. & Weber, F. (Eds.), 1984. Angewandte Geophysik Band 1 - Gravimetrie und Magnetik, Springer Verlag Wien - New York & Akademie Verlag Berlin, 353 pp.

Morat, P., Mouel, J.-L.L., Poirier, J.-P. & Kossobokov, V., 1999. Heat and water transport by oscillatory convection in an underground cavity. C.R. Acad. Sci. Paris, Sciences de la terre et des planètes **328**: 1-8.

Muhlethaler, C., 1931. Étude Géologique de la région des Verrières (Canton de Neuchâtel). Bulletin de la Société neuchâteloise des Sciences naturelles **56**: 123-300.

Müller, I., 1981. La grotte de "Chez le Brandt" (Jura Neuchâtelois, Coord; 526 425/ 199 000). Essai de synthèse des donnees géologiques et hydroéologiques. Cavernes (Neuchâtel) **25**(1): 8-14.

Müller, I., 1982a. Premières prospections électromagnétiques VLF (very low frequency) dans le karst en Suisse. Proceed. of the 7e congrès national de spéléologie, Schwyz: 173-181.

Müller, I., 1982b. Résultats préliminaires des sondages géophysiques pluridirectionels (résistivité, polarisation induite, microsismique) dans la région de la Baume (Jura Neuchâtelois, Suisse). Bulletin de la Société Neuchâteloise des Sciences Naturelles **105**: 191-204.

Müller, I., 1982c. Role de la prospection électromagnétique VLF (Very Low Frequency) pour la mise en valeur et la prospection des aquifères calcaires. Annales Scintifiques de l' Université de Besancon **1**: 219-226.

Müller, I., 1983. Résultats préliminaires des sondages géoélectriques adaptés à la recherche du réseau karstique. Proceed. of the Atti Convegno Int.le sul carso di alta montagna Imperia (30.04. - 04.05.1982), Imperia, **1**: 367-380.

Müller, I. & Zötl, J., 1980. Karsthydrologische Untersuchungen mit natürlichen und künstlichen Tracern im Neuenburger Jura (Schweiz). Steirische Beiträge zur Hydrogeologie **32**: 5-100.

Paal, G., 1965. Ore prospecting based on VLF-radio signals. Geoexploration **3**: 139-147.

Palacky, G.J., Ritsema, I.L. & Jong, S.J.D., 1981. Electromagnetic prospecting for groundwater in precambrian terrains in the Republic of Upper Volta. Geophysical Prospecting **29**: 932-955.

Parasnis, D.S., 1986. Principles of applied geophysics.

Patella, D., 1997. Introduction to ground surface self-potential tomography. Geophysical Prospecting **45**: 653-681.

Pedersen, L.B., Dynesius, L., Bastani, M., Gharibi, M. & Matzander, U., 1999. "ENVIRO MT": A new radio controlled source system. Proceed. of the 5th meeting of the Environmental and Engeneering Geophysical Society European Section.

Piro, S., Tsourlos, P.I. & Tsokas, G.N., 2001. Cavity detection employing advanced geophysical techniques: Acase study. European Journal Of Environmental And Engeneering Geophysics **6**: 3-31.

Pracser, E., 1999. Annual report about the activity of the geoelectric laboratory in 1988. 3D d.c. modeling, Internal report, Eötvös Lorand Geophysical Institute, Budapest, Hungary.

Pracser, E., Adam, A., Szarka, L., Mueller, I. & Turberg, P., 2000. Slingram measurements in the Mecsek Mountains, Hungary. Acta Geodaetica et Geophysica Hungarica **35**(4): 397-414.

Radic, T. & Becken, M., 2000. Berechnung der Widerstandsverteilung aus im Radiofrequenzbereich gemessenen magnetische Übertragungsfunktionen. Proceed. of the Elektromagnetische Tiefenforschung, Altenberg, Germany, **18**, Deutsche Geophysikalische Gesellschaft: 274-278, ISSN 0946-7467.

Revil, A., Pezard, P.A. & al., e., 1999a. Streaming potential in porous media, 1: Theory of the zeta potential. Journal of Geophysical Research **104**(B9): 20021-20031.

Revil, A., Schwaeger, H. & al., e., 1999b. Streaming potential in porous media, 2: Theory and application to geothermal systems. Journal of Geophysical Research **104**(B9): 20033-20048.

Sailhac, P., Marquis, G. & Aubert, M., 2000. A wavelet based technique applied to characterise subsurface fluid flow from SP data. Proceed. of the 6th Meeting Environmental and Engeneering Geophysics - Explore Tomorrows Fundaments - Sept. 3-7 2000, Bochum, Germany, EEGS-ES.

Sato, M. & Mooney, H.M., 1960. The Electrochemical Mechanism of Sulfide Self-Potentials. Geophysics **XXV**(1): 226-249.

Sattel, D. & Macnae, J., 2001. The feasibility of electromagnetic gradiometer measurements. Geophysical Prospecting **49**: 309-320.

Schmeling, H., 1986. Numerical models on the influence of partial melt on elastic, anelastic and electrical properties of rocks. Part II, electrical conductivity. Phys. Earth Planet. Inter. **43**: 123-135.

Schmid, S.M., Rück, P. & Schreurs, G., 1990. The significance of the Schams nappes for the reconstruction of the paleotectonic and orogenic evolution of the Penninic zone along the NFP-20 East traverse (Grisons, eastern Switzerland). Mém. Soc. géol. Fr. **156**: 263-287.

Schmucker, U., 1986. Erfahrungen mit magnetischen Untertageregistrierungen. Proceed. of the Elektromagnetische Tiefensondierung, Lerbach bei Köln, Germany, **11**: 63-73.

Schnegg, P.-A., 1998. The magnetotelluric survey of the Penninic Alps of Valais. Swiss Geophysical Commission, Bern, 76 pp.

Schnegg, P.A. & Bossy, F., 2001. Sonde for downhole measurement of water turbidity and dye tracer concentration. Swets & Zeitlinger Lisse, 795-798 pp.

Schnegg, P.-A., Fisher, G., Le Quang, B.V. & Ranieri, G., 1987. A magnetotelluric study in the Campidano Graben of Sardinia. Journal of Geophysics **61**: 30-38.

Shankland, T.J. & Waff, H.S., 1977. Partial melting and conductivity anomalies in the upper mantle. J. Geophys. Res. **82**: 5409-5417.

Sivenas, P. & Beales, F.W., 1982a. Natural geobatteries associated with sulphide ore deposits, I. Theoretical Studies. J. geochem. Explor. **17**: 123-144.

Sivenas, P. & Beales, F.W., 1982b. Natural geobatteries associated with sulphide ore deposits, I. Theoretical Studies. Journal of Geochemical Exploration **17**: 123-144.

Smith, J.T. & Booker, J.R., 1991. Rapid Inversion of two- and three-dimensional magnetotelluric data. J. Geophys. Res. **96**: 3905-3922.

Song, Y., Kim, H.J. & Lee, K.H., 2002. High-frequency electromagnetic impedance method for subsurface imaging. Geophysics **67**(2): 501-510.

Spitzer, K., 1998. The three-dimensional DC sensitivity for surface and subsurface sources. Geophysical Journal International **134**: 736-746.

Spitzer, K., Fluche, B. & Storz, W., 2000. Investigating the near-surface conductance with an integrated EM experiment in Bad Königshofen. Proceed. of the Elektromagnetische Tiefenforschung, Altenberg, Germany, **18**, Deutsche Geophysikalische Gesellschaft: 70-80, ISSN 0946-7467.

Steiner, T., de Carvalho Dill, A., Szarka, L. & Müller, I., 1992. Comparative studies of VLF-R and VLF-EM geophysical methods; 1-D and 2-D numerical modelling at the tracer test-field Wilerwald (BE, Switzerland). Bull. du Centre d'Hydrogéologie de l'Université de Neuchatel **11**.

Stiefelhagen, W., 1998. Radio Frequency Electromagnetics (RF-EM): Kontinuierlich messendes Breitband-VLF, erweitert auf hydrogeologische Problemstellungen. PhD thesis, Centre of Hydrogeology, University of Neuchâtel, Neuchâtel, Switzerland, 243 pp.

Stiefelhagen, W. & Müller, I., 1997. Radio Frequency Electromagnetics (RF-EM) - Extended VLF applied to hydrogeology. Proceed. of the EAGE 59th Conference and Technical Exhibition, Geneva, Switzerland, 26.-30. May 1997, Geophysical Division.

Stoll, J., Bigalke, J. & Grabner, E.W., 1995. Electrochemical Modelling of Self-Potential Anomalies. Surveys in Geophysics **16**: 107-120.

Streiff, V., Jäckli, H. & Neher, J., 1971. Geologischer Atlas der Schweiz, Blatt: 1235 Andeer, Kommissionsverlag: Kümmerly & Frey AG Geographischer Verlag Bern, Bern.

Streiff, V., Jäckli, H. & Neher, J., 1976. Erläuterungen zu Blatt: 1235 Andeer. Kommissionsverlag: Kümmerly & Frey AG. Geographischer Verlag Bern, Bern, 106 pp.

Szalai, S., 1993. Multielectrode DC measurements for leakage monitoring. Diploma thesis, Eötvös Lorand University, Budapest, Hungary.

Szalai, S. & Szarka, L., 2000. An approximate analytical approach to compute geoelectric dipole-dipole responses due to a small buried cube. Geophysical Prospecting **48**(871-885).

Szalai, S., Szarka, L., Pracser, E., Bosch, F., Müller, I. & Turberg, P., 2002. Geoelectric mapping of near-surface karstic fractures by using null-arrays. Geophysics: accepted.

Szarka, L., 1991. Detectability of high-condzctivity plates by CSAMT method on basis of analogue modelling results. - An interesting analogue modelling experience. Acta Geod. Geoph. Mont. Hung. **26**: 273-285.

Szarka, L., 1994. Three-dimensional electromagnetic imaging. Doctor of the Academy thesis, Geodetic and Geophysical Research Institute of the Hungarian Academy of Sciences, Sopron, Hungary.

Szarka, L. & Menvielle, M., 1999. A possibility for an enhanced 3D parameter-sensitivity - the keyhole imaging. Geophysical Prospecting **47**: 59-71.

Szarka, L. & Nagy, Z., 1992. A possibility of an electromagnetic technique to locate oil reservoir boundaries on basis of analogue modelling experiments. Acta Geod. Geoph. Mont. Hung. **27**: 131-138.

Tabbagh, A., Benderitter, Y., Andrieux, P., Decriaud, J.-P. & Guerin, R., 1991. VLF resistivity mapping and verticalization of the electric field. Geophysical Prospecting **39**(8): 1083-1097.

Tchalenko, J.S., 1970. Similarities between shear zones of different magnitudes. Geological Society of America Bulletin **81**: 1625-1640.

Tchalenko, J.S. & Ambraseys, N.N., 1970. Structural analysis of the Dasht-e Bayaz (Iran) earthquake fractures. Geological Society of America Bulletin **81**: 41-60.

Telford, W.M., Geldart, L.P. & Sheriff, R.E., 1990. Applied Geophysics Second Edition. Cambridge University Press, Cambridge, UK, 770 pp.

Tezkan, B., Goldman, M., Greinwald, S., Hördt, A., Müller, I., Neubauer, F.M. & Zacher, G., 1996. A joint application of radiomagnetotellurics and transient electromagnetics to the investigation of a waste deposit in Cologne (Germany). Journal of Applied Geophysics **34**: 199-212.

Tezkan, B., Hördt, A. & Gobashy, M., 2000. Two-dimensional radiomagnetotelluric investigation of industrial and domestic waste sites in Germany. Journal of Applied Geophysics **44**: 237-256.

Tezkan, B., Zacher, G. & Dautel, S., 1997. On the application of radiomagnetotellurics to waste site exploration in Germany. Proceed. of the Symposium on the Application of geophysics to engineering and environmental problems (SAGEEP '97), Wheat Ridge, CO, United States, Environmental and Engineering Geophysical Society: 825-833.

Thierrin, J. & Müller, I., 1988. La méthode VLF/Résistivité multifréquence, un example d' eploration hydrogéologique dans un synclinal Crétacé à la Bré vine. Annales Scientifiques de l' Universté de Besancon, Mémoire hors série **6**: 17-24.

Tikhonov, A.N., 1950. On determining the electric properties of deep layers of the earth's crust. Proc (Doklady) Acad. Sci. USSR **83-2**.

Tsokas, G.N., Tsuorlos, P.I. & Szymanski, J.E., 1997. Square array resistivity anomalies and inhomogeneity ratio calculated by the finite element method. Geophysics **62**: 426-435.

Turberg, P., 1994. Apport de la cartographie Radiomagnétotellurique a l'hydrogéologie des milieux fractures. PhD thesis, Centre d'Hydrogéologie de l'Institut de Géologie, Université de Neuchâtel, Neuchâtel, Switzerland, 132 pp.

Turberg, P. & Barker, R., 1996. Joint application of radio-magnetotelluric and electrical imaging surveys in complex subsurface environments. First Break **14**(3): 105-112.

Turberg, P. & Müller, I., 1992. La méthode inductive VLF-EM pour la prospection hydrogéologique en continu du milieu fissuré. Annales Scientifique de l' Université de Besancon, Mémoire hors série **11**: 207-214.

Turberg, P. & Müller, I., 1997. Contribution de la méthode radiomagnétotellurique à la délimitation des structures hydrogéologiques en milieu hétérogène de subsurface. Proceed. of the Colloque GEOFCAN Géophysik des sols et des formations superficielles, 11-12 septembre 1997, Bondy, France, Abstracts et Résumés étendus.

Turberg, P., Müller, I. & Flury, B., 1994. Hydrogeological investigation of porous environments by radio magnetotelluric-resistivity (RMT-R 12-240 kHz). Journal of Applied Geophysics **31**: 133-143.

Turberg, P. & Persson, L., 1997. Radiomagnetotelluric measurements for detection of faults and fracture zones in Sweden. Proceed. of the EAGE 59th Conference and Technical Exhibition (26-30.05.1997), Geneva, Switzerland.

Vrba, J. & Zaporozec, A. (Eds.), 1994. Guidebook on mapping groundwater vulnerability. International Contributions to Hydrogeology **16**, I.A.o. Hydrogeologists, Verlag Heinz Heise, Hannover, 131 pp.

Wanfang, Z., Beck, B.F. & Stephenson, J.B., 1999. Investigation of groundwater flow in karst areas using component separation of natural potential measurements. Environmental Geology **37**(1-2): 19-25.

Wannamaker, P.E., Stodt, J.A. & Rijo, L., 1985. PW2D - Finite element program for solution of magnetotelluric responses of two-dimensional earth resistivity structure, Earth Sciences Laboratory, University of Utah, Utah.

Wannamaker, P.E., Stodt, J.A. & Rijo, L., 1986. Two dimensional topographic responses in magnetotellurics modeled using finite elements. Geophysics **51**: 2131-2144.

Weh, M., Mählmann, R.F. & Froitzheim, N., 1996. Strukturelle und metamorphe Diskontinuitäten im Penninikum am Westrand der Ostalpen. Proceed. of the Tektonik und Strukturgeologisches Kolloqium.

Wenger, B., 2001. Traceurs fluorescents en hydrogéologie: Description des propriétés optiques, de la conservativité, la toxicité et le prix des principaux colorants utilisés pour le traçage des eaux souterraines., Centre of Hydrogeology, University of Neuchâtel, Switzerland, pers.com.

Wexsteen, P., Jaffé, F.C. & Mazor, E., 1988. Geochemistry of cold CO2 -rich springs of the Scuol-Tarasp region, Lower Engadine, Swiss Alps. Journal of Hydrology **104**: 77-92.

Wiese, H., 1962. Geomagnetische Tiefentellurik Teil II: Die Streichrichtung der Untergrundsstrukturen des elektrischen Widerstandes, erschlossen aus geomagnetischen Variationen. Geofis pura Appl. **52**: 83-102.

Williams, P.W., 1983. The role of the subcutaneous zone in karst hydrology. Journal of Hydrology **61**: 45-67.

Wright, J.L., 1988. VLF Interpretation Manual, Technical Note. EDA Instruments, Toronto, Ontario, Canada.

Wu, N., Booker, J.R. & Smith, J.T., 1993. Rapid two-dimensional inversion of COPROD2 Data. J. Geomag. Geoelec. **45**: 1073-1087.

Zacher, G., Tezkan, B. & Müller, I., 1994. Flächenhafte RMT-Messungen auf einer Altlast bei Schongau (Bayern) und deren zweidimensionale Interpretation. Proceed. of the 3. DGG-Seminar Umweltgeophysik, Neustadt/Weinstrasse 30.8.-2.9.1994, **Sonderband III/ 1996**, Deutsche Geophysikalische Gesellschaft e. V.

Zacher, G., Tezkan, B., Neubauer, F.M., Hördt, A. & Müller, I., 1996. Radiomagnetotellurics: A powerful tool for waste-site exploration. European Journal of Environmental and Engeneering Geophysics **1**: 139-159.

Zhou, W., Beck, B.F. & Stephenson, J.B., 2000. Reliability of dipole-dipole electrical resistivity tomography for defining depth to bedrock in covered karst terranes. Environmental Geology **39**(7): 760-766.

Zwahlen, F. & Dörfliger, N., 1995. Hydrogeological aspects of groundwater protection in karstic areas. in Final report of the COST 65 action, European Comission, Directorate General Science, Research and Development.

Appendix A

VLF-EM GRAD Operation Manual

The VLF-EM GRAD antenna is compatible to the formerly developed RF-EM equipment components: RECEIVER, DATALOGGER and BATTERY-PACK. A detailed description of the RF-EM components, the measurement procedure and the data download and processing-software is explained in the appendix of the PhD thesis of Stiefelhagen (1998) (appendix in English). Nevertheless, a short description is given here.

While using the DATALOGGER, the data are recorded to one binary file to the PCMCIA memory card. These cards can be read by notebooks for instance. With the help of the "VLF-EM" program package (included on this PhD CD-ROM) the data can be downloaded and converted to ASCI files to the computer. Furthermore, additional data processing is possible with this package. For the detailed description of the "VLF-EM" program package the reader is referred to the appendix of Stiefelhagen (1998).

Components

GRADIENT ANTENNA (15 – 25 kHz)

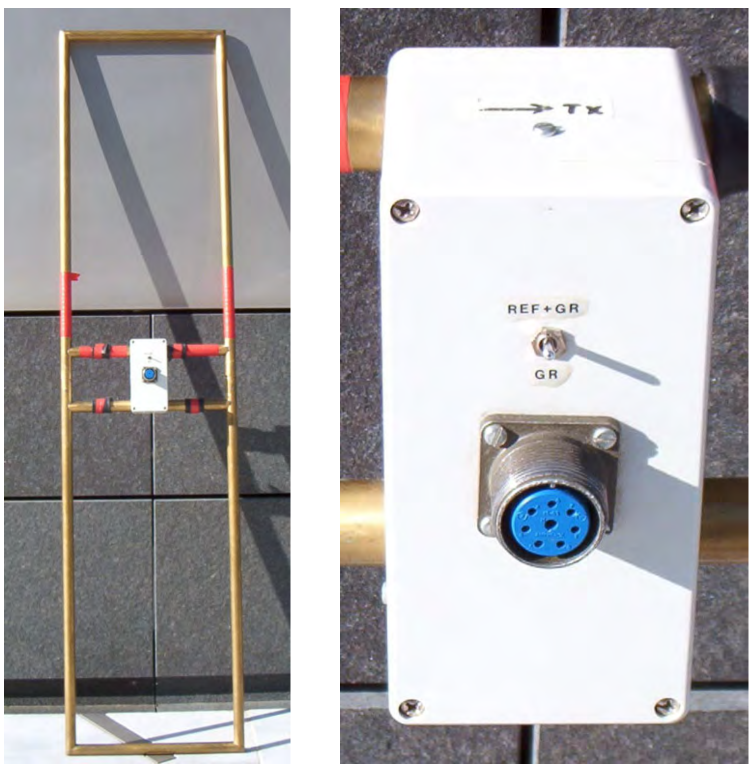

Fig. A - 1: (l): Complete antenna; (r): Detailed view of the electronic box (from top to bottom): "TRANSMITTER DIRECTION LABEL T_X", SWITCHER "REF+GR" (measurement mode) or "GR" (transmitter direction estimation mode), SOCKET for CABLE1.

RF-EM RECEIVER (15 – 300 kHz)

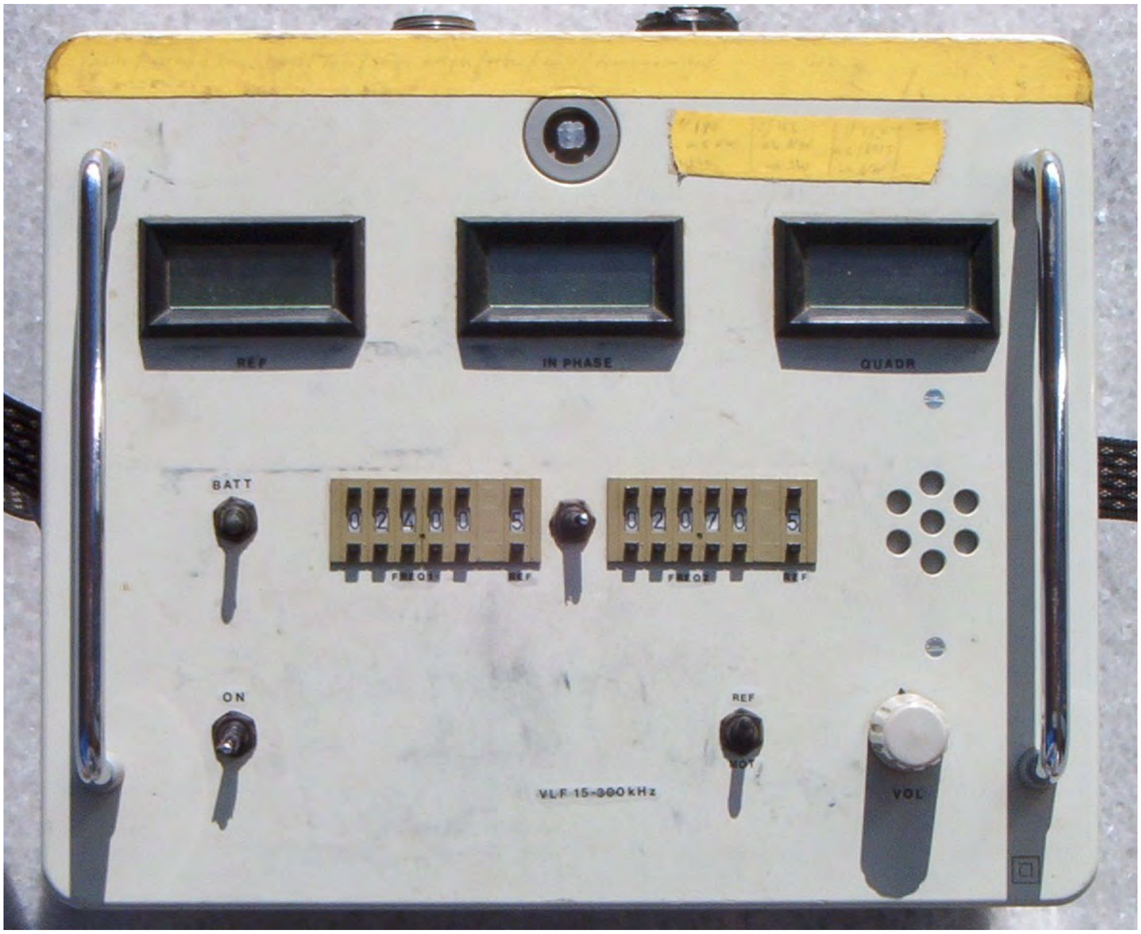

Fig. A - 2: Front view of RF-EM receiver. Two different frequencies can be pre-tuned. Switcher "REF/MOT" has to be in position "REF" while measuring.

DATALOGGER

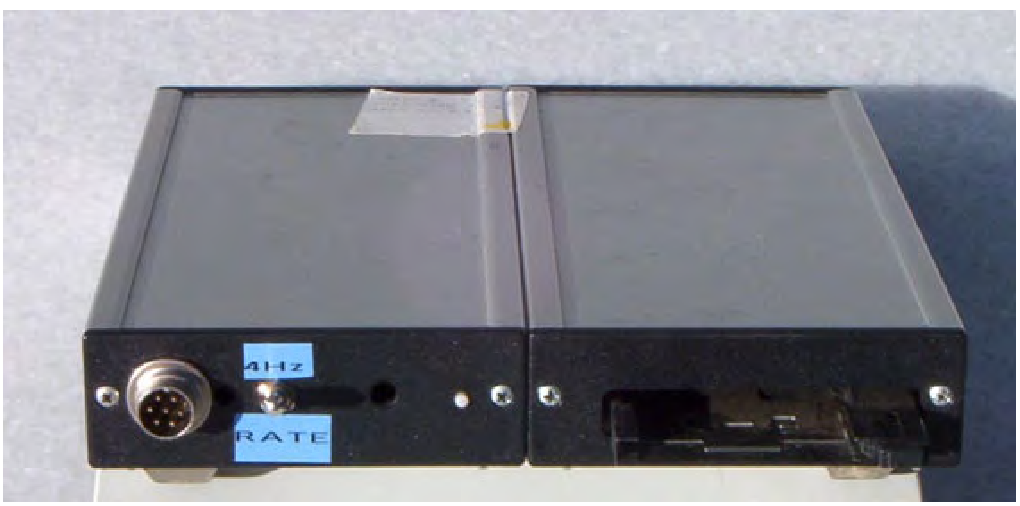

Fig. A - 3: Front panel of Datalogger. From left to right: Socket for Remote Control; Switcher for Sample Frequency (up = 4 Hz, down = 1 Hz); Memory Card slot.

Datalogger Remote Control

Fig. A - 4: Datalogger RemoteControl with cable. Box (from left to right): (1) Switcher position "STP" = STOP, "S/S" = RECORD; (2) LED; (3) Switcher "MARK"

Memory card (2 MB) and Memory Card Battery (3V, BR2325)

Fig. A - 5: Memory Card with Battery (Type: BR2325, 3V)

BATTERY-PACK for DATALOGGER- and RF-EM RECEIVER-power supply

Fig. A - 6: Front panel of BATTERY-PACK with "ON/OFF Switcher", Fuses and Sockets for power supply cables to DATALOGGER and RECEIVER. Pack includes two 12 Volt PB Accus.

CABLE 1: GRADIENT ANTENNA ↔ RECEIVER

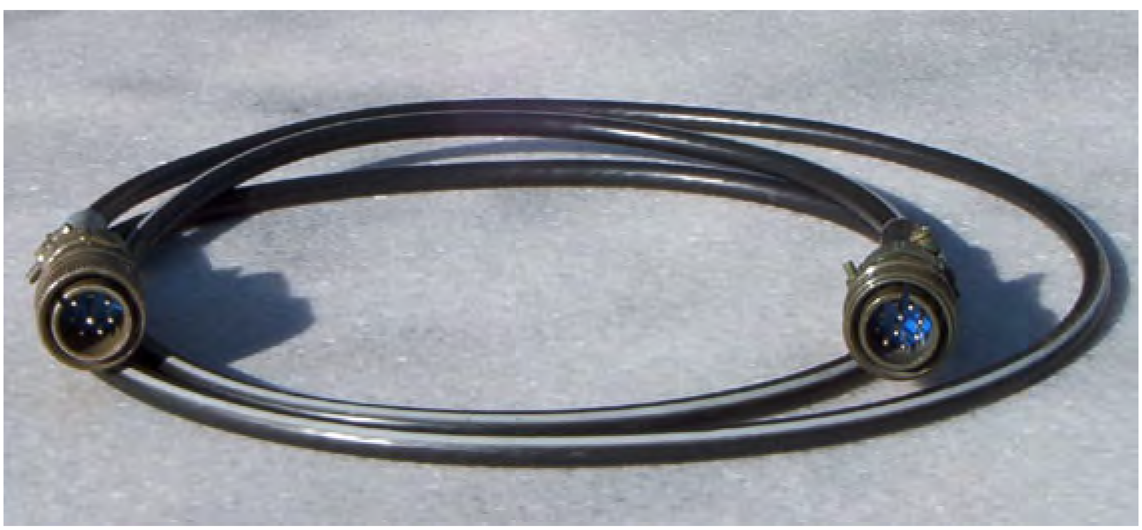

Fig. A - 7: Cable1: Connection between ANTENNA and RECEIVER. Left plug connects to ANTENNA; right plug connects to RECEIVER.

CABLE 2: BATTERY PACK ↔ RECEIVER

Fig. A - 8: Cable 2: for power supply of the RECEIVER.

CABLE 3: DATALOGGER ↔ RECEIVER, BATTERY PACK (has 3 plugs)

Fig. A - 9: Cable 3: for power supply of DATALOGGER and data transfer from RECEIVER to DATALOGGER. Plugs to connect to (from left to right): (1) DATALOGGER back panel; (2) BATTERY-PACK; (3) RECEIVER

CABLE 4: Battery Pack Charging Cable

Fig. A - 10: Cable 4: for charging the Battery-Pack. Use chargers for PB Accus!

Operating procedure

Important Note: When making connections to the BATTERY-PACK, always plug in the cable to the device first, then afterwards to the BATTERY-PACK in order to prevent short circuits caused by the open end of the cable touching the (wet) ground or grass!

Assembling the system

1. Connect ANTENNA to RECEIVER with CABLE 1.
2. Connect RECEIVER to BATTERY-PACK with CABLE 2
3. Connect REMOTE CONTROL to DATALOGGER
4. Connect DATALOGGER to RECEIVER with CABLE 3 (Data Plug)
5. Connect DATALOGGER to BATTERY-PACK with CABLE 3 (Battery Plug)
6. Plug in MEMORY CARD into DATALOGGER slot (check MEMORY CARD BATTERY before with voltmeter)
7. Deactivate the write protection of the MEMORY CARD

Carrying out measurements

Preparation

1. Switch on RECEIVER
2. Choose frequency
   a. Transmitter position should be parallel to assumed structure strike direction and vertical to profile direction to guarantee E-Polarisation situation). Two frequencies can be pre-tuned.

3. Check transmitter orientation with the help of signal sound:
    a. Turn ANTENNA (antenna-switcher position "GR", Fig. A - 1) to find the sound minimum: The "transmitter-direction-label T_X" indicates then the transmitter orientation with an uncertainty of 180°.
    b. Once the transmitter orientation is checked, push the "antenna-switcher" to the position "REF+GR" (Fig. A - 1). This is then the signal maximum position, which is used for the measurement. **Note: The "TRANSMITTER-DIRECTION-LABEL T_X" has to show into the real position of the remote radio transmitter (known from lists); otherwise, the recorded signals are of switched mathematical signs.** If the real position is unknown, make sure that for all profiles, which are carried out with the same frequency, the arrow is consistently orientated towards the same direction. The real orientation can be figured out later by comparing the results from known transmitters. If necessary, the recorded data may be corrected by multiplying with -1.
4. Choose DATALOGGER frequency (Fig. A - 3)
    a. 1 Hz mode: Inphase, Quadrature and Reference Signal is stored.
    b. 4 Hz mode: Inphase and Quadrature is stored.
5. Switch DATALOGGER power on (switcher at BATTERY-PACK; Fig. A - 1)
6. Wait one minute for finishing of MEMORY CARD erasing

Profiling and using the Remote Control

7. Start walking and push left switcher on REMOTE CONTROL down to position "S/S" to start recording (Fig. A - 4).
    a. Check, if the red LED on the REMOTE CONTROL blinks (slow at 1 Hz mode, fast at 4 Hz mode). If the LED does not blink, check the system.
8. Use the "MARK" switcher to make marks in the recorded data.
    a. The marks can later be used for converting the samples into distances (view "VLF-EM" program package in the appendix of Stiefelhagen (1998)).
    b. The marks may also be used to record the position of geographical prominent features along profiles.
9. If for any reason you have to stop recording on a profile, switch the left switcher on the REMOTE CONTROL back to the position "STP".
    a. To continue the profile just switch to "S/S" again.
10. **End of profile**: Switch to position "STP" **and** make a MARK **afterwards**.
    a. This switcher sequence creates an "End Of Profile-Mark" in the data and opens a new file for recording the next profile.

Downloading the data

11. Activate the write protection of the MEMORY CARD
12. Switch off DATALOGGER power on the BATTERY-PACK
13. Remove the MEMORY CARD out of the DATALOGGER
14. Deactivate the MEMORY CARD write protection and plug in the MEMORY CARD into the PCMCIA slot of a PC, where the "VLF-EM" program package is installed.
15. Use the command "bt" to download and convert the data from binary to ASCI format (further necessary details in Stiefelhagen (1998))

Once the DATALOGGER power was switched off, the MEMORY CARD will be erased when switching the power on again (view step 6: one minute waiting time!).

VLF-EM program package

The detailed explication can be found in Stiefelhagen (1998). The program was originally written for the Microsoft platforms DOS, Windows 95 and Windows 98. For the use under Windows 2000 some little modifications must be done manually. The program package must be installed from Floppy Disks. To create a three-disk installation set, copy the content of each of the folders "install", "install2" and "sinstall", which are found on the "PhD CD-ROM", to one floppy disk respectively.

To install the program, run the command "VLF_INST.BAT" from the "install" or the "sinstall" (lighter version without source codes) floppy disk. During the installation process, the AUTOEXEC.BAT file is modified. Under Windows 2000 skip this step. These modifications must be done manually in the "Environmental Variables" mask of the system properties under Windows 2000. The sample parameters are found in AUTOEXEC_VLF-EM_WIN98.BAT, which is also stored on this "PhD CD-ROM". Use these values.

Some of the default installed batch files (BT.BAT, GNUPLOT.BAT and TX.BAT) must be modified to run under Windows 2000. The appropriate files can be found on this PhD CD-ROM.